



The
University
Of
Sheffield.

Formalisation of bespoke fatigue approaches to design aluminium-to-steel thin hybrid welded joints

By:

Ibrahim Abdulkarim Thabet Al Zamzami

A thesis submitted in partial fulfilment of the requirements for the degree of
Doctor of Philosophy

The University of Sheffield
Faculty of Engineering.
Department of Civil and Structural Engineering

Supervisors:

Prof. Luca Susmel

Prof. Buick Davison

Submission Date

September 2019

This page left intentionally blank

Abstract

The present research was designed to investigate experimentally and numerically the fatigue behaviour of aluminium-to-steel hybrid-welded joints. It has always been a challenge to weld dissimilar materials because of the significant difference in their mechanical, thermo-physical and metallurgical properties, which causes the formations of hard and brittle intermetallic phases in the welding region. Recently, EWM® Welding has developed a new welding technology (known as coldArc®) to solve this problem which is capable of providing a strong joint on condition that the steel sheet is galvanized. Various welding configurations were manufactured using the coldArc® welding including butt, lap, cruciform and tee welded joints.

Before investigating the fatigue behaviour of the hybrid-welded joints, the static behaviour was investigated to better understand the overall mechanical behaviour of these joints. As far as the static investigation is concerned, the visual examination of the fracture surfaces revealed that, regardless of the geometry of the welded connections, the fracture of the joint always took place in the heat-affected zone (HAZ) on the aluminium side. This inspection indicated that the use of EWM® coldArc welding technology had improved the strength of the hybrid welded joint significantly and removed the problem of having a brittle phase in the welding zone. The results obtained from this investigation shows that Eurocode9 (EC9) can also be used to design aluminium-to-steel thin welded joints.

The fatigue lifetime estimation of aluminium-to-steel thin welded joints was carried out using the nominal stresses, effective notch stresses, the Notch Stress Intensity Factors (N-SIFs) and the Modified Wöhler Curve Method (MWCM) in conjunction with the Theory of Critical Distances (TCD). The results of the fatigue investigation showed that for the nominal and effective notch stresses, the available Standards and Codes of Practice (EC9 and the International Institution of Welding (the IIW)) are only suitable for thick welded joints. However, the negative inverse slope of 5 for thin materials suggested by Sonsino¹ was seen to provide conservative fatigue life estimations in terms of nominal stresses.

Furthermore, the effective notch stresses and the N-SIF approaches make it evident that the strength of the aluminium alloy used in this investigation was very low compared to the aluminium alloys used in the structural applications and hence another design curves are required. In this context, a FAT of 90 was proposed for the notch stresses to perform an accurate fatigue design of the hybrid-welded joints. For the N-SIFs, a design curve

¹ Sonsino C.M. A consideration of allowable equivalent stresses for fatigue design of welded joints according to the notch stress concept with the reference radii $r_{ref} = 1.00$ and 0.05 mm. *Welding in the World* 2009; 53: R64-R74.

Abstract

characterised by negative inverse slope equal to 5 million cycles to failure is recommended. Finally, the MWCM was calibrated for the structural details being investigated. The validation process demonstrated the high level of accuracy in estimating the fatigue strength of hybrid welded joints.

Acknowledgments

Firstly, I would like to express my gratitude to my supervisors Professor Luca Susmel, and Professor Buick Davison for their continuous support, guidance and encouragement throughout my PhD. I also would like to give a special thank you to the technicians who supported my experimental work, Paul Blackburn and Richard Kay. I would like to take this opportunity to express my gratitude to my family who was the hero behind the scenes, and supporting me in every matter during my PhD. I would like to thank EWM® Welding for providing the welding machine to support this research work.

Contents

Abstract.....	i
Acknowledgments.....	iii
Contents.....	iv
List of Figures.....	vii
List of Tables	xiv
Nomenclature.....	xviii
Abbreviations	xxii
1 Introduction.....	1
1.1 Background	1
1.2 Aims and objectives	4
1.3 Thesis outline	5
1.4 Publications.....	6
1.5 References	7
2. Literature Review	9
2.1 Metal joining processes	9
2.1.1 Explosion-bonding.....	10
2.1.2 Friction welding	10
2.1.3 Friction Stir Welding (FSW)	11
2.1.4 Laser Welding.....	12
2.1.5 ColdArc Welding	13
2.2 Fatigue loading in welded joints.....	15
2.2.1 Uniaxial cyclic loading.....	15
2.2.2 Fatigue assessment methods.....	22
2.2.3 Multiaxial cyclic loading	37
2.3 Conclusions	43
2.4 References	44
3. Global and local stress-based approaches to estimate the fatigue strength of aluminium welded joints	51
3.1 Introduction	52

3.2	Methodology.....	53
3.3	Fatigue assessment results and discussion	55
3.3.1	Nominal stress based approach	55
3.3.2	Hot-spot stress approach.....	59
3.3.3	Effective notch stress approach.....	63
3.3.4	N-SIF approach	66
3.3.5	TCD	69
3.3.6	Mean stress effect on the fatigue strength of aluminium weldments.....	72
3.4	Conclusions	76
3.5	Reference	77
4.	Fatigue assessment of inclined welded joints subjected to uniaxial cyclic loading.	81
4.1	Introduction	81
4.2	Methodology.....	82
4.2.1	Experimental data	82
4.2.2	Finite Element Analysis (sub-modelling).....	85
4.3	The MWCM to estimate the fatigue lifetime of inclined welds subjected to uniaxial fatigue loading	87
4.3.1	MWCM applied along with the nominal stress approach	87
4.3.2	The MWCM applied along with the hot-spot stress approach.....	93
4.3.3	The MWCM applied along with the effective notch stress approach	98
4.3.4	The MWCM applied along with the Point Method	103
4.4	Conclusions	108
4.5	References	109
5.	Experimental Procedure	111
5.1	Materials.....	111
5.2	Welding Process	112
5.3	Investigated configurations.....	113
5.3.1	Static investigation	113
5.3.2	Fatigue investigation.....	115
5.4	Static test	117
5.5	Fatigue test	117
6.	Static strength and design of aluminium-to-steel thin welded joints.....	123
6.1	Introduction	124
6.2	Experimental Results.....	124
6.3	Design against static loading.....	132
6.4	Discussion	133

Contents

6.5	Conclusion.....	135
6.6	References	136
7.	Fatigue behaviour of aluminium-to-steel thin welded joints.....	137
7.1	Introduction	137
7.2	Lifetime estimation in terms of nominal stress approach	138
7.3	Lifetime estimation in terms of the effective notch stress approach	142
7.4	Lifetime estimation in terms of the N-SIFs approach.....	145
7.5	Lifetime estimation in terms of the MWCN along with the Point Method.....	147
7.5.1	Method formalisation	148
7.5.2	Method validation	153
7.6	Conclusions	155
7.7	References	156
8.	Conclusions and recommendation for future work	158
8.1	Conclusion.....	158
8.2	Recommendation for future work	162
A	Appendix A Fatigue results generated by testing aluminium alloys (Chapter 3)	163
B	Appendix B Fatigue results generated by testing steel inclined welded joints (chapter 4)	181
C	Appendix C Static data of aluminium-to-steel welded joints (chapter 6)	185
	Static experimental data of the hybrid joints (Long-term).	185
	Force vs. displacement curves of the hybrid joints.	188
	Static fracture surface of the hybrid joints (Short-term).....	200
	Static fracture surface of the hybrid joints (Long-term)	209
	Metallurgical Analysis.....	216
D	Appendix D Fatigue data of aluminium-to-steel welded joints (chapter 7).....	221

List of Figures

Figure 1.1 Fatigue damage model showing the PSBs and the micro cracks.	1
Figure 1.2. Different stages of the fatigue life of the structural components.	2
Figure 1.3 Comparison between the strength of plain, notch and welded steel components [1].	3
Figure 2.1 Explosion-bonding weld processes [5].	10
Figure 2.2 Schematization of the Friction Stir Welding [11].	11
Figure 2.3 Set up of laser welding process for the investigated hybrid welded joint done by Gao [16].	12
Figure 2.4 Current and voltage of the EWM coldArc process and the standard short arc process.	13
Figure 2.5 the Power comparison of standard and coldArc welding processes [19].	14
Figure 2.6 Sequence of the metal transfer and drop separation in the coldArc process [21].	14
Figure 2.7 Spatter-free welding achieved by using EWM coldArc welding technology.	15
Figure 2.8 Plain specimens subjected to fatigue loading with a load ratio equal -1 (a) Wöhler diagram (b).	16
Figure 2.9 Fatigue behaviour of metals in the form of Wöhler curves including ferrous metal under control condition (a) non-ferrous metal (b) ferrous metal in real condition (c).	17
Figure 2.10 Wöhler diagram showing fatigue curves calculated for different probabilities of survival.	18
Figure 2.11 The effect of non-zero mean stress and load ratio on the Wöhler diagrams [24].	21
Figure 2.12 Nominal sections in welded details [26].	23
Figure 2.13 Examples of axial misalignment (a) and angular misalignment (b), (c) [34]. ...	24
Figure 2.14 Fatigue class recommendation (FAT) based on the nominal stress and hot-spot stress approaches according to the IIW [34].	25
Figure 2.15 Example of the linear surface stress extrapolation (a) and through thickness stress linearization procedure (b) [43].	26
Figure 2.16 Hot spot stress determination according to Dong method [43].	26

List of Figures

Figure 2.17 Type "a" and "b" hot spots [34].	27
Figure 2.18 Neuber's micro-support theory [45].	29
Figure 2.19 Notch stress and stress intensity [45].	30
Figure 2.20 Definition of the local coordinates (Polar coordinates).	31
Figure 2.21 Definition of the loading modes [26].	32
Figure 2.22 Fatigue strength of steel and aluminium welded joints based on the N-SIF approach [58].	34
Figure 2.23 Definition of the local coordinate system (a), the formalisation of the TCD in form of Point Method (b) and Line Method (c).	36
Figure 2.24 The MWCM to estimate fatigue lifetime of welded components applied in terms of nominal and hot spot stresses.	39
Figure 2.25 The MWCM to estimate fatigue lifetime of welded components applied in terms of effective notch stress as well as along with the PM.	40
Figure 2.26 Modified Wöhler diagram.	41
Figure 3.1 Geometry of the investigated welded details.	52
Figure 3.2 Accuracy of the Nominal Stress approach in estimating the fatigue strength of the investigated welded joints see Figure 3.1 for the definition of the different welded geometries.	57
Figure 3.3 Example of the refined area around the focus path according to the hot spot stress approach.	60
Figure 3.4 Definition of hot-spot stress.	61
Figure 3.5 Accuracy of the Hot-Spot Stress approach in estimating the fatigue strength of the investigated welded joints.	62
Figure 3.6 Weld toe and root rounded according to the reference radius concept.	63
Figure 3.7 Example of FE model being solved using the Effective notch Stress approach.	64
Figure 3.8 Accuracy of the Effective Notch Stress approach in estimating the fatigue strength of the investigated welded joints.	65
Figure 3.9 Example of FE model being solved using the N-SIFs and Point Method.	67
Figure 3.10 Accuracy of the N-SIF approach in estimating the fatigue strength of the investigated welded joints.	68

Figure 3.11 Determination of the critical distance value using two calibration fatigue curves (a); Local stress-distance curve and critical distance LW-AI according to the PM (b).	69
Figure 3.12 Accuracy of the PM in estimating the fatigue strength of the investigated welded joints.	71
Figure 3.13 Effect of load ratio R on the fatigue strength of aluminium welded joints.	74
Figure 4.1 Fatigue specimens tested by Booth and Maddox [4] (a) and load carrying cruciform specimens tested by Kim and Kainuma [5] (b).	83
Figure 4.2 Out-of-plane gusset specimens (a) and non-load carrying cruciform specimens (b) tested by Kim and Yamada [6].	84
Figure 4.3 example of 3D FE global model (a) and sub-model (b).	86
Figure 4.4 Nominal and hot spot stresses in inclined welded joints subjected to uniaxial cyclic loading.	87
Figure 4.5 Mohr's circle to calculate the stress components relative to the critical plane.	89
Figure 4.6 Accuracy of the recommended reference design curves in estimating the fatigue strength of the the welded joints in terms of nominal stresses (toe failure (a) and root failure (b)).	90
Figure 4.7 Accuracy of the MWCM applied along with nominal stresses in estimating fatigue strength in the presence of inclined welds (geometry BM).	91
Figure 4.8 Accuracy of the MWCM applied along with nominal stresses in estimating fatigue strength in the presence of inclined welds. (Geometry KY-N and KY-G).	92
Figure 4.9 Accuracy of the MWCM applied along with nominal stresses in estimating fatigue strength in the presence of inclined welds (geometry KK).	92
Figure 4.10 definition nominal and shear hot-spot stresses.	93
Figure 4.11 Examples of mesh refinement (a); and the linear-elastic FE models solved by following a solid-to-solid sub-modelling procedure (b); using the hot-spot stress approach.	94
Figure 4.12 the procedure followed to determine the required hot spot stresses.	95
Figure 4.13 Accuracy of the recommended reference design curves in estimating the fatigue strength of the investigated welded joints in terms of hot-spot stresses.	96
Figure 4.14 Accuracy of the MWCM applied along with hot-spot stresses in estimating fatigue strength in the presence of inclined welds (for geometry BM).	97
Figure 4.15 Accuracy of the MWCM applied along with hot-spot stresses in estimating fatigue strength in the presence of inclined welds (for geometry KY-N and KY-G).	97

List of Figures

Figure 4.16 Examples of mesh refinement (a); and the linear-elastic FE models solved by following a solid-to-solid sub-modelling procedure (b); using the effective notch stress approach.	99
Figure 4.17 Accuracy of the recommended reference design curves in estimating the fatigue strength of the investigated welded joints in terms of 1 st principal stresses.....	100
Figure 4.18 Accuracy of the MWCM applied along with effective notch stresses in estimating fatigue strength in the presence of inclined welds (for geometry BM).	100
Figure 4.19 Accuracy of the MWCM applied along with effective notch stresses in estimating fatigue strength in the presence of inclined welds (for geometry KK).	101
Figure 4.20 Accuracy of the MWCM applied along with effective notch stresses in estimating fatigue strength in the presence of inclined welds (for geometry KY-N and KY-G).	102
Figure 4.21 Examples of the linear-elastic FE models solved by following a solid-to-solid sub-modelling procedure using the TCD.	104
Figure 4.22 Schematic illustration of the focus path used to calculate the effective stresses of 15° inclination angle welded joints using the PM.	105
Figure 4.23 Accuracy of the MWCM to estimate the fatigue strength of the inclined welded joints using the Theory of Critical Distances in the form of Point Method (Geometry BM)..	105
Figure 4.24 Accuracy of the MWCM to estimate the fatigue strength of the inclined welded joints using the Theory of Critical Distances in the form of Point Method (Geometry KK)..	106
Figure 4.25 Accuracy of the MWCM to estimate the fatigue strength of the inclined welded joints using the Theory of Critical Distances in the form of Point Method (Geometry KY)..	107
Figure 5.1 EWM welding machine.	112
Figure 5.2 EWM alpha Q puls including codes list for various material combination (a) the machine interface showing values for different welding parameters (b).....	113
Figure 5.3 Geometry of the investigated aluminium-to-steel welded components (a). Schematisation of the tensile specimens (b).....	114
Figure 5.4 Geometry of the investigate aluminium-to-steel welded joints, butt-welded joints (a); and the load carrying cruciform welded joints (b).	115
Figure 5.5 Geometry of the investigate aluminium-to-steel welded joints, lap-welded hybrid welded joints (a); and the tee welded joints (b).....	116
Figure 5.6 MAYSE uniaxial fatigue machine (a), hydraulic grips (b).....	118

Figure 6.1 Force vs extension for different aluminium-to-steel welded joints.	128
Figure 6.2 Tensile static failure of double butt, 45°, and 60 ° inclined butt, cruciform and lap hybrid welded joints (a) Tensile static failure modes of single butt, 15° and 30° inclined butt hybrid welded joints (b).....	129
Figure 6.3 the average tensile strength results of Al-St butt, lap and cruciform Welded Joints ((short-term ageing).	130
Figure 6.4 the average tensile strength results of Al-St butt Welded Joints with various inclination angles (short-term ageing).	131
Figure 6.5 Comparison between the short term and long-term tensile static strength of butt-welded, cruciform-welded and lap-welded aluminium-to-steel hybrid joints.	131
Figure 6.6 Effective and equivalent design stresses of aluminium-to-steel welded joints compared with standard design codes.	132
Figure 7.1 Fatigue Failure of butt, lap and cruciform welded joints.	139
Figure 7.2 Accuracy of the nominal stress approach to estimate the fatigue strength of the thin hybrid welded joints.....	141
Figure 7.3 Examples of linear elastic 2D FE models solved using effective notch stress approach.	142
Figure 7.4 Weld toe and root rounded according to the reference radius concept (a); accuracy of the effective notch stress approach to estimate the fatigue strength of the thin hybrid welded joints (b); results generated for the whole data and FAT90 design curve (c).	143
Figure 7.5 FE model for the tee welded joints	144
Figure 7.6 schematization of the weld details used in the FE model for the NSIF approach.	146
Figure 7.7 Accuracy of the N-SIF approach to estimate the fatigue strength of the thin hybrid welded joints (a); statistical reanalysis for the data with a proposed design curve (b).	146
Figure 7.8 Examples of linear elastic FE models (a) solved using a 2-dimentional models (b) solved using a 3-dimentional models following the standard solid-solid sub-modelling procedure.....	149
Figure 7.9 2D and 3D linear elastic stress distribution along the weld seam for the cruciform welded joints.....	150

List of Figures

Figure 7.10 the procedure used to calibrate the MWCM constants and estimate the fatigue strength of hybrid welded joint according to the PM.	152
Figure 7.11 Accuracy of the MWCM applied along with the Point Method in estimating fatigue strength of thin hybrid welded components (2D FE models).	153
Figure 7.12 Accuracy of the MWCM applied along with the Point Method in estimating fatigue strength of thin hybrid welded components (3D FE models).	154
Figure C.1 Force vs. displacement curve for single sided Butt-welded joints (short term). ..	189
Figure C.2 Force vs. displacement curve for double sided Butt-welded joints (short term).	190
Figure C.3 Force vs. displacement curve for 15° inclined butt-welded joints (short term)..	191
Figure C.4 Force vs. displacement curve for 30° inclined butt-welded joints (short term).	192
Figure C.5 Force vs. displacement curve for 45° inclined butt-welded joints (short term).	194
Figure C.6 Force vs. displacement curve for 60° inclined butt-welded joints (short term).	195
Figure C.7 Force vs. displacement curve for cruciform-welded joints (short term).....	197
Figure C.8 Force vs. displacement curve for Lap-welded joints (short term)	198
Figure C.9 Tensile static failure of single-butt-welded joints (short-term).	200
Figure C.10 Tensile static failure of double-butt-welded joints (short-term).	201
Figure C.11 Tensile static failure of 15° inclined butt-welded joints (short-term).	202
Figure C.12 Tensile static failure of 30° inclined butt-welded joints (short-term).	203
Figure C.13 Tensile static failure of 45° inclined butt-welded joints (short-term).	204
Figure C.14 Tensile static failure of 60° inclined butt-welded joints (short-term).....	205
Figure C.15 Tensile static failure of lap-welded joints (short-term).....	206
Figure C.16 Tensile static failure of cruciform-welded joints (short-term).	207
Figure C.17 Tensile static failure of single-butt-welded joints (long-term).	209
Figure C.18 Tensile static failure of 15° inclined butt-welded joints (long-term).	210
Figure C.19 Tensile static failure of 30° inclined butt-welded joints (long-term).	211
Figure C.20 Tensile static failure of 45° inclined butt-welded joints (long-term).	212
Figure C.21 Tensile static failure of 60° inclined butt-welded joints (long-term).	213
Figure C.22 Tensile static failure of lap-welded joints (long-term).	214

Figure C.23 Tensile static failure of cruciform-welded joints (long-term).	215
Figure C.24 the position of the investigated sections in the aluminium-to-steel welded joints for the metallurgical analysis.	216
Figure C.25 Map of main metallic elements taken further from melting zone.....	216
Figure C.26 Zinc –aluminium interface.	217
Figure C.27 Steel –filler interface.	218
Figure C.28 Distribution of Zinc in the Filler.	219
Figure C.29 Steel – Filler – Aluminium interfaces.....	220
Figure C.30 Map of the main metallic elements in the welding zone: a) Steel, b) Aluminium and c) Zinc.	220
Figure D.1 Fatigue failure of butt-welded joints with load ratio, $R=0.1$	221
Figure D.2 Fatigue failure of butt-welded joints with load ratio, $R=-1$	223
Figure D.3 Fatigue failure of lap-welded joints with load ratio, $R=0.1$	224
Figure D.4 Fatigue failure of lap-welded joints with load ratio, $R=0.5$	225
Figure D.5 Fatigue failure of tee-welded joints with load ratio, $R=0.1$	226
Figure D.6 Fatigue failure of tee-welded joints with load ratio, $R=-1$	227
Figure D.7 Fatigue failure of cruciform-welded joints with load ratio, $R=0.1$	228
Figure D.8 Fatigue failure of cruciform-welded joints with load ratio, $R=-1$	229
Figure D.9 2D and 3D linear elastic stress distribution along the weld seam for the lap-welded joints.....	233
Figure D.10 2D and 3D linear elastic stress distribution along the weld seam for the butt-welded joints.....	233

List of Tables

Table 2.1 Index q for a confidence level equal to 0.95% [30].	19
Table 2.2 FAT for different welded geometries [34].	23
Table 2.3 Definition of the types of hot spots.	27
Table 2.4 FAT normal stresses according to the IIW for the effective notch stress approach [49].	30
Table 2.5 Notch opening angles and their corresponding constants and exponents.	32
Table 3.1 EC9 and the IIW recommended values in terms of stress ranges and negative inverse slope to design aluminium welded joints using the nominal and hot spots stress approaches.	54
Table 3.2 Fatigue results generated by testing ground butt-welded joints (geometry Aa in Figure 3.1) statistically re-analysed in terms of nominal stresses.	56
Table 3.3 Summary of the statistical re-analyses for the different welded geometries in terms of nominal stress approach.	58
Table 3.4 A summary of the amount of data fall below the design curve and the percentage of the data above the design curve	59
Table 3.5 Summary of the statistical re-analyses for the different approaches/welded geometries and corresponding recommended curves.	61
Table 3.6 Summary of the statistical re-analyses for the different approaches/welded geometries and corresponding recommended curves.	64
Table 3.7 Summary of the statistical re-analyses for the different approaches/welded geometries and corresponding recommended curves.	67
Table 3.8 Influence of the welded joint's absolute dimensions on the estimated value for L_{w-Al} .	70
Table 3.9 Summary of the statistical re-analyses for the different approaches/welded geometries and corresponding recommended curves.	72
Table 5.1 Mass chemical composition of the used materials by weight percentage.	112
Table 5.2 Fatigue results generated by testing butt-welded joints (Figure 5.4a).	119
Table 5.3 Fatigue results generated by testing cruciform welded joints (Figure 5.4b).	120
Table 5.4 Fatigue results generated by testing lap welded joints (Figure 5.5a).	121

Table 5.5 Fatigue results generated by testing tee welded joints (Figure 5.5b).....	122
Table 6.1 Ultimate tensile strength of plain, single and double-sided butt-welded joints (short term).	125
Table 6.2 Ultimate tensile strength of single-sided butt-welded joints with various inclination angles (short term).....	126
Table 6.3 Ultimate tensile strength of lab welded joints (short term).....	127
Table 6.4 Ultimate tensile strength of cruciform welded joints (short term).	127
Table 6.5 Ultimate tensile strength comparison of the short-term and long-term experiments.	130
Table 7.1 Summary of the statistical re-analyses for the different welded geometries in terms of nominal stress approach (the experimental results are presented in chapter 5).	140
Table 7.2 Summary of the statistical re-analyses for the different welded geometries in terms of effective notch stress and the N-SIFs approaches (the experimental data are presented in chapter 5).	145
Table A.1 The ultimate tensile strength (UTS) of different parent aluminium alloys.....	163
Table A.2 Fatigue results generated by testing butt-welded joints (geometry Ab) statistically re-analysed in terms of nominal stresses.	164
Table A.3 Fatigue results generated by testing ground butt-welded joints (geometries Ae) statistically re-analysed in terms of nominal stresses.	168
Table A.4 Fatigue results generated by testing non-load carrying fillet welded joints (geometries Ba, Bd and Be) statistically re-analysed in terms of nominal stresses.	169
Table A.5 Fatigue results generated by testing non-load carrying fillet welded T-joints (geometry Bb) statistically re-analysed in terms of nominal stresses.	171
Table A.6 Fatigue results generated by testing cruciform full-penetration welded joints (geometry Ca) statistically re-analysed in terms of nominal stresses.	173
Table A.7 Fatigue results generated by testing load carrying fillet cruciform welded joints (geometries Cb and Cc) statistically re-analysed in terms of nominal stresses.....	175
Table A.8 Fatigue results generated by testing non-load carrying fillet cruciform welded joints (geometry Ba) and non-load carrying fillet welded T-joints (geometry Bb) statistically re-analysed in terms of hot-spot stresses and effective notch stresses approaches.....	177

List of Tables

Table A.9 Fatigue results generated by testing cruciform full-penetration welded joints (geometry Ca) and load carrying fillet cruciform welded joints (geometry Cb) statistically re-analysed in terms of hot-spot stresses and effective notch stress approaches.	178
Table A.10 Fatigue results generated by testing non-load carrying fillet cruciform welded joints (geometry Ba) and non-load carrying fillet welded T-joints (geometry Bb) statistically re-analysed in terms of N-SIFs and the TCD.	179
Table A.11 Fatigue results generated by testing cruciform full-penetration welded joints (geometry Ca) and load carrying fillet cruciform welded joints (geometry Cb) statistically re-analysed in terms of N-SIFs and the TCD.	180
Table B.1 Experimental data and stress components relative to the critical plane calculated in terms of nominal stresses and hot-spot stresses (Geometry BM).	181
Table B.2 Experimental data and stress components relative to the critical plane calculated in terms of nominal stresses and hot-spot stresses (Geometry KK).	181
Table B.3 Experimental data and stress components relative to the critical plane calculated in terms of nominal stresses and hot-spot stresses (Geometry KN-G).	182
Table B.4 Experimental data and stress components relative to the critical plane calculated in terms of nominal stresses and hot-spot stresses (Geometry KY-N).	182
Table B.5 Experimental data and stress components relative to the critical plane calculated in terms of notch stresses and Point Method (Geometry BM).	183
Table B.6 Experimental data and stress components relative to the critical plane calculated in terms of notch stresses and Point Method (Geometry KK).	183
Table B.7 Experimental data and stress components relative to the critical plane calculated in terms of notch stresses and Point Method (Geometry KN-G).	184
Table B.8 Experimental data and stress components relative to the critical plane calculated in terms of notch stresses and Point Method (Geometry KY-N).	184
Table C.1 Ultimate tensile strength of single and double sided butt-welded joints (long term).	185
Table C.2 Ultimate tensile strength of single-sided butt-welded joints with various inclination angles (long term)	186
Table C.3 Ultimate tensile strength of lap welded joints (long term).	187
Table C.4 Ultimate tensile strength of cruciform welded joints (long term).	187

Table C.5 Weight and atomic percentages of elements found in Spot 1 and Area2 (Figure C.26).....	217
Table C.6 Weight percentages of elements found in Spot 1, 2 and 3 (Figure C.27).....	219
Table C.7 Weight percentages of elements found in Spot 1, 2, 3, 4, 5 and 6 (Figure C.29).....	220
Table D.1 Experimental data and stress components relative to the critical plane calculated in terms of Pint Method for the butt-welded joints (2D and 3D FE models).	230
Table D.2 Experimental data and stress components relative to the critical plane calculated in terms of Pint Method for the lap welded joints (2D and 3D FE models).	231
Table D.3 Experimental data and stress components relative to the critical plane calculated in terms of Pint Method for the cruciform welded joints (2D and 3D FE models).	232

Nomenclature

c_0, c_1	constants in the linear regression function
$f(R)$	mean stress enhancement factor
k_I	non-dimensional parameter to estimate K_I and ΔK_I
K_I, K_{II}	notch-stress intensity factor (N-SIF) for Mode I and Mode II loading
L	thickness of secondary attachment
L_{W-Al}	critical distance for aluminium welded joints
n	number of experimental data
N_A	reference number of cycles to failure
N_f	number of cycles to failure
P	proportion of the distribution
P_S	probability of survival
q	factor for one-sided tolerance limits for normal distribution
r, θ	polar coordinates
r_n	notch root radius
r_{ref}	reference radius
R	load ratio ($R = \sigma_{min} / \sigma_{max}$)
t	Thickness
T_σ	scatter ratio of the endurance limit range for PS=90% and PS=10%
z	weld leg length
ΔK_I	mode I N-SIF range

$\Delta K_{I,50\%}$	mode I N-SIF range extrapolated at NA cycles to failure for PS=50%
$\Delta K_{I,97.7\%}$	mode I N-SIF range extrapolated at NA cycles to failure for PS=97.7%
$\Delta\sigma$	stress range
$\Delta\sigma_{0.4t}$	range of the superficial stress at a distance from the weld toe equal to 0.4·t
$\Delta\sigma_t$	range of the superficial stress at a distance from the weld toe equal to t
$\Delta\sigma_1$	range of the maximum principal stress
$\Delta\sigma_{A,50\%}$	endurance limit range at NA cycles to failure for PS=50%
$\Delta\sigma_{A,95\%}$	endurance limit range at NA cycles to failure for PS=95%
$\Delta\sigma_{A,97.7\%}$	endurance limit range at NA cycles to failure for PS=97.7%
$\Delta\sigma_{HS}$	hot-spot stress range
$\Delta\sigma_{NS}$	notch stress range
$\Delta\sigma_{PM}$	range of the Point Method local stress
$\lambda_1, \lambda_2, \chi_1, \chi_2$	constants in William's equations
σ_{max}	maximum stress in the cycle
σ_{min}	minimum stress in the cycle
σ_θ, σ_r	linear-elastic local normal stresses
τ_{r0}	linear-elastic local shear stress
a, b, α , β	fatigue constants for the MWCM's calibration curves
k	negative inverse slope of the uniaxial fatigue curve
k_0	negative inverse slope of the torsional fatigue curve
k_t	negative inverse slope of the modified Wöhler curve

Nomenclature

$\Delta\sigma_x$	stress range normal to the weld seam
$\Delta\sigma_{nom}$	axial nominal stress range
$\Delta\sigma_n$	stress range perpendicular to the critical plane
$\Delta\sigma_A$	stress range of the uniaxial design curve extrapolated at a reference number of cycles to failure
$\Delta\sigma_{0.4t}$	normal superficial stress range at a distance from the weld toe equal to 0.4t
$\Delta\sigma_t$	superficial normal stress range at a distance from the weld toe equal to t
$\Delta\sigma_{R,d}, \Delta\tau_{R,d}$	design resistance stress range for a specific number of cycles and appropriate FAT class
$\Delta\tau_{xy}$	shear stress range parallel to the weld seam
$\Delta\tau$	shear stress range relative to the critical plane
$\Delta\tau_{0.4t}$	superficial shear stress range at a distance from the weld toe equal to 0.4t
$\Delta\tau_t$	superficial shear stress range at a distance from the weld toe equal to t
$\Delta\tau_A$	stress range of the torsional design curve extrapolated at a reference number of cycles to failure
ρ_w	critical plane stress ratio
$\Delta\tau_{Ref}$	reference shear stress range extrapolated at N_{Ref} cycles to failure
r_{Ref}	reference radius
θ	inclination angle with respect to the applied cyclic loading
σ_{Ed}	the design normal stress, perpendicular to the weld axis
τ_{Ed}	the design shear stress, parallel to the weld axis
σ_{eq}	the combined normal and shear stresses
f_w	characteristic strength weld metal

γ_{Mw}	Partial safety factor for welded joints
$\sigma_{eq,fillet}$	the combined normal and shear stresses for the fillet weld
σ_{\perp}	direct stress perpendicular to the weld throat
τ_{\perp}	shear stresses in the perpendicular direction to the fillet weld
τ_{\parallel}	shear stresses in the parallel direction to the fillet weld

Abbreviations

AM	<u>A</u> rea <u>M</u> ethod
EC	<u>E</u> uro <u>C</u> ode
FE	<u>F</u> inite <u>E</u> lement
FSW	<u>F</u> ri <u>S</u> tion <u>S</u> tir <u>W</u> elding
HAZ	<u>H</u> eat <u>A</u> ffacted <u>Z</u> one
IIW	<u>I</u> nternational <u>I</u> nstitution of <u>W</u> elding
IMC	<u>I</u> nter <u>M</u> etallic <u>C</u> ompound
LM	<u>L</u> ine <u>M</u> ethod
MIG	<u>M</u> etal <u>I</u> ntert <u>G</u> as
MWCM	<u>M</u> odified <u>W</u> öhler <u>C</u> urve <u>M</u> ethod
N-SIF	<u>N</u> otch <u>S</u> tress <u>I</u> ntensity <u>F</u> actor
PM	<u>P</u> oint <u>M</u> ethod
PSB	<u>P</u> ersistent <u>S</u> lip <u>B</u> ands
TCD	The <u>T</u> heory of <u>C</u> ritical <u>D</u> istances
UTS	<u>U</u> ltimate <u>T</u> ensile <u>S</u> trength
VM	<u>V</u> olume <u>M</u> ethod

Chapter 1

1 Introduction

1.1 Background

Fatigue failure of metals is a very complicated process, which was explored initially in the mid-19th century. In general, fatigue occurs when the material is experiencing a repeated cyclic loading, which is lower than the ultimate tensile strength or the yield strength of the material [1-3]. The damage caused by the fatigue process is accumulated cycle by cycle during the lifetime of the structural component and, after a certain number of cycles; the component suddenly fails without any visible warning signs.

The fatigue life of the components is usually composed of two stages, the crack initiation stage and the crack growth stage followed by the fracture of the component. The first stage is the crack initiation; this involves the formation of the persistent slip bands (PSBs) and invisible microcracks (Figure 1.1), which are related to the cyclic slips [1, 4-5].

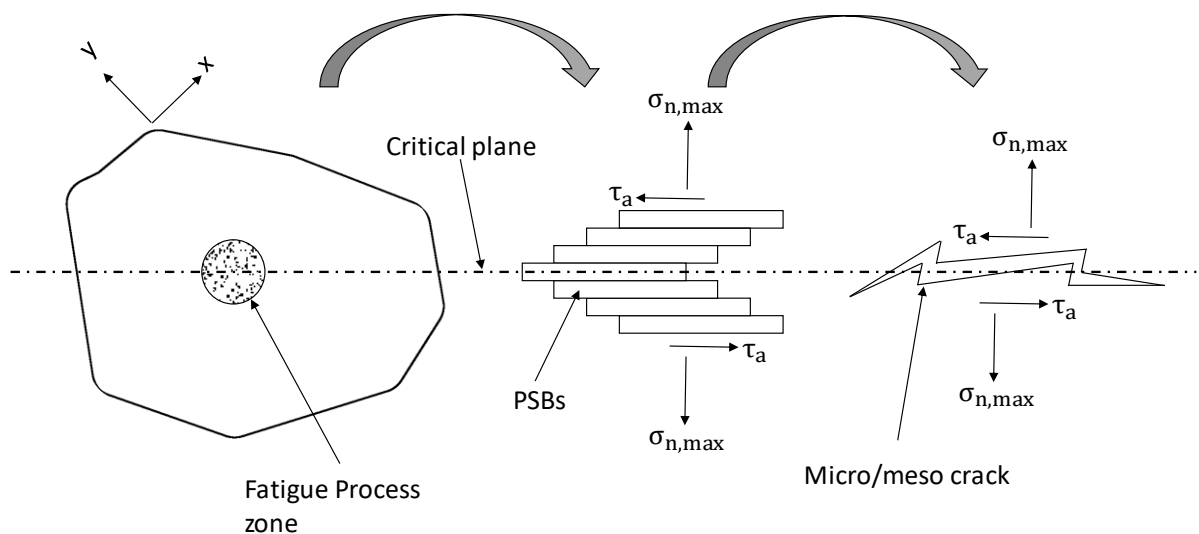


Figure 1.1 Fatigue damage model showing the PSBs and the micro cracks.

1.1 Background

Due to the effect of the grain boundaries, the microcracks grow slowly extending the crack length in each cycle. Then, the second stage begins as the macro-cracks penetrate inside the component in directions perpendicular to the applied stress load.

The growth of the macro-cracks is much faster in this phase until the crack extends to its critical length causing the fracture of the components. However, the rate of crack propagation can vary considerably depending on different factors including the material used, the type of component (i.e. welded, notched or plain) and the nature of the applied stresses (i.e. axial, bending and/or torsion)[1]. Figure 1.2 shows the different stages of the fatigue life of the structural components.

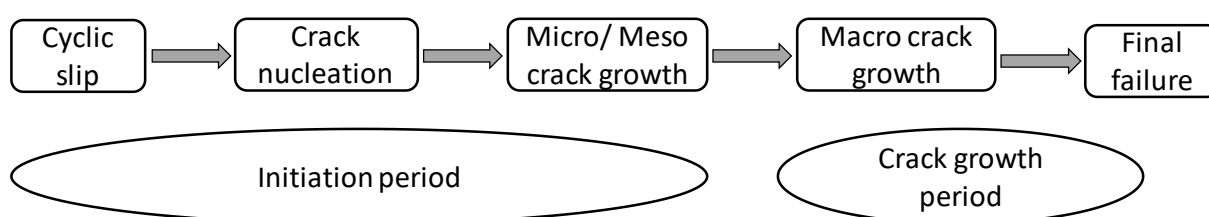


Figure 1.2. Different stages of the fatigue life of the structural components.

The welding process was invented in the Bronze Age; however, the use of welding techniques to join structural components was introduced more than a century ago to replace the use of bolted joints [7]. Fatigue problems associated with the welding process were identified from the outset. A considerable amount of research that can be found in literature has been carried out to investigate the effect of the welding process on the overall fatigue behaviour of the structural components. The research indicates that the fatigue life of the welded components is considerably lower than the un-welded components made from the same metal, as shown in Figure 1.3 [1]. The reason behind the strength reduction is that the welding process induces residual stresses, defects, imperfections and distortion, which strongly affect the fatigue strength of the welded components [8-9]. A severe stress concentration could occur at the weld seams and weld root resulting in sharp stress/strain gradients [6]. Consequently, the fatigue failure of the structural welded components usually appears in the welds rather than on the parent material, even if the parent material contains notches such as opening or re-entrant corners [2]. Further, the filler material disturbs the homogeneity of the parent material leading to the change of the microstructure of the component in the heat-affected zone [2].

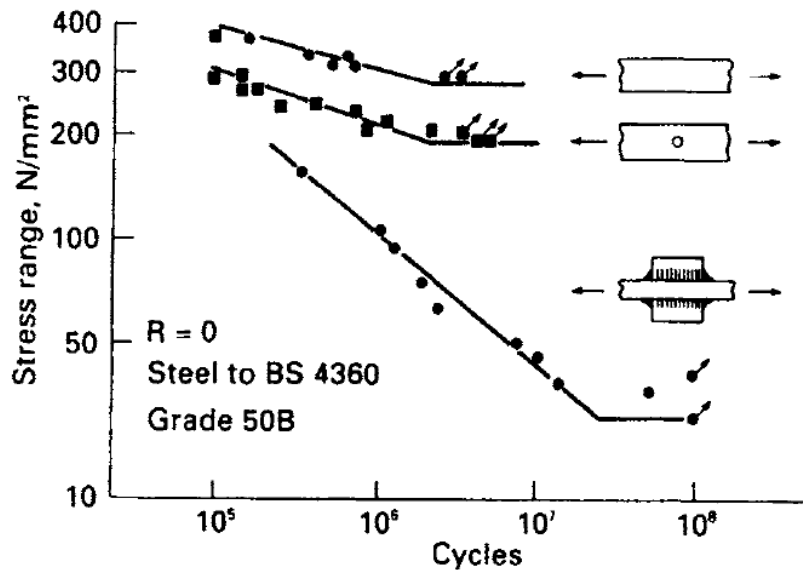


Figure 1.3 Comparison between the strength of plain, notch and welded steel components [1].

In recent years, using aluminium as a structural material has become an interesting alternative solution in important applications such as automotive frames, offshore structures and in the railway industry. The reason behind this growth is the ability to utilise the various mechanical/physical properties of aluminium alloys to manufacture high-performance lightweight structures having increased strength-to-weight ratio. Further, aluminium is a “green” material that can efficiently be recycled ad infinitum.

Recently, many government policies have been established to lower the carbon dioxide emissions from land vehicles. The transportation industry has been challenged to reduce fuel consumption and comply with such policies. To this end, fuel-efficient engines and mass efficient structural materials are required to reduce the total weight of the vehicle [10-11]. To tackle this issue effectively, aluminium has widely replaced steel parts in the automotive industry to reduce the overall weight of the vehicles [10].

The necessity of welding aluminium-to-steel has recently increased in the shipbuilding, energy production and the automotive industry. However, using the conventional fusion welding technology to weld aluminium-to-steel was seen to cause many problems as the aluminium and steel have very different physical properties (e.g. thermal expansion, conductivity and melting temperature). The differences in physical properties result in the formation of hard and brittle phases (such as Fe-Al) at the weld, which severely deteriorates the mechanical properties of the aluminium-to-steel hybrid welded joints [10, 12].

Since the early 2000s, many researchers in the field of dissimilar metal welding have been conducted with the aim of achieving stronger hybrid joints with higher productivity [13-16]. As a result, low energy input welding technologies were developed (e.g. ARC Welding method) to

1.2 Aims and objectives

join aluminium-to-steel that improves the tensile strength of the joint, with the tensile strength being more than 70% of the parent material's strength [16].

The literature on the fatigue behaviour of similar structural materials has highlighted different fatigue assessment approaches to estimate the fatigue lifetime of the structural components. The design codes and guidelines suggested three different design methods: (1) the nominal stresses, (2) the hot-spot stresses, and (3) the effective notch stresses [17, 1]. These methods were studied extensively and seen to estimate the fatigue lifetime of the components reasonably accurately, on condition that the correct reference curves for each particular geometry are applied. More attention is recently focused on the utilisation of the Theory of Critical Distances (TCD). The TCD provides a very accurate estimation of the fatigue lifetime of the structural components with much less computational effort required.

1.2 Aims and objectives

The novelty of my research stems from the fact that, the fatigue behaviour of aluminium-to-steel welded joints has never before examined in a systematic and structured way. The main aim of this research is to investigate experimentally in details the fatigue behaviour of aluminium-to-steel thin welded joints. Hence, investigating the effectiveness of the existing stress-based approaches in designing the hybrid welded joints subjected to fatigue loading. However, to understand better the mechanical properties of the hybrid welded joints, the static behaviour is investigated by manufactured the aluminium-to-steel hybrid welded joints using the coldArc® welding technology provided by EWM Welding.

The following objectives are required to achieve the aims:

1. Manufacture various configurations of aluminium-to-steel thin welded joints using the coldArc® welding technology. Then run tensile static loading tests to investigate the static strength of the welded joints and examine the capability of this welding technology to make a robust hybrid joint.
2. Perform a metallurgical analysis to quantify the micro-geometrical parameters of the weld.
3. Conduct systematic experimental and numerical work to investigate the fatigue behaviour and extend the use of the existing design approaches (the nominal stresses, the effective notch stresses and the Notch Stress Intensity Factors (N-SIFs)) to design aluminium-to-steel hybrid welded joints.
4. Formalise a numerical procedure suitable for using the Theory of Critical Distance (TCD) to perform the fatigue assessment of hybrid-welded joints.

1.3 Thesis outline

The research work presented in this thesis is structured as follow: **Chapter 2** reviews in detail the available information on the static and fatigue behaviour of aluminium-to-steel welded joints. The chapter gives a quick overview of the available welding technologies and provides more detail about the advanced welding technology used in this thesis. Moreover, the chapter describes the fundamental aspects of the stress-based approaches that represent the core part of this research including the nominal stresses, hot-spot stresses, the effective notch stresses, the N-SIFs, the TCD and the Modified Whöler Curve Method (MWCM).

Chapter 2 showed that most of the literature was focusing on the fatigue strength of steel welded joints and much less attention paid to the aluminium-welded joints. Therefore, **Chapter 3** provides a full statistical reanalysis of more than two thousands of experimental data, taken from the literature, generated by testing various aluminium configurations to check the accuracy and reliability of the existing stress-based approach in designing aluminium-welded joints.

In Chapter 4, the MWCM was used to estimate the fatigue lifetime of steel inclined welded joints subjected to uniaxial loading. The importance of chapter 4 comes from the fact that in real life the structural components are experiencing stresses that are always at an angle to the direction of the weld. **Chapter 5** presents the experimental procedure conducted to manufacture and test the aluminium-to-steel hybrid-welded joints.

Chapter 6 and **Chapter 7** studied the static and fatigue behaviour of the hybrid-welded joints, respectively. These two chapters provide suggestions, design curves and equations to design the welded joints subjected to static or fatigue loading more accurately. **Chapter 8** gave an overall conclusion followed by recommendations for further work.

1.4 Publications

From the work presented in this thesis, the following papers were published or submitted for publication:

Journal Papers:

- Al Zamzami I, Susmel L. On the accuracy of nominal, structural, and local stress-based approaches in designing aluminium welded joints against fatigue. *International Journal of Fatigue* 2017; 101: 137-158. <https://doi.org/10.1016/j.ijfatigue.2016.11.002>.
- Al Zamzami L, Cocco V.Di, Davison J.B, Iacoviello F, Susmel L. Static strength and design of aluminium-to-steel thin welded joints. *Welding in the World* 2018; <https://doi.org/10.1007/s40194-018-0634-2>.
- Al Zamzami I, Susmel L. On the use of hot-spot stresses, effective notch stresses and the Point Method to estimate lifetime of inclined welds subjected to uniaxial fatigue loading. *Int J Fatigue* 2018; 117: 432-449. <https://doi.org/10.1016/j.ijfatigue.2018.08.032>.
- Al Zamzami I, Davison J.B, Susmel L. Nominal and local stress quantities to design aluminium-to-steel thin welded joints against fatigue. *Int J Fatigue* 2019; 279-295. <https://doi.org/10.1016/j.ijfatigue.2019.02.018>.

Conference proceedings Papers:

- Al Zamzami I, Davison J.B, Susmel L. Static Strength of aluminium-to-steel thin welded joints: preliminary results. BSSM 12th International Conference on Advances in Experimental Mechanics, 29 Aug 2017 - 31 Aug 2017. <http://www.bssm.org/uploadeddocuments/Conf 2017/2017 papers/28 Ibrahim AlZamzami formatted.pdf>.
- Al Zamzami I, Susmel L. Static and fatigue behaviour of aluminium-to-steel thin welded joints. 19th International Colloquium on Mechanical Fatigue of Metals, 05 Sep 2018 - 07 Sep 2018. Proceedings of the 19th International Colloquium on Mechanical Fatigue of Metals. 05 Sep 2018.

1.5 References

- [1] Maddox S.J. Fatigue strength of welded structures, second edition ed., Cambridge : Abington Publishing, 1991.
- [2] Fricke W. Review Fatigue analysis of welded joints: state of development. *Marine Structures* 2003; 185-200.
- [3] Campbell F. Fatigue and Fracture- Understanding the basics, ASM International 2012.
- [4] Susmel L. Multiaxial notch fatigue- From nominal to local stress/strain quantities. Cambridge: Woodhead Publishing Limited, 2009.
- [5] Radaj D, Sonsion C.M, Fricke W. Fatigue assessment of welded joints by local approaches, Cambridge: Woodhead Publishing Limited, 2006.
- [6] Schijve J. Fatigue of Structures and Materials, Second Edition ed., Springer, 2009.
- [7] Schijve J. Fatigue predictions of welded joints and the effective notch stress concept. *Int J Fatigue* 2012; 45: 31-38.
- [8] Haryadi G.W, Kim S.J. Influences of post weld heat treatment on fatigue crack growth behavior of TIG welding of 6013 T4 aluminium alloy joint (part 1. Fatigue crack growth across the weld metal). *J Mech Sci & Tech* 2001; 25 (9): 2161-2170.
- [9] Borrego L.P, Costa J.D, Jesus J.S, Loureiro A.R, Ferreira J.M. Fatigue life improvement by friction stir processing of 5083 aluminium alloy MIG butt welds. *Theor & Appl Fract Mech* 2014; 70:68-74.
- [10] Kimapong K, Watanabe T. Lap Joint of A5083 Aluminium Alloy and SS400 Steel by Friction Welding. *Materials Transactions* 2005; 46(4):835-841.
- [11] Meco S, Pardal G, Ganguly S, Williams S, McPherson N. Application of laser in seam welding of dissimilar steel to aluminium joints for thick structural components. *Optics and Laser in Engineering* 2015: 22-30.
- [12] Qin G-L, Su Y-H, Wang S-J. Microstructures and properties of welded joint of aluminium alloy to galvanized steel by Nd: YAG laser + MIG arc hybrid brazing-fusion welding. *Transactions of Nonferrous Metals Society of China* 2004; 24:989-995.
- [13] Okamura H, Aota K. Joining of dissimilar materials with friction stir welding. *Welding International* 2004; 18(11):852-860.
- [14] Katayama S. Laser welding of aluminium alloys and dissimilar metals. *Welding International* 2004; 18(8): 618-625.
- [15] Kato K, Tokisue H. Dissimilar friction welding of aluminium alloys to other materials. *Welding International* 2004; 18(11):861-867.

1.5 References

- [16] Lu Z, Huang P, GAO W, Li Y, Zhang H, Yin S. ARC welding method for bonding steel with aluminium. *Front. Mech. Eng. China* 2009; 4(2):134-143.
- [17] Hobbacher A. *Recommendations For Fatigue Design of Welded Joints and Components*. International Institute of Welding, Paris, 2007.
- [18] "EuroCode 9: Design of aluminium structures- Part 1-3: Structures susceptible to fatigue," 2011.

Chapter 2

2.Literature Review

The purpose of this chapter is to review the technical literature on the fatigue behaviour of steel and aluminium welded joints. Various stress-based design approaches have been employed to determine the fatigue lifetime of notched, cracked and welded structural components. In this context, the nominal stresses, hot-spot stresses, the effective notch stresses, the Notch Stress Intensity Factors (N-SIFs), the TCD and the MWCM have been reviewed explicitly to extend the use of these approaches and apply them to estimate the fatigue lifetime of the aluminium-to-steel thin welded joints. This chapter also examines the state of the art on the development of the existing welding technologies to join dissimilar materials, particularly aluminium alloy and steel.

2.1 Metal joining processes

One of the most challenging aspects associated with the design and fabrication of a high-performance mechanical assembly is how to join efficiently its different parts. There are many issues related to the use of modern and advanced composite materials to create complex, and lightweight hybrid structures. The most critical issue is the joining process. It is a difficult and expensive process to join composite to other composites as well as to other structural materials. In contrast, metallic materials can efficiently be joined together at a relatively low cost by welding. For this reason, manufacturing structures and components by metallurgically welding aluminium to steel represents an innovative solution for the fabrication of future low-cost and environmentally friendly lightweight structural assemblies. Accordingly, in recent years, the issue of joining aluminium to steel has received considerable attention.

The main problem associated with the use of conventional fusion welding technologies to weld aluminium to steel is that these two materials have different physical properties (e.g., thermal expansion, conductivity, and melting temperature). Furthermore, their different metallurgical

2.1 Metal joining processes

characteristics lead to the formation of hard and brittle intermetallic phases (such as Fe-Al) at the interface between the two materials, with these intermetallic phases markedly deteriorating the mechanical properties of the welded connections [1-2].

2.1.1 Explosion-bonding

Certainly, explosion-bonding represents a revolutionary technology allowing both similar and dissimilar materials to be joined together. This process was developed in the late 1950s in the shipbuilding industry to weld aluminium to steel so that connections with improved corrosive, mechanical, and strength properties could be manufactured effectively. It is a solid phase process where welding takes place by accelerating one of the components at extremely high velocity using chemical explosives. A schematic illustration of the explosion bonding process is shown in Figure 2.1. The drawback of this method is that dis-bonding is likely to occur during construction and in-service operations, with this resulting in extra time and cost associated with repairing/removing [3-5].

To overcome the above problems, over the past decade, there has been a remarkable increase in the research work done in the field of dissimilar metal welding with the aim not only of achieving stronger and of more flexible hybrid welded joint solutions, but also of increasing manufacturing productivity [6-9].

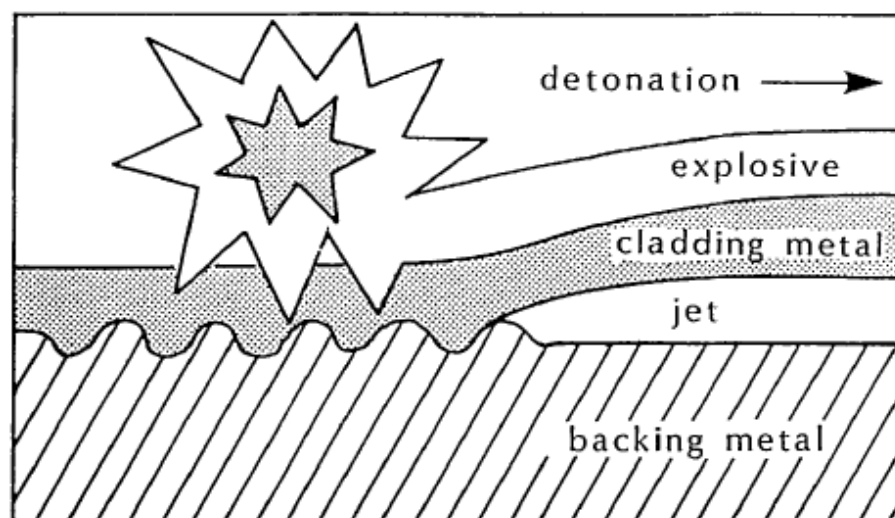


Figure 2.1 Explosion-bonding weld processes [5].

2.1.2 Friction welding

Owing to the intrinsic limitations of explosion bonding, in recent years, different attempts have been made to explore alternative technological solutions. Friction welding is another process, which can be used to welded aluminium to steel. It works by moving one plate against another stationary plate under very high pressure to generate the required heat to join the components

together. For instance, Fukumoto [10] used the friction welding process to manufacture hybrid-welded joints made of 5052 aluminium alloy and 304 stainless steel. This investigation showed that longer friction time causes the formation of intermetallic layers at the weld interfaces. Further, as the intermetallic layer thickness increased, the connections become more and more brittle, with fracture occurred at the interface [10].

2.1.3 Friction Stir Welding (FSW)

FSW is another joining process that has been used to manufacture aluminium-to-steel connections. Figure 2.2 illustrates how the FSW process works. First, the rotating pin is plunged into the aluminium plate and then pushed into the faying steel surface as shown in Figure 2.2. The rubbing motion of the rotating pin generates the heat required to melt the aluminium. Consequently, the molten aluminium adheres to the faying steel surface making the joint.

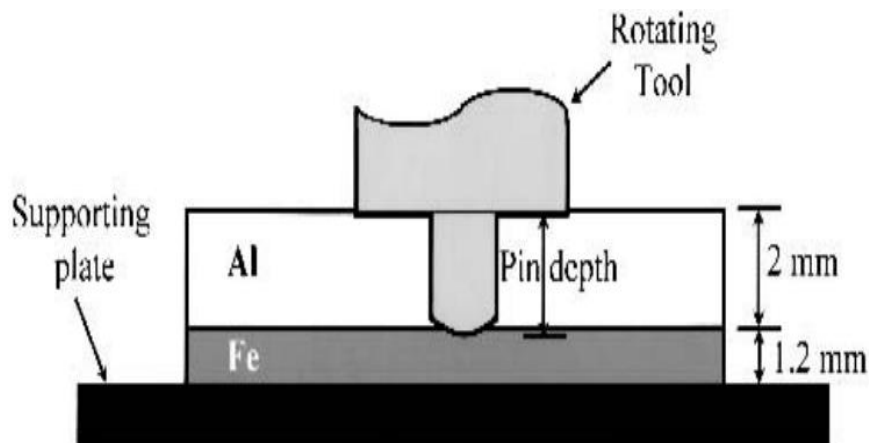


Figure 2.2 Schematization of the Friction Stir Welding [11].

FSW was used to produce mainly lap and butt-welded joints. These investigations demonstrate that, as far as FSW is concerned, the joint strength tended to increase as the rotation speed increased. In contrast, the strength tended to decrease as the travelling speed increased [1, 3, 11-12]. Lately, this process was further developed so that aluminium-to-steel welded joints are manufactured using a multi-pass welding strategy. The results obtained using FSW showed that the use of this technology led to the elimination of the intermetallic layers, with this resulting in an increase of the overall strength of the joints. The main disadvantage of this method is that friction stir welded connections are characterised by a non-uniform distribution of the mechanical properties across the weld [13].

2.1.4 Laser Welding

The laser welding is a fusion joining process that produces the joining of materials with the required heat obtained from a concentrated beam of coherent, monochromatic light affecting the joint to be welded (Figure 2.3). The laser beam provides a concentrated heat source resulting in narrow, deep welds and high welding rates. The laser welding has a high power density, which results in high and cooling rates as well as a small HAZ compared with other technologies. Laser welding-based processes have been used to weld aluminium to steel effectively. The use of laser welding results in a microstructural damage reduction at the interface associated with the presence of intermetallic compound (IMC) layers. With this joining technology, promising results can be achieved if the correct temperature at the interface is controlled during the welding process so that the growth of the IMC layers is limited [4, 14-15]. Gao [16] investigated the hybrid-welded joints using AA6060 aluminium alloy and 304SS steel. The set-up of the laser welding process is shown in Figure 2.3. Gao proposed that to limit the growth of the IMC layers, the temperature at the interface should be lower than 1120°C.

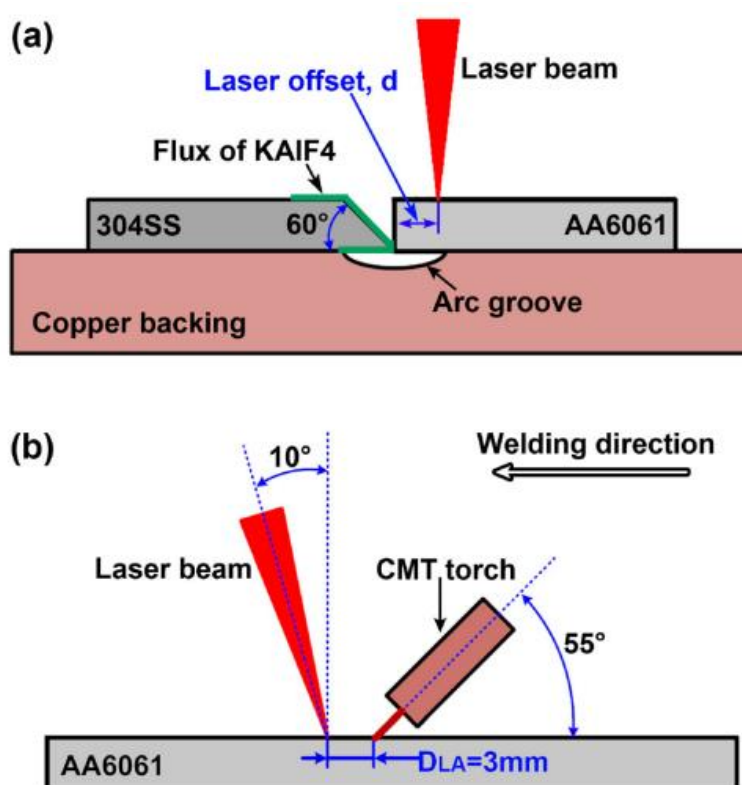


Figure 2.3 Set up of laser welding process for the investigated hybrid welded joint done by Gao [16].

2.1.5 ColdArc Welding

Examination of the state of the art suggests that the main challenges to be faced when welding aluminium-to-steel are as follow:

- i. Minimise the presence of the IMC layers at the interface.
- ii. Control the thickness of IMC layers to avoid the formation of brittle phases.
- iii. Prevent the formation of pores and cracks, which reduce the overall strength of aluminium-to-steel welded joints.

As a result, a variety of low-energy-input welding technologies was developed in recent years to join aluminium to steel effectively [17, 18]. In this context, EWM coldArc® undoubtedly represents the most advanced technology solution that is available in the market (www.ewm-group.com). It is an advanced form of welding that allows excellent control over the rate of heat input and the metal transfer. Its lower heat input enables welding professionals to weld thin metal sheets without causing any burn through. It can join thin sheets from 0.3 mm using an automated welding machine and from 0.7 mm using manual welding machine [19].

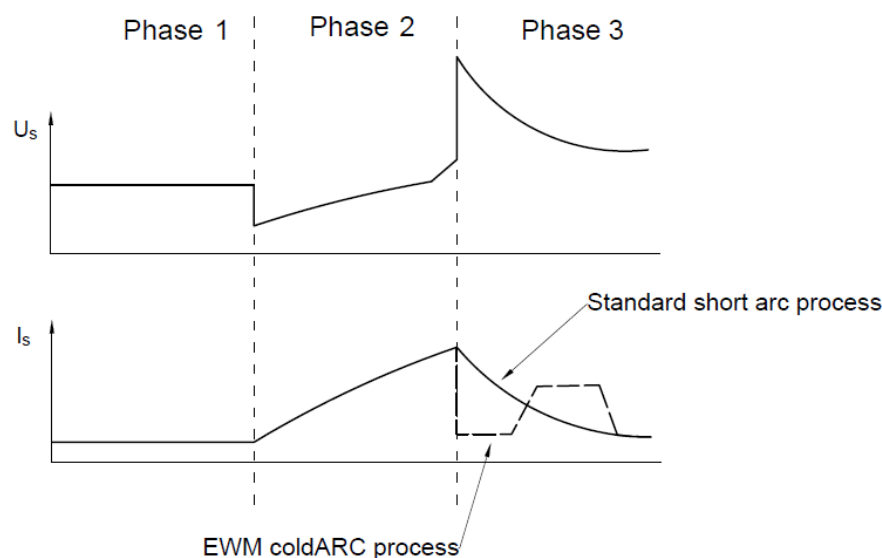


Figure 2.4 Current and voltage of the EWM coldArc process and the standard short arc process.

It is a modified short-arc process for root welding of pipes or thin materials and has excellent gap bridging capabilities. Due to the low-heat used during the process, it causes no damage to the zinc coating and less warping formed. Therefore, it is an ideal solution to weld aluminium to steel, provided that the steel sheet is zinc coated to minimise the formation of the hard and brittle intermetallic phases [19-20].

2.1 Metal joining processes

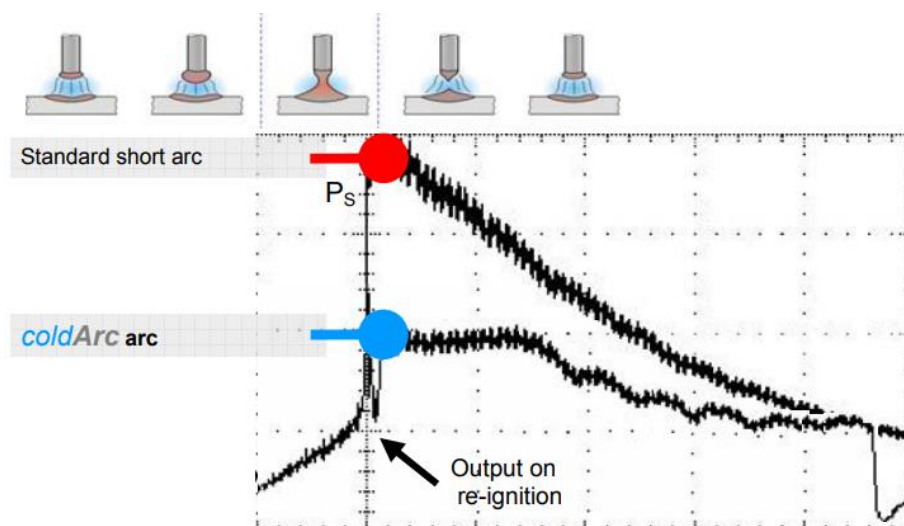


Figure 2.5 the Power comparison of standard and coldArc welding processes [19].

Figure 2.4 compares the welding current, I_s and voltage, U_s of the coldArc welding process and traditional short-arc-welding process. This figure shows that the first two phases are the same. However, the advantage of the coldArc process is shown in phase 3, at the moment of arc re-ignition and immediately afterwards. At the moment of arc re-ignition, it is apparent that the output is considerably lower (see Figure 2.5). Moreover, there is a reduction in the output shortly after the arc ignites which occurs in an exceptionally dynamic and controlled way. After the stabilization of the arc, there is a slight increase in the current for a defined short period, known as melt pulse, to create regular separations [18] as shown in Figure 2.6.

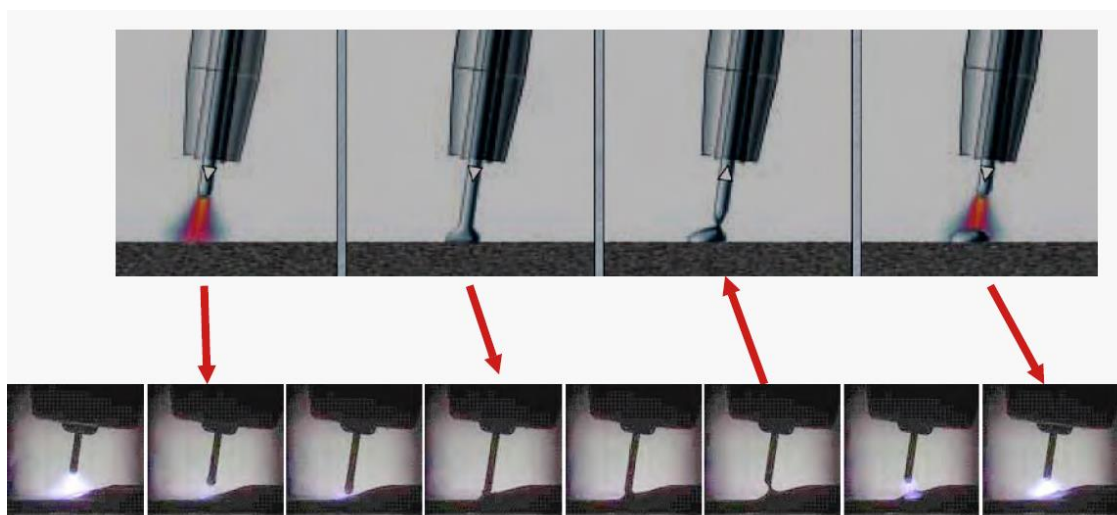


Figure 2.6 Sequence of the metal transfer and drop separation in the coldArc process [21].

A widespread occurrence in the inert metal gas (MIG) welding is the formation of spatter, which is essentially droplets of molten materials generated around or on the weld seam. The problem of having a spatter during welding is that it is a material waste and it requires more time and cost more money to clean it up. However, due to the power reduction during arc re-ignition, the use of the coldArc® welding process provides a spatter-free weld (see Figure 2.7).



Figure 2.7 Spatter-free welding achieved by using EWM coldArc welding technology.

2.2 Fatigue loading in welded joints

2.2.1 Uniaxial cyclic loading

2.2.1.1 Wöhler curve

Wöhler was one of the first researchers to investigate the fatigue phenomenon. He started by studying train axles and tried to understand the reason of axle failure under repeated loads which were lower than the static strength of the material [22- 23]. A few years later, L. Spangenberg [24] plotted the experimental data obtained from Wöhler's investigation on a linear scale, with stress range in the y-axis and the number of cycles to failure in the x-axis. In 1910 Basquin was the first researcher represented the fatigue results in a log-log diagram described by a simple formula (Eq.(2.1)), where Basquin gave some numerical values for C and n based on Wöhler's fatigue experimental data [25].

$$\sigma_a = CR^n \quad (2.1)$$

These diagrams, which are now known as Wöhler curves or S-N curves, were developed over the years and are still in use to predict the fatigue lifetime of welded structures, by using one of the well-known methods either the nominal stresses, hot-spot stresses or the effective notch stresses.

2.2 Fatigue loading in welded joints

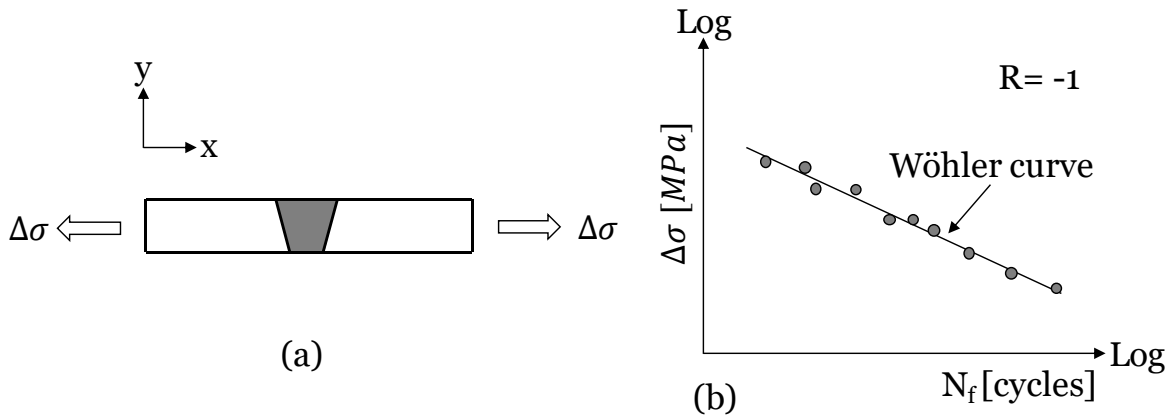


Figure 2.8 Plain specimens subjected to fatigue loading with a load ratio equal -1 (a) Wöhler diagram (b).

The Wöhler curve is a powerful tool that describes the relationship between the applied stress amplitude/range to the number of cycles to failure of the material. Figure 2.8a shows a conventional ground butt-welded specimen subjected to fully reversed cyclic loading ($R = \frac{\sigma_{\min}}{\sigma_{\max}} = -1$), meaning that during the test the mean stress is controlled and have a value of zero. By running a series of tests under the same load ratio of the same material and at different stress amplitudes, the Wöhler curve can be constructed in a log-log diagram as shown in Figure 2.8b. In a log-log chart, the Wöhler curve is a straight line, which can be described by using the well-known relationship also known as Wöhler equation (Eq.(2.2)):

$$\sigma_{x,a}^k \cdot N_f = \sigma_0^k \cdot N_0 = \text{constant} \quad (2.2)$$

Where k is the negative inverse slope. The Wöhler curves shown in Figure 2.9 describes the fatigue behaviour of metals. For ferrous metal (i.e. steel, see Figure 2.9a) tested under controlled condition, the fatigue behaviour exhibit a knee point which means that if the applied stress is lower than the stress amplitude at the knee point, the material will never fail and therefore the number of cycle to failure would be equal to infinity. The stress amplitude, σ_0 at which the material will never fail is known as the fatigue limit, however, this fatigue limit does not exist on real situations (Figure 2.9c), it only exists in labs under controlled conditions (Figure 2.9a) [26].

Figure 2.9b illustrates the fatigue behaviour of non-ferrous metals and a good example of non-ferrous metal is aluminium. It is clear from the graph that there is no knee point and the fatigue limit does not exist. In this case, to design non-ferrous metal subjected to fatigue loading it is essential to define an artificial fatigue limit known as the endurance limit, σ_A , extrapolated at

a given number of cycles to failure, N_A , which ranges from 10^6 to 10^8 cycles to failure. As long as aluminium is concerned, it is a common practice to define the endurance limit at $2 \cdot 10^6$ cycles to failure [26].

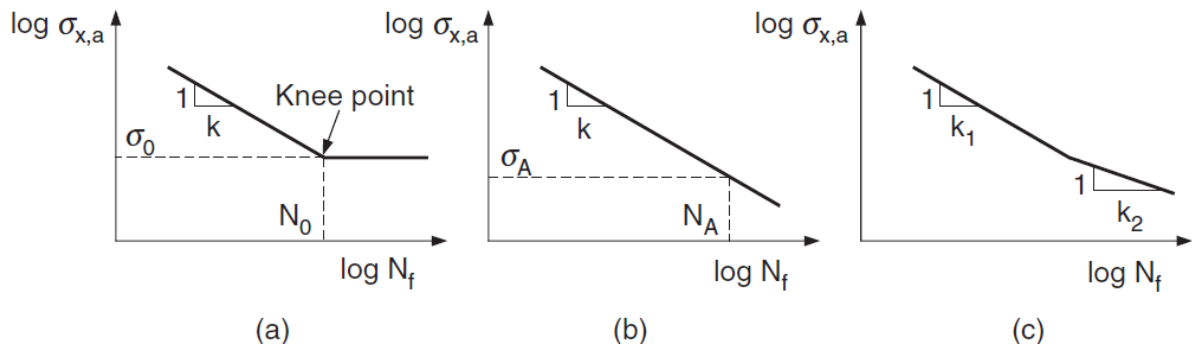


Figure 2.9 Fatigue behaviour of metals in the form of Wöhler curves including ferrous metal under control condition (a) non-ferrous metal (b) ferrous metal in real condition (c).

Figure 2.9c shows the typical S-N curve for ferrous metal in real conditions, where the material can have two different slopes. In the high cyclic fatigue regime, the material behaves differently, and the relationship between the applied stress and the cycles to failure tend to be steeper than the line describing the relationship in the medium cycle fatigue regime [23- 26].

2.2.1.2 Statistical determination of fatigue curves

As mentioned in Section 2.2.1.1, the fatigue curves are schematised as straight lines in log-log diagrams, and therefore described mathematically via the Wöhler-relationship (Eq.(2.2)). Fatigue curves are usually determined through a least square linear regression. This optimisation is performed under the hypothesis of a log-normal distribution of the cycles to failure at any stress level (Figure 2.10) [27]. Accordingly, for a given number of experimental results, the fatigue curve for a probability of survival, P_s , equal to 50% is determined by calibrating constants c_0 and c_1 in the following linear regression function:

$$\log(N_f) = c_0 + c_1 \cdot \log(\Delta\sigma) \quad (2.3)$$

Where, $\Delta\sigma$ is the independent variable and N_f is the dependent variable.

2.2 Fatigue loading in welded joints

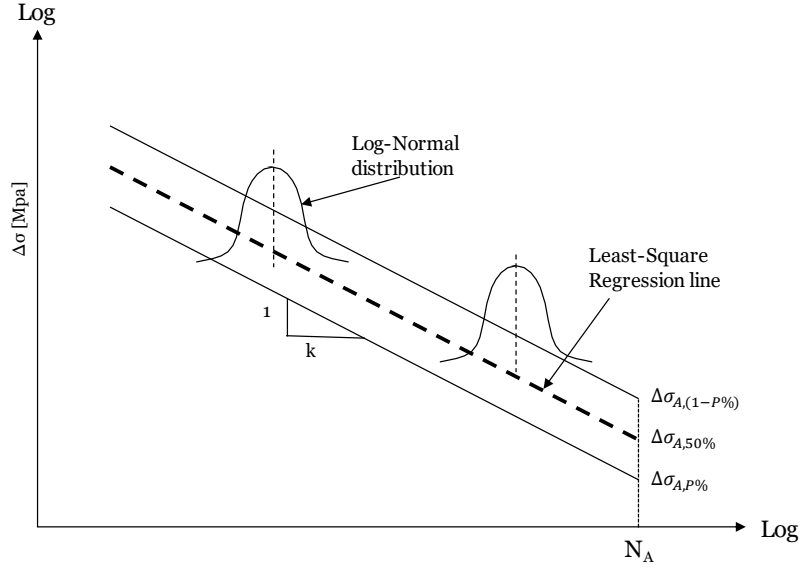


Figure 2.10 Wöhler diagram showing fatigue curves calculated for different probabilities of survival.

By assuming that the number of experimental results to be used to calibrate Eq. (2.3) is equal to n . Given the population of data, the i^{th} specimen (for $i=1, 2, \dots, n$) is assumed to be tested at a stress level equal to $\Delta\sigma_i$, the corresponding experimental number of cycles to failure being equal to $N_{f,i}$. Using the least square method, the values for constants c_0 and c_1 in Eq. (2.3) can then be calculated as [28]:

$$c_1 = \frac{\sum_{i=1}^n [\log(\Delta\sigma_i) - x_m] \cdot [\log(N_{f,i}) - y_m]}{\sum_{i=1}^n [\log(\Delta\sigma_i) - x_m]^2} \quad (2.4)$$

$$c_0 = y_m - c_1 \cdot x_m \quad (2.5)$$

Where,

$$x_m = \frac{\sum_{i=1}^n \log(\Delta\sigma_i)}{n} \quad (2.6)$$

$$y_m = \frac{\sum_{i=1}^n \log(N_{f,i})}{n} \quad (2.7)$$

As soon as constants c_0 and c_1 are known, both the negative inverse slope, k , and the endurance limit, $\Delta\sigma_{A,50\%}$, extrapolated for $P_S=50\%$ at N_A cycles to failure can directly be determined by simply rewriting Eq. (2.2) in the form of Eq. (2.3), so that:

$$k = -c_1 \quad (2.8)$$

$$\Delta\sigma_{A,50\%} = \left(\frac{10^{c_0}}{N_A} \right)^{\frac{1}{k}} \quad (2.9)$$

To determine the scatter band characterising the population of experimental data being post-processed, initially the associated standard deviation is calculated according to the following standard formula:

$$s = \sqrt{\frac{\sum_{i=1}^n \left\{ \log(N_{f,i}) - \log \left[\left(\frac{\Delta\sigma_{A,50\%}}{\Delta\sigma_i} \right)^k \right] \right\}^2}{n-1}} \quad (2.10)$$

Standard deviation s allows the endurance limit at N_A cycles to failure to be estimated directly for $P_s = P\%$ and $P_s = (1-P)\%$, respectively, i.e.:

$$\Delta\sigma_{A,P\%} = \Delta\sigma_{A,50\%} \left[\frac{N_A}{10^{\log(N_A) + q \cdot s}} \right]^{\frac{1}{k}} \quad (2.11)$$

$$\Delta\sigma_{A,(1-P)\%} = \Delta\sigma_{A,50\%} \left[\frac{N_A}{10^{\log(N_A) - q \cdot s}} \right]^{\frac{1}{k}} \quad (2.12)$$

In Eq. (2.11) and (2.12), q is a statistical index that depends on the adopted confidence level, the chosen probability of survival, and the number of tested samples [29].

Table 2.1 Index q for a confidence level equal to 0.95% [30].

n	q			
	$P_s=90\%$	$P_s=95\%$	$P_s=97.7\%$	$P_s=99\%$
3	6.158	7.655	9.445	10.552
4	4.163	5.145	6.317	7.042
5	3.407	4.202	5.152	5.741
6	3.006	3.707	4.544	5.062
7	2.755	3.399	4.167	4.641
8	2.582	3.188	3.907	4.353
9	2.454	3.031	3.719	4.143
10	2.355	2.911	3.573	3.981
15	2.068	2.566	3.155	3.52
20	1.926	2.396	2.951	3.295
25	1.838	2.292	2.828	3.158
30	1.778	2.22	2.742	3.064
35	1.732	2.166	2.678	2.994
40	1.697	2.126	2.630	2.941
45	1.669	2.092	2.589	2.897
50	1.646	2.065	2.559	2.863
55	1.626	2.042	2.531	2.833
60	1.609	2.022	2.507	2.807
65	1.594	2.005	2.487	2.785
70	1.581	1.990	2.471	2.765
75	1.570	1.976	2.453	2.748
80	1.559	1.964	2.439	2.733

2.2 Fatigue loading in welded joints

Table 2.1 lists, for different probabilities of survival, some values of index q determined, under the hypothesis of a log-normal distribution, by taking the confidence level equal to 95% [30].

In conclusion, it is worth highlighting that the curves determined for P_S equal to $P\%$ and $(1-P)\%$ have both negative inverse slope, k , equal to that of the Wöhler curve determined for $P_S=50\%$ (Eq. (2.8)). Finally, as soon as $\Delta\sigma_{A, (1-P)\%}$ and $\Delta\sigma_{A, P\%}$ are known for the population of fatigue data being post-processed, the associated T_σ ratio takes on the following value:

$$T_\sigma = \frac{\Delta\sigma_{A, (1-P)\%}}{\Delta\sigma_{A, P\%}} \quad (2.13)$$

2.2.1.3 Non-zero mean stress effects

The effect of the non-zero mean stress is a well-known factor that influences the fatigue strength of the engineering materials. In particular, under uniaxial cyclic loading, the fatigue damage is seen to increase as the applied superimposed static stress, $\sigma_{x,m}$ increased, as shown in Figure 2.11a. Likewise, by decreasing the load ratio, R , the fatigue curves are shifted upwards in the Wöhler diagrams (Figure 2.11b), resulting in the reduction of the material fatigue/endurance limit.

Independent of the definition being adopted to determine the required design stresses, much experimental evidence suggested that as far as-welded connections are concerned; the presence of superimposed static stresses plays a minor role in the overall fatigue strength of welded joints [31]. This is a consequence of the fact that the residual stresses arising from the welding process alter the actual value of the load ratio in the vicinity of the crack initiation locations. Therefore, in the presence of high tensile residual stresses, the local value of R is seen to be different from the nominal load ratio characterising the load history under investigation, with the local R ratio becoming larger than zero also under fully reversed nominal fatigue loading. Accordingly, connections in the as-welded condition are usually assessed via reference design curves that are determined experimentally under $R>0$. Whilst the above simplification is seen to result in reasonable fatigue life predictions for steel welded joints, unfortunately, it does not always return satisfactory results with aluminium weldments. This is because nominal load ratios lower than zero can affect the fatigue behaviour not only of stress relieved, but also of as-welded aluminium joints [32].

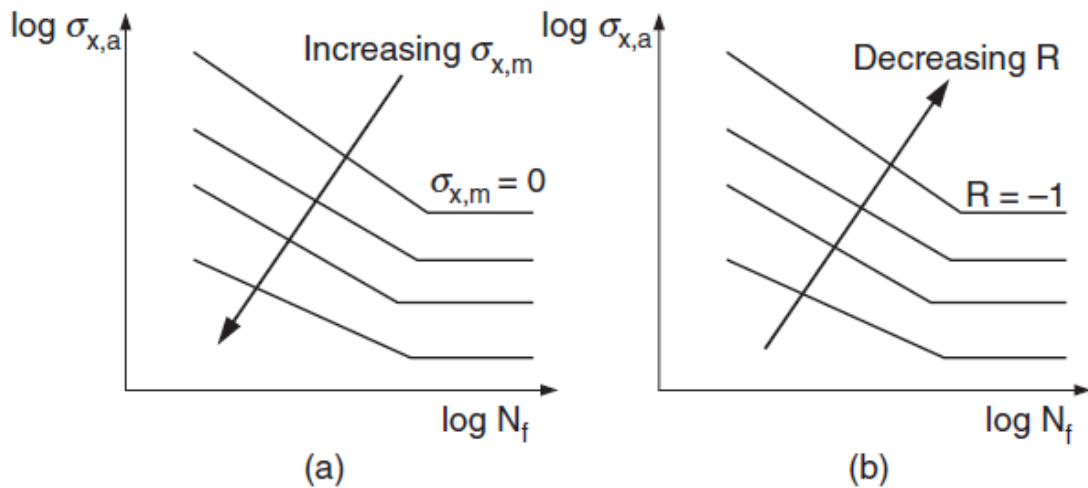


Figure 2.11 The effect of non-zero mean stress and load ratio on the Wöhler diagrams [24].

Accordingly, under nominal load ratios lower than zero, fatigue assessment performed by following the recommendations of the available standard can lead to an excessive level of conservatism. The effect of residual stresses can be mitigated by relieving the material in the weld regions via appropriate technological processes. However, by so doing, aluminium weldments' fatigue strength is seen to increase, with the role played by non-zero mean stresses becoming more and more important as load ratio R decreases [31].

Both EC9 and the IIW suggest using specific enhancement factors in order to take into account the effect of the load ratio characterising the load history being assessed. Enhancement factor $f(R)$ is defined as the ratio between the actual value of the endurance limit at $2 \cdot 10^6$ cycles to failure and the corresponding design endurance limit recommended as being used for the design of the specific welded geometry. In other words, from a fatigue assessment point of view, under $R < 0.5$ the fatigue strength of the specific welded detail being designed can be increased by multiplying the corresponding fatigue class by $f(R)$. Both EC9 [33] and the IIW [34] considers the following three scenarios:

- Case I. Un-welded base material and wrought products with negligible residual stresses; stress relieved welded components, in which the effects of constraints or secondary stresses have been considered in analysis; no constraints in assembly:

$$\begin{aligned}
 f(R) &= 1.6 && \text{for } R < -1 \\
 f(R) &= -0.4 \cdot R + 1.2 && \text{for } -1 \leq R \leq 0.5 \\
 f(R) &= 1 && \text{for } R > 0.5
 \end{aligned} \tag{2.14}$$

2.2 Fatigue loading in welded joints

- Case II. Small scale thin-walled simple structural elements containing short welds; parts or components containing thermally cut edges; no constraints in assembly:

$$\begin{aligned} f(R) &= 1.3 && \text{for } R < -1 \\ f(R) &= -0.4 \cdot R + 0.9 && \text{for } -1 \leq R \leq -0.25 \\ f(R) &= 1 && \text{for } R > -0.25 \end{aligned} \quad (2.15)$$

- Case III. Complex two- or three-dimensional welded components; components with global residual stresses; thick-walled components; normal case for welded components and structures:

$$f(R) = 1.3 \quad (2.16)$$

2.2.2 Fatigue assessment methods

2.2.2.1 *The nominal stress approach*

The nominal stress-based approach is one of the most widely used methods that is employed in situations of practical interest to perform the fatigue assessment of welded components. This approach postulates that the required design stresses have to be calculated according to classic continuum mechanics by directly referring to the nominal cross-sectional area. The fatigue curves to be used in conjunction with the nominal stress approach take into account the stress gradient resulting from those macro-geometrical features characterising the welds zones [34-36]. In contrast, nominal stresses are determined without taking into account those localised stress raising phenomena due to the presence of the weld toe as these phenomena are already included in the reference fatigue design curves being provided by the available design codes (such as EC9 and the IIW). Consequently, the selection of an appropriate design curve is essential to ensure that accurate fatigue design is achieved [34-36]. Examples of fatigue design curves suggested by the IIW are shown in Table 2.2.

Table 2.2 FAT for different welded geometries [34].

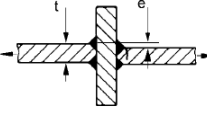
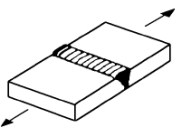
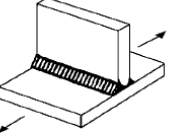
Structural detail	Description	Requirements	FAT St	FAT Al
	Cruciform joint or T-joint, full penetration.		80	32
	Single sided T-joints and cruciform joints without misalignment.	Misalignment < 15% of primary plate	90	32
	Transverse butt welds welded from one side without backing bar, full penetration	Root controlled by NDT	71	28
	Transverse non-load carrying attachment, not thicker than main plate K-butt weld, toe ground	Grinding parallel to stress	100	36

Figure 2.12 shows the nominal sections for different welded configurations. In simple structures, the nominal design stresses, where the component is under tension, are calculated using the simple beam theory, see Eq.(2.17) [34],

$$\sigma_{nom} = F/A \tag{2.17}$$

Where σ_{nom} is the nominal stress, F is the applied force, and A is the cross-sectional area. In contrast, the FE code may be used to calculate the nominal stresses for complicated statically overdetermined structures.

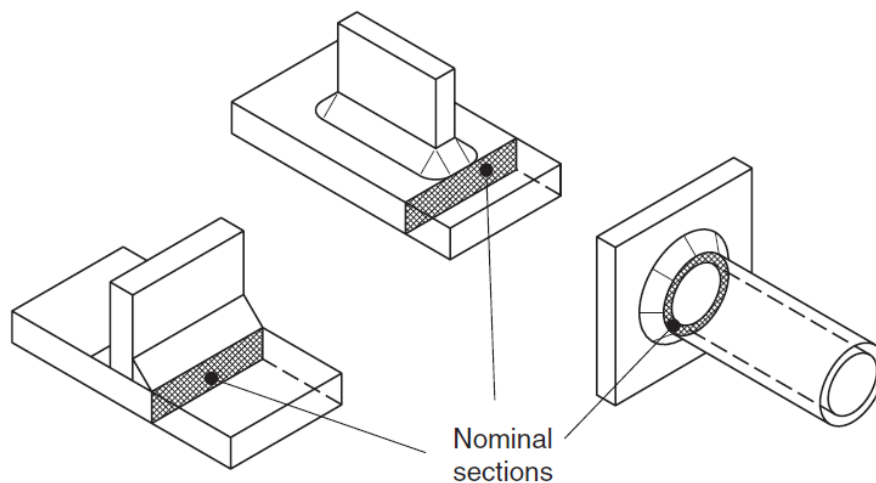


Figure 2.12 Nominal sections in welded details [26].

2.2 Fatigue loading in welded joints

Another important aspect to consider while using the nominal stress approach is the misalignment of the welded joints. It reduces the fatigue strength of the joints. The fatigue resistance S-N curves for the specific structural detail already covers the misalignment of the welded joints (see Figure 2.13). However, secondary bending stresses that formed from the axial or angular misalignment should be considered if the misalignment exceeds the amount that is already covered in the S-N curves, and therefore an additional stress-raising factor, $K_{m,eff}$, should be introduced.

$$K_{m,eff} = \frac{K_m \text{ calculated}}{K_m \text{ already covered}} \quad (2.18)$$

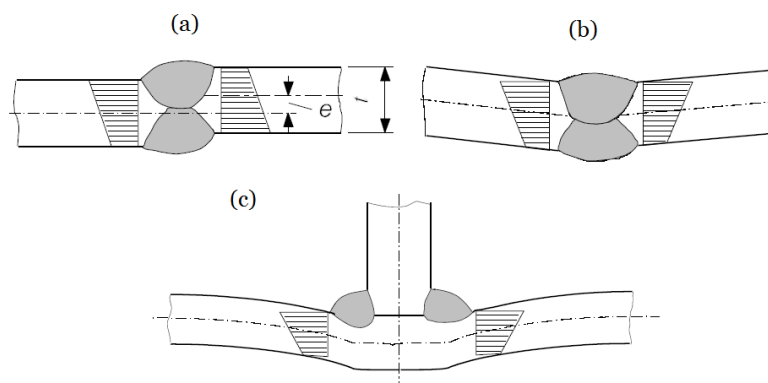


Figure 2.13 Examples of axial misalignment (a) and angular misalignment (b), (c) [34].

To conclude, although the nominal stress approach is the easiest and widely used approach in practice, the details of the designed components should be similar to the corresponding details found in the design codes and guidelines. Nevertheless, the use of the appropriate S-N curves results in a reasonably accurate fatigue lifetime estimation of the designed components.

The limitation of this approach is that, due to complexities and irregularities of the designed welded components, either the nominal stresses cannot be calculated unambiguously or a reference fatigue curve for the specific geometry of the welded component is not available. Hence, this approach is not directly applicable, and another stress-based approach is needed to assess such complex geometries. Unless the specific design curve being needed is generated by running appropriate experiments.

2.2.2.2 The hot-spot stress approach

The hot-spot stress approach also known as the structural stress approach have traditionally employed to assess the fatigue strength of tubular welded joints in offshore structures. This approach has been extended to estimate successively the fatigue lifetime of various welded joints in different structural applications. It was introduced to allow the evaluation of the fatigue strength when either the nominal stresses cannot be calculated unambiguously or a reference fatigue curve for the specific geometry of the welded detail being assessed is not available [32, 37-39].

The main advantage of the hot-spot stress approach is that it considers the stress raising effect in the vicinity of the weld toe, except the non-linear effect, which has been considered indirectly in the reference design curve suggested by the standard design codes and guidelines. Another advantage of this approach is that the number of S-N curves required to assess the fatigue lifetime of the welded components is reduced to a single S-N curve for each welded configurations as shown in Figure 2.14 [32, 34, 37-39].







Nominal Stress Approach					Hot spot stress approach		
No	Butt Welds	Description	FAT St.	FAT Al.	Butt Welds	FAT St.	FAT Al.
211			112	45		100	40
212		Weld reinforcement <0.1 thickness	90	36			
213		Al. Butt weld with toe angle $\leq 50^\circ$ Butt weld with toe angle $> 50^\circ$	80	32 25			
214			80	28			
216		Root controlled by inspection procedure (NDT)	71	28			
		No NDT	36	12			

Figure 2.14 Fatigue class recommendation (FAT) based on the nominal stress and hot-spot stress approaches according to the IIW [34].

2.2 Fatigue loading in welded joints

The hypothesis of this approach is to neglect the non-linear notch effect at the weld toe and model the welded joints by determining the linear-elastic stress states at two or three reference points at a distance away from the weld toe in the direction of the applied stress. Subsequently, the hot-spot stress can be calculated as shown in Figure 2.15. This approach is limited to the fatigue assessment of the weld toe, and it not applicable to assess the fatigue behaviour of welded structures where the crack initiated at the weld root and propagate through the weld metal [31, 32, 40].

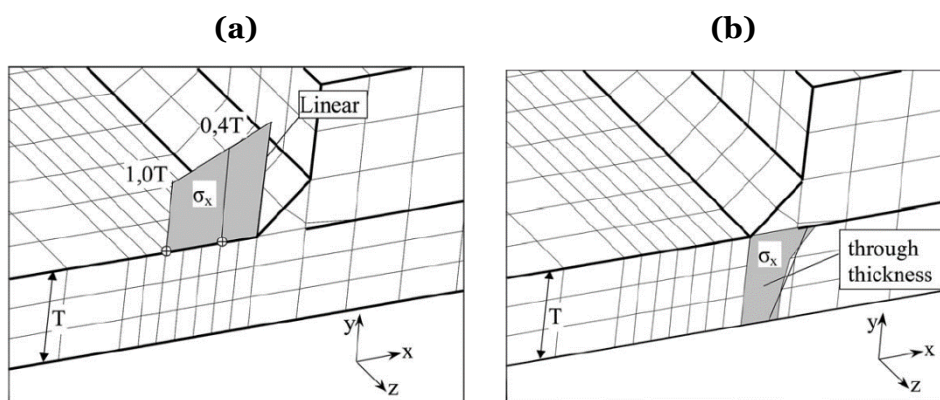


Figure 2.15 Example of the linear surface stress extrapolation (a) and through thickness stress linearization procedure (b) [43].

There are two ways to calculate the hot-spot stresses either experimentally by using strain gauges at reference distances away from the weld toe or by solving a linear-elastic finite element (FE) models. The hot-spot stresses, using the FE models, can be estimated using either the surface stress extrapolation or through-thickness stress linearization [31, 34] (see section 2.2.2.2.1 and 2.2.2.2.2 below). Another interesting method is the one suggested by Dong [41-42] (Figure 2.16), which is based on linearized equilibrium stresses from normal and shear stresses in a distance from the weld toe where the stress singularity effect has vanished.

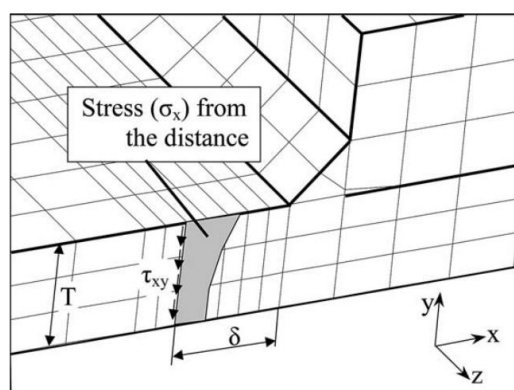


Figure 2.16 Hot spot stress determination according to Dong method [43].

2.2.2.2.1 Surface stress extrapolation

The linear surface stress extrapolation involves the determination of the linear elastic stresses at two or three superficial points away from the vicinity of the weld toe. These superficial points are defined with respect to the thickness of the plate (t) (see Eq. (2.19) to (2.21)). This is the most widely used method to determine the hot-spot stresses from the FE models. There are two types of hot-spots have to be distinguished according to their location on the plate and their orientation to the weld toe as shown in Figure 2.17. Table 2.3 describes the definitions of type a and type b hot spots.

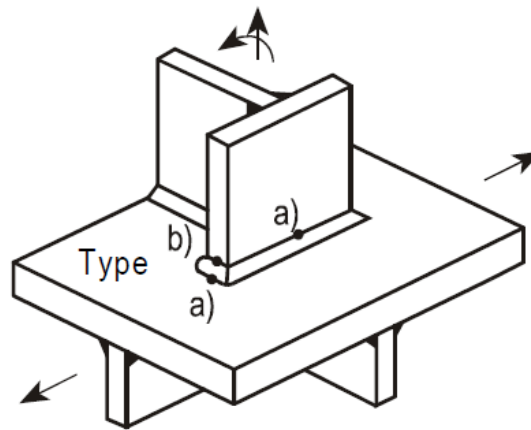


Figure 2.17 Type "a" and "b" hot spots [34].

Table 2.3 Definition of the types of hot spots.

Type	Description
a	The stress transfers to the weld toe on the surface of the plate
b	The stress transfers to the weld toe on the edge of the plate

As long as type "a" hot spot is concerned, the linear elastic stresses (Figure 2.17), for fine mesh with element length not more than $0.4t$, can be evaluated at two reference points $0.4t$ and $1t$. Then the hot-spot stresses are calculated using Equation (2.19). In contrast, for coarse meshes, $0.5t$ and $1.5t$ extrapolation points from the weld toe can be used. Then Eq. (2.20) is used to calculate the corresponding hot-spot stresses. In situations where the stress gradient is steeper, the quadratic extrapolation at three reference points $0.4t$, $0.9t$ and $1.4t$ may be used and Eq. (2.21) is therefore applied to find the hot-spot stresses σ_{HS} .

2.2 Fatigue loading in welded joints

$$\sigma_{\text{Hs}} = 1.67\sigma_{0.4t} - 0.67\sigma_{1t} \quad (2.19)$$

$$\sigma_{\text{Hs}} = 1.5\sigma_{0.5t} - 0.5\sigma_{1.5t} \quad (2.20)$$

$$\sigma_{\text{Hs}} = 2.52\sigma_{0.4t} - 2.24\sigma_{0.9t} + 0.72\sigma_{1.4t} \quad (2.21)$$

For type “b” hot spot (Figure 2.17), the stress distribution in the vicinity of the weld toe is not dependent on the plate thickness. Consequently, the reference points are given at absolute distance from the weld toe. For a fine mesh with element length less than or equal to 4 mm at the hot-spot, the linear elastic stresses are evaluated at three reference points 4 mm, 8 mm and 12 mm, and the structural stresses are calculated using Eq. (2.22). However, for coarse mesh with element length equal to 10 mm, the linear elastic stresses are calculated at two reference points 5 mm and 15 mm from the weld toe then the structural stress is calculated using Eq. (2.23).

$$\sigma_{\text{Hs}} = 3\sigma_{4\text{mm}} - 3\sigma_{8\text{mm}} + \sigma_{12\text{mm}} \quad (2.22)$$

$$\sigma_{\text{Hs}} = 1.5\sigma_{5\text{mm}} - 0.5\sigma_{15\text{mm}} \quad (2.23)$$

2.2.2.2.2 Through thickness stress linearization

The second technique to calculate the hot-spot stress is the through thickness stress linearization procedure. Here, the hot-spot stress is calculated directly from the stresses in the cross-sectional thickness of the plate at the weld toe as shown in Figure 2.15b. The linear stress can be expressed by integrating the non-linear distribution and then creating a linear distribution, which produces the same membrane and bending force components [43].

2.2.2.2.3 Conclusion

To conclude, the hot-spot stress approach has successively evaluated the stress raising effect in the vicinity of the weld toe and estimates the fatigue behaviour of the complex welded components reasonably accurate. The main drawback of this approach is the sensitivity to the mesh density. Another drawback of this approach is that it is restricted to the fatigue lifetime estimation where the crack initiated at weld toe. In other word, this approach is not applicable where the crack initiates at the weld root.

2.2.2.3 The effective notch stress approach

The effective notch stress approach is the most advanced fatigue design method recommended by the IIW [34]. This method assumes that fatigue strength can be estimated by using linear-elastic notch stresses determined by adding a fictitious notch radius to the actual radius of the weld toes or the weld roots [44]. The weld imperfection critically affects the accuracy of determining the actual radius of the welded component. Consequently, the actual radius is assumed to have a zero value, to take into account the worst-case scenario. Neuber suggested the following formula for the fictitious radius ρ_f :

$$\rho_f = \rho + s \cdot \rho^* \quad (2.24)$$

Where ρ the actual notch radius, s is the factor for stress multiaxiality and strength criterion and ρ^* is the substituted micro-structural length. The fictitious radius is derived from the integration of the stress distribution in the real notch as shown in Figure 2.18. By taking advantage of the micro-support theory proposed by Neuber to model sharp cracks, Radaj [45] has proposed a fictitious weld toe/root notch radius of 1 mm for thickness greater than or equal to 5 mm. The reference radius of 1 mm proposed by Radaj is based on the fictitious radius $\rho_f = 1\text{mm}$ derived from Equation (2.24). For the worst-case scenario, the actual notch radius ρ is assumed to have a value of 0 mm, and the factor s is assumed to be 2.5 for plane strain conditions at the roots of sharp notches. The value of the substitute micro-structural length ρ^* depends on the type of the material, by considering typical welds in low strength steel and $\rho^* = 0.4$ was chosen [46].

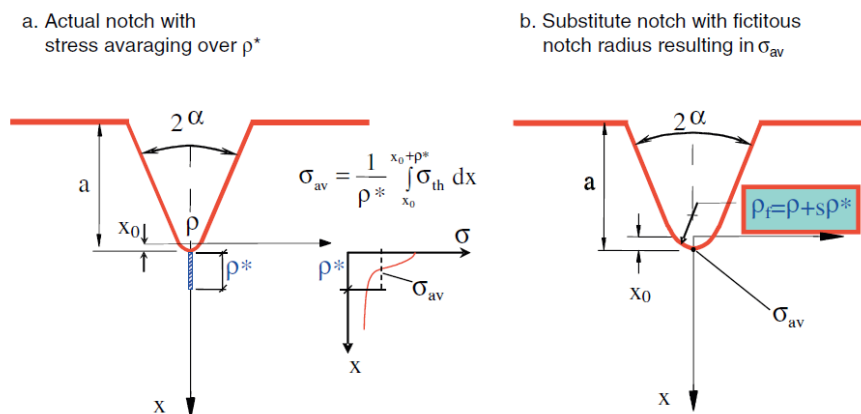


Figure 2.18 Neuber's micro-support theory [45].

In contrast, for thin-walled structures with a thickness less than 5 mm, mainly applied in the automotive industry, the fictitious notch radius of 0.05 mm is recommended as being employed [32, 47]. The background of the reference radius $r_f=0.05$ mm is based on the relationship between the stress intensity factor and the notch stresses. It is a compromise

2.2 Fatigue loading in welded joints

between the FE modelling and the calculation of reasonable local stress components at a given stress intensity (Figure 2.19). Zhang and Richter [48] introduced the use of a fictitious radius $r_f=0.05$ mm at the tip of the spot weld based on the relationship mentioned above.

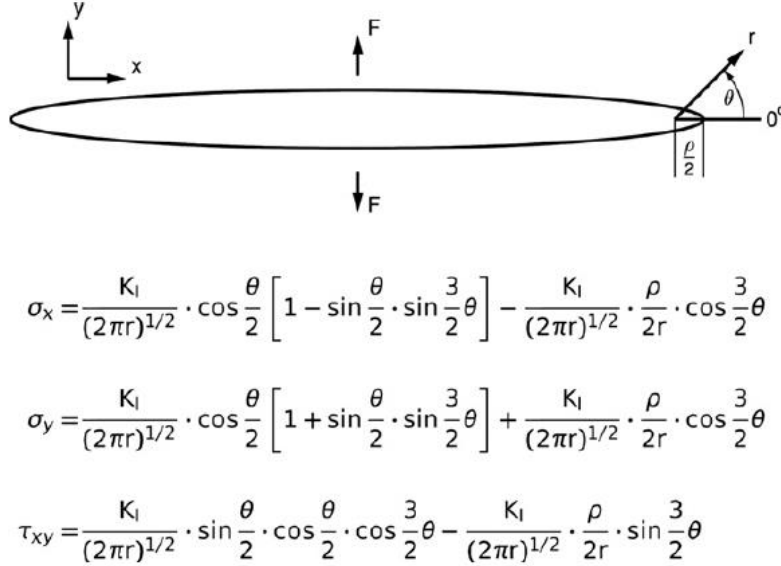


Figure 2.19 Notch stress and stress intensity [45].

To perform a fatigue assessment for welded joints with a thickness larger than 5mm, the IIW [34] suggests two master reference curves for steel and aluminium welded joints extrapolated at two million cycles to failure and calculated for a probability of survival equal to 97.7%. These design curves for steel and aluminium are characterised by a negative inverse slope, k , equal to 3 and a notch stress endurance limit range $\Delta\sigma_{A,97.7\%}$, equal to 225 MPa and 71 MPa respectively. On the other hand, to design thin welded joints against fatigue ($t<5$ mm), Sonsino [49] suggested a reference design curve for steel and aluminium having a negative inverse slope equal to 3 and a notch stress endurance limit range $\Delta\sigma_{A,97.7\%}$, equal to 630 MPa and 180 MPa, respectively, extrapolated at two million cycles to failure for probability of survival equal 97.7%. These values are based on the principal stress hypothesis. Table 2.4 summarises the different FAT values for steel and aluminium using the principal stress and the von Mises stress hypotheses suggested by the IIW and Sonsino.

Table 2.4 FAT normal stresses according to the IIW for the effective notch stress approach [49].

r_f in mm	1.00	1.00	0.05	0.05
Hypothesis	Principal stress	Von Mises	Principal stress	Von Mises
Steel	225	200	630	560
Aluminium	71	63	180	160

*All given allowable stress range are in MPa, for $N=2 \times 10^6$; $R=0.5$; $P_s=97.7\%$; $k=3$

A number of researchers have investigated the applicability and the accuracy of the effective notch stress approach. C. Morgenstern et al. [39] D. Radaj [50], Z. Barsoum et al. [51], investigated the applicability of the effective notch stress approaches using various configurations of steel and aluminium welded joints. The results obtained from these investigations proved the applicability and the high accuracy of this approach and results in a good agreement with designed S-N curves proposed by the IIW.

2.2.2.4 The Notch Stress Intensity Factors (N-SIFs) approach

Verreman and Nie first proposed the N-SIFs approach back in the mid-1990s, [52], which is based on William's equations. Figure 2.20 shows the definition of the polar coordinate (local coordinate) and a cruciform welded joint subjected to uniaxial loading where the toe radius is assumed to be zero.

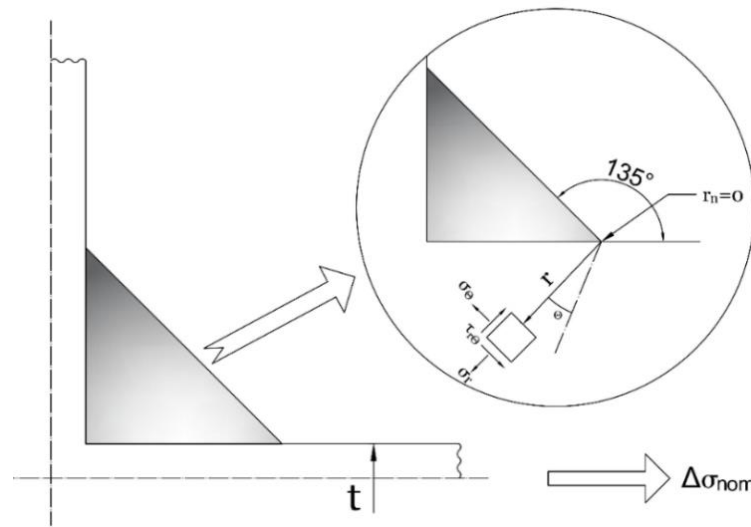


Figure 2.20 Definition of the local coordinates (Polar coordinates).

According to the definition of the polar coordinate in Figure 2.20, under uniaxial fatigue loading the linear elastic stress field in the vicinity of the V-notches subjected to the opening and sliding loading modes (Mode I and Mode II see Figure 2.21) can be described efficiently through the equations below [53- 55]:

$$\begin{Bmatrix} \sigma_{\theta} \\ \sigma_r \\ \tau_{r\theta} \end{Bmatrix}_{\rho=0} = \frac{1}{\sqrt{2\pi}} \frac{r^{\lambda_1-1} K_{I}}{(1+\lambda_1)+\chi_1(1-\lambda_1)} \begin{Bmatrix} (1+\lambda_1)\cos(1-\lambda_1)\theta \\ (3-\lambda_1)\cos(1-\lambda_1)\theta \\ (1-\lambda_1)\sin(1-\lambda_1)\theta \end{Bmatrix} + \chi_1 \begin{Bmatrix} \cos(1+\lambda_1)\theta \\ -\cos(1+\lambda_1)\theta \\ \sin(1+\lambda_1)\theta \end{Bmatrix} \quad (2.25)$$

$$\begin{Bmatrix} \sigma_{\theta} \\ \sigma_r \\ \tau_{r\theta} \end{Bmatrix}_{\rho=0} = \frac{1}{\sqrt{2\pi}} \frac{r^{\lambda_2-1} K_{II}}{(1+\lambda_2)+\chi_2(1-\lambda_2)} \begin{Bmatrix} -(1+\lambda_2)\sin(1-\lambda_2)\theta \\ -(3-\lambda_2)\sin(1-\lambda_2)\theta \\ (1-\lambda_2)\cos(1-\lambda_2)\theta \end{Bmatrix} + \chi_2 \begin{Bmatrix} -\sin(1+\lambda_2)\theta \\ \sin(1+\lambda_2)\theta \\ \cos(1+\lambda_2)\theta \end{Bmatrix} \quad (2.26)$$

2.2 Fatigue loading in welded joints

Where λ_i and χ_i are parameters depending on the opening angle of the V-notch. Values for different opening angles are shown in Table 2.5. K_I and K_{II} are N-SIFs associated with the opening and sliding loading modes and based on the stress field components, the N-SIFs can be written as follows:

$$K_I = \sqrt{2\pi} \lim_{r \rightarrow 0} (\sigma_\theta)_{\theta=0} r^{1-\lambda_1} \quad (2.27)$$

$$K_{II} = \sqrt{2\pi} \lim_{r \rightarrow 0} (\sigma_\theta)_{\theta=0} r^{1-\lambda_2} \quad (2.28)$$

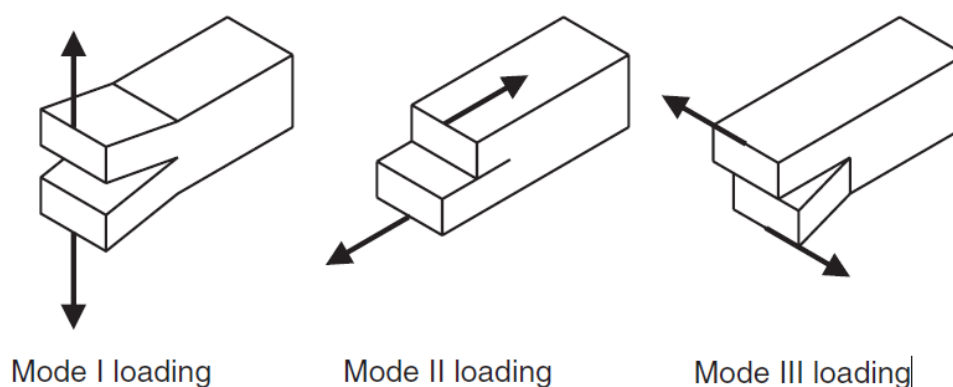


Figure 2.21 Definition of the loading modes [26].

Verreman and Nie [52], have observed the stress intensity factor of singular stress states at the V-notch of the welded components and suggested that these stress parameters can be applied directly to investigate and rationalize the initiation of the crack occurs on welded components, subjected to fatigue loading, with a crack propagation between 0-0.5mm.

Table 2.5 Notch opening angles and their corresponding constants and exponents.

Opening angle (°)	q	r_0/ρ	Mode I			Mode II		
			λ_1	χ_1	μ_1	λ_2	χ_2	μ_2
0	2.00	0.50	0.50	1.00	-0.50	0.50	1.00	-0.50
30	1.83	0.46	0.50	1.07	-0.42	0.60	0.92	-0.26
45	1.75	0.43	0.51	1.17	-0.39	0.66	0.81	-0.15
60	1.67	0.40	0.51	1.31	-0.35	0.73	0.66	-0.03
90	1.50	0.33	0.54	1.84	-0.28	0.91	0.22	0.19
135	1.25	0.20	0.67	4.15	-0.15	1.30	-0.57	0.55

A couple of years later, Lazzarin and Tovo [56] developed this approach even further, by determining the contribution of the opening and sliding loading modes (Mode I and Mode II). In particular, they observed that in fillet welded joints under axial loading the contribution due

to Mode II stress components can be neglected with a little loss of accuracy [56]. This is because, as the opening angle of the notch is greater than 100° , Mode II stresses are no longer singular.

To validate the applicability of this approach, Lazzarin and Tovo applied this approach using many experimental steel data made by Maddox and Gurney for transverse non-load-carrying fillet welds. The original S-N curve was largely scattered, due to the large variations of the main plate thickness, weld and attachment sizes. The scatter band for the same data was greatly reduced when using the N-SIFs approach in particular for $N_f \geq 10^6$ cycle [56].

Then, Tovo and Lazzarin [57] compared and investigated the relationship between the N-SIFs approach and the hot-spot stress approach. They demonstrated that for some cases, the hot-spot stress approach was not able to estimate accurately the fatigue behaviour of the welded joints, as the structural stresses were not sufficient for evaluating the local stress field. On the other hand, the combination of the structural stress field and the N-SIFs based field was more precise in evaluating the local stresses and it increased the accuracy in estimating the fatigue behaviour of the welded joints [57].

A couple of years later, Lazzarin and Livieri [58] extended this approach to explore the fatigue behaviour of aluminium alloys welded joints considering Tee and cruciform non-load and load carrying fillet welded joints. The aluminium-welded joints were characterised by a thickness ranging between 3 and 24 mm to investigate the scale effect. They proved that the theoretical exponent value quantifying the scale effect of 0.25 proposed by Eurocode is not conservative and by statistically re-analysing the fatigue data, a value of 0.3 seems to be more realistic for both aluminium and steel welded joints [58].

Specific design curves were derived by reanalysing a large number of experimental data with various welded joints configurations and various thicknesses. The master curves for steel and aluminium suggested by Lazzarin and Livieri [58] are presented in Figure 2.22. The master curves are characterised by Mode I N-SIF ranges $\Delta K_I = 155 \text{ MPa mm}^{0.326}$ and $\Delta K_I = 74 \text{ MPa mm}^{0.326}$ with a negative inverse slope of 3 and 4 calculated at $P_s = 97.7\%$ at five million cycles to failure for steel and aluminium respectively.

2.2 Fatigue loading in welded joints

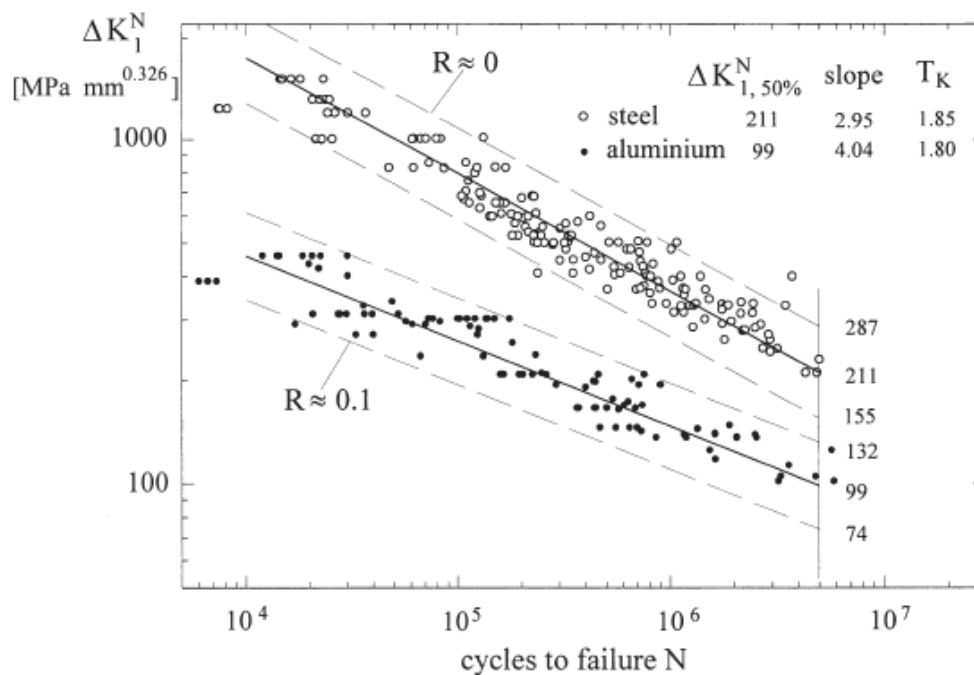


Figure 2.22 Fatigue strength of steel and aluminium welded joints based on the N-SIF approach [58].

B. Atzori et al. [59] demonstrated that the N-SIFs approach could be directly applied in conjunction with the well-established fracture mechanics approach to evaluate the stress intensity factor of a crack that is propagating from the weld toe as soon as the entire stress field of the un-cracked geometry is known. The results obtained by the local stress analysis showed a good agreement with the published data that was based on the fracture mechanics when a virtual crack length of 0.3mm was introduced at the weld toe.

To conclude, the N-SIFs approach proved that the linear elastic stress quantities in the vicinity of the weld toe could be used successively to predict the fatigue behaviour of welded joints and seen to be highly accurate in considering the scale effect in the welded joints.

2.2.2.5 The Theory of Critical Distance (TCD)

The Theory of Critical Distances (TCDs) was first proposed by Neuber [60] at the mid of the last century. Neuber believed that the continuum mechanics theorem used to predict the elastic stresses in situations of a high-stress gradient (cracks or notches.) is not valid and the results obtained are over conservative [61-62]. Accordingly, he suggested that to calculate the effective stress damaging the material at the fatigue process zone, the linear elastic stresses closer to the stress concentrator apex must be averaged over a certain length equal to the crystal or structural particles length, which now known as the Line Method (LM). A few years later, Peterson [63] simplified the approach proposed by Neuber [60] by suggesting that the effective

stress damaging the material can be directly calculated at a given distance from the notch apex, this method is now referred to as the Point Method (PM) [62].

In 1974, Whitney and Nuismer [64] were investigating the monotonic failure of fibre composite materials. They obtained their experimental data by testing many laminated composite samples with different hole diameters and crack lengths. Whitney and Nuismer were not aware of the prior work done by Neuber and Peterson and they developed two methods, which are identical to the LM and PM. Furthermore, they proved that there is a direct link between the Mode I fracture toughness and the ultimate tensile strength of the laminate composites and therefore the critical lengths a_0 and d_0 , related to their methods, are considered as material properties.

In 1983, Tanaka [65] established a theoretical relationship between the fatigue limit and the threshold stress intensity factor, which can be used to calculate the critical length. However, Tanaka has not compared his theoretical finding with experimental data to validate his method. Surprisingly, Tanaka work was largely ignored, and the same relationship was rediscovered by Taylor [66- 68] by assuming that the stress intensity range will be equal to the threshold when the stress range is equal to the fatigue limit, so the critical length can be determined as follow:

$$L = \frac{1}{\pi} \cdot \left(\frac{\Delta K_{th}}{\Delta \sigma_0} \right)^2 \quad (2.29)$$

Where, ΔK_{th} is the threshold stress intensity range, and $\Delta \sigma_0$ is the endurance fatigue limit of the un-notched sample.

Later in the 1990s and early 2000s, Taylor [66- 67] has introduced two different forms of the TCD, which are called the Area Method (AM), and the Volume Method (VM). The Area method is based on the assumption that the effective stresses damaging the material can be calculated by averaging the linear stresses within a semi-circular area in the vicinity of the notch/ crack apex with a radius equal to the critical distance [66]. Similarly, the Volume Method estimate the effective stress damaging the material by averaging the linear stresses within a specific volume in the vicinity of the notch/ crack tip [61]. For 2D FE analysis, the VM and AM are exactly the same [66]. In 2002, Taylor [68] extended the use of the TCD to estimate the fatigue strength of welded joints by treating the welds as notches.

Figure 2.23 shows the different formalisation of the TCD according to PM and LM to estimate the fatigue strength of welded components. To apply the TCD to estimate the fatigue lifetime of welded structural components, the materials properties mentioned in Eq. (2.29) must be known for specific loading case (i.e. load ratio, R). The required properties can be obtained by

2.2 Fatigue loading in welded joints

running an appropriate experimental investigation. However, Susmel [26] has recorded materials parameters for many commonly used materials.

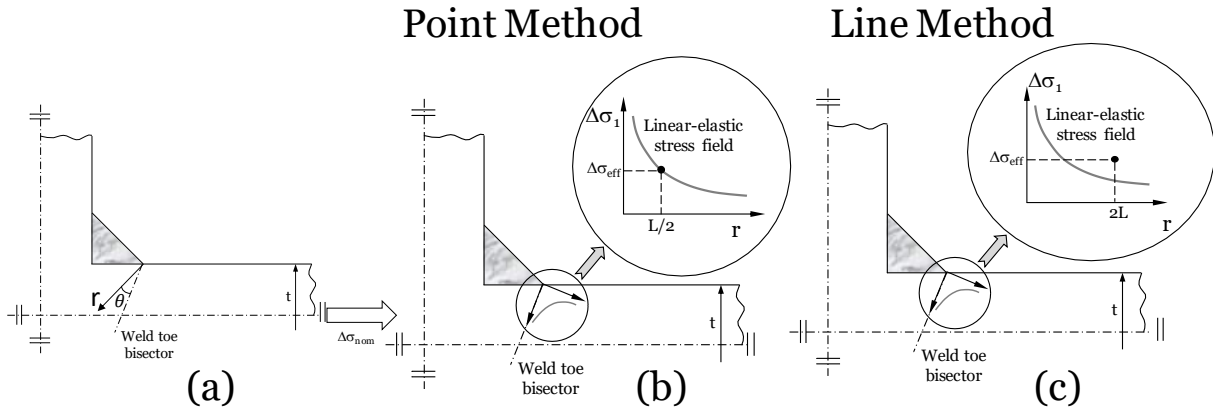


Figure 2.23 Definition of the local coordinate system (a), the formalisation of the TCD in form of Point Method (b) and Line Method (c).

The TCD assumed that the fatigue damaged caused by the presence of stress concentrator can be estimated by using the stress quantity that represents the entire linear elastic stress field damaging the fatigue process zone. Furthermore, the structural components containing stress concentrator are assumed to be in their fatigue limit condition when the effective stress, $\Delta\sigma_{eff}$ is equal to the material plain fatigue limit, $\Delta\sigma_0$ so that:

$$\Delta\sigma_{eff} = \Delta\sigma_0 \quad (2.30)$$

The effective stress, $\Delta\sigma_{eff}$, can be calculated by using one of the TCD approaches, where the focus path is taken at the notch/weld toe tip (i.e. θ is equal zero, Figure 2.23a). By using the Point Method, the failure of the component will occur when the stress at a distance ($L/2$) from the weld tip is equal to $\Delta\sigma_0$. Accordingly, the effective stress $\Delta\sigma_{eff}$ can be calculated using Eq.(2.31).

$$\Delta\sigma(L/2) = \Delta\sigma_0 \quad (2.31)$$

The Line Method uses a similar strategy as the Point Method, and the effective stress is taken as the average stresses along the bisector from the notch to a certain distance equal to $2L$. Thus, the LM criterion can be written as:

$$\frac{1}{2L} \int_0^{2L} \Delta\sigma(r) dr = \Delta\sigma_0 \quad (2.32)$$

The applicability and reliability of the Theory of Critical Distances approaches have been investigated by many researchers, where the TCD was seen to predict the fatigue life of metals with a high level of accuracy [69- 75]. Taylor and Wang [67] reanalysed a set of data from the

literature using the TCD. These data covered various notch geometries, loading types and several load ratios. The predicted results using the PM, LM and AM fell within 20% of the experimental fatigue limits. They stated that the TCD is very successful in predicting the fatigue limits of complex notched components from elastic FE analysis.

As far as the welded joints are concerned, G. Grupi et al. [76] used the TCD to predict the high-cycle fatigue behaviour of welded components. He showed that the TCD in the form of PM and LM is capable of predicting the endurance limit of welded joint with the combination of high accuracy and ease of use.

To conclude, the TCD is seen to be highly accurate in assessing the strength of the structural components subjected to cyclic loading. It is relatively easy to determine the accurate stresses in the vicinity of the notch/welds by running a simple finite element analysis.

2.2.3 Multiaxial cyclic loading

2.2.3.1 Inclined welded joints

The available Design Codes [33, 34, 77] recommend specific design rules that can be used primarily in those situations where the cyclic force being applied is either normal or parallel to the weld seams. However, this is not always the case. In fact, in real welded structures, in-service forces can be applied also at different angles to the weld seams. To address this type of design problem, Eurocode 9 [33] and Eurocode 3 [77] suggest estimating fatigue damaged by considering the effect of the stress ranges that are both normal and parallel to the weld toe using Eq. (2.33).

$$\left(\frac{\gamma_{Ff} \cdot \Delta\sigma_{E,2}}{\Delta\sigma_C / \gamma_{Mf}} \right)^3 + \left(\frac{\gamma_{Ff} \cdot \Delta\tau_{E,2}}{\Delta\tau_C / \gamma_{Mf}} \right)^5 \leq 1 \quad (2.33)$$

Here, $\Delta\sigma_{E,2}$ and $\Delta\tau_{E,2}$ are equivalent constant amplitude stress ranges, whereas $\Delta\sigma_C$ and $\Delta\tau_C$ are reference values of fatigue strength at two million cycles to failure. γ_{Ff} and γ_{Mf} are partial factors related to the applied stress ranges and fatigue strength, respectively.

Similarly, to address this specific problem, the IIW [34] recommends using a relationship that is directly derived from the classic equation due to Gough, i.e.:

$$\left(\frac{\Delta\sigma_{eq,S,d}}{\Delta\sigma_{R,d}} \right)^2 + \left(\frac{\Delta\tau_{eq,S,d}}{\Delta\tau_{R,d}} \right)^2 \leq CV \quad (2.34)$$

2.2 Fatigue loading in welded joints

In Eq. (2.34), $\Delta\sigma_{eq,s,d}$ and $\Delta\tau_{eq,s,d}$ are equivalent constant amplitude stress ranges, whereas $\Delta\sigma_{R,d}$ and $\Delta\tau_{R,d}$ are the design stress ranges for a specific number of cycles estimated from appropriate uniaxial and torsional FAT curves. Finally, CV is a reference comparison index that is directly provided in Ref. [34].

Turning to the research work that has been done to address the problem of designing against fatigue uniaxially loaded inclined welds, Kim and Kainuma [78] argued that the fatigue life can be evaluated by the stress range ($\Delta\sigma_a \cos^2 \alpha$) at the weld throat in the normal direction of the crack propagation, irrespective of the inclination angle. Then, they proposed that the existing S-N curves found in the design codes for 0-degree joints are applicable to be used to design the inclined welded joints when used in conjunction with $\Delta\sigma_a \cos^2 \alpha$. Recently, Susmel [79] has proposed a simple formula that was derived by tackling the problem from a multiaxial fatigue angle. In particular, he obtained very accurate estimates by simply applying the Modified Wöhler Curve Method (MWCM) [80- 83] along with the nominal stresses approach [84].

2.2.3.2 The Modified Wöhler Curve Method (MWCM)

Examination of the state of the art shows that the MWCM is one of the most advanced tools that can be used to assess the strength of welded components subjected to multiaxial fatigue loading. In particular, this method – that can be applied in terms of either nominal, hot-spot or local stresses - has proven to be highly accurate and reliable in estimating lifetime of steel and aluminium welded joints subjected to in-phase/out-of-phase constant/variable amplitude uniaxial/multiaxial fatigue loading [35, 62, 82-91].

The procedure to design welded joints against fatigue according to the MWCM is summarised in Figure 2.24 and Figure 2.25, with this general theoretical framework being valid independently of the type of stresses being used (i.e., either nominal, hot-spot, or local stresses).

Initially, the hypothesis is formed that the welded component being designed is subjected to a cyclic load history that results in a multiaxial stress state, $[\Delta\sigma]$, at the critical location/section. Stress tensor $[\Delta\sigma]$ is then post-processed to calculate the shear stress range, $\Delta\tau$ and the normal stress range, $\Delta\sigma_n$, relative to that material plane experiencing the maximum shear stress range (i.e., the so-called critical plane) [35, 92].

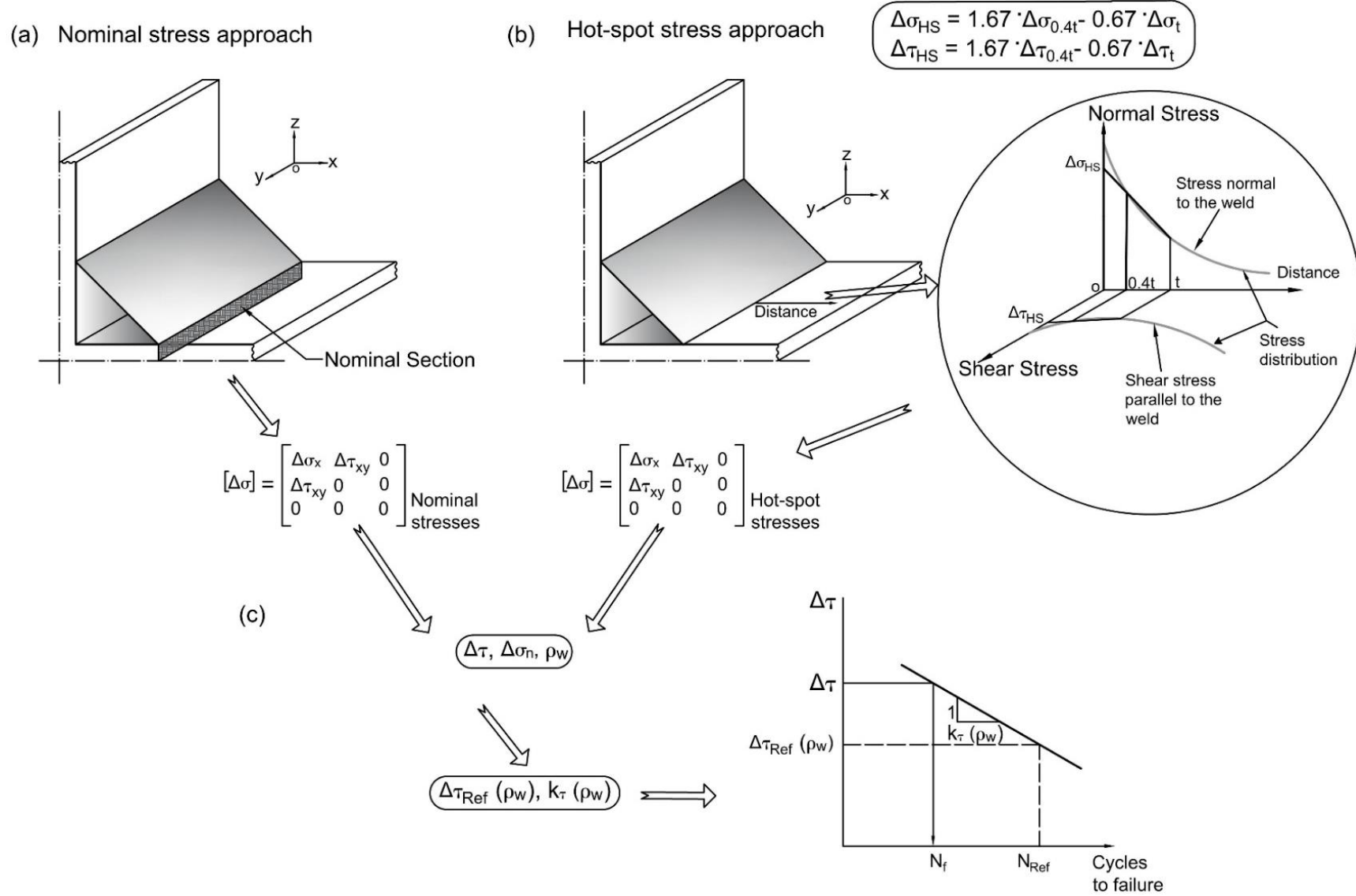


Figure 2.24 The MWCM to estimate fatigue lifetime of welded components applied in terms of nominal and hot spot stresses.

2.2 Fatigue loading in welded joints

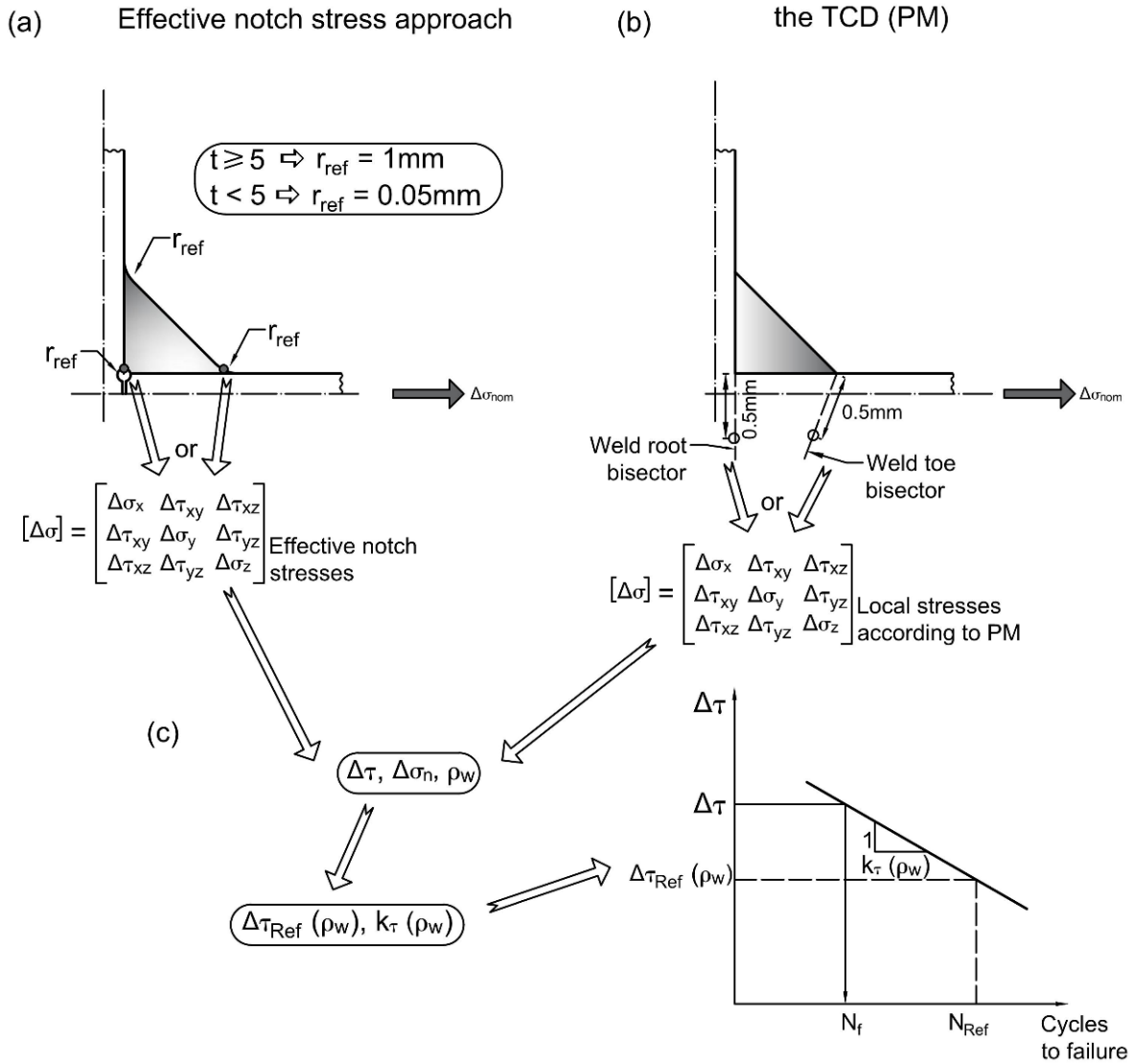


Figure 2.25 The MWCM to estimate fatigue lifetime of welded components applied in terms of effective notch stress as well as along with the PM.

The MWCM takes into account the combined effect of $\Delta\tau$ and $\Delta\sigma_n$ through a stress ratio, ρ_w which is defined as follows (Eq. (2.35)) [26, 84]:

$$\rho_w = \frac{\Delta\sigma_n}{\Delta\tau} \quad (2.35)$$

According to the way it is defined, stress ratio ρ_w is sensitive to the degree of multiaxiality and non-proportionality of the assessed cyclic load history [26, 34]. In particular, it is straightforward to see that ρ_w is invariably equal to unity under fully reversed axial cyclic loading and invariably equal to zero under pure torsional fatigue loading [26].

In order to explain how the MWCM works, consider the maximum shear stress range, $\Delta\tau$ vs. number of cycles to failure, N_f , diagram that is reported in Figure 2.26 (which is usually referred to as “modified Wöhler diagram”). According to this log-log schematisation, welded

components are designed using a modified Wöhler curve whose position varies as ratio ρ_w changes. Any of these design curves is defined unambiguously via its negative inverse slope, $k_\tau(\rho_w)$ and its endurance limit, $\Delta\tau_{\text{Ref}}(\rho_w)$, extrapolated at N_{Ref} cycles to failure.

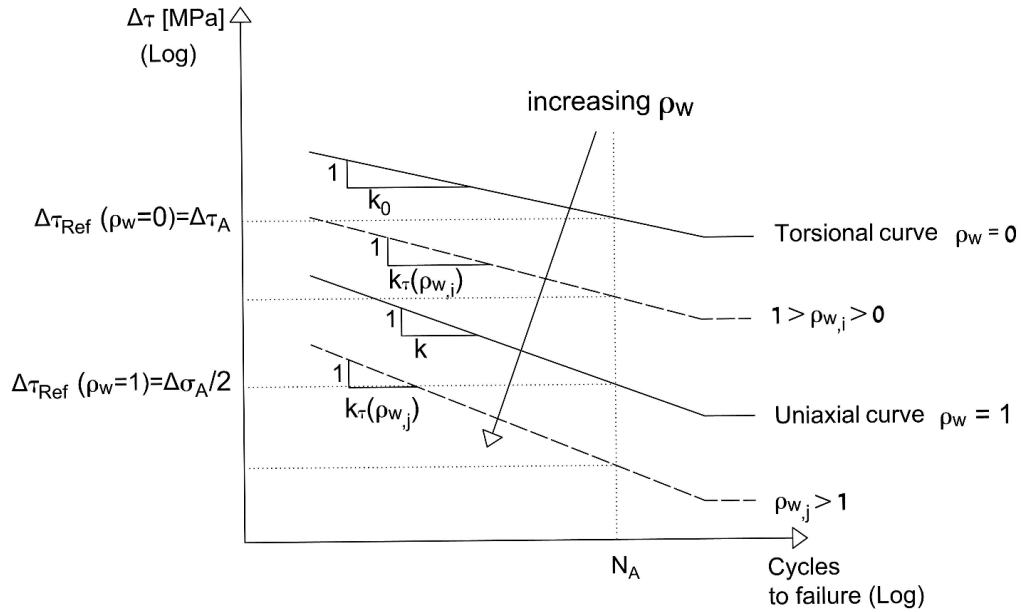


Figure 2.26 Modified Wöhler diagram.

The schematic diagram of Figure 2.26 makes it evident that fatigue lifetime can be assessed provided that the specific modified Wöhler curve is known for the value of ρ_w calculated, according to Eq. (2.35), by post-processing the load history under investigation. Since the S-N curves that are available to perform the fatigue assessment are usually those experimentally determined/estimated under fully-reversed uniaxial and torsional fatigue loading, the modified Wöhler curves for ρ_w ratios different from unity (uniaxial case) and zero (torsional case) have to be derived via the following linear relationships [23, 80-83]:

$$k_\tau(\rho_w) = \alpha \cdot \rho_w + \beta \tag{2.36}$$

$$\Delta\tau_{\text{Ref}}(\rho_w) = a \cdot \rho_w + b \tag{2.37}$$

In Equations (2.36) and (2.37) α , β , a and b are fatigue constants to be determined from suitable experimental fatigue curves. In particular, by observing that $\rho_w = 1$ under fully-reversed uniaxial cyclic loading and $\rho_w = 0$ under torsional fatigue loading, Eqs (2.36) and (2.37) can directly be rewritten as follows [26, 83]:

$$k_\tau(\rho_w) = (k - k_0) \cdot \rho_w + k_0 \tag{2.38}$$

$$\Delta\tau_{\text{Ref}}(\rho_w) = \left(\frac{\Delta\sigma_A}{2} - \Delta\tau_A \right) \cdot \rho_w + \Delta\tau_A \tag{2.39}$$

2.2 Fatigue loading in welded joints

Where, k and k_0 are the negative inverse slopes of the uniaxial and torsional fatigue curves, respectively, whereas $\Delta\sigma_A$ and $\Delta\tau_A$ are the ranges of the corresponding endurance limits determined at a number of cycles to failure equal to at N_{Ref} .

Turning back to the way the MWCM quantifies fatigue damage, after using Eqs (2.38) and (2.39) to estimate the modified Wöhler curve associated with the value of ρ_w characterising the load history under investigation, the number of cycles to failure can be predicted directly via the following standard power law:

$$N_f = N_{Ref} \cdot \left[\frac{\Delta\tau_{Ref}(\rho_w)}{\Delta\tau} \right]^{k_\tau(\rho_w)} \quad (2.40)$$

In summary, it is worth recalling here that, according to the way it is defined, ratio ρ_w is not sensitive to the presence of non-zero mean stress [26, 35, 84]. This implies that the MWCM as reviewed in the present section can be used to perform the fatigue assessment of welded joints characterised by high tensile residual stresses – i.e., in the as-welded condition. In contrast, the fatigue assessment of stress-relieved welded connections is recommended to be performed by adopting appropriate enhancement factors as extensively discussed in Ref. [35].

2.3 Conclusions

To conclude this chapter, the literature shows a massive interest in the use of hybrid-welded joints, in particular, aluminium-to-steel to reduce the overall weight of the structures and provide environmentally friendly solutions. To date, the static behaviour of hybrid-welded joints has still not yet been comprehensively examined. The existing literature on the hybrid-welded joints is focused extensively on the microstructure of the hybrid joints and the welding technology to optimise the welding parameters and hence eliminate the presence of IMC that deteriorate the strength of the joint. Some studies are investigating the ability of welding aluminium-to-steel, with limited research investigating the static strength of hybrid-welded joints. Unexpectedly there is a very limited investigation of the fatigue behaviour of the hybrid-welded joints, and yet there is no guideline or codes to design these joints against fatigue loading.

The literature highlighted several stress-based approaches that are capable to accurately perform the static and fatigue assessment of welded joints made from the same material. It was noticeable that a large body of the literature investigating the fatigue assessment of steel welded joints with much less attention paid to the fatigue assessment of aluminium-welded joints. In addition, the Standards and Codes of Practice (IIW, and EC9) have provided design curves for aluminium and steel assuming the welded components are subjected to either normal or perpendicular loading to the weld. However, in reality, the welded component can experience a loading that is at an angle to the weld seam.

The work presented in this thesis aims to fill in the gaps mentioned above and use the existing knowledge to solve these problems. To do that, the following tasks were performed:

- From the literature, aluminium welded fatigue data were collected and reanalysed according to the existing fatigue design approaches. Also formalising the TCD to estimate the fatigue strength of aluminium subjected to uniaxial loading (chapter 3).
- The MWCM is used to estimate the fatigue strength of inclined welded joints (made of steel) subjected to uniaxial loading. (see chapter 4)
- Aluminium-to-steel welded joints were manufactured using coldArc® welding and investigated the static and fatigue behaviour. The aim was to propose suitable design curves and equations to be able to design these joint accurately (see chapter 6 and 7).

2.4 References

- [1] Kimapong K, Watanabe T. Lap Joint of A5083 Aluminium Alloy and SS400 Steel by Friction Welding. *Materials Transactions* 2005; 46(4): 835-841. .
- [2] Qin G, Su Y, Wang S. Microstructures and properties of welded joint of aluminium alloy to galvanized steel by Nd: YAG laser + MIG arc hybrid brazing-fusion welding. *Transactions of Nonferrous Metals Society of China* 2004; 24: 989-995..
- [3] Chao R, Yang J, Lay S. Interfacial Toughness for the Shipboard Aluminium/Steel Structural Transition Joint. *Marine Structures* 1997; 10: 353-362. .
- [4] McKenney C, Banker J. Explosion-Bonded Metals for Marine Structural Applications. *Marine Technology* 1971: 285-292. .
- [5] Trethewey K.R. Explosion-bonded transition joints for structural applications. *Construction and Building Materials* 1989; 3(2): 64-72. .
- [6] Okamura H, Aota K. Joining of dissimilar materials with friction stir welding. *Welding International* 2004; 18(11): 852-860. .
- [7] Katayama S. Laser welding of aluminium alloys and dissimilar metals. *Welding International* 2004; 18(8): 618-625..
- [8] Kato K, Tokisue H. Dissimilar friction welding of aluminium alloys to other materials. *Welding International* 2004; 18(11): 861-867. .
- [9] Lu Z, Huang P, Gao W, Li Y, Zhang H, Yin S. ARC welding method for bonding steel with aluminium. *Front. Mech. Eng. China* 2009; 4(2): 134-143..
- [10] Fukumoto S, Tsubakino H, Okita K, Aritoshi M, Tomita T. Friction welding process of 5052 aluminium alloy to 304 stainless steel. *Materials Science and Technology* 1999; 15(9): 1080-1086. .
- [11] Elrefaey A, Gouda M, Takahashi M, Ikeuchi K. Characterization of Aluminium/Steel Lap Joint by Friction Stir Welding. *Journal of Materials Engineering and Performance* 2005; 14(1): 12-17..
- [12] Liu H, Maeda M, Fujii H, Nogi K. Tensile properties and fracture locations of friction-stir welded joints of 1050-H24 aluminum alloy. *Journal of materials science letters* 2003; 22: 41-43. .
- [13] Leitao C, Arruti E, Aldanondo E, Rodrigues D. Aluminium-steel lap joining by multipass friction stir welding. *Materials and Design* 2016; 106: 153-160..

- [14] Meco S, Pardal G, Ganguly S, Williams S, McPherson N. Application of laser in seam welding of dissimilar steel to aluminium joints for thick structural components. *Optics and Laser in Engineering* 2015; 67: 22-30. .
- [15] Wang P, Chen X, Pan Q, Madigan B, Long J. Laser welding dissimilar materials of aluminum to steel: an overview. *the Internation Journal of Advanced Manufacturing Technology* 2016; 87: 3081-3090..
- [16] Gao M, Chen C, Mei S, Wang L, Zeng X. Parameter optimization and mechanism of laser–arc hybrid welding of dissimilar Al alloy and stainless steel. *International Journal of Advanced Manufacturing Technology* 2014; 74: 199-208..
- [17] Era T, Isw A, UezonoT, Ueyama T, Hitata Y. Controlled bridge transfer (CBT) gas metal arc process for steel sheets joining. *Welding International* 2013; 27(4): 268-273. .
- [18] Cao R, Sun J.H, , Chen J.H, Wang P. Cold metal transfer joining aluminum alloys-to-galvanized mild steel. *Journal of Manufacturing Science and Engineering* 2014; 136: 051015-1 to 051015-10..
- [19] Goecke S.F. *Low Energy Arc Joining Process for Materials Sensitive to Heat*, EWM Mündersbach, (2005) Germany..
- [20] Kah P, Suoranta R, Martikainen J. Advanced gas metal arc welding processes. *Int J Adv Manuf Technol* 2013; 67: 655-674. .
- [21] Zech F, Cramer H, Baum L. *GMAW welding and brazing of thin sheet metal using modern power sources. Innovative technologies for joing advanced materials*, Trimisoara..
- [22] Wöhler A. *Versuche zur Ermittlung der auf die Eisenbahnwaggnachsen einwirkenden Krafte and di Widerstandsfahigkeit der Wagen-Achsem.*1860:583-616. [In German].
- [23] Naser J.M, Toledano F.S. *Analysis of vibration-induced fatigue cracking in steel bridge.* Chalmers University of Technology, Goteborg, Sweden, 2011..
- [24] Spangnburg L. *The fatigue of metal under repeated strains.* New York, USA: Van Nostrand Publisher, 19876..
- [25] Schutz W. *A history of fatigue.* *Engineering Fracture Mechanics* 1996; 54(2): 263- 300. .
- [26] Susmel L. *Multiaxial notch fatigue from nominal to local stress/strain quantities.* Cambridge, UK: Woodhead Publishing Limited, 2009. .
- [27] Sinclair GM, Dolan TJ. *Effect of stress amplitudes on statistical variability in fatigue life of 75S–T6 Aluminium Alloy.* *Trans ASME* 1953; 75: 867–872..

2.4 References

- [28] Lee Y-L, Pan J, Hathaway R, Barkey M. Fatigue testing and analysis. Butterworth-Heinemann, Elsevier; 2005..
- [29] Hertzberg RW. Deformation and fracture mechanics of engineering materials. 4th ed. Chichester, New York, USA: Wiley; 1996..
- [30] Gibbons Natrella M. Experimental statistics. National Bureau of Standards, Handbook 91; 1963..
- [31] Radaj D, Sonsino C.M, Fricke W. Recent developments in local concepts of fatigue assessment of welded joints. *International Journal of Fatigue* 2009; 31: 2-11..
- [32] Morgenstern C, Sonsino CM, Hobbacher A, Sorbo F. Fatigue design of aluminium welded joints by the local stress concept with the fictitious notch radius of $r_f=1\text{mm}$. *Int J Fatigue* 2006;28:881–890..
- [33] Eurocode 9: design of aluminium structures – Part 2: structures susceptible to fatigue, prENV; 1999..
- [34] Hobbacher A. Recommendations For Fatigue Design of Welded Joints and Components. International Institute of Welding, Paris, 2007..
- [35] Susmel L. Four Stress analysis strategies to use the Modified Woler Curve Method to perform the fatigue assessment of weldments subjected to constant and variable amplitude multiaxial fatigue loading. *International Journal of Fatigue* 2014; 67: 38-54. .
- [36] Djavit D.E, Strande E. Fatigue failure analysis of fillet welded joints used in offshore structures. Master's thesis, Chalmers University of Technology, Goteborg, Sweden, 2013..
- [37] Niemi E, Fricke W, Maddox SJ. Fatigue analysis of welded components: designer's guide to the structural hot-spot stress approach (IIW-1430-00). Cambridge, UK: Woodhead Publishing Limited; 2006..
- [38] Niemi E. Structural stress approach to fatigue analysis of welded components. IIW-document XIII-1819-00/XV-1090-01; 2000..
- [39] Hobbacher AF. New developments at the recent update of the IIW recommendations for fatigue of welded joints and components. *Steel Construction* 2010;3(4):231–42..
- [40] Radaj D, Sonsino C.M, Fricke W. Fatigue assessment of welded joints by local approaches. Cambridge: Woodhead Publishing, 2006. .
- [41] Dong P. A structural stress definition and numerical implementation for fatigue analysis of welded joints. *International Journal of Fatigue* 2001; 23: 865-876. .

- [42] Dong P, Hong J.K, Osage D, Prager M. Assessment of ASME'S FSRF rules for vessel and piping welds using a new structural stress method. *Welding in the World* 2003; 47(1/2): 31-43. .
- [43] Poutiainen I, Tanskanen P, Marquis G. Finite element methods for structural hot-spot stress determination- a comparison of procedures. *International Journal of Fatigue* 2004; 26: 1147-1157. .
- [44] Sonsino C.M, Fricke W, Bruyne F.de Hopper A, Ahmadi A, Zhang G. Notch stress concepts for the fatigue assessment of welded joints-Background and applications. *International Journal of Fatigue* 2012; 34: 2-16..
- [45] Radaj D. Design and analysis of fatigue resistant welded structures. Cambridge: Woodhead Publishing, 1990..
- [46] Fricke W. Fatigue assessment by notch stress analysis, Woodhead Publishing, 2012..
- [47] Karakas Ö, Morgenstern C, Sonsino C.M. Fatigue design of welded joints from the wrought magnesium alloy AZ31 by the local stress concept with the fictitious notch radii of $r_f=1.0$ and 0.05mm . *International Journal of Fatigue* 2008; 30: 2210-2219. .
- [48] Zhang G, Richter B. A new approach to the numerical fatigue-life prediction of spot-welded structures. *Fatigue Fract Engng Mater Struct* 2000; 23: 499-508..
- [49] Sonsino C.M. A consideration of allowable equivalent stresses for fatigue design of welded joints according to the notch stress concept with the reference radii $r_{ref} = 1.00$ and 0.05 mm . *Welding in the World* 2009; 53: R64-R74. .
- [50] Radaj D, Lazzarin P, Berto F. Fatigue assessment of welded joints under slit-parallel loading based on strain energy density or notch rounding. *International Journal of Fatigue* 2009; 31: 1490-1504. .
- [51] Barsoum Z, Khurshid M, Barsoum I. Fatigue strength evaluation of friction stir welded aluminium joints using the nominal and notch stress concepts. *Materials and Design* 2012; 41: 231-238. .
- [52] Verreman Y, Nie B. EARLY DEVELOPMENT OF FATIGUE CRACKING AT MANUAL FILLET WELDS. *Fatigue Fract. Engng Mater. Struct* 1996; 19: 669-681. .
- [53] Lazzarin P, Tovo R. A unified approach to the evaluation of linear elastic stress fields in the neighborhood of cracks and notches. *International Journal of Fracture* 1996; 78: 3-19..
- [54] Lazzarin P, Lassen T, Livieri P. A notch stress intensity approach applied to fatigue life predictions of welded joints with different local toe geometry. *Fatigue Fract Engng Mater Struct* 2003; 26: 49-58. .

2.4 References

- [55] B Atzori B, Lazzarin P, Tovo R. Stress field parameters to predict the fatigue strength of notched components. *Journal of Strain Analysis* 1999; 34(6): 437-453..
- [56] Lazzarin P, Tovo R. A notch Intensity Factor Approach to the Stress Analysis of Welds. *Fatigue & Fracture of Engineering Materials & Structures* 1998; 21: 1089-1103..
- [57] Tovo R, Lazzarin P. Relationships between local and structural stress in the evaluation of the weld toe stress distribution. *International Journal of Fatigue* 1999; 21: 1063-1078. .
- [58] Lazzarin P, Livieri P. Notch stress intensity factors and fatigue strength of aluminium and steel welded joints. *International Journal of Fatigue* 2001; 23: 225-232. .
- [59] Atzori B, Lazzarin P, Tovo R. From a local stress approach to fracture mechanics: a comprehensive evaluation of the fatigue strength of welded joints. *Fatigue Fract Engng Mater Struct* 1999; 22: 369-381..
- [60] Neuber H. *Theory of notch stresses: principles for exact calculation of strength with reference to structural form and material*. Berlin, Germany: Springer Verlag; 1958..
- [61] Taylor D. *The Theory of Critical Distances: A new perspective in Fracture Mechanics*. Oxford: Elsevier, 2007. .
- [62] Susmel L, Taylor D. A novel formulation of the theory of critical distances to estimate lifetime of notched components in the medium-cycle fatigue regime. *Fatigue Fract Engng Mater Struct* 2007; 30: 567-581.. .
- [63] Peterson R.E. Notch sensitivity. In: Sines G, Waisman JL, editors. *Metal fatigue*. New York: McGraw Hill; 1959. p. 293–306..
- [64] Whitney J.M, Nuismer R.J. Stress Fracture Criteria for Laminated Composites Containing Stress Concentrations. *Journal of Composite Materials* 1974; 8: 253-265..
- [65] Tanaka K. Engineering Formula for Fatigue Strength Reduction due to Crack-like Notches. *International Journal of Fracture* 1983; 22: R39-R46. .
- [66] David Taylor, “Geometrical effects in fatigue: a unifying theoretical model,” *International Journal of Fatigue*, vol. 21, pp. 413-420, 1999. .
- [67] Taylor D, Wang G. The validation of some methods of notch fatigue analysis,” *Fatigue Fract Engng Mater Struct* 2000; 23: 387-394..
- [68] Taylor D, Barrett N, Lucano G. Some new methods for predicting fatigue in welded joints. *Int J Fatigue* 2002; 24: 509–18..
- [69] Araújo J.A, Susmel L, Taylor D, Ferro, Ferreira J.L. On the prediction of high-cycle fretting fatigue strength: Theory of critical distances vs. hot-spot approach. *Eng. Fract. Mech.* 2008; 75(7): 1763-1778..

- [70] Susmel L Taylor D. Two methods for predicting the multiaxial fatigue limits of sharp notches. *Fatigue Fract. Eng. Mater. Struct.* 2003; 26(9): 821-833. .
- [71] Susmel L, Taylor D. Acritical distance/plane method to estimate finite life of notched components under variable amplitude uniaxial/multiaxial fatigue loading. *International Journal of. Fatigue* 2012; 38: 7-24..
- [72] Bellett D, Taylor D, Marco S, Mazzeo E, Guillois J, Pircher T. The fatigue behaviour of three-dimensional stress concentrations. *International Journal of Fatigue* 2005; 27(3): 207-221..
- [73] Araujo J, Susmel L, Taylor D, Ferro J, Mamiya E. On the use of the Theory of Critical Distances and the Modified Wöhler Curve Method to estimate fretting fatigue strength of cylindrical contacts. *International Journal of Fatigue* 2007; 29(1): 95-107..
- [74] Susmel L, Taylor D. An Elasto-Plastic Reformulation of the Theory of Critical Distances to Estimate Lifetime of Notched Components Failing in the Low/Medium-Cycle Fatigue Regime. *J. Eng. Mater. Technl.* 2010; 13: 021002-1 to 021002-8..
- [75] Taylor D. Predicting the fracture strength of ceramic materials using the theory of critical distances. *Eng. Fract. Mech.* 2004; 71(16-17): 2407-2416. .
- [76] Grupi G, Grupi V, Gugielmino E, Taylor D. Fatigue assessment of welded joints using critical distance and other methods,” *Engineering Failure Analysis* 2005; 12: 129-142. .
- [77] Design of steel structures. ENV 1993-1-1, EUROCODE 3; 1988..
- [78] Kim I-K, Kainuma S. Fatigue life assessment of load-carrying fillet welded cruciform joints inclined to uniaxial cyclic loading. *International Journal of Pressure Vessels and Piping* 2005; 82(11): 807-813..
- [79] Susmel L. Nominal stresses and Modified Wohler Curve Method to perform the fatigue assessment of uniaxially loaded inclined welds. *Journal of Mechanical Engineering Science* 2014; 228(16): 2871-2880...
- [80] Susmel L, Lazzarin P. A Bi-parametric modified wöhler curve for high cycle multiaxial fatigue assessment. *Fatigue Fract Eng Mater Struct* 2002;25: 63–78..
- [81] Lazzarin P, Susmel L. A stress-based method to predict lifetime under multiaxial fatigue loadings. *Fatigue Fract Eng Mater Struct* 2003; 26: 1171–87..
- [82] Susmel L. Multiaxial fatigue limits and material sensitivity to non-zero mean stresses normal to the critical planes. *Fatigue Fract Eng Mater Struct* 2008;31: 295–309..
- [83] Susmel L, Tovo R, Lazzarin P. The mean stress effect on the high-cycle fatigue strength from a multiaxial fatigue point of view. *Int J Fatigue* 2005;27:928 43..

2.4 References

- [84] Susmel L, Tovo R. On the use of nominal stresses to predict the fatigue strength of welded joints under biaxial cyclic loading. *Fatigue Fract Eng Mater Struct* 2004;27:1008–24..
- [85] Susmel L, Tovo R. Local and structural multiaxial stress states in welded joints under fatigue loading. *Int J Fatigue* 2006;28:564–75..
- [86] Susmel L. Modified Wöhler Curve Method, Theory of Critical Distances and EUROCODE 3: a novel engineering procedure to predict the lifetime of steel welded joints subjected to both uniaxial and multiaxial fatigue loading. *Int J Fatigue* 2008;30:888–907..
- [87] Susmel L, Tovo R, Benasciutti D. A novel engineering method based on the critical plane concept to estimate the lifetime of weldments subjected to variable amplitude multiaxial fatigue loading. *Fatigue Fract Eng Mater Struct* 2009;32:441–59..
- [88] Susmel L. Three different ways of using the Modified Wöhler Curve Method to perform the multiaxial fatigue assessment of steel and aluminium welded joints. *Eng Fail Anal* 2009;16:1074–89..
- [89] Susmel L. Estimating fatigue lifetime of steel weldments locally damaged by variable amplitude multiaxial stress fields. *Int J Fatigue* 2010;32:1057–80..
- [90] Susmel L, Sonsino CM, Tovo R. Accuracy of the Modified Wöhler Curve Method applied along with the $r_{ref}=1$ mm concept in estimating lifetime of welded joints subjected to multiaxial fatigue loading. *Int J Fatigue* 2011;33:1075–91..
- [91] Susmel L, Askes H. Modified Wöhler Curve Method and multiaxial fatigue assessment of thin welded joints. *Int J Fatigue* 2012;43:30–42..
- [92] Susmel L. A simple and efficient numerical algorithm to determine the orientation of the critical plane in multiaxial fatigue problems. *Int J Fatigue* 2010;32: 1875–83..

Chapter 3

3. Global and local stress-based approaches to estimate the fatigue strength of aluminium welded joints

The work presented in this chapter was published in the International Journal of Fatigue with the following title:

Al Zamzami I, Susmel L. On the accuracy of nominal, structural, and local stress based approaches in designing aluminium-welded joints against fatigue. International Journal of Fatigue 2017; 101:137-158. <https://doi.org/10.1016/j.ijfatigue.2016.11.002>.

Even though aluminium as a structural material plays an important role in many different engineering applications, examination of state of the art indicate that the fatigue behaviour of steel weldments has been studied extensively since the beginning of last century. On the other hand, there are less theoretical and experimental work has been conducted to effectively design and estimate the fatigue strength of aluminium-welded joints. To this end, a large number of data taken from the technical literature was used to investigate in detail the accuracy and reliability of the existing fatigue design approaches in designing aluminium weldments subjected to uniaxial fatigue loading. This chapter presents a detailed investigation of the use of nominal stresses, hot-spot stresses, effective notch stresses, the Notch Stress Intensity Factors (N-SIFs) and the Theory of Critical Distances (TCD).

3.1 Introduction

More recently, there has been increased emphasis on the use of aluminium as a structural material to replace the use of steel in many structural applications such as automotive frames, offshore structures and in the railway industry. The reason behind this growth is the ability to utilise the various mechanical and physical properties of aluminium alloys where the strength to weight ratio is increased resulting in a high-performance lightweight and high corrosion resistance structures. Moreover, aluminium is considered as a green material, which implies that it can be efficiently recycled in perpetuity.

The available Standards and Codes of Practice (i.e. EC9 and the IIW) take as a starting point the assumption that welded aluminium alloys have the same fatigue strength regardless of their chemical composition. Although this assumption results in a considerable simplification of the design problem, it increases the level of uncertainty associated with the fatigue assessment process [1]. These design uncertainties lead to components and structures that are bigger and heavier than necessary, with this resulting in inefficient usage of materials and energy during manufacturing.

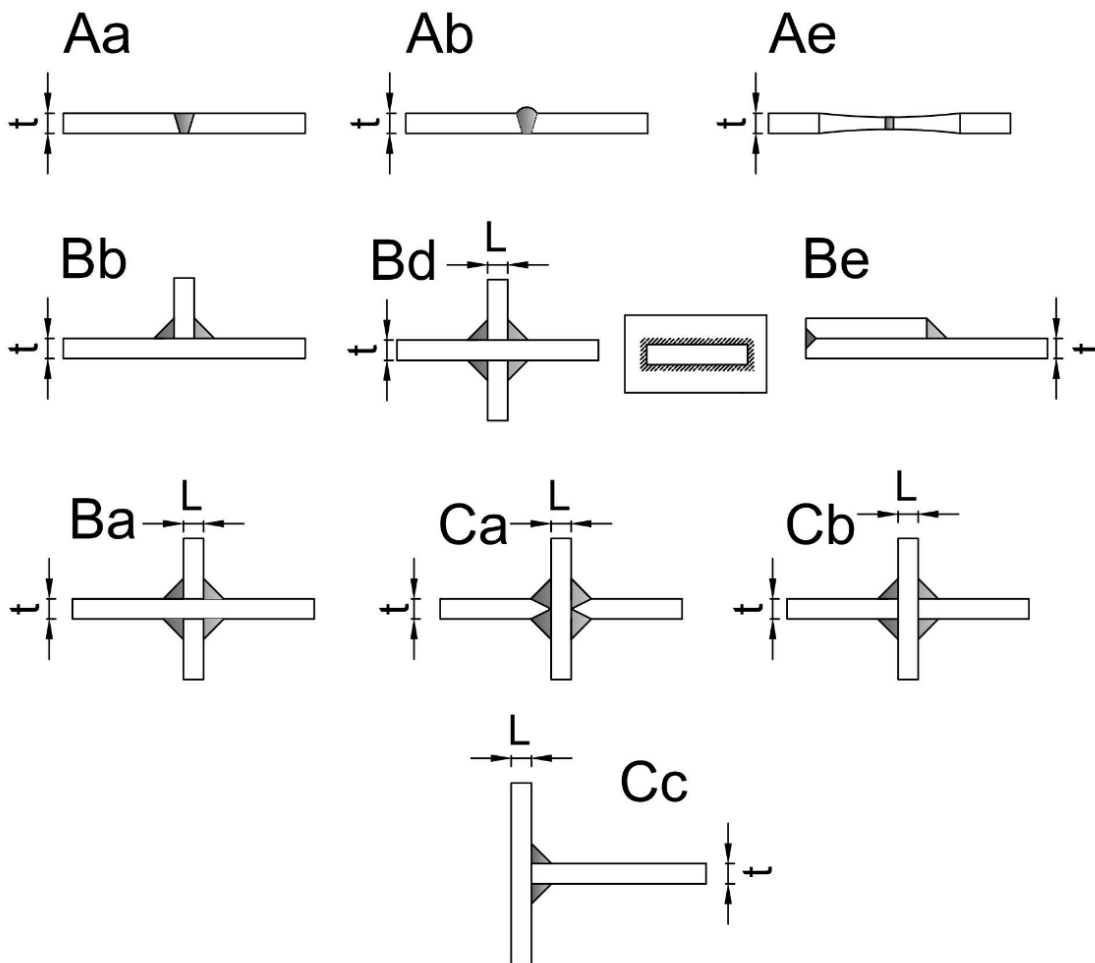


Figure 3.1 Geometry of the investigated welded details.

In this investigation, the accuracy of the design approaches mentioned above was assessed systematically against a large number of experimental data taken from the technical literature [2-23]. The selected data were generated by testing aluminium-welded joints under either cyclic axial loading or cyclic bending. The geometries of the structural details being investigated are shown in Figure 3.1. Furthermore, owing to the important role played by the presence of superimposed static stress, the influence of non-zero mean stresses on aluminium-welded joints' overall fatigue strength was also investigated in detail.

To use both the hot-spot approach and the considered local stress methods to post-process the experimental data being selected, a number of linear-elastic FE models was solved using commercial FE code ANSYS®. The N-SIF approach was applied also by using the empirical formulas devised by Lazzarin and Tovo that allow the N-SIF range, ΔK_I , for standard welded geometries to be estimated directly [24, 25, 26]. Finally, the N-SIF master curve proposed by Lazzarin and Livieri [25, 27, 28] was used to determine a unifying value for the TCD critical distance suitable for accurately estimating the fatigue lifetime of aluminium welded joints.

3.2 Methodology

To investigate the accuracy and reliability of the design approaches, mentioned in section 3.1, in estimating fatigue lifetime of aluminium-welded joints, more than two thousand experimental results were selected from the technical literature [2-23]. These data were generated by testing, under either cyclic axial loading or cyclic bending loading, a variety of welded specimens (Figure 3.1) made of different aluminium alloys. The specimens considered in the present investigation were tested under load ratios, $R = \sigma_{\min}/\sigma_{\max}$ ranging from -1 up to 0.75.

According to the design strategies recommended by Eurocode 9 (EC9) [29] and the International Institute of Welding (IIW) [30, 31], initially, the experimental results being considered were post-processed in terms of stress ranges by disregarding the presence of superimposed static stress. Subsequently, the same data were re-analysed to investigate the effect of non-zero mean stresses on the fatigue behaviour of aluminium-welded joints (Section 3.3.6).

Figure 3.1 summarises the different types of welded specimens that were assessed according to the nominal stress approach. On the other hand, the hot-spot stresses, effective notch stresses, N-SIF and the TCD were applied only to series Ba, Bb, Ca and Cb (Figure 3.1). Because, for the other series, the relevant local dimensions of the welds were not reported in the original sources.

3.2 Methodology

For a given definition of the design stress range, the data sets being investigated were post-processed to obtain the corresponding fatigue curves. These curves were determined by reanalysing the fatigue results under the hypothesis of a log-normal distribution of the number of cycles to failure, N_f , for each stress level, with a confidence level being taken equal to 95% [32, 33]. The mathematical procedure followed to post-process the considered experimental data is summarised in Chapter 2, Section 2.2.1.2.

Table 3.1 EC9 and the IIW recommended values in terms of stress ranges and negative inverse slope to design aluminium welded joints using the nominal and hot spots stress approaches.

Approach	Welded Geometry	EC9		IIW	
		$\Delta\sigma_{A,97.7\%}$ [MPa]	k	$\Delta\sigma_{A,97.7\%}$ [MPa]	k
The nominal stress	Aa	55	4.5	45	3
	Ab	36	4.3	36	3
	Ae	55	4.5	45	3
	Ba	23	3.4	36	3
	Bb	23	3.4	36	3
	Bd	23	3.4	36	3
	Be	23	3.4	36	3
	Ca	36	3.4	32	3
	Cb	25	3.4	36	3
	Cc	25	3.4	36	3
The hot-spot stress	Ba	-	-	40	3
	Bb	-	-	40	3
	Ca	-	-	40	3
	Cb	-	-	36	3
The effective notch stress	Ba			71	3
	Bb			71	3
	Ca			71	3
	Cb			71	3

According to this standard procedure, in what follows the results from the statistical re-analyses will be reported in terms of: negative inverse slope, k, range of the endurance limit, $\Delta\sigma_{A,97.7\%}$, extrapolated at $2 \cdot 10^6$ cycles to failure for a Probability of Survival, P_s , equal to 97.7%, and scatter ratio, $T\sigma$, of the endurance limit range for 90% and 10% probabilities of survival (i.e., $T\sigma = \Delta\sigma_{10\%} / \Delta\sigma_{90\%}$). The scatter ratio, $T\sigma$, is a useful index allowing the level of scattering associated with a population of fatigue data to be quantified. As to the recommended values for $T\sigma$, Haibach [34] has demonstrated that, on average, the series of fatigue data generated by testing steel welded joints are characterised by a $T\sigma$ ratio equal to 1.5. This reference value was derived by post-processing a large number of experimental results from different welded structural details made of steel [34].

For what concerns the nominal stress approach, the required reference design curves were taken from EC9 [29] as well as from the IIW Recommendations [30] (see Table 3.1). The accuracy of the estimates obtained by applying both the hot-spot stress approach and the effective notch stress approach were compared with the reference curves supplied by the IIW [30].

It is worth recalling here that the EC9 design curves refer to $P_s=97.7\%$, whereas those reported in the IIW Recommendations refer to $P_s=95\%$. The values for the endurance limits suggested both by EC9 and the IIW are extrapolated at $2 \cdot 10^6$ cycles to failure. The IIW recommends a constant negative inverse slope, k , equal to 3, whilst EC9 supplies different negative inverse slopes for different welded geometries.

Finally, Lazzarin and Livieri's master curve (shown in Figure 2.22) for aluminium welded joints [25, 26, 28] was used to assess the predictions made according to the N-SIF approach.

3.3 Fatigue assessment results and discussion

3.3.1 Nominal stress based approach

As far as the nominal stress approach is concerned, design stresses are calculated using the classic continuum mechanics concepts. In particular, nominal stresses have to be determined by explicitly taking into account those stress gradients resulting from the macro-geometrical features characterising the welds regions [35, 36]. On the contrary, the stress concentration phenomena arising from the weld toes have to be disregarded, since the effect of the local stress gradients is already included in the fatigue strength values supplied by both EC9 and the IIW. Accordingly, the selection of an appropriate design curve is essential to achieve accurate fatigue design [30, 37].

Table 3.2 summarises the results obtained by using the nominal stress approach (for geometry Aa) by post-processing, according to the statistical procedure reviewed in Section 2.2.1.2, the individual data sets being investigated. Endurance limit ranges $\Delta\sigma_{A,50\%}$ and $\Delta\sigma_{A,97.7\%}$ reported in Table 3.2 were extrapolated at $2 \cdot 10^6$ cycles to failure for P_s equal to 50% and 97.7%, respectively. The results obtained for the rest of the geometries are presented in Appendix A (Table A.2 to Table A.7).

3.3 Fatigue assessment results and discussion

Table 3.2 Fatigue results generated by testing ground butt-welded joints (geometry Aa in Figure 3.1) statistically re-analysed in terms of nominal stresses.

Series	Ref.	No of Data	Load Type ⁽¹⁾	R	t [mm]	k	T _σ	Nominal Stress		Parent material	Filler material
								Δσ _{A,50%} [MPa]	Δσ _{A,97.7%} [MPa]		
Aa-1	[13]	9	Ax	0	4.8	8.5	2.27	117.3	77.9	5083	5356
Aa-2	[13]	9	Ax	0	4.8	6.9	2.13	116.7	80.0	5083	5356
Aa-3	[13]	9	Ax	0	4.8	10.6	2.89	132.4	77.9	5083	5356
Aa-4	[13]	9	Ax	0	4.8	9.5	3.03	132.5	76.1	5083	5356
Aa-5	[13]	9	Ax	0	4.8	5.9	2.37	110.4	71.6	5083	5356
Aa-6	[13]	9	Ax	0	4.8	14.8	2.18	129.8	87.9	5083	5356
Aa-7	[13]	9	Ax	0	4.8	5.1	2.06	100.6	70.1	5083	5356
Aa-8	[13]	9	Ax	0	4.8	10.6	2.02	127.1	89.3	5083	5356
Aa-9	[13]	9	Ax	0	4.8	7.9	2.78	120.1	72.0	5083	5356
Aa-10	[5]	11	Be	-1	6.4	4.9	1.84	163.0	120.0	NP 5/6	NG 6
Aa-11	[5]	18	Be	-1	6.4	7.2	1.76	189.6	143.0	NP 5/6	NG 6
Aa-12	[5]	8	Be	-1	6.4	5.4	1.28	159.2	140.7	NP 5/6	NG 6
Aa-13	[5]	8	Be	-1	6.4	5.0	2.49	164.0	104.0	NP 5/6	NG 6
Aa-14	[5]	5	Be	-1	6.4	8.2	5.36	236.3	102.0	NP 5/6	NG 6
Aa-15	[5]	7	Be	-1	6.4	3.9	2.25	115.1	76.8	NP 5/6	NG 6
Aa-16	[4]	16	Be	-1	9.5	5.6	1.78	188.3	141.1	5083-H113	5183
Aa-17	[4]	12	Be	-1	9.5	6.4	1.72	211.1	161.1	5456-H321	5556
Aa-18	[15]	10	Be	-1	7.6	7.1	1.92	288.8	208.4	5456-H321	n/a
Aa-19	[14]	12	Be	-1	7.6	11.6	1.20	308.6	281.8	5083-H113	5183
Aa-20	[14]	15	Be	-1	7.6	5.3	1.84	185.6	136.8	5083-H113	5183
Aa-21	[12]	20	Ax	0.08	12.0	4.1	1.80	73.4	54.8	Al Zn Mg1	S-Al Mg5
Aa-22	[4]	9	Ax	0	9.5	5.5	1.51	112.4	91.4	5083-H113	5183
Aa-23	[4]	11	Ax	0	9.5	5.9	1.65	114.3	88.9	5083-H113	5356
Aa-24	[4]	12	Ax	0	9.5	4.7	2.02	99.2	69.9	n/a	n/a
Aa-25	[12]	17	Ax	0	12	4.0	1.63	79.3	62.1	Al Mg5 F28	S-Al Mg5
Aa-26	[8]	8	Ax	0	6.4	8.5	1.12	128.8	121.9	5083-H113	5356
Aa-27	[8]	10	Ax	0	9.5	7.3	1.42	105.0	88.2	5083-H113	5356
Aa-28	[8]	10	Ax	0	9.5	11.1	1.53	128.0	103.4	5083-H113	5356

Chapter 3: Global and local stress-based approaches to estimate the fatigue strength of aluminium welded joints

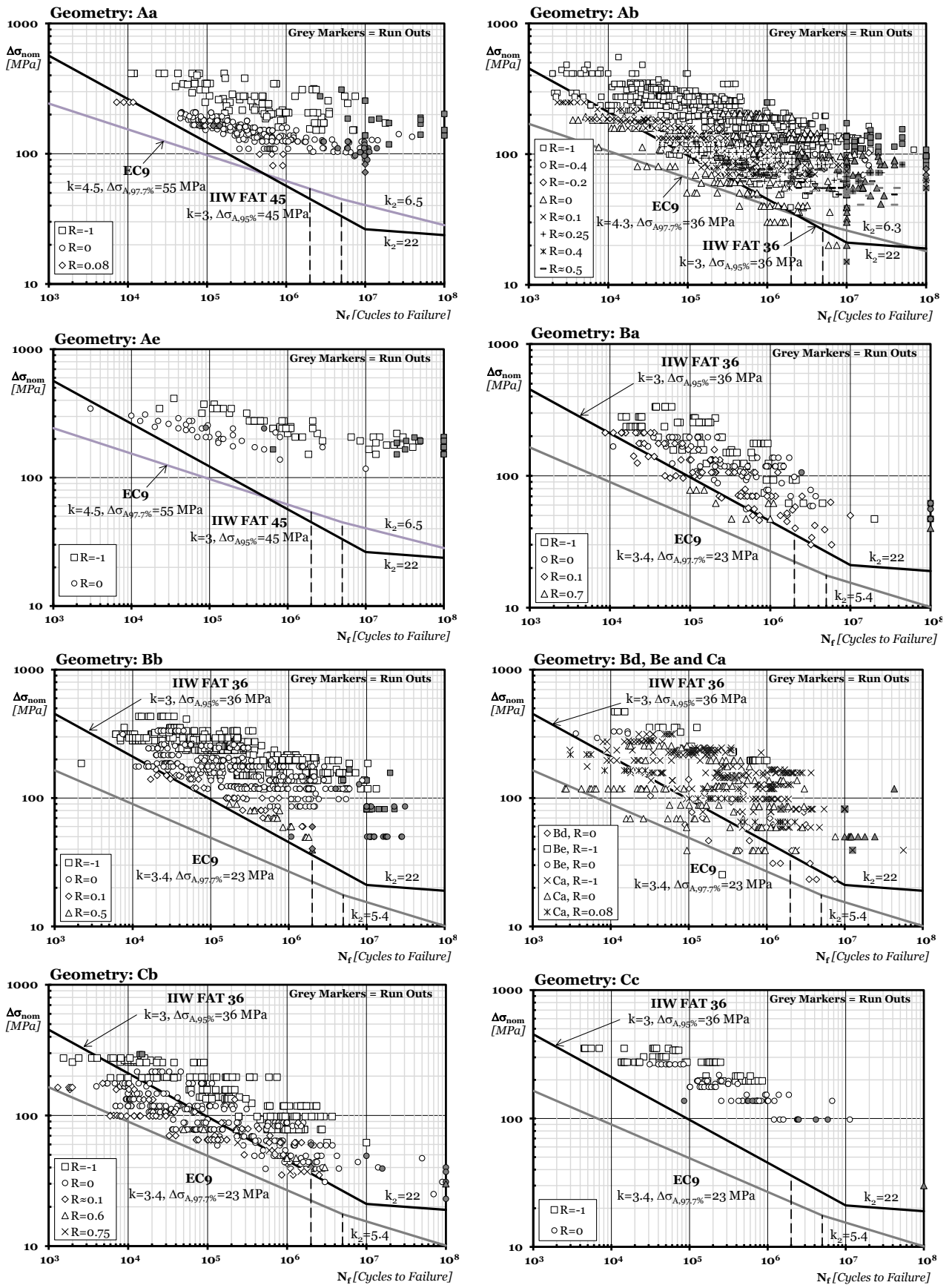


Figure 3.2 Accuracy of the Nominal Stress approach in estimating the fatigue strength of the investigated welded joints see Figure 3.1 for the definition of the different welded geometries.

3.3 Fatigue assessment results and discussion

It is apparent from the tables that, on average, the negative inverse slope of the fatigue curves determined from the individual series is larger than the values that are recommended both by EC9 and by the IIW. Another important aspect is that, according to Table 3.2 and Table A.2 to Table A.7, the average value of T_{σ} is equal to 2.2 with a standard deviation of 1.3. This suggests that, as far as aluminium welded joints are concerned; the expected value for T_{σ} is larger than the reference value of 1.5 that is suggested by Haibach for steel weldments [34].

The experimental results listed in Table 3.2 and Table A.2 to Table A.7 are also summarised in the Wöhler diagrams reported in Figure 3.2. In more detail, these log-log charts plot the range of the nominal stress, $\Delta\sigma_{nom}$, vs. the number of cycles to failure, N_f , for the different structural details being considered (Figure 3.1). For each welded geometry, the fatigue curves suggested by EC9 and the IIW are also plotted in these figures to allow the experimental results to be contrasted with the standard and recommended design guidelines.

The fatigue curves for $P_s=50\%$ and $P_s=97.7\%$ determined by post-processing all the experimental results generated by testing the same type of structural detail are summarised in Table 3.3. In this table, the obtained values are directly compared to the corresponding design curves in terms of negative inverse slope and endurance limit range extrapolated at $2 \cdot 10^6$ cycles to failure.

Table 3.3 Summary of the statistical re-analyses for the different welded geometries in terms of nominal stress approach.

Welded Geometry	Nominal Stress			
	$\Delta\sigma_{A,50\%}$ [MPa]	$\Delta\sigma_{A,97.7\%}$ [MPa]	k	T_{σ}
Aa	72.1	13.0	1.8	30.88
Ab	65.0	17.3	2.4	14.21
Ae	185.3	89.2	7.0	4.32
Ba	45.7	15.5	2.1	8.69
Bb	73.3	22.6	2.5	10.53
Bd	30.8	6.5	2.0	22.31
Be	54.5	7.6	1.9	51.79
Ca	40.1	6.6	1.8	36.60
Cb	36.3	11.6	2.7	9.81
Cc	109.8	67.2	3.8	2.67

Figure 3.2 show that, in general, the design curves recommended by EC9 result in more conservative fatigue lifetime estimation than those obtained by using the IIW design curves. Further, these Wöhler diagrams together with Table 3.3 demonstrate that, for a given welded geometry, the negative inverse slope calculated from the entire population of data is lower than the corresponding value suggested by both EC9 and the IIW. This is an interesting aspect,

Chapter 3: Global and local stress-based approaches to estimate the fatigue strength of aluminium welded joints

especially in light of the fact that, as shown in Table 3.2 and Table A.2 to Table A.7, the negative inverse slope of the individual data sets is, in general, larger than the corresponding standard value.

To conclude, the nominal stress approach is a suitable and straightforward method to estimate the fatigue strength of aluminium-welded joints in particular EC9 was seen to provide a high-level of accuracy. Finally, it is important to highlight that the use of the design curves recommended both by EC9 and by the IIW to assess butt (Ab) and load-carrying cruciform Ca and Cb (Figure 3.2) welded joints is seen to result in estimates that are slightly non-conservative. Table 3.4 summarises the number of non-conservative prediction using EC9 ($P_s=97.7\%$) and the IIW ($P_s=95\%$).

Table 3.4 A summary of the amount of data fall below the design curve and the percentage of the data above the design curve

Welded Geometry		No. of samples below the design curve	Total No. of samples	% of samples above the design curve
Aa	EC9	0	360	100
	IIW	4		98.8
Ab	EC9	21	1372	98.5
	IIW	150		89.1
Ae	EC9	0	123	100
	IIW	1		99.2
Ba	EC9	0	251	100
	IIW	21		91.6
Bb	EC9	0	761	100
	IIW	7		99.1
Bd, Be, Ca	EC9	7	499	98.6
	IIW	62		87.6
Cb	EC9	2	512	99.6
	IIW	200		60.9
Cc	EC9	0	127	100
	IIW	0		100

3.3.2 Hot-spot stress approach

In the present investigation, hot-spot stresses were determined numerically according to the IIW procedure which is based on the use of different reference distances, with these lengths depending on the type of hot-spot stress and quality of mesh [30] (more details in Section 2.2.2.2). Linear-elastic bi-dimensional FE models were solved via commercial software ANSYS®. Weld beads were modelled as sharp V-notches, i.e., by taking the fillet radius along the intersection line between the weld and parent material invariably equal to zero.

3.3 Fatigue assessment results and discussion

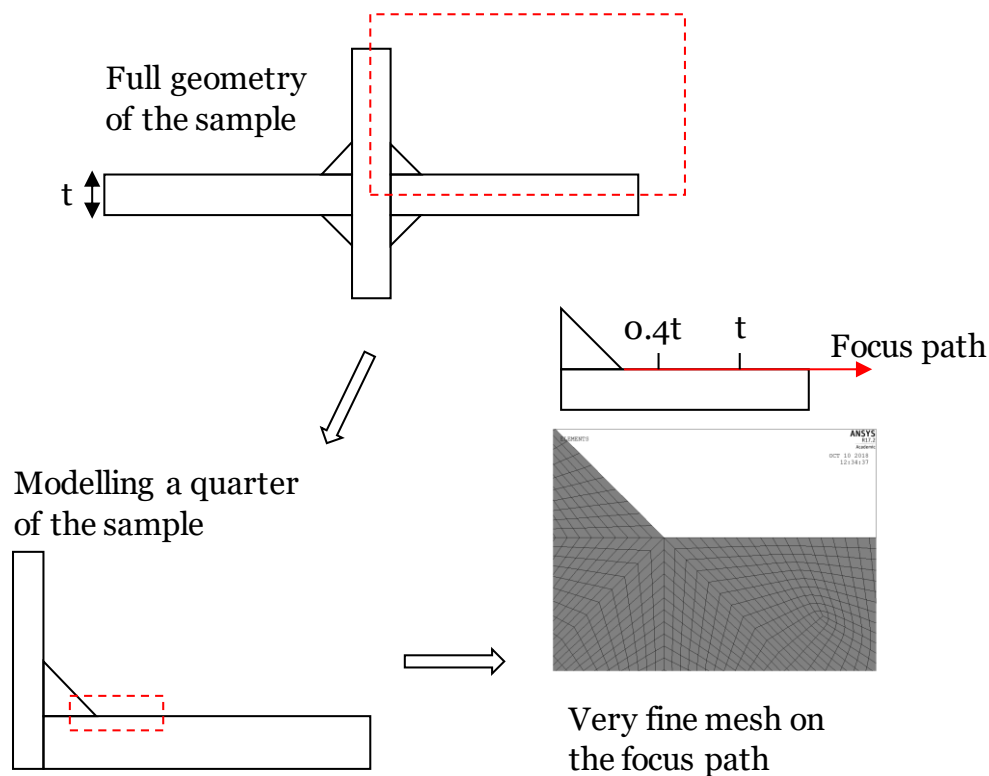


Figure 3.3 Example of the refined area around the focus path according to the hot spot stress approach.

The models were meshed according to the rules recommended by the IIW via eight-node solid quadratic elements (Plane 183). According to the symmetrical pattern of the investigated geometries and the need to achieve accurate results with less computing time, the FE models were solved by only modelling a quarter of the cruciform joints and a half of the T-joints. Figure 3.3 shows an example of a cruciform welded joints and the procedure followed to solve the 2D model. The mesh density was varied throughout the welded details to obtain fine mesh in the vicinity of the weld toes regions with element size in the range of 0.2–0.3 mm (Figure 3.3).

Parent and filler aluminium alloys were treated as linear-elastic, isotropic and homogeneous materials with Young's modulus equal to 68 GPa and Poisson's ratio equal to 0.33 [38]. Via these FE models, the corresponding hot-spot stresses were calculated using the surface stress extrapolation method as reviewed in Section 2.2.2.2.1. In particular, normal stresses were determined at two reference points positioned at a distance from the weld toe equal to $0.4t$ and t , respectively, with t being the thickness of the main plate as defined in Figure 3.4 [30].

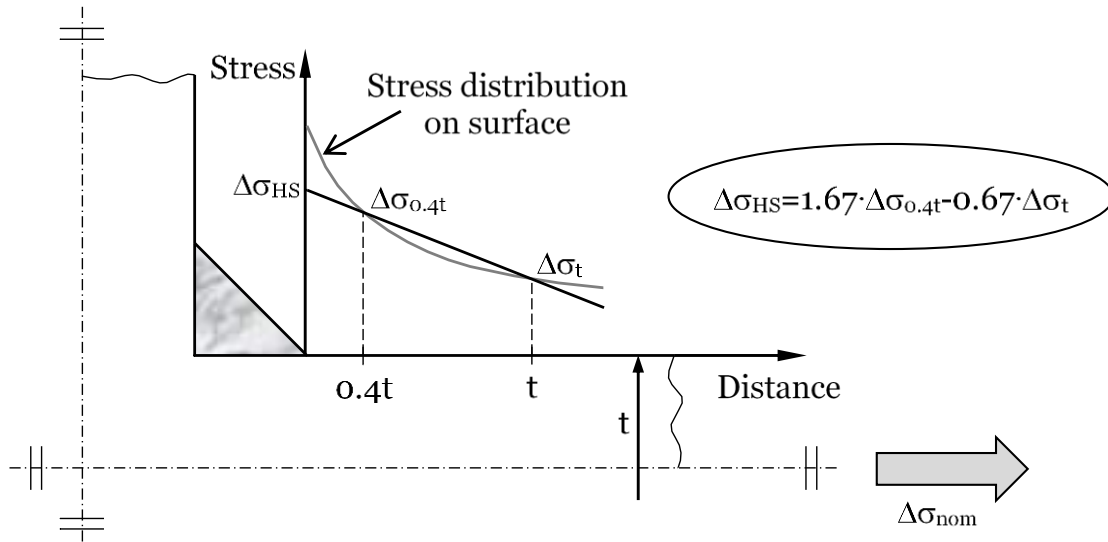


Figure 3.4 Definition of hot-spot stress.

The results from the statistical re-analysis performed by post-processing structural welded details Ba, Bb, Ca and Cb (Figure 3.1) according to the hot-spot stress approach are summarised in Appendix A (Table A.8 and Table A.9). The same data are also plotted in the Wöhler diagrams reported in Figure 3.5. The values of both the negative inverse slope, k , and the endurance limit ranges ($\Delta\sigma_{A,50\%}$ and $\Delta\sigma_{A,97.7\%}$) at $2 \cdot 10^6$ cycles to failure that were determined by reanalysing, for any given welded geometry, the entire population of data are reported in Table 3.5.

Table 3.5 Summary of the statistical re-analyses for the different approaches/welded geometries and corresponding recommended curves.

Welded Geometry	Hot-spot Stress			
	$\Delta\sigma_{A,50\%}$ [Mpa]	$\Delta\sigma_{A,97.7\%}$ [Mpa]	k	T_σ
Ba	51.2	13.3	1.9	14.87
Bb	75.8	20.1	2.2	14.30
Ca	65.4	17.3	2.2	14.36
Cb	40.7	11.4	2.4	12.67

3.3 Fatigue assessment results and discussion

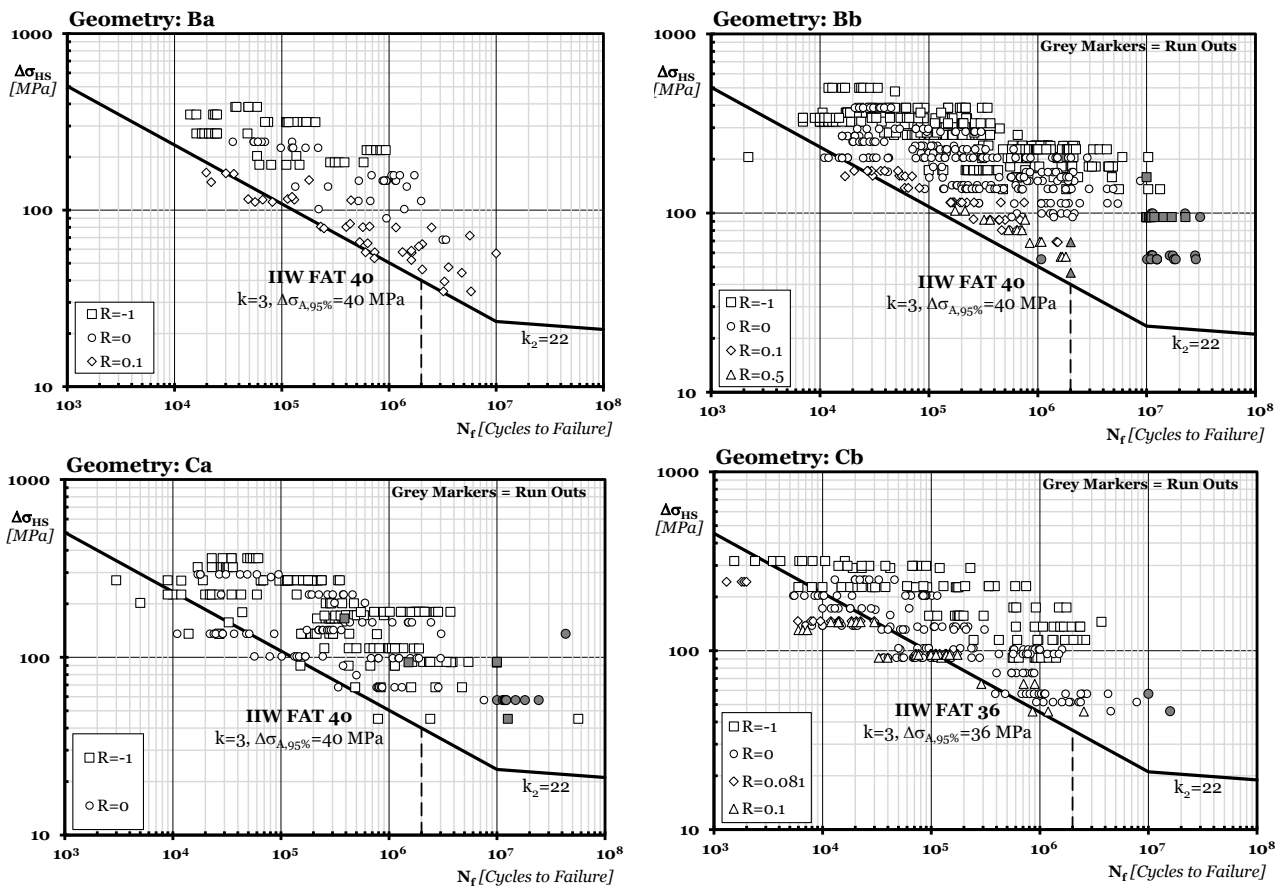


Figure 3.5 Accuracy of the Hot-Spot Stress approach in estimating the fatigue strength of the investigated welded joints.

The Wöhler diagrams of Figure 3.5 demonstrate that, as long as non-load-carrying cruciform connections (Ba) and T-joints (Bb) are concerned, the use of the hot-spot approach together with the design fatigue curves supplied by the IIW resulted in estimates that are not only accurate but also characterised by an adequate level of conservatism. On the contrary, it is clear that the use of the IIW design curves returned estimates that are characterised by a certain degree of non-conservatism when they are employed to assess the strength of load-carrying fillet welded joints (series Ca and Cb). As to this aspect, it is interesting to observe that for these welded geometries the level of non-conservatism is seen to increase as the load ratio increases.

To conclude, from Figure 3.5 it can be seen clearly that, compared to the nominal stress approach the accuracy in estimating the fatigue lifetime of welded joints has been improved. To conclude, according to both Figure 3.5 and Table 3.4, it can be noted that, for a given type of structural detail, the negative inverse slopes determined by reanalysing the entire population of data are lower not only than the k values associated with the individual data sets (Table A.8 and Table A.9) but also lower than the unifying value of 3 recommended by the IIW.

3.3.3 Effective notch stress approach

By taking advantage of the micro-support theory proposed by Neuber to model sharp cracks, back in the 1980s Radaj [39] has proposed to use a fictitious weld toe/root radius, r_{ref} , of 1 mm to assess the fatigue strength of welded connections having thickness larger than (or equal to) 5 mm. In contrast, for thin welded details having thickness lower than 5 mm, a fictitious radius, r_{ref} , of 0.05 mm is recommended as being employed [34, 40- 42]. The notch stress approach is restricted to welded joints in which fatigue cracks initiate either at the weld toe or at the weld root and, under uniaxial fatigue loading, the required stress analyses have to be performed in terms of maximum principal stress range.

As far as thick aluminium welded joints (i.e., $t \geq 5$ mm) are concerned, the IIW suggests performing the fatigue assessment via a master design curve characterised by an inverse negative slope equal to 3 and a notch stress endurance limit range, $\Delta\sigma_{A,97.7\%}$, at $2 \cdot 10^6$ cycles to failure equal to 71 MPa (for $P_S=97.7\%$). Turning to aluminium welded joints having a thickness lower than 5 mm, as mentioned earlier, weld toes and roots are recommended to be rounded by adopting a fictitious radius of 0.05 mm. To design thin aluminium welded joints against fatigue, Sonsino [42] suggests employing a reference design curve having an inverse negative slope equal to 3 and a notch stress endurance limit range, $\Delta\sigma_{A,97.7\%}$, at $2 \cdot 10^6$ cycles to failure equal to 180 MPa (for $P_S=97.7\%$). Figure 3.6 illustrates the fundamental aspects of the effective notch stress approach and the suggested radius reference values.

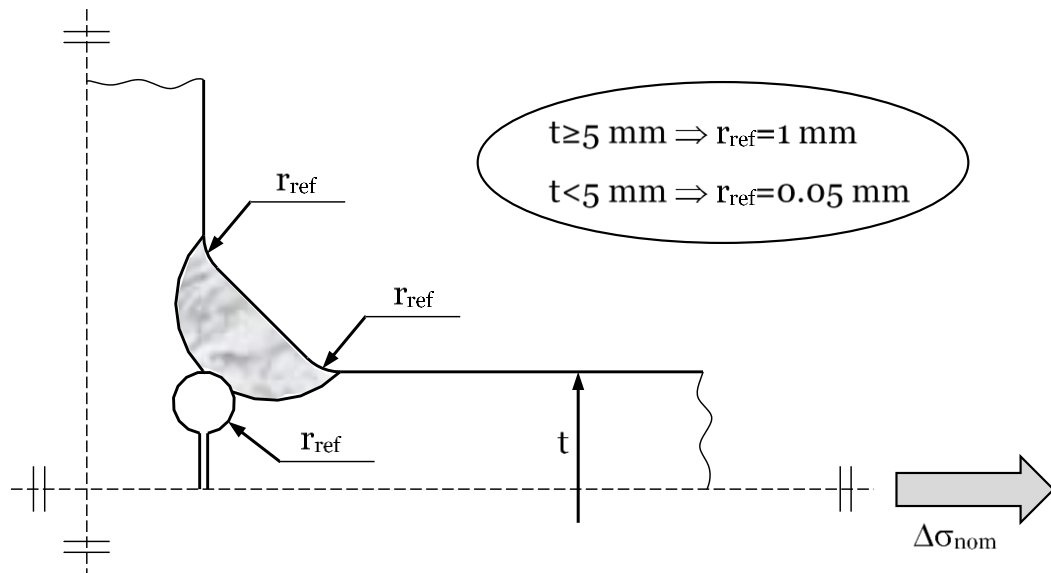


Figure 3.6 Weld toe and root rounded according to the reference radius concept.

The collected data were re-analysed by using FE code ANSYS® to solve linear-elastic bi-dimensional models. In these models, the same element type and the same material properties

3.3 Fatigue assessment results and discussion

as those used to calculate hot-spot stresses were employed. According to the thickness value, the structural details being investigated were modelled by rounding the toes/roots with a circular fillet having a radius equal to either 1 mm or 0.05 mm, this depending on the actual thickness of the main plate.

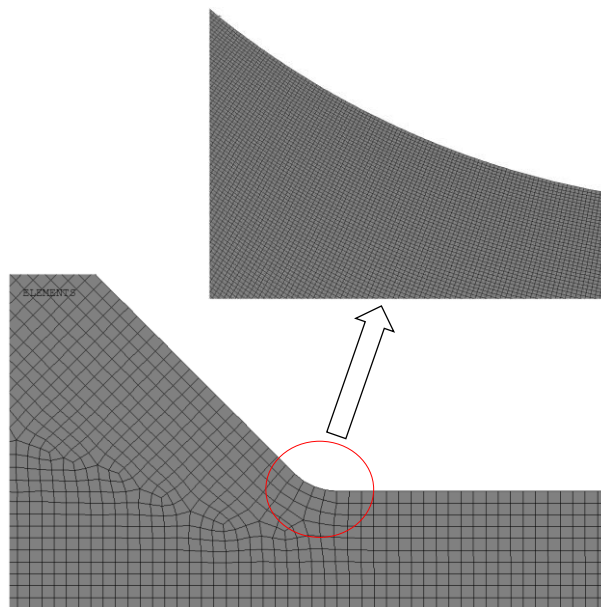


Figure 3.7 Example of FE model being solved using the Effective notch Stress approach.

As recommended by the IIW, the mesh in the vicinity of the fictitious fillets was refined until convergence occurred (Figure 3.7). This refinement process led to elements having a size in the critical regions ranging between 0.04- 0.06 mm for $r_{ref}=1$ mm and between 0.0025-0.0035 mm for $r_{ref}=0.05$ mm.

Table 3.6 Summary of the statistical re-analyses for the different approaches/welded geometries and corresponding recommended curves.

Welded Geometry	Effective notch Stresses			
	$\Delta\sigma_{A,50\%}$ [Mpa]	$\Delta\sigma_{A,97.7\%}$ [Mpa]	k	T_σ
Ba \geq 5	113.2	35.1	2.0	10.40
Ba $<$ 5	314.6	85.1	4.3	2.13
Bb \geq 5	145.7	33.3	2.0	19.17
Bb $<$ 5	218.9	85.9	3.1	6.50
Ca \geq 5	129.8	34.0	2.2	14.55
Cb \geq 5	121.3	40.8	2.7	8.83
Cb $<$ 5	297.9	26.2	2.5	20.05

Chapter 3: Global and local stress-based approaches to estimate the fatigue strength of aluminium welded joints

The results from the statistical re-analysis performed by post-processing welded geometries Ba, Bb, Ca and Cb (Figure 3.1) in terms of linear-elastic notch stress are listed in Appendix A, Table A.8 and Table A.9. The individual experimental results are plotted instead in the log-log charts of Figure 3.8. Table 3.6 lists the values of k as well as of $\Delta\sigma_A$, 50% and $\Delta\sigma_A$, 97.7% at $2 \cdot 10^6$ cycles to failure determined by re-analysing the entire population of data for any welded geometry being considered.

The Wöhler diagrams of Figure 3.8 shows that the use of the Effective Notch Stress approach along with the design fatigue curve supplied by the IIW [25] for $t \geq 5$ mm and by Sonsino [42] for $t < 5$ mm resulted in estimates that are not only accurate, but also characterised by an adequate level of conservatism.

To conclude, according to Figure 3.8 and Table 3.6, although the in-field usage of this approach requires a considerable computational effort, the Effective Notch Stress approach certainly is the most accurate design method amongst those recommended by the IIW.

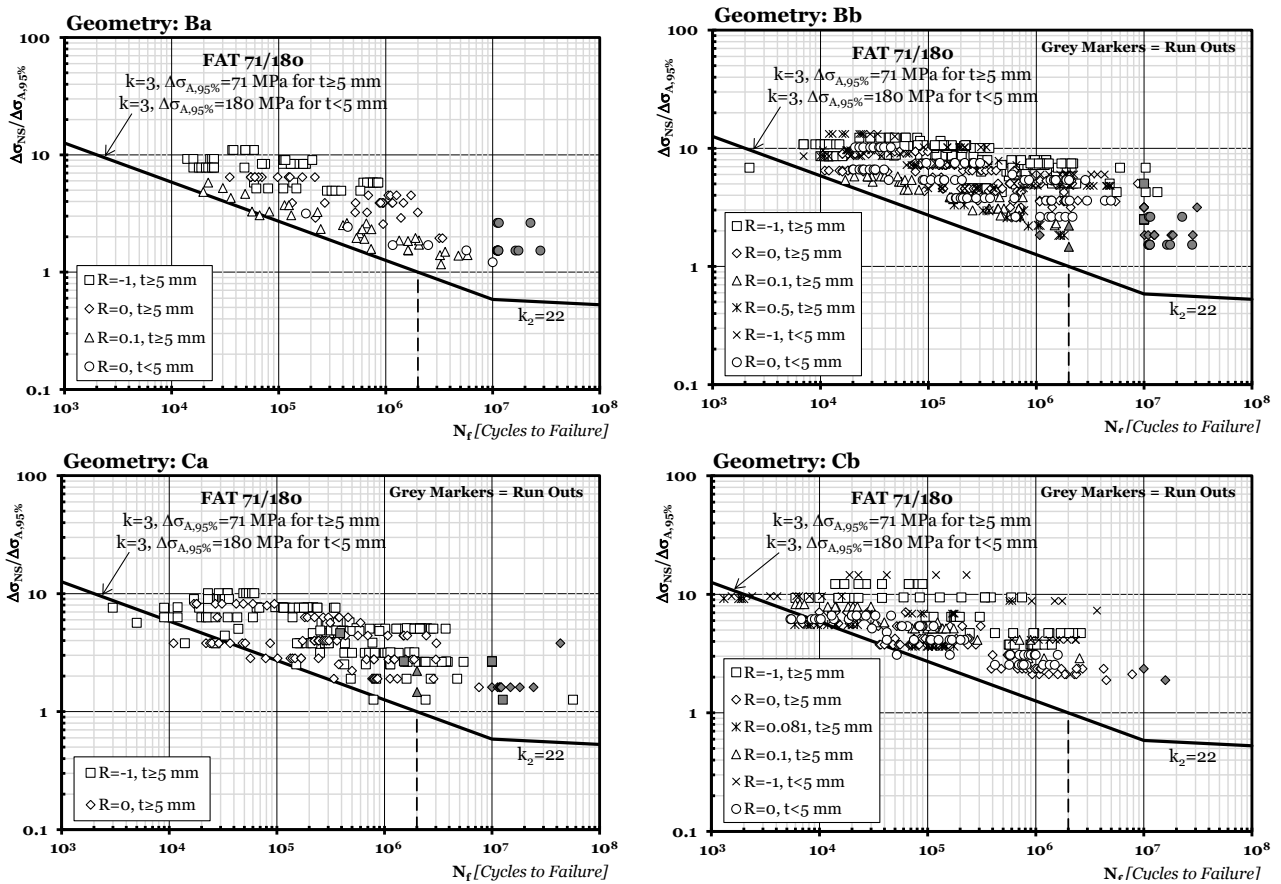


Figure 3.8 Accuracy of the Effective Notch Stress approach in estimating the fatigue strength of the investigated welded joints.

3.3.4 N-SIF approach

As mentioned in chapter 2, section 2.2.2.4, the N-SIFs approach takes as a starting point the fact that linear-elastic stress fields in the vicinity of sharp V-notches can be described concisely by using N-SIFs. The accuracy and reliability of the N-SIF approach was initially checked by considering steel fillet welded joints with thickness varying in the range 13-100 mm. Subsequently, Lazzarin and Livieri extended the use of this design method to aluminium-welded joints by proposing a specific design curve that was derived by considering a large number of experimental data [28]. This master curve is characterised by a reference Mode I N-SIF range, $\Delta K_{I,97.7\%}$, at $5 \cdot 10^6$ cycles to failure equal to $74 \text{ MPa} \cdot \text{mm}^{0.326}$ (for $P_S=97.7\%$) and a negative inverse slope equal to 4.

In the present investigation, to re-analyse the experimental data generated by testing non-load carrying fillet welded joints, Mode I N-SIF ranges were estimated using the following relationship [24, 43]:

$$\Delta K_I = k_I \cdot \Delta \sigma_{\text{nom}} \cdot t^{1-\lambda_1} \quad (3.1)$$

Where, k_I is a non-dimensional parameter, which depends on the absolute dimensions of the joint, $\Delta \sigma_{\text{nom}}$, is the range of the nominal stress, and t is the thickness of the main plate. The Mode I N-SIF ranges associated with the other geometries were instead determined numerically according to definition (3.2):

$$\left\{ \begin{array}{c} \sigma_\theta \\ \sigma_r \\ \tau_{r\theta} \end{array} \right\}_{\rho=0} = \frac{1}{\sqrt{2\pi}} \frac{r^{\lambda_1-1} K_I}{(1+\lambda_1) + \chi_1(1-\lambda_1)} \left[\left\{ \begin{array}{c} (1+\lambda_1)\cos(1-\lambda_1)\theta \\ (3-\lambda_1)\cos(1-\lambda_1)\theta \\ (1-\lambda_1)\sin(1-\lambda_1)\theta \end{array} \right\} + \chi_1 \left\{ \begin{array}{c} \cos(1+\lambda_1)\theta \\ -\cos(1+\lambda_1)\theta \\ \sin(1+\lambda_1)\theta \end{array} \right\} \right] \quad (3.2)$$

In the solved FE models, fillet welds were modelled by setting the toe radius equal to zero. The mesh density in the weld region (Figure 3.9) and the associated N-SIF values were then determined according to the numerical procedure proposed by Tovo and Lazzarin in Ref. [24, 43]. First, the resulting stress field was determined along the bisector using FE models. By applying Eq.(3.3) and (3.4) and to the results generated from the FE models, the stresses along the bisector closer to the tip can be used to calculate the N-SIFs.

$$K_1 = \sqrt{2\pi} \lim_{r \rightarrow 0} (\sigma_\theta)_{\theta=0} r^{1-\lambda_1} \quad (3.3)$$

$$K_2 = \sqrt{2\pi} \lim_{r \rightarrow 0} (\tau_{r\theta})_{\theta=0} r^{1-\lambda_2} \quad (3.4)$$

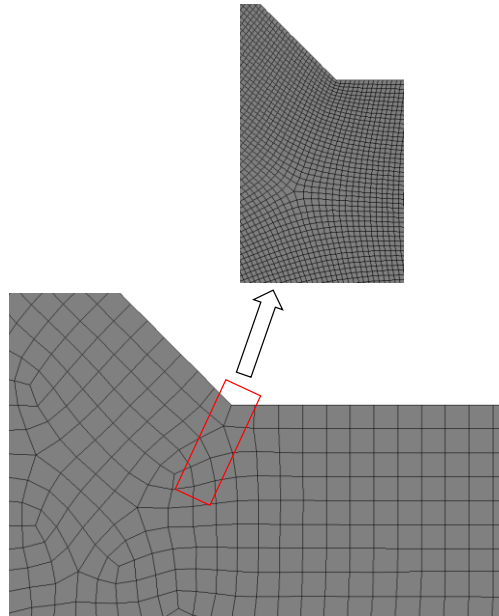


Figure 3.9 Example of FE model being solved using the N-SIFs and Point Method.

The results from the statistical re-analysis performed by post-processing welded geometries Ba, Bb, Ca and Cb (Figure 3.1) according to the N-SIF approach are listed in Appendix A (Table A.10 and Table A.11). The corresponding individual experimental data are instead plotted in the ΔK_I vs. N_f diagrams reported in Figure 3.10. The values of both the negative inverse slope, k , and the endurance limits expressed in terms of N-SIF range extrapolated at $2 \cdot 10^6$ cycles to failure (i.e., $\Delta K_{I,50\%}$ for $P_S=50\%$ and $\Delta K_{I,97.7\%}$ for $P_S=97.7\%$) that were determined by re-analysing, for any given welded geometry, the entire population of data are reported in Table 3.7.

Table 3.7 Summary of the statistical re-analyses for the different approaches/welded geometries and corresponding recommended curves.

Approach	Welded Geometry	Nominal Stress			
		$\Delta\sigma_{A,50\%}$ [Mpa]	$\Delta\sigma_{A,97.7\%}$ [Mpa]	k	T_σ
N-SIF	Ba	119.5	43.7	2.3	7.46
	Bb	150.4	34.9	2.1	18.57
	Ca	112.0	21.6	1.9	26.91
	Cb	120.7	48.9	3.0	6.09

3.3 Fatigue assessment results and discussion

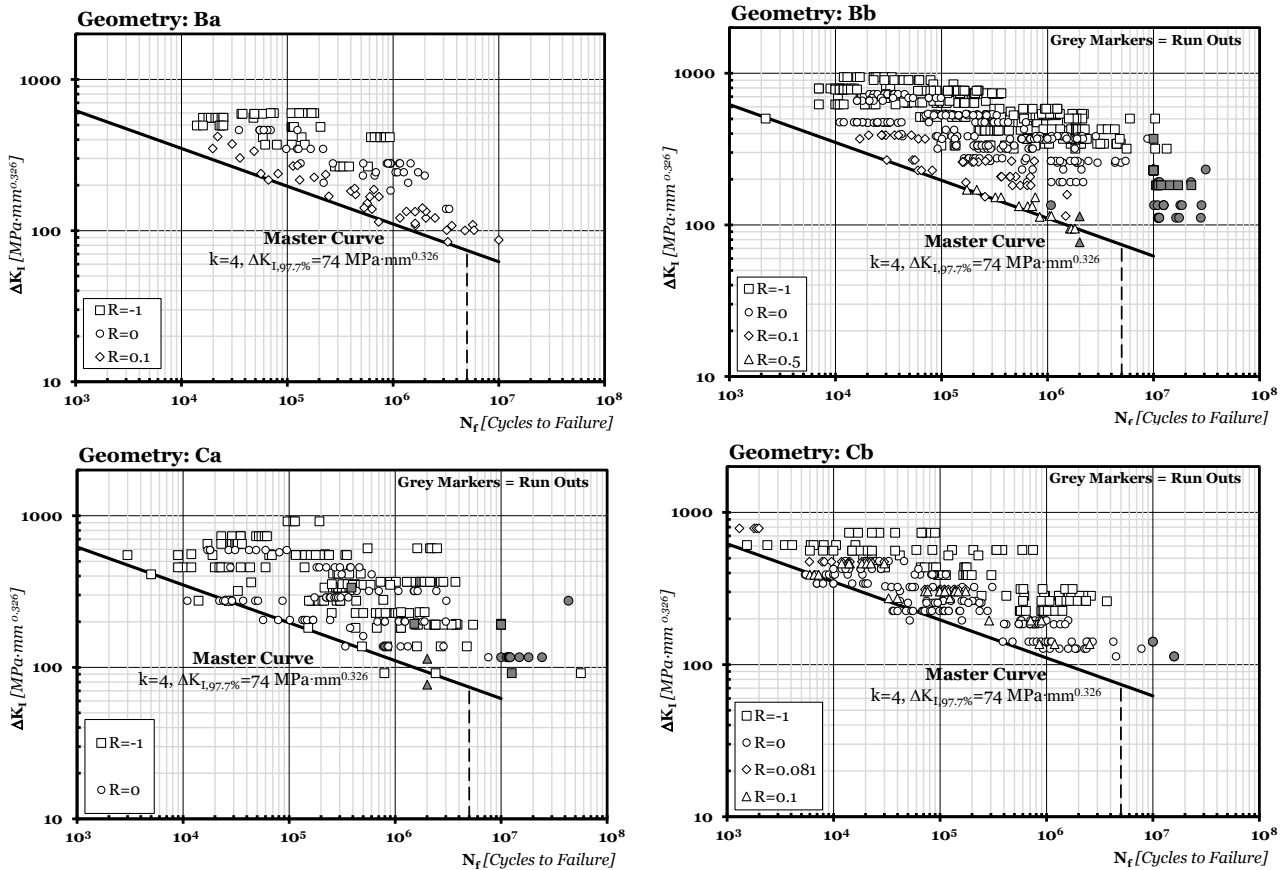


Figure 3.10 Accuracy of the N-SIF approach in estimating the fatigue strength of the investigated welded joints.

According to the charts of Figure 3.10, Lazzarin and Livieri’s master curve was capable of estimating the considered experimental results with a high level of accuracy, with this holding true independently of the type of joint being considered. It is interesting to observe that, as for the approaches investigated in the previous sections, the level of conservatism characterising the N-SIF approach is seen to decrease as the applied load ratio increases. Nevertheless, the aforementioned diagrams further confirm that the N-SIF approach is a powerful design tool suitable for designing aluminium welded joint against fatigue by systematically reaching an adequate level of accuracy/safety.

3.3.5 TCD

The PM represents the simplest formalisation of the TCD and postulates that the stress to be used to estimate the fatigue damage extent is equal to the linear elastic-stress determined at a given distance from the assumed crack initiation location. Its simplicity makes the PM a straightforward design tool suitable for being used in situations of practical interest to perform the fatigue assessment of real welded components. Accordingly, in the present investigation the accuracy of the TCD in estimating fatigue lifetime of aluminium-welded joints was checked by applying this powerful theory solely in the form of the PM.

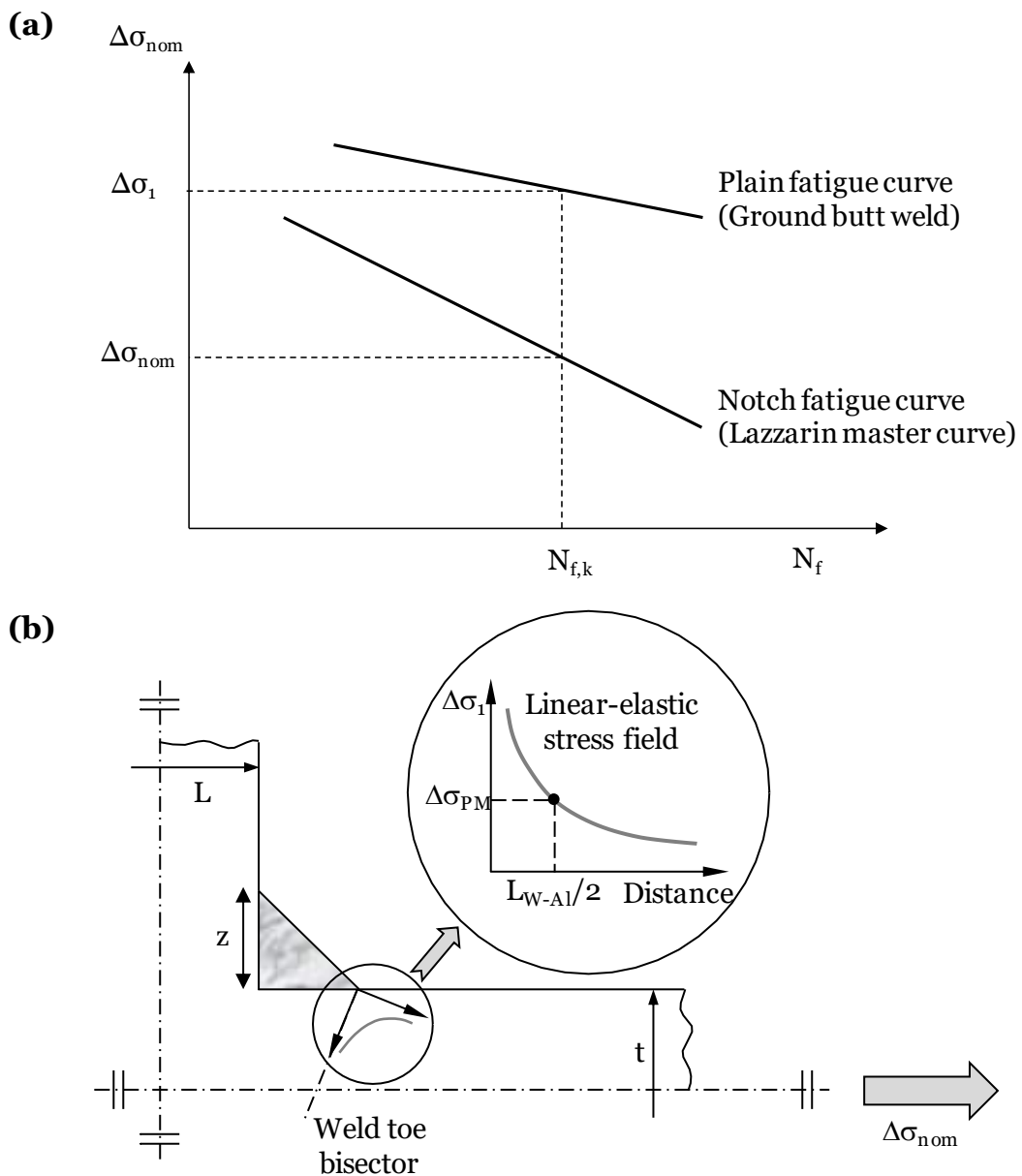


Figure 3.11 Determination of the critical distance value using two calibration fatigue curves (a); Local stress-distance curve and critical distance L_{W-AI} according to the PM (b).

3.3 Fatigue assessment results and discussion

Following a strategy similar to the one adopted in Ref. [1], the PM was calibrated by making the following assumptions:

- The fatigue strength of ground butt welded joints under uniaxial fatigue loading is modelled via the EC9 fatigue curve recalculated for $P_S=50\%$ (i.e., $\Delta\sigma_{A,50\%}=79.2$ MPa at $2\cdot 10^6$ cycles to failure and $k=4.5$);
- The $P_S=50\%$ reference master curve suggested by Lazzarin and Livieri for aluminium welded joints ($\Delta K_{I,50\%}=124.5$ MPa \cdot mm $^{0.326}$ at $2\cdot 10^6$ cycles to failure and $k=4$ [31]) is used as reference notch fatigue curve.

By using these two pieces of calibration information, a unifying value for the critical distance, L_{W-Al} , suitable for designing aluminium-welded joints was then determined as follows:

- by making t , L and z vary (see welded geometry in Figure 3.11), the $P_S=50\%$ N-SIF master curve and Eq. (3.1) were used to estimate the corresponding nominal stress range, $\Delta\sigma_{nom,50\%}$, at $2\cdot 10^6$ cycles to failure;
- subsequently, under the estimated values for $\Delta\sigma_{nom,50\%}$, the corresponding local stress distributions were determined along the weld toe bisector in terms of maximum principal stress $\Delta\sigma_1$ (Figure 3.11) [1, 44], with these stress-distance curves being estimated both numerically (Fig. 4c) and analytically via Eq. (3.2);
- Finally, according to the PM, by plotting, at $2\cdot 10^6$ cycles to failure, the linear-elastic stress field for the welded geometry being considered as well as the ground butt weld endurance limit, i.e. $\Delta\sigma_{A,50\%}=79.2$ MPa, critical distance value L_{W-Al} was estimated directly via the abscissa of the point at which these two stress-distance curves crossed each other (Figure 3.11).

Table 3.8 Influence of the welded joint's absolute dimensions on the estimated value for L_{W-Al} .

$\Delta\sigma_{A,50\%}^{(1)}$ [MPa]	$\Delta K_{I,50\%}^{(1)}$ [MPa \cdot mm $^{0.326}$]	$t=L=Z$ [mm]	$\Delta\sigma_{nom,50\%}^{(1)}$ [MPa]	L_{W-Al} [mm]
79.2	124.5	8	52.7	0.50
		12	46.2	0.49
		16	42.1	0.49
		20	39.1	0.48

⁽¹⁾ at $2\cdot 10^6$ cycles to failure.

Since Lazzarin and Livieri's N-SIF master curve was determined by post-processing a large number of experimental data generated by testing aluminium cruciform joints having absolute dimensions in the range 3-24mm [26, 28], the procedure describe above was applied by considering different values for t , L and z (see welded geometry Ca in Figure

Chapter 3: Global and local stress-based approaches to estimate the fatigue strength of aluminium welded joints

3.1)). This was done in order to check whether the estimated critical distances were affected by the absolute dimensions of the welded joint being used for calibration (scale effect in fatigue).

Table 3.8 summarises the results of this sensitivity analysis that was performed by taking t , L and z equal to 8, 12, 16 and 20mm. Table 3.7 demonstrates that, from an engineering point of view, the influence of the welded connection's absolute dimensions on the estimated values for length L_{W-AI} can be neglected with little loss of accuracy. Accordingly, for the sake of design simplicity, the $L_{W-AI/2}$ value to apply the PM to design aluminium-welded joints against fatigue was taken invariably equal to 0.25 mm, i.e.:

$$L_{W-AI} = 0.5 \text{ mm} \tag{3.5}$$

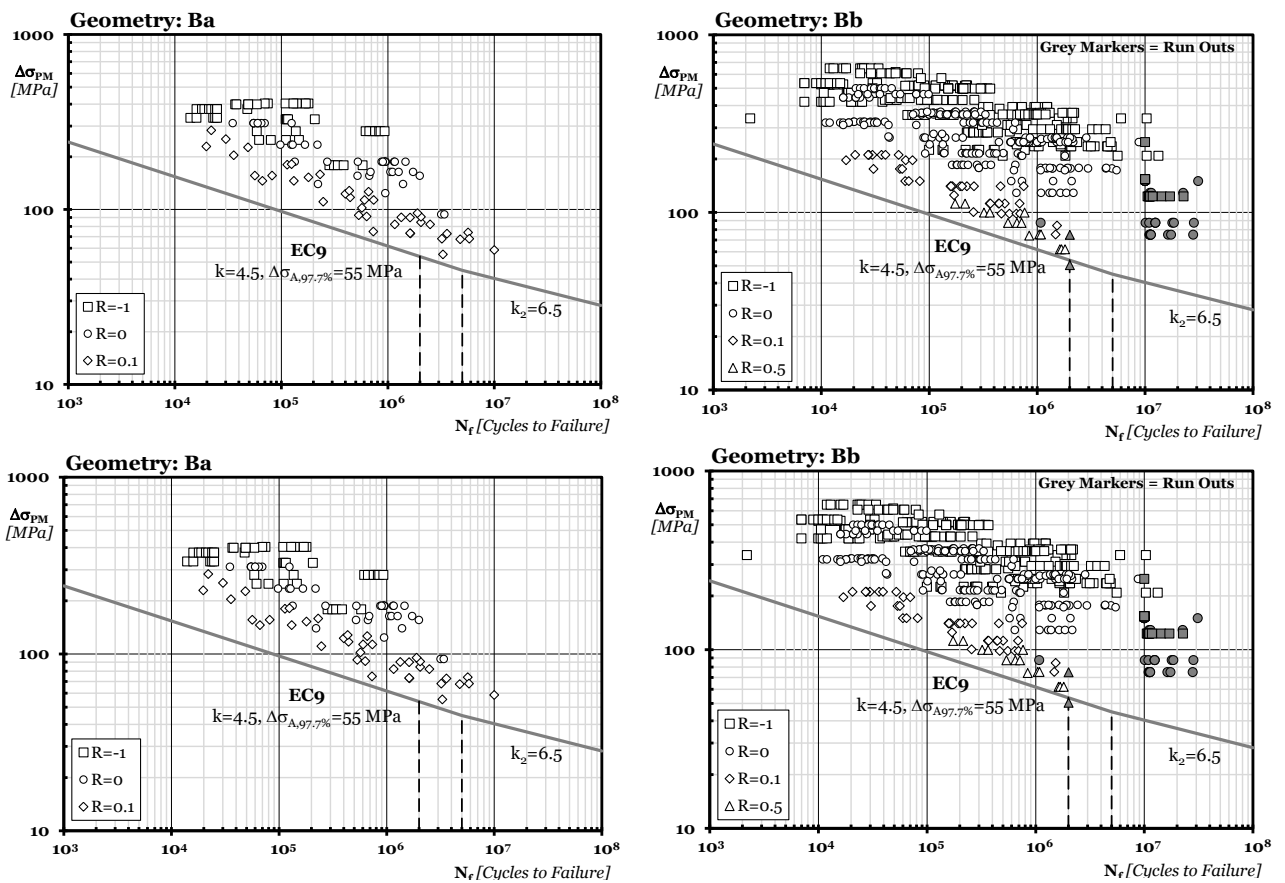


Figure 3.12 Accuracy of the PM in estimating the fatigue strength of the investigated welded joints.

Once the critical distance was determined, the experimental results summarised in Table A.10 and Table A.11 (Appendix A) were post-processed to determine the linear-elastic PM stress range, $\Delta\sigma_{PM}$, at a distance from the weld toe equal to $L_{W-AI/2}=0.25$ mm, the required linear-elastic stress fields being determined by taking the weld toe radius invariably equal to zero.

3.3 Fatigue assessment results and discussion

The experimental results summarised in those tables are also plotted in the $\Delta\sigma_{PM}$ vs. N_f log-log diagrams reported in Figure 3.12, the $P_S=97.7\%$ reference design curve being that recommended by EC9 to assess the fatigue strength of ground butt welded joints (i.e., $\Delta\sigma_{A,97.7\%}=55$ MPa at $2 \cdot 10^6$ cycles to failure and $k=4.5$). These charts make it evident that the TCD applied by taking $L_{W-Al/2}=0.25$ mm resulted in highly accurate estimates, with this holding true independently of type of joint and absolute dimensions. It is also interesting to observe that, according to Table 3.9, the negative inverse slope, k , determined, for any considered welded geometry, by post-processing the entire population of data was seen to be lower than the value of 4.5 characterising the EC9 design curve used as reference information not only to estimate L_{W-Al} , but also to assess the overall accuracy of the PM (Figure 3.12). This results in the fact that, as for the other design methods being considered in the present investigation, the endurance limits for series Ba, Bb, Ca and Cb were seen to be lower than the corresponding endurance limit of the EC9 reference design fatigue curve being adopted (see Table 3.9).

To conclude, the charts of Figure 3.12 fully support the idea that the TCD can be used to perform the fatigue assessment of aluminium weldments by directly post-processing the linear-elastic stress fields acting on the material in the weld regions. Its systematic usage was seen to result in highly accurate estimates, the computational effort required for its in-field usage being lower than the one required to apply both the Effective Notch Stress method and the N-SIF approach.

Table 3.9 Summary of the statistical re-analyses for the different approaches/welded geometries and corresponding recommended curves.

Approach	Welded Geometry	Nominal Stress			
		$\Delta\sigma_{A,50\%}^{(1)}$ [Mpa]	$\Delta\sigma_{A,97.7\%}^{(2)}$ [Mpa]	k	T_σ ⁽³⁾
TCD	Ba	80.0	29.0	2.3	7.62
	Bb	88.5	16.8	1.8	27.74
	Ca	89.2	23.4	2.2	14.6 0
	Cb	81.4	33.0	3.0	6.09

3.3.6 Mean stress effect on the fatigue strength of aluminium weldments

In order to check the accuracy and reliability of the enhancement factors reported in chapter 2, section, section 2.2.1.3 for Case I and Case II, all the data considered in the present investigation were post-processed to compare the experimental value of $f(R)$ to the corresponding value estimated according to Eqs. (2.14) and (2.15) in section 2.2.1.3. In

Chapter 3: Global and local stress-based approaches to estimate the fatigue strength of aluminium welded joints

particular, independently of the type of welded joint and adopted definition for the design stress, the experimental values for the enhancement factors were calculated as follows:

$$f(R) = \frac{\Delta\sigma_{A,97.7\%}|_{\text{experimental}}}{\Delta\sigma_{A,97.7\%}|_{\text{fatigue class}}} \text{ or } f(R) = \frac{\Delta\sigma_{A,95\%}|_{\text{experimental}}}{\Delta\sigma_{A,95\%}|_{\text{fatigue class}}} \quad (3.6)$$

In a similar way, the enhancement factors for the N-SIF approach were determined as:

$$f(R) = \frac{\Delta K_{I,97.7\%}|_{\text{experimental}}}{\Delta K_{I,97.7\%}|_{\text{master curve}}} \quad (3.7)$$

The results of this analysis are summarised in the $f(R)$ vs. R diagrams of Figure 3.13 (a-f). These charts make it evident that, independently of the adopted design strategy, the experimentally determined values for enhancement factor $f(R)$ are highly scattered. However, in spite of such a large level of scattering, the diagrams of Figure 3.13 (a-f) confirm that, on average, the fatigue strength of aluminium-welded joints tends to increase as the load ratio decreases.

In order to assess the experimental values obtained for $f(R)$ from the different data sets being re-analysed, in these diagrams also the straight lines plotted according correction rules Eqs. (2.14) and (2.15) are also reported. These charts make it evident that the strategies being suggested by both EC9 and the IIW to enhance the strength of aluminium-welded joints subjected to in-service load ratios lower than zero are highly conservative.

This precautionary approach is clearly justified by the fact that the effect of non-zero mean stresses on the overall fatigue strength of aluminium-welded joints depends on a large number of variables, which include, amongst other: technological aspects characterising the specific welding technique being employed, quality of the joints, environmental conditions, and type of applied loading. Accordingly, given a specific welded connection, the only way to accurately quantify its sensitivity to the presence of superimposed static stresses is by running appropriate experiments, with this clearly increasing the time and costs associated with the design problem.

However, it has to be said that real structures are seen to be much less sensitive to the presence of non-zero mean stresses than the laboratory specimens [44]. This explains the reason why in situations of practical interest, aluminium welded joints are usually designed by taking the enhancement factor, $f(R)$, invariably equal to unity – i.e., Case III, Eq. (2.16).

3.3 Fatigue assessment results and discussion

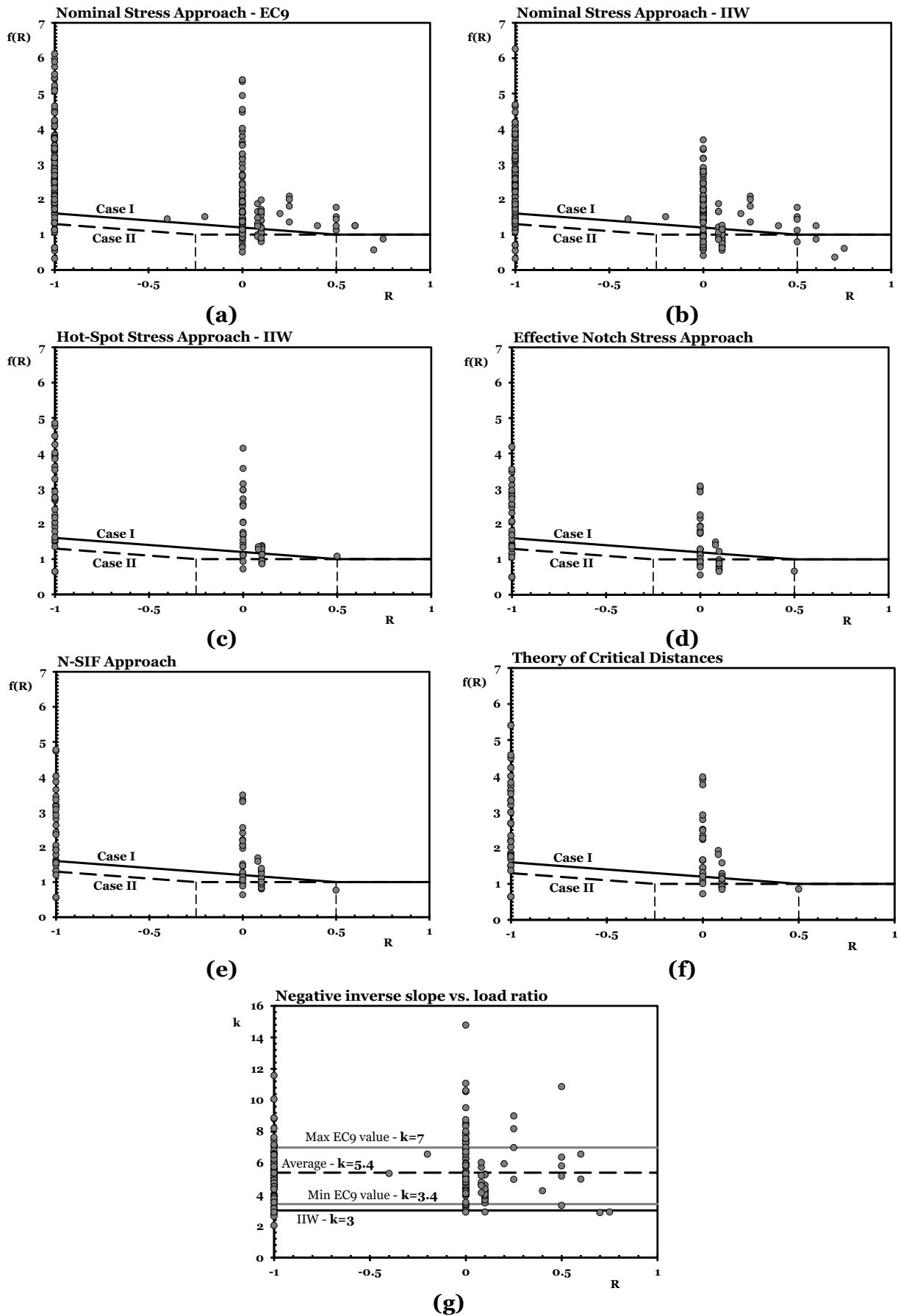


Figure 3.13 Effect of load ratio R on the fatigue strength of aluminium welded joints.

To conclude, the chart of Figure 3.13g plots the experimental values for the negative inverse slope vs. the applied load ratio, the reported k values being those calculated by post-processing the data sets considered in the present investigation. The above chart makes it evident that, on average, the negative inverse slope is not affected by the applied value of load ratio R , with this fully confirming the validity of the assumptions on which the standard corrections recommended as being used to take into account the presence of non-zero mean stresses are based. Finally, Figure 3.13g confirms that the value of 3 suggested by the IIW is conservative, whilst the values for the negative inverse slope supplied by EC9 are capable of capturing the observed experimental reality more accurately.

3.4 Conclusions

- The use of the design curves recommended both by EC9 and the IIW to perform the fatigue assessment of aluminium-welded joints according to the Nominal Stress approach is seen to result in an adequate level of accuracy, with the estimates being, on average, conservative.
- The data sets considered in the present investigation fully confirm the fact that the Hot-Spot approach can be used successfully to design real aluminium welded joints against fatigue.
- The Effective Notch Stress approach is seen to be the most accurate design methodology recommended by the IIW. However, it requires intensive computational effort to model weld toes and roots by introducing the required fillet radii (with this holding true especially in the presence of complex three-dimensional welded geometries).
- The re-analysis discussed in the present paper further confirms the well-known accuracy of the N-SIF approach in estimating fatigue lifetime of aluminium-welded joints.
- The TCD applied in the form of the PM is seen to be highly accurate in assessing the strength of aluminium-welded joints subjected to fatigue loading.
- The TCD can be used in situations of practical interest to design, in terms of maximum principal stress, aluminium welded joints against fatigue by taking the required critical distance value, L_{W-Al} , invariably equal to 0.5 mm.
- As far as aluminium welded, joints are concerned, the enhancement factors recommended both by EC9 and the IIW are seen to result in conservative estimates. Accordingly, experimental trials should be run in order to assess accurately the sensitivity of the specific welded joints being designed to the presence of non-zero mean stresses.

3.5 Reference

- [1] Susmel L. The Modified Wöhler Curve Method calibrated by using standard fatigue curves and applied in conjunction with the Theory of Critical Distances to estimate fatigue lifetime of aluminium weldments. *Int J Fatigue* 2009; 31:197-212. 226.
- [2] Neumann A. Theoretische Grundlagen der Austwertung von Dauerfestigkeitsversuchen aus Schweißverbindungen und geschweißten Bauteilen aus Al Mg- Legierungen *Wissenschaftl. Wissenschaftliche Zeitschrift der Technischen Universität Karl-Marx-Stadt, Chemnitz, G.*
- [3] Anon. Minutes of the meeting of the Working Group on fatigue issues in shipbuilding. The Shipbuilding Engineering Society, Blohm & Voss AG, Hamburg, 1973 (www.blohmvooss.com). .
- [4] Person NL, Fatigue of aluminium alloy welded joints. *Welding Research Supplement* 1971;3:77s-87s. .
- [5] Wood JL. Flexural fatigue strength of butt welds in Np.5/6 type aluminium alloy. *British Welding Journal* 1970;7(5):365-380. .
- [6] Atzori B, Bufano R. Raccolta di dati sulla resistenza a fatica dei giunti saldati in Al Mg5. University of Bari, Bari, Italy, Report no. 76/4, November 1976 .
- [7] Haibach E, Kobler HG. Beurteilung der Schwingfestigkeit von Schweißverbindungen aus AlZnMg_i auf dem Weg einer örtlichen Dehnungsmessung. *Aluminium* 1971;47:725-730. .
- [8] Mindlin H. Fatigue of Aluminium Magnesium Alloys. *Welding Research Supplement* 1963;1:276-281. .
- [9] Gunn KW, McLester R. Effect of Mean Stress on Fatigue Properties of Aluminium Butt Welded Joints. *Welding Research Abroad*, 1960;6(7):53-60. .
- [10] Newman RP. Fatigue tests on butt welded joints in Aluminium Alloys HE.30 and NP. 5/6. *British Welding Journal* 1959;6(7):324-332. .
- [11] Gunn KW, Lester MC. Fatigue Strength of welded joints in Aluminium Alloys. *British Welding Journal* 1962;9(12):634-649. .
- [12] Jacoby G. Über das Verhalten von Schweißverbindungen aus Aluminiumlegierungen bei Schwingbeanspruchung. Dissertation, Technische Hochschule, Hannover, 1961. .

3.5 Reference

- [13] Andrew RC, Waring J. Axial-Tension Fatigue in Aluminium MIG Welding. *Met Const and Brit Weld Journal* 1974; 6:8-11. .
- [14] De Money FW, Wolfer GC. Fatigue Properties of plate and Butt Weldment of 5083-H 113 at 75 and- 300F. *Advances in Cryogenic Engineering*, Plenum Press, NY, USA, 1961; 6:590-603. 28 .
- [15] Haibach E, Atzori B. A Statistical Re-analysis of Fatigue Test Results on Welded Joints in AlMg5. Fraunhofer-Gesellschaft, Report No. FB-116, 1974. .
- [16] Kiefer TF, Keys RD, Schwartzberg FR. Determination of low-Temperature Fatigue Properties of Structural Metal Alloys. Martin Company Report CR, pp. 65-70, October 1965. .
- [17] Atzori B, Indrio, P. Comportamento a fatica dei ciunti saldati in Al Zn Mg1, Al Zn4 Mg1 ED Al Mg Si. University of Bari, Bari, Italy, Report No. 76/5, December 1976. .
- [18] Kosteas D. Zur systematische Auwertung von Schwingfestigkeit von Schwingfestigkeitsuntersuchungen bei Aluminiumlegierungen. Dissertation, University of Munich, Germany, 1970. .
- [19] Kosteas D. Versuchsergebnisse aus Schwingfestigkeitsuntersuchungen mit Al Zn Mg1 und Al Mg4.5 Mn. VA Berich NR 5889/2, 25 2, 1973. .
- [20] Sidhom N, Laamouri A, Fathallah R, Braham C, Lieurade HP. Fatigue strength improvement of 5083 H11 Al-alloy T-welded joints by shot peening: experimental characterization and predictive approach. *Int J Fatigue* 2005;27:729-745. .
- [21] Maddox SJ. Scale effect in fatigue of fillet welded aluminium alloys. *Proceedings of the Sixth International Conference on Aluminium Weldments*, Cleveland, Ohio, pp. 77–93, 1995..
- [22] Meneghetti G. Design approaches for fatigue analysis of welded joints. PhD Thesis, Univeristy of Padova, Padova, Italy, 1998. .
- [23] Riberio AS, Goncalves JP, Oliveria F, Castro PT, Fernandes AA. A comparative study on the fatigue behaviour of aluminium alloy welded and bonded Joints. *Proceeding of the Sixth International Conference on Aluminium Weldments*, Cleveland, Ohio, 65–76..
- [24] Lazzarin P, Tovo R. A notch intensity factor approach to the stress analysis of welds. *Fatigue Fract Engng Mater Struct* 1998;21:1089-1103..
- [25] Lazzarin P, Lassen T, Livieri P. A notch stress intensity approach applied to fatigue life predictions of welded joints with different local toe geometry. *Fatigue Fract Engng Mater Struct*, 2003;26:49-58..

Chapter 3: Global and local stress-based approaches to estimate the fatigue strength of aluminium welded joints

- [26] Lazzarin P, Livieri P. Notch stress intensity factors and fatigue strength of aluminium and steel welded joints. *Int J Fatigue* 2001;23:225-232..
- [27] Susmel L, Taylor D. A novel formulation of the theory of critical distances to estimate lifetime of notched components in the medium-cycle fatigue regime. *Fatigue Fract Engng Mater Struct* 2007;30:567-581..
- [28] Livieri P, Lazzarin P. Fatigue strength of steel and aluminium welded joints based on generalised stress intensity factors and local strain energy values. *Int J Fracture* 2005;133(3):247–276..
- [29] Eurocode 9: Design of aluminium structures – Part 2: Structures susceptible to fatigue, prENV 1999. .
- [30] Hobbacher A. Recommendations For Fatigue Design of Welded Joints and Components IIW document XIII-2151-07/XV-1254-07, 2007. .
- [31] Hobbacher AF. New developments at the recent update of the IIW recommendations for fatigue of welded joints and components. *Steel Construction* 2010; 3(4):231-242. .
- [32] Spindel JE, Haibach E. Some considerations in the statistical determination of the shape of S-N curves. In: *Statistical Analysis of Fatigue Data*, ASTM STP 744 (Edited by R. E. Little and J. C. Ekvall), pp. 89–113, 1981. .
- [33] Hertzberg RW. *Deformation and Fracture Mechanics of Engineering Materials*, 4th edn, Chichester, Wiley, New York, USA, 1996. .
- [34] Haibach E. *Service fatigue-strength – methods and data for structural analysis*. VDI, Düsseldorf, Germany, 1992..
- [35] Fricke W. Review Fatigue analysis of welded joints: state of development. *Mar Struc* 2003;16(3):185-200..
- [36] Fricke W. IIW guideline for the assessment of weld root fatigue. *Welding in the World*, 2013;57:753-791..
- [37] Djavit DE, Strande E. Fatigue failure analysis of fillet welded joints used in offshore structures. MSc Thesis, Chalmers University of Technology, Goteborg, Sweden, 2013..
- [38] Taylor D, Barrett N, Lucano G. Some new methods for predicting fatigue in welded joints. *Int J Fatigue* 2002; 24:509-518..
- [39] Radaj D. *Design and analysis of fatigue resistant welded structures*. Abington publishing, Cambridge, England, 1990..

3.5 Reference

- [40] Morgenstern C, Sonsino CM, Hobbacher A, Sorbo F. Fatigue design of aluminium welded joints by the local stress concept with the fictitious notch radius of $r_f=1\text{mm}$. *Int J Fatigue* 2006;28:881-890..
- [41] Karakas O, Morgenstern C, Sonsino CM. Fatigue design of welded joints from the wrought magnesium alloy AZ31 by the local stress concept with the fictitious notch radii of $r_f=1.0$ and 0.05mm . *Int J Fatigue* 2008;30:2210-2219..
- [42] Sonsino CM. A consideration of allowable equivalent stresses for fatigue design of welded joints according to the notch stress concept with the reference radii $r_{ref} = 1.00$ and 0.05 mm . *Welding in the World* 2009; 53(3/4):R64-R75..
- [43] Lazzarin P, Tovo R. A unified approach to the evaluation of linear elastic stress fields in the neighbourhood of cracks and notches. *Int J Fracture* 1996; 78:3-19. .
- [44] Susmel L. *Multiaxial notch fatigue: from nominal to local stress/strain quantities*. Woodhead Publishing Limited, Cambridge, UK 2009. .
- [45] Atzori B. Trattamenti termici e resistenza a fatica delle strutture saldate. *Rivista Italiana della Saldatura*, Edited by A.T.A, Genova, Italy, 1983; 1:3-16. 30 .

Chapter 4

4. Fatigue assessment of inclined welded joints subjected to uniaxial cyclic loading.

The work presented in this chapter was published in the International Journal of Fatigue with the following title:

Al Zamzami I, Susmel L. On the use of hot-spot stresses, effective notch stresses and the Point Method to estimate lifetime of inclined welds subjected to uniaxial fatigue loading. Int J Fatigue 2018; 117: 432-449. <https://doi.org/10.1016/j.ijfatigue.2018.08.032>.

4.1 Introduction

The present chapter addresses the problem of estimating fatigue strength of welded joints when the weld seams are inclined with respect to the direction of the applied axial cyclic loading. As mentioned in section 2.2.3.1, the available Design codes, in particular the IIW [1], EC3 [2] (for steel) and EC9 [3] (for aluminium), have suggested different design rules to estimate the fatigue strength of welded components that experiencing either normal or parallel cyclic loading with respect to the weld seams. However, this is not always the case. In fact, in real welded structures, the direction of the applied forces are at different angles to the weld seams. The Design codes suggest some rules to estimate the fatigue damage by considering the effect of the combined normal and parallel stresses (see section 2.2.3.1).

From a fatigue design point of view, the main complexity lies in the fact that, with these particular welded geometries, although the applied loading is uniaxial, the stress state damaging the weld toe/root is multiaxial. However, an accurate fatigue assessment can be performed as long as the degree of multiaxiality of the nominal/structural/local stress states at the weld toes/roots is modelled effectively.

To this end, in this present chapter the Modified Wöhler Curve Method (MWCM) is used to assess the fatigue strength of steel joints with inclined welds by using this multiaxial fatigue criterion in conjunction with nominal stresses, hot-spot stresses, effective notch stresses, and the Theory of Critical Distances (TCD). A large number of experimental results taken from the literature and generated by testing steel inclined fillet welds was used to check the accuracy and reliability of the MWCM applied along with these different ways of determining the relevant stress states.

4.2 Methodology

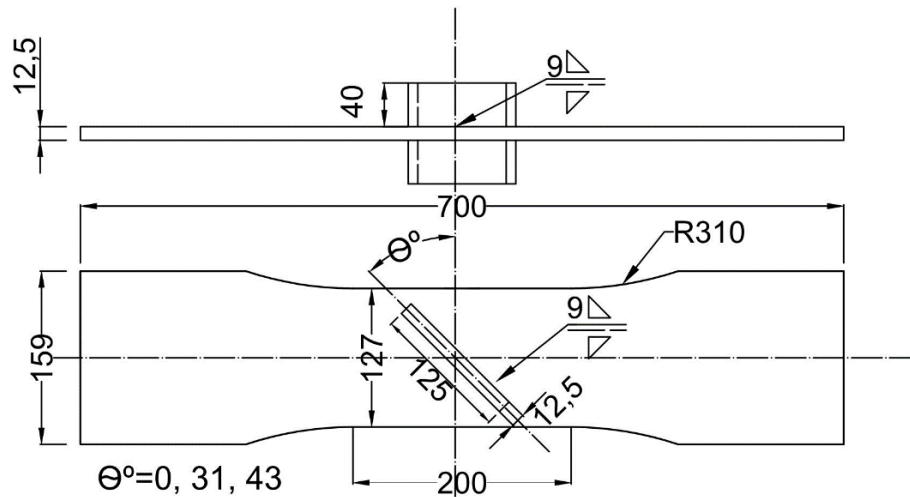
4.2.1 Experimental data

To assess the accuracy of the MWCM in estimating the fatigue strength of inclined welds, a number of experimental datasets were selected from the technical literature. These results were generated by testing, under zero-tension (i.e., $R=0$), uniaxial cyclic loading steel specimens manufactured by making the weld inclination angle, θ , vary in the range 0° - 45° . In particular, the welded specimens tested by Booth and Maddox (Figure 4.1a) [4], the load-carrying fillet welded joints tested by Kim and Kainuma (Figure 4.1b) [5] and the out-of-plane gusset geometry (Figure 4.2a) as well as the non-load carrying fillet welded joint (Figure 4.2b) tested by Kim and Yamada [6].

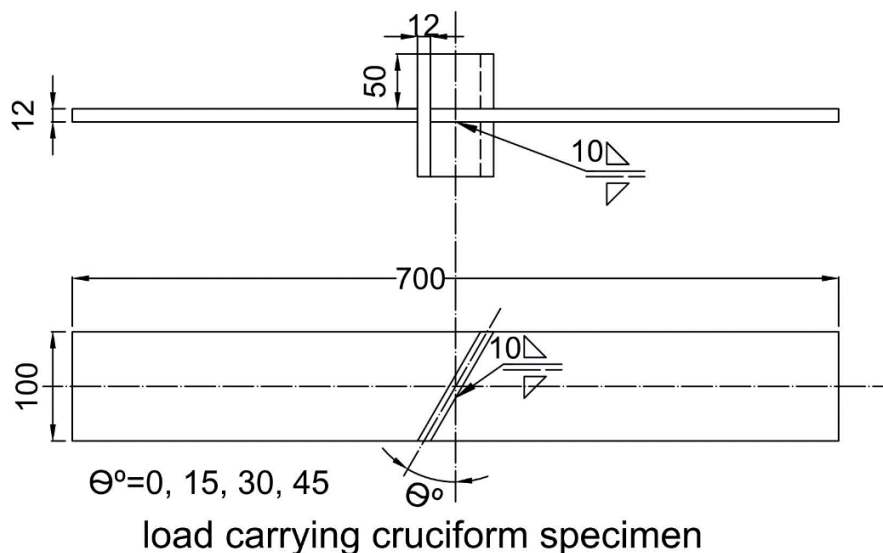
These welded specimens were all in the as-welded condition, i.e., no heat treatment was used to relieve the internal residual stresses arising from the welding process. After welding, all the samples were mechanically treated to force the fatigue cracks to initiate at the middle section of the weld seams (either at the weld toes or at the weld roots). In particular, the out-of-plane gusset specimens (specimen type KY-G in Figure 4.2a [6]) were either grounded with a disc grinder or needle peened to ensure that the fatigue cracking process did not occur at the weld edges. The length of the gusset was fixed so that the distance between the end of the gusset and the edge of the specimen was 20 mm wide. Accordingly, the gusset length varied with an inclination angle, θ .

Chapter 4: Fatigue assessment of inclined welded joints subjected to uniaxial cyclic loading.

For the non-load carrying fillet (specimen type KY-N in Figure 4.2b [6]), the two stiffeners and the area in between were widened with a fillet radius equal to 15 mm to reduce the stress concentration effect and ensure no fatigue cracks initiates at the edges. For the load-carrying fillet welded joints (specimen type KK in Figure 4.1b [5]), the root gap was less than 0.1 mm and the specimens were grounded with a disc grinder at the weld toe to prevent fatigue failures to occur in these locations.

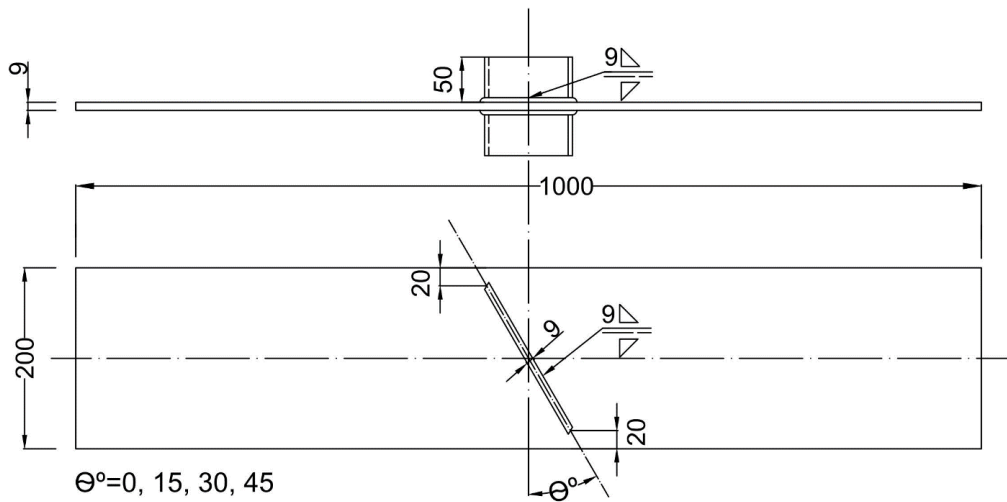


(a) Welded Specimen BM



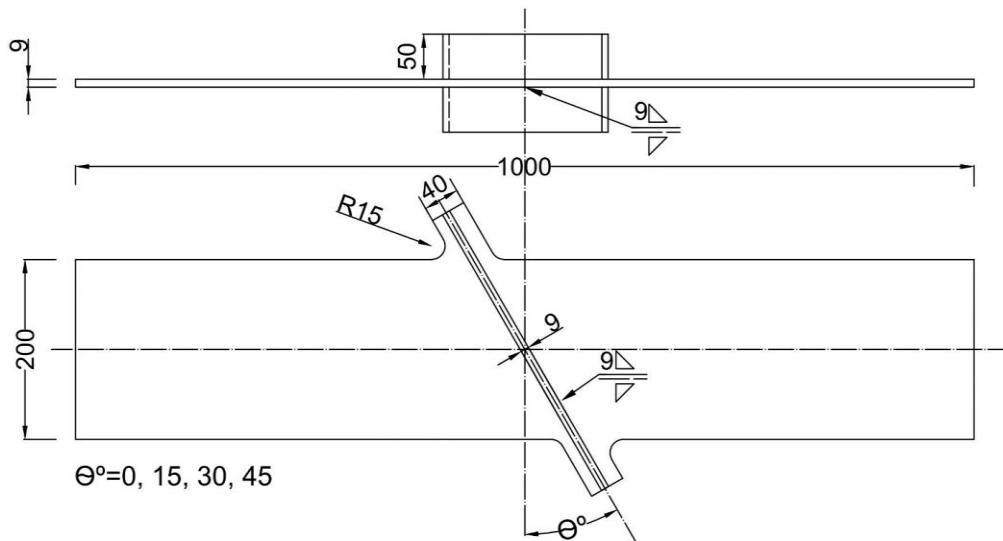
(b) Welded Specimen KK

Figure 4.1 Fatigue specimens tested by Booth and Maddox [4] (a) and load carrying cruciform specimens tested by Kim and Kainuma [5] (b).



Out-of-plane gusset specimen

(a) Welded Specimen KY-G



Non-load carrying cruciform specimen

(b) Welded Specimen KY-N

Figure 4.2 Out-of-plane gusset specimens (a) and non-load carrying cruciform specimens (b) tested by Kim and Yamada [6].

Finally, it is worth observing that the welded geometries sketched in Figure 4.1 and Figure 4.2 were used to check the accuracy of the MWCM when this approach is applied in terms of nominal and effective notch stress as well as in conjunction with the TCD. The hot-spot stress approach was used instead solely to post-process the results

generated by testing the welded specimens shown in Figure 4.1a, and Figure 4.2. This is due to the fact that in the load-carrying fillet welded joints tested by Kim and Kainuma (Figure 4.1b) [5] fatigue cracks were seen to initiate from the weld roots and the hot-spot stress approach cannot be used to assess this type of failure [7- 8].

4.2.2 Finite Element Analysis (sub-modelling)

In order to check the accuracy and the reliability of the MWCM in estimating the fatigue strength of inclined welded joints, a linear-elastic tri-dimensional Finite Element (3D FE) models were solved via the commercial software package ANSYS ®. These models were created to determine the corresponding stress distribution according to the stress-based approaches (i.e. hot-spot stresses, effective notch stresses and the Point Method (PM)).

Weld beads were modelled as sharp V-notches, i.e., by taking the fillet radius along the intersection line between the weld and parent material invariably equal to zero. The investigated welded components were treated as linear-elastic, isotropic and homogeneous materials with Young's modulus equal to 210 GPa and Poisson's ratio equal to 0.3. These assumptions are used for the Finite Element Analysis, however, in reality, the manufacturing process can cause geometrical irregularities on the welding zone and disturb the homogeneity in the Heat Affected Zone. These irregularities can have an effect on the strength of the samples, particularly if located near the point of maximum stress (i.e. toe tip). The variations in the actual geometry are typically accounted for in the statistical analysis and will attribute to the level of scattering.

For the hot-spot stresses and the effective notch stresses, the meshing process was completed according to the rules recommended by the IIW via eight-noded solid brick elements (Solid 185). The mesh density was varied throughout the welded details to achieve a fine mesh with element size equal to 0.6 mm for the hot-spot stresses and an element size equal to 0.2 mm for the effective notch stresses.

A massive number of elements are generated using a fine-meshed 3D FE model. Therefore, solving such FE model is time-consuming and it would require a significant computational effort. To solve this problem, ANSYS® provides a technique called solid-solid sub-modelling to refine the mesh with less time required. In more details, solve a global model with a coarse mesh. Then create a sub-model using the same global coordinate system, by cutting the volumes away from the vicinity of the weld. After that, keep repeating the sub-modelling procedure until reaching convergence. The solid-solid sub-modelling procedure is as follow:

1. Create a global model (as shown in Figure 4.3a)

4.2 Methodology

2. The mesh should be relatively coarse
3. Apply the loads and boundary conditions.
4. Solve the model and save it in a .db format.

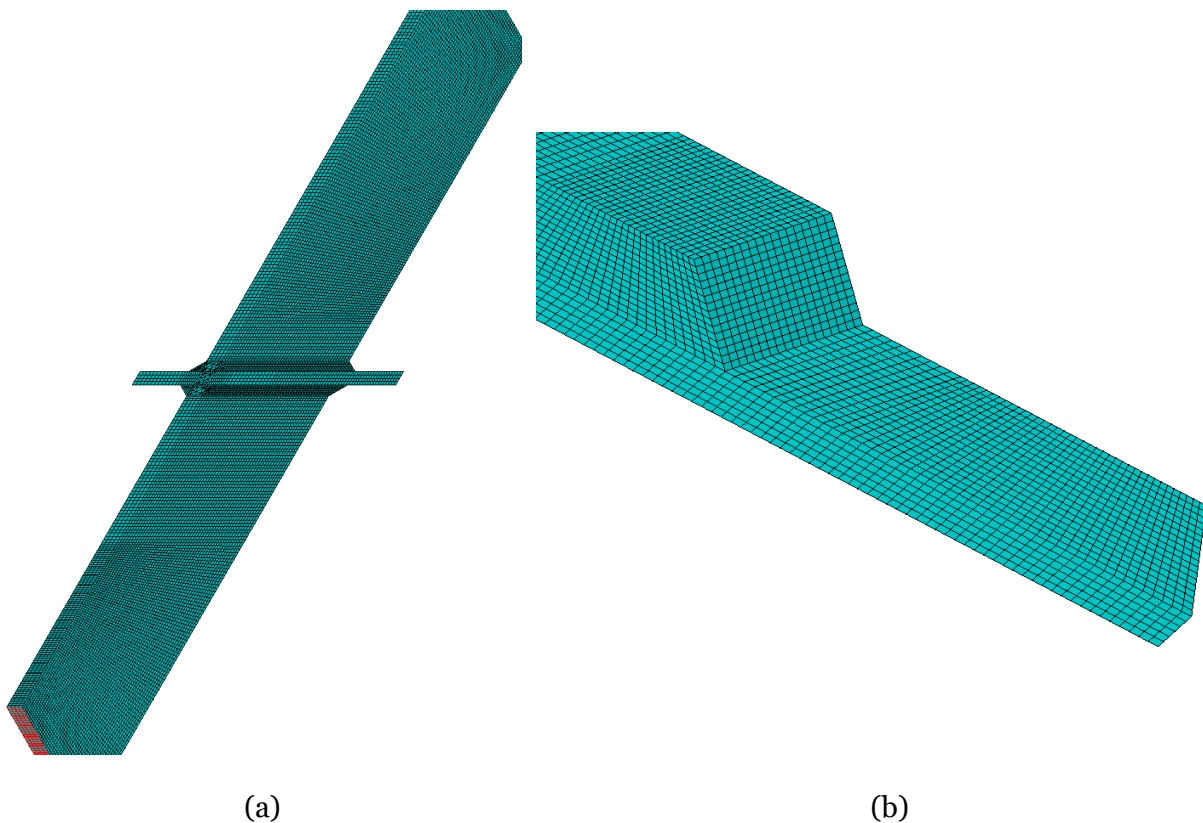


Figure 4.3 example of 3D FE global model (a) and sub-model (b).

5. Create a sub-model using the same coordinate system used in the global model (as shown in Figure 4.3b).
6. Use a smaller element size.
7. Select all the nodes on the sub-model boundaries that are in common with the global model and save the file.
8. Interpolate the cut boundary by using the node file generated in step (7) and the results file from step (4). The interpolation process will create .cbdo file.
9. Select the .cbdo file, which will transfer the boundary condition from the global to the sub-model.

10. Solve the sub-model and compare the results at the common boundaries between the two models.
11. Repeat step 5 to 10 to obtain a finer mesh until the required accuracy is achieved. Note that the sub-model for the second iteration is now the coarse model and so on.

4.3 The MWCM to estimate the fatigue lifetime of inclined welds subjected to uniaxial fatigue loading

4.3.1 MWCM applied along with the nominal stress approach

Back in 2004, the MWCM applied in terms of nominal stresses was seen to be successful in estimating fatigue lifetime of aluminium and steel welded joints when the loads were applied parallel and perpendicular to the weld seams [9- 12]. Recently, the combined use of the MWCM and the nominal stress approach was also extended to the fatigue assessment of uniaxially loaded inclined welds [13]. For these welded geometries, although the global load history is uniaxial, the nominal stress state in the vicinity of the weld is not only multiaxial but also varies proportionally, with the degree of proportionality changing as the weld inclination angle increases [13].

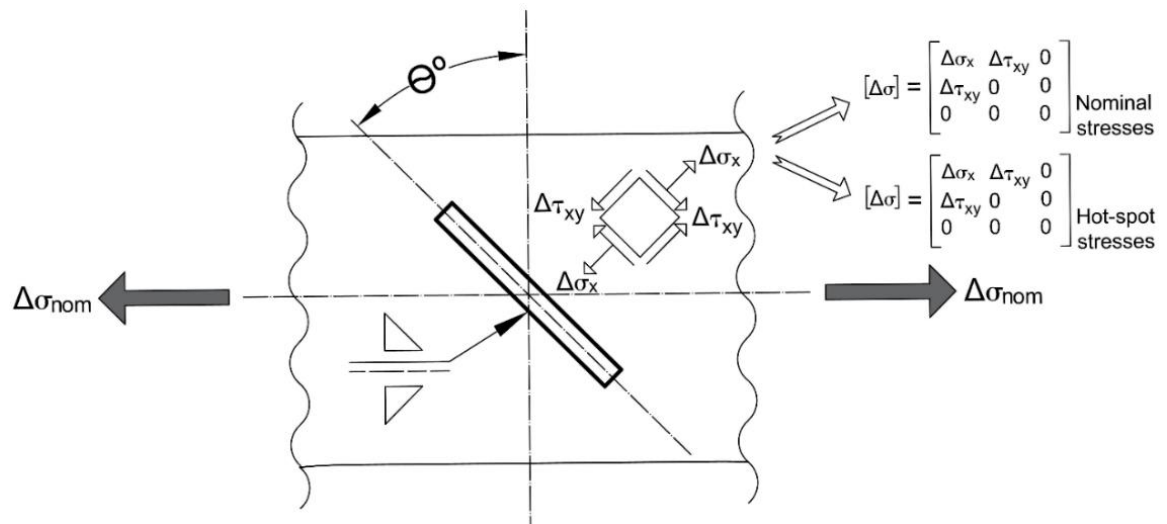


Figure 4.4 Nominal and hot spot stresses in inclined welded joints subjected to uniaxial cyclic loading.

4.3 The MWCM to estimate the fatigue lifetime of inclined welds subjected to uniaxial fatigue loading

According to the sketch reported in Figure 4.4, the nominal stresses perpendicular, $\Delta\sigma_x$ and parallel, $\Delta\tau_{xy}$ to the weld seam can easily be determined as follows [14]:

$$\Delta\sigma_x = \Delta\sigma_{nom} \cdot \cos^2\theta \quad (4.1)$$

$$\Delta\tau_{xy} = \Delta\sigma_{nom} \cdot \cos\theta \cdot \sin\theta \quad (4.2)$$

Where, θ is the angle between the weld seam and the straight line normal to the direction along which the uniaxial cyclic force is applied (Figure 4.4). The use of the nominal stresses determined according to Eqs (4.1) and (4.2) to estimate the fatigue strength of welded joints can be justified by advocating the Notch-Stress Intensity Factor (N-SIF) approach [15, 16]. In particular, for a notch-opening angle larger than 100° , Mode II stresses are no longer singular, so that they can be neglected with a little loss of accuracy. In contrast, the overall fatigue strength of welded joints is seen to be depending predominantly on Mode I and Mode III stress components, with the corresponding linear-elastic stress fields being still singular also for weld opening angles equal to 135° [16, 17]. Since, Mode I and Mode III stresses are proportional to nominal stresses $\Delta\sigma_x$ and $\Delta\tau_{xy}$, respectively, the stress quantities determined according to Eqs (4.1) and (4.2) can directly be used to assess fatigue strength when the weld seams are subjected to a multiaxial system of normal and shear forces [13, 17].

Having clarified this important aspect, as per the schematic Mohr circle reported in Figure 4.5, the ranges of the normal and shear nominal stresses relative to the critical plane can then be determined as [13]:

$$\Delta\sigma_n = \frac{\Delta\sigma_x}{2} = \frac{\Delta\sigma_{nom}}{2} \cdot \cos^2\theta \quad (4.3)$$

$$\Delta\tau = \sqrt{\frac{\Delta\sigma_x^2}{4} + \Delta\tau_{xy}^2} = \frac{\Delta\sigma_{nom}}{2} \cdot \cos^2\theta \sqrt{1 + 4\tan^2\theta} \quad \text{for } \theta \neq \frac{\pi}{2} \quad (4.4)$$

If q is used to define the following trigonometric quantity:

$$q = \frac{1}{\sqrt{1 + 4\tan^2\theta}} \quad (4.5)$$

Then, the critical plane stress ratio, ρ_w can directly be determined as:

$$\rho_w = \frac{\Delta\sigma_n}{\Delta\tau} = \frac{1}{\sqrt{1 + 4\tan^2\theta}} = q \quad (4.6)$$

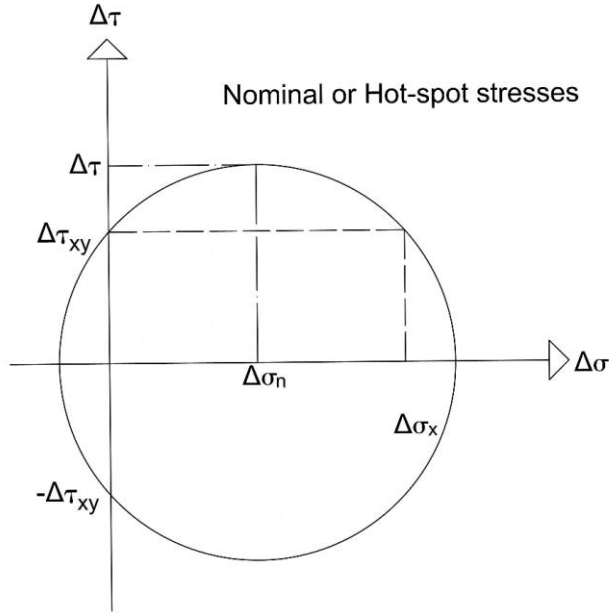


Figure 4.5 Mohr's circle to calculate the stress components relative to the critical plane.

Eq. (4.6) makes it evident that, as far as uniaxially loaded inclined welds are concerned, ρ_w depends solely on the inclination angle, θ . Since $\rho_w = q$, then the MWCM's calibration equations (see section 2.2.3.2– i.e., Eqs (2.38) and (2.39), can be rewritten as [13] :

$$k_\tau(\rho_w) = k_\tau(q) = (k - k_0) \cdot q + k_0 \quad (4.7)$$

$$\Delta\tau_{Ref}(\rho_w) = \Delta\tau_{Ref}(q) = \left(\frac{\Delta\sigma_A}{2} - \Delta\tau_A \right) \cdot q + \Delta\tau_A \quad (4.8)$$

Finally, according to Eq. (2.39) (see section 2.2.3.2) the number of cycles to failure can be estimated via the following relationship:

$$N_f = N_{Ref} \cdot \left[q \cdot \frac{q\Delta\sigma_A + 2\Delta\tau_A(1 - q)}{\Delta\sigma_{nom} \cdot \cos^2\theta} \right]^{(k-k_0) \cdot q + k_0} \quad (4.9)$$

4.3 The MWCM to estimate the fatigue lifetime of inclined welds subjected to uniaxial fatigue loading

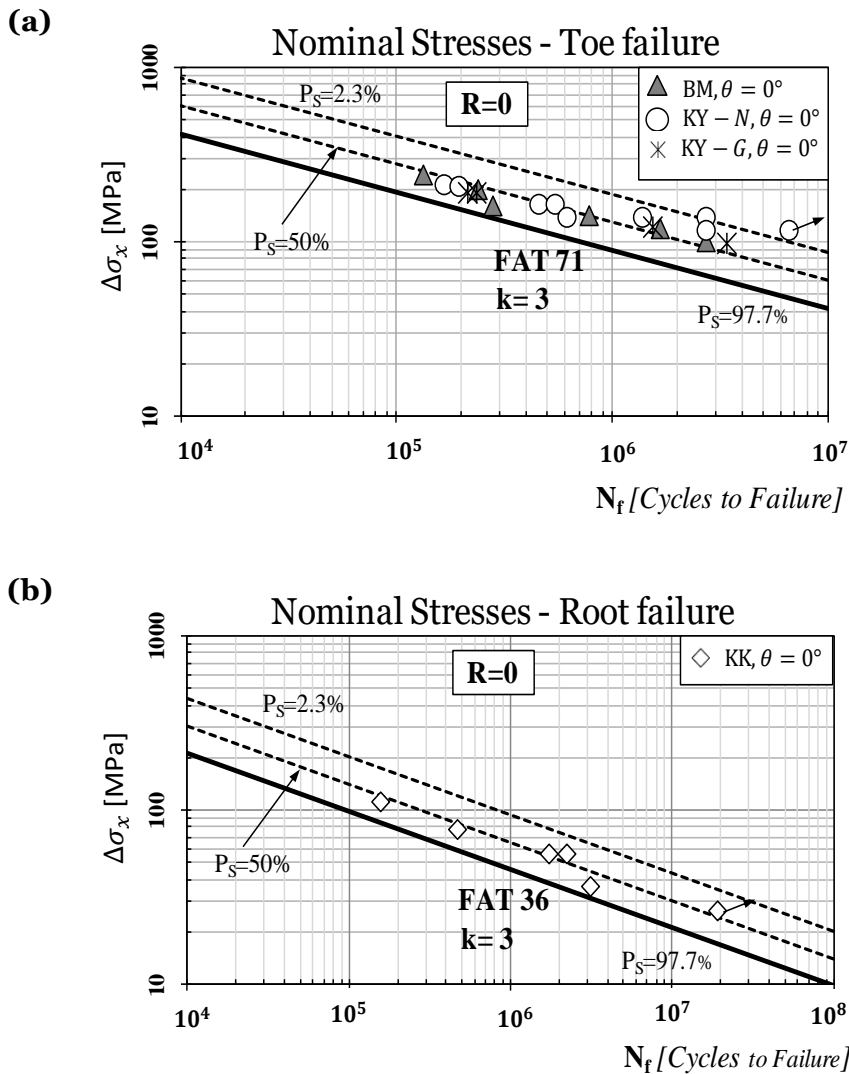


Figure 4.6 Accuracy of the recommended reference design curves in estimating the fatigue strength of the welded joints in terms of nominal stresses (toe failure (a) and root failure (b)).

The check the overall level of accuracy of the MWCM used along with the nominal stress approach, Eqs (4.7) and (4.8) were calibrated as described in what follows. As far as non-loading transverse fillet-welded joints are concerned, the IIW [1] recommends using uniaxial and torsional fatigue curves having endurance limits $\Delta\sigma_A$ and $\Delta\tau_A$ (extrapolated at $N_{Ref} = 2 \cdot 10^6$ cycles to failure and determined for a probability of survival, P_S , of 97.7%) equal to 71 MPa (with $k=3$) and 80 MPa (with $k_0=5$), respectively. The $\Delta\sigma_{nom}$ vs. N_f log-log diagram of Figure 4.6a confirms that the FAT 71 curve was capable of accurately modelling the fatigue behaviour of the $\theta = 0^\circ$ configurations for specimens BM (Figure 4.1a), KY-G (Figure 4.2a), and KY-N (Figure 4.2b).

When cracks originate from the weld roots - as it was observed in the KK specimens (Figure 4.1b) [5], the IIW suggests using instead a uniaxial fatigue curve having $\Delta\sigma_A = 36$

Chapter 4: Fatigue assessment of inclined welded joints subjected to uniaxial cyclic loading.

MPa (at $N_{Ref} = 2 \cdot 10^6$ cycles to failure) with $k=3$ and a torsional design curve having $\Delta\tau_A = 80$ MPa (at $N_{Ref} = 2 \cdot 10^6$ cycles to failure) and $k_0=5$. As expected, the chart of Figure 4.6b fully confirms that the FAT 36 design curve was suitable for modelling the fatigue strength of the KK specimens (Figure 4.1b), i.e., for assessing those situations where final breakage took place as a result of weld root cracking.

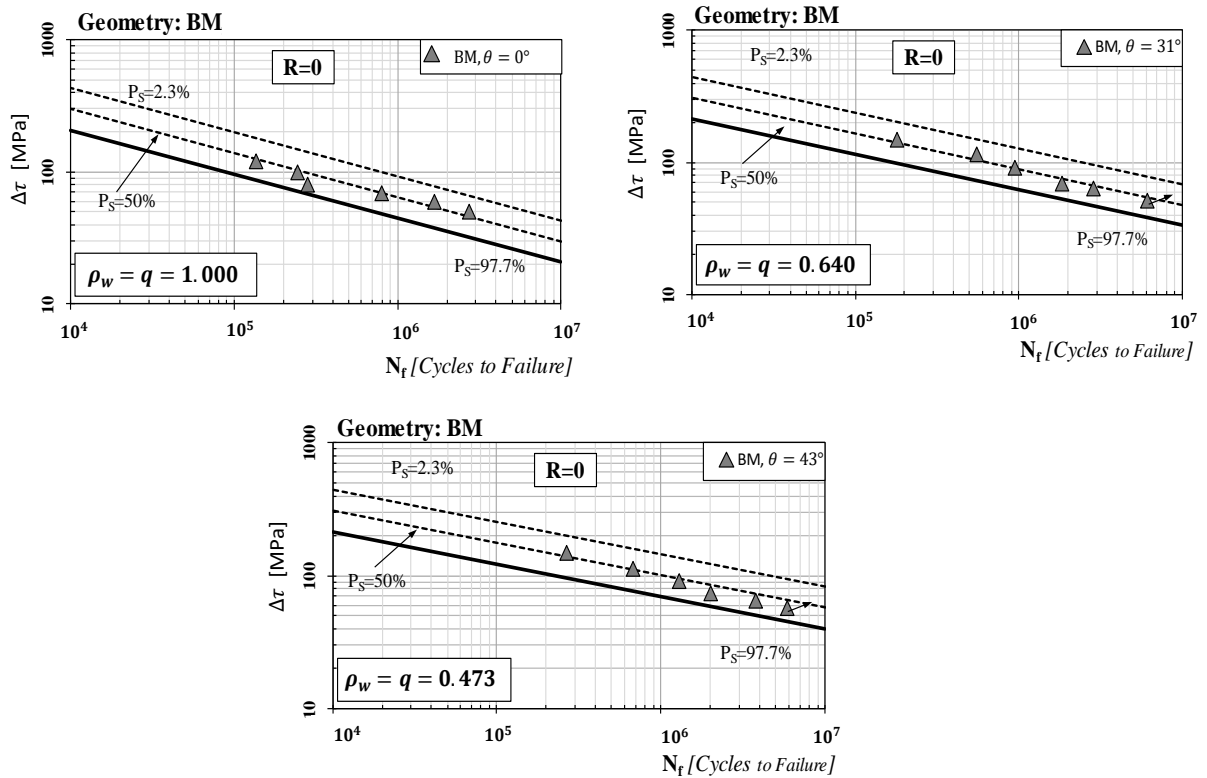


Figure 4.7 Accuracy of the MWCM applied along with nominal stresses in estimating fatigue strength in the presence of inclined welds (geometry BM).

Figure 4.7 to Figure 4.9 shows the results obtained from the MWCM analysis for the different geometries/inclination angles. The scatter band plotted in these charts are derived from the reference value of 1.5 suggested by Haibach [18]. It is worth mentioning that this value was calculated for a probability of survival equal to 90% and 10%. However, in this investigation the scatter band are plotted with a probability of survival equal to 97.7% and 2.3% and hence the scatter band value was recalculated and the value used is 1.85.

4.3 The MWCM to estimate the fatigue lifetime of inclined welds subjected to uniaxial fatigue loading

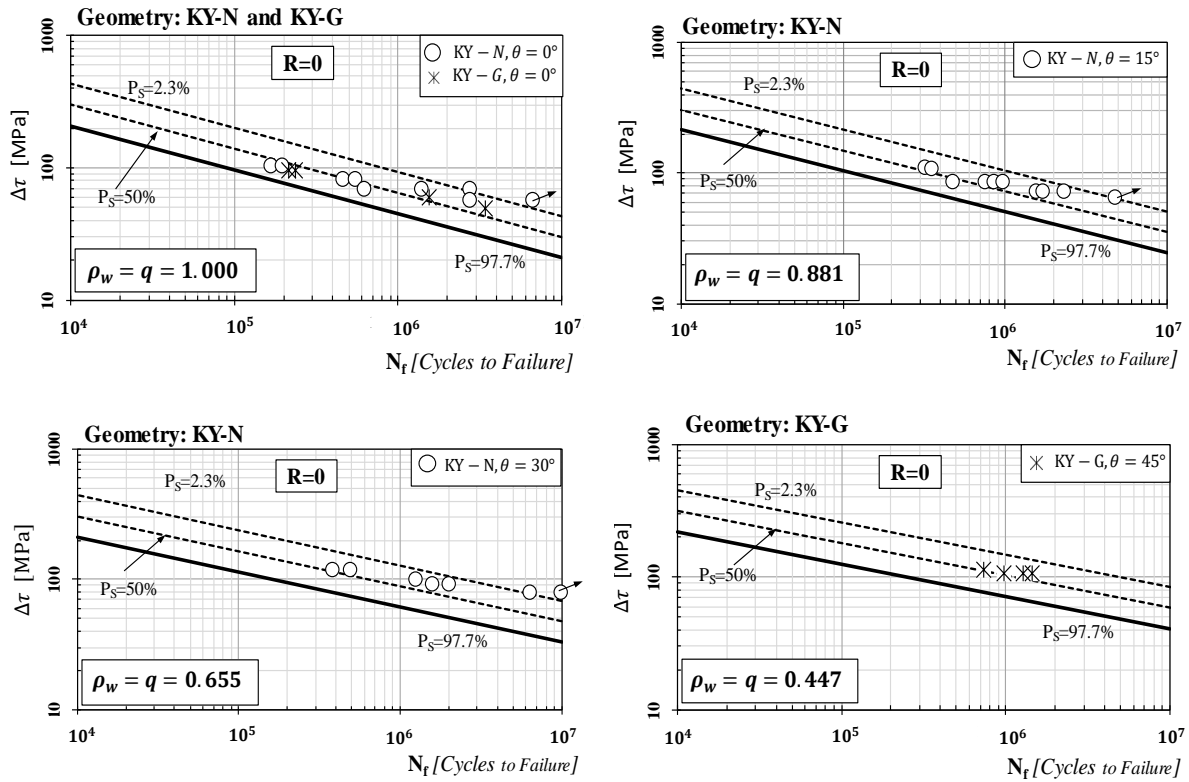


Figure 4.8 Accuracy of the MWCM applied along with nominal stresses in estimating fatigue strength in the presence of inclined welds. (Geometry KY-N and KY-G).

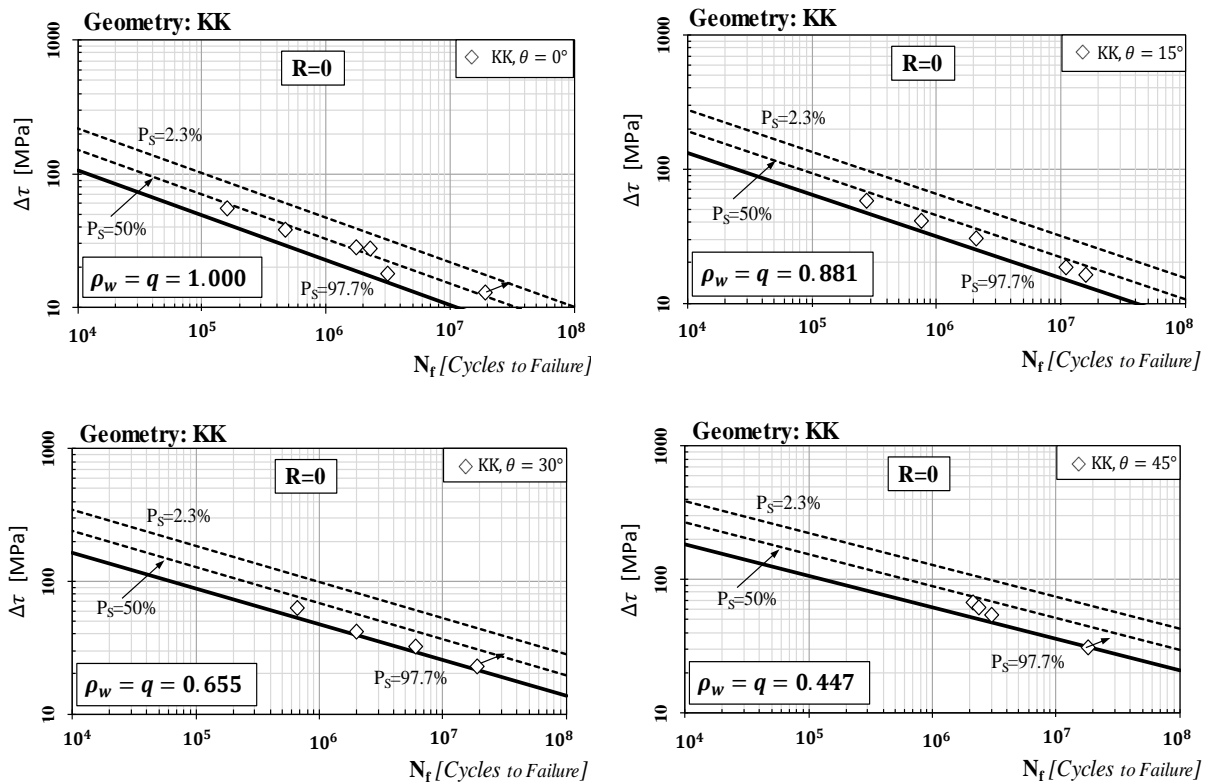


Figure 4.9 Accuracy of the MWCM applied along with nominal stresses in estimating fatigue strength in the presence of inclined welds (geometry KK).

In summary, the modified Wöhler diagrams of Figure 4.7 to Figure 4.9 (see also Table B.1 to Table B.4, Appendix B), confirms that the MWCM applied in conjunction with the nominal stress approach is successful in estimating the extent of fatigue damage in the presence of uniaxially loaded inclined welds. With this holding true independently of the type of failure (i.e., either toe or root cracking).

4.3.2 The MWCM applied along with the hot-spot stress approach

To check the accuracy of the MWCM applied along with the global stress approach in estimating fatigue lifetime of uniaxially loaded inclined welds, the hot-spot stress components parallel, $\Delta\tau_{HS}$, and perpendicular, $\Delta\sigma_{HS}$, to the weld seam (Figure 4.10) [9, 19] were determined using the surface extrapolation method (see section 2.3.2.3.1) [1] as follows:

$$\Delta\sigma_{HS} = 1.67\Delta\sigma_{0.4t} - 0.67\Delta\sigma_t \quad (4.10)$$

$$\Delta\tau_{HS} = 1.67\Delta\tau_{0.4t} - 0.67\Delta\tau_t \quad (4.11)$$

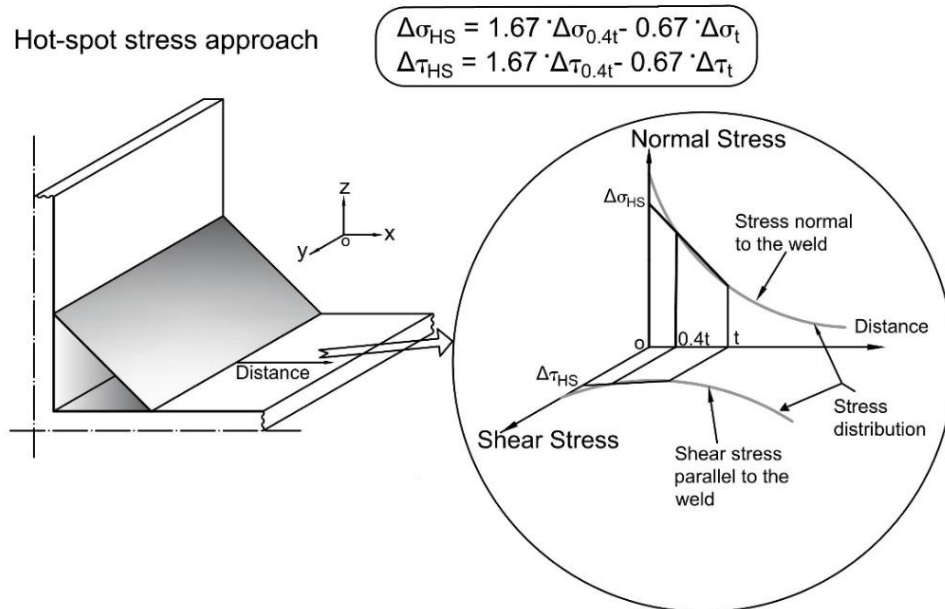


Figure 4.10 definition nominal and shear hot-spot stresses.

In more detail, according to Figure 4.10, stress components $\Delta\sigma_{0.4t}$ and $\Delta\tau_{0.4t}$ were determined at a distance from the weld toe equal to $0.4t$ (with t being the thickness), whereas stress components $\Delta\sigma_t$ and $\Delta\tau_t$ were determined at a distance from the weld toe

4.3 The MWCM to estimate the fatigue lifetime of inclined welds subjected to uniaxial fatigue loading

equal to t . The commercial FE code ANSYS® was used to determine the required stresses by solving three-dimensional linear-elastic FE models where the mesh density was set according to the IIW recommendations [1, 20] (see the example shown in Figure 4.11).

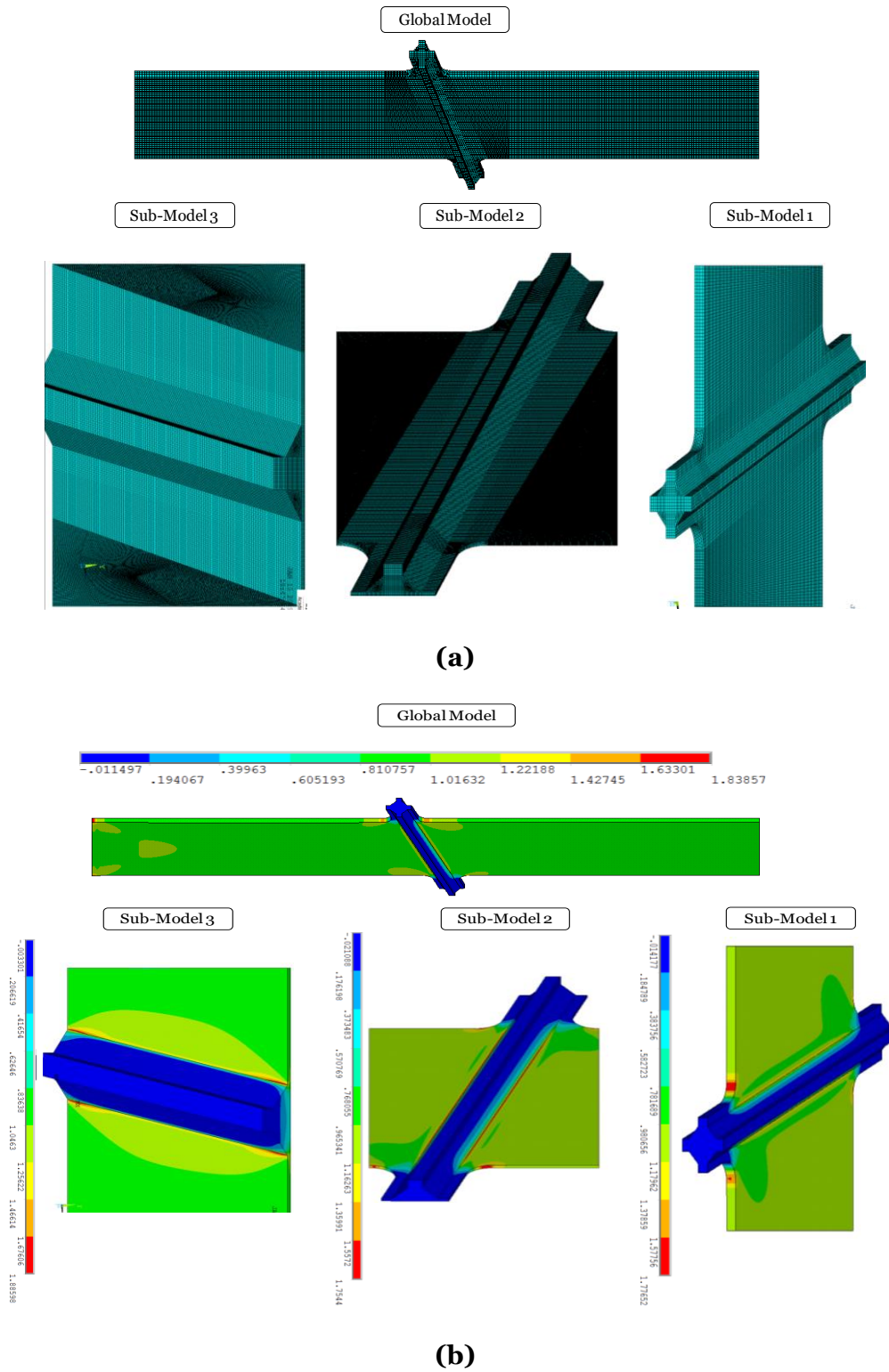


Figure 4.11 Examples of mesh refinement (a); and the linear-elastic FE models solved by following a solid-to-solid sub-modelling procedure (b); using the hot-spot stress approach.

Chapter 4: Fatigue assessment of inclined welded joints subjected to uniaxial cyclic loading.

Figure 4.12 shows the procedure followed to determine the required local stresses for the inclined welds. Following the mesh refinement and obtaining the required level of accuracy (Figure 4.11); the local stresses were obtained along the focus path perpendicular to the weld seams (Figure 4.12).

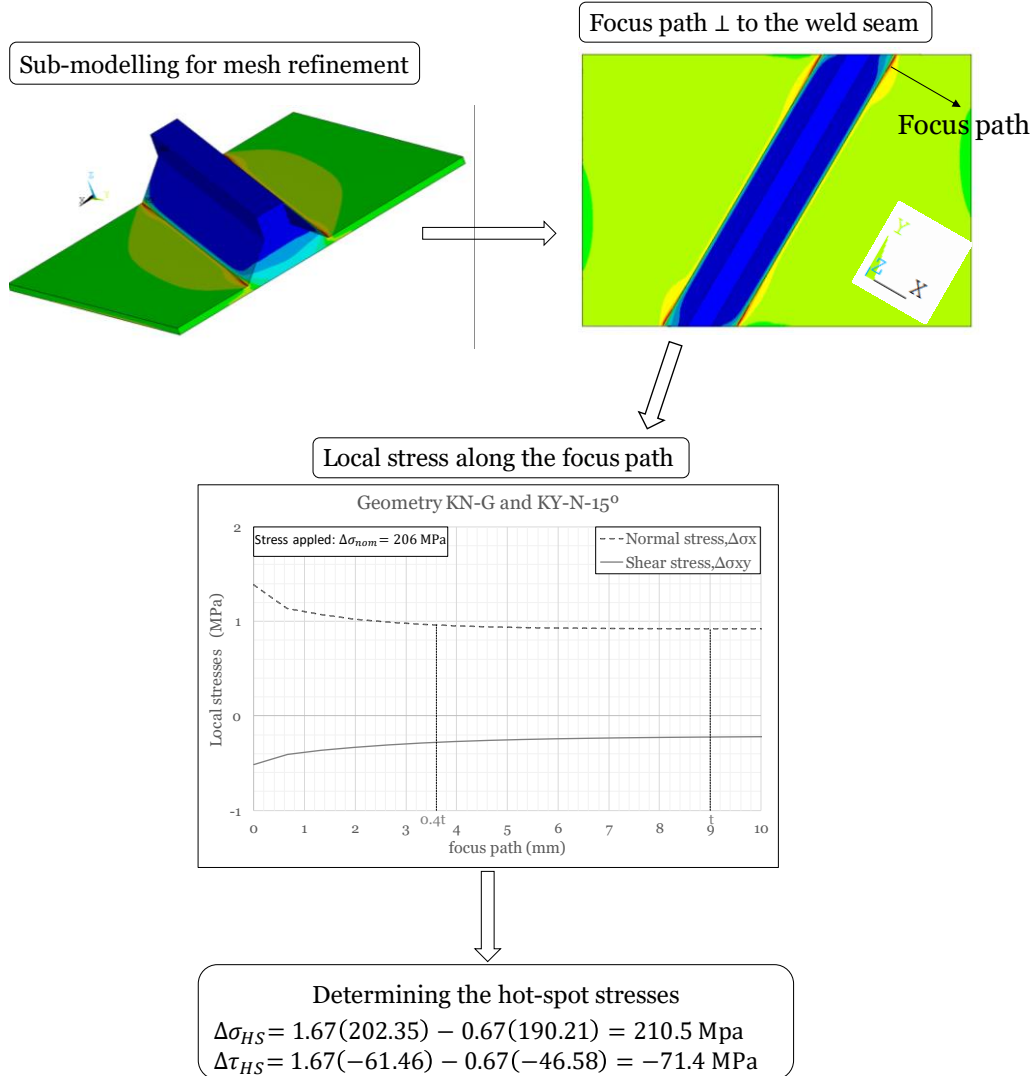


Figure 4.12 the procedure followed to determine the required hot spot stresses.

The MWCM's governing equations Eqs (2.38) and (2.39) (see section 2.2.3.2), were calibrated using the FAT 100 uniaxial fatigue curve ($\Delta\sigma_A = 100$ MPa at $N_{Ref} = 2 \cdot 10^6$ cycles to failure for $P_s = 97.7\%$ and $k = 3$) and the FAT 80 torsional fatigue curve ($\Delta\tau_A = 80$ MPa at $N_{Ref} = 2 \cdot 10^6$ cycles to failure for $P_s = 97.7\%$ and $k_o = 5$) [1], obtaining:

$$k_t(\rho_w) = -2 \cdot \rho_w + 5 \quad (4.12)$$

$$\Delta\tau_{Ref}(\rho_w) = -47.5 \cdot \rho_w + 80 \text{ [MPa]} \quad (4.13)$$

4.3 The MWCM to estimate the fatigue lifetime of inclined welds subjected to uniaxial fatigue loading

As far as weld toe failures are concerned, the $\Delta\sigma_{HS}$ vs. N_f log-log diagram of Figure 4.13 makes it evident that the FAT 100 uniaxial fatigue curve was capable of accurately assessing in terms of hot-spot stresses the fatigue strength of the $\theta=0^\circ$ welded specimens being considered.

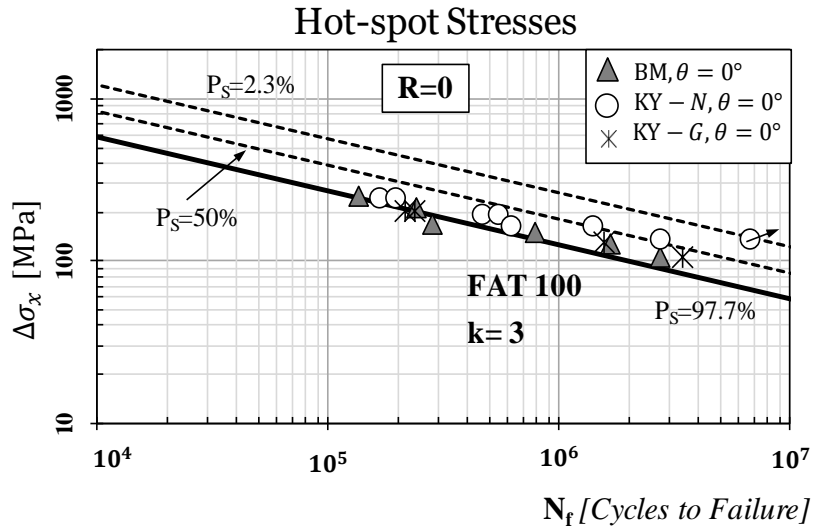


Figure 4.13 Accuracy of the recommended reference design curves in estimating the fatigue strength of the investigated welded joints in terms of hot-spot stresses.

The overall accuracy obtained by applying the MWCM in conjunction with the hot-spot stress approach to estimate the fatigue strength of welded geometries is shown in the modified Wöhler diagrams of Figure 4.14 and Figure 4.15 (see also Table B.1 to Table B.4, Appendix B). These charts make it evident that the MWCM is successful in estimating fatigue lifetime of uniaxially loaded connections with inclined welds also when it is applied along with the global stress approach. It is noticeable from these charts that the obtained level of conservatism slightly increasing as the inclination angle, θ , increases.

Chapter 4: Fatigue assessment of inclined welded joints subjected to uniaxial cyclic loading.

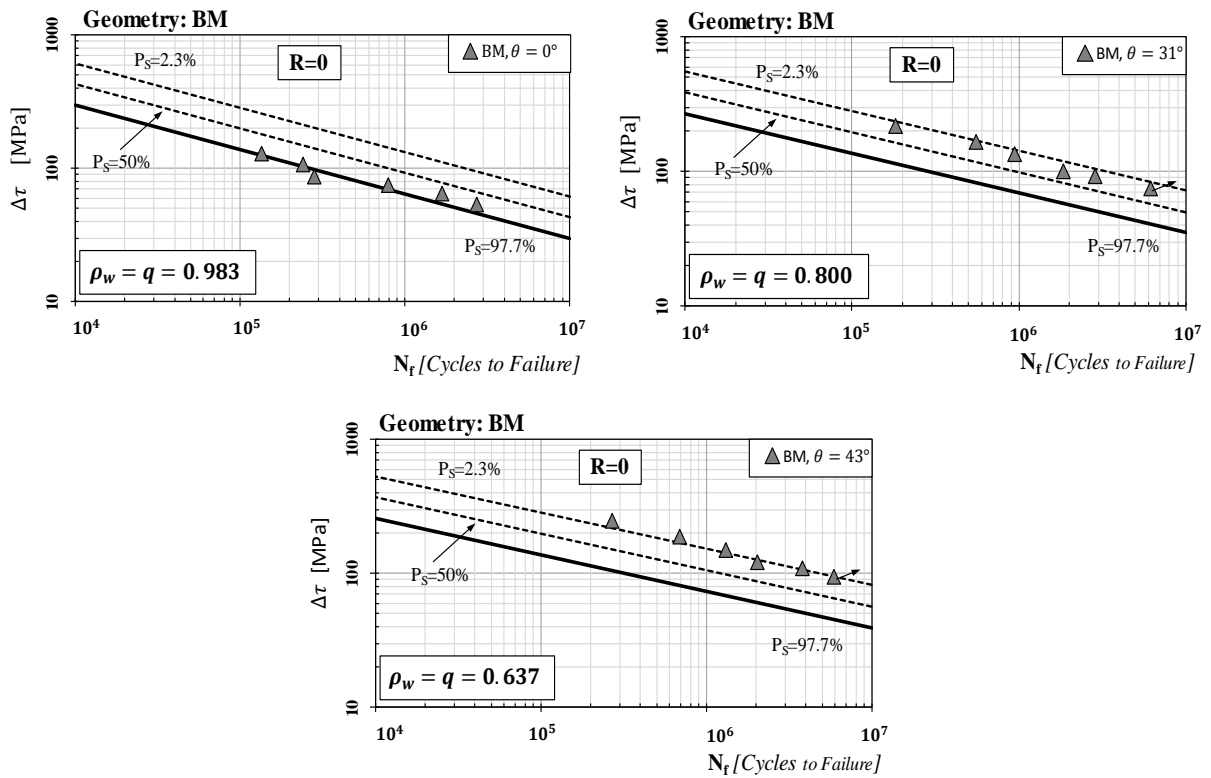


Figure 4.14 Accuracy of the MWCM applied along with hot-spot stresses in estimating fatigue strength in the presence of inclined welds (for geometry BM).

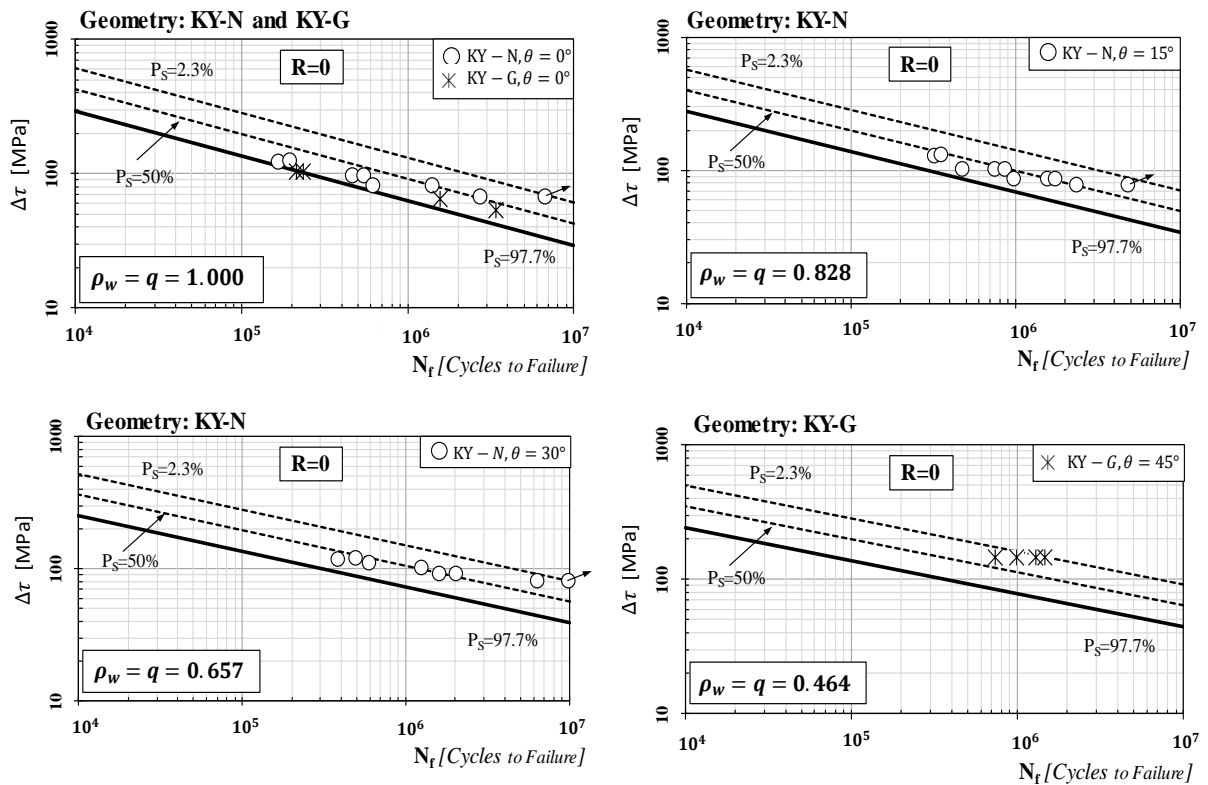


Figure 4.15 Accuracy of the MWCM applied along with hot-spot stresses in estimating fatigue strength in the presence of inclined welds (for geometry KY-N and KY-G).

4.3.3 The MWCM applied along with the effective notch stress approach

Since all the welded joints considered in the present investigation had a thickness larger than 5 mm, notch stresses were determined using FE code ANSYS® by rounding the weld toes of specimens BM, KY-G, and KY-N and the weld roots of specimens KK (Figure 4.1b) by setting r_{ref} invariably equal to 1 mm. The stress analysis was performed via three-dimensional FE models solved by following a conventional solid-to-solid sub-modelling procedure (section 4.2.2), with the mesh density being gradually increased until convergence occurred (see the example shown in Figure 4.16).

The MWCM was applied along with the reference radius concept [20] by calibrating its governing equations, Eqs (2.38) and (2.39) (see section 2.2.3.2), using the FAT 225 uniaxial fatigue curve [1, 21] and the FAT 160 torsional fatigue curve [21]. In more detail, the uniaxial calibration curve had endurance limit, $\Delta\sigma_A$, extrapolated at $N_{Ref} = 2 \cdot 10^6$ cycles to failure for $P_S=97.7\%$ equal to 225 MPa, the negative inverse slope, k , being equal to 3. The torsional calibration curve had instead $\Delta\tau_A=160$ MPa (again at $N_{Ref} = 2 \cdot 10^6$ cycles to failure for $P_S=97.7\%$) and $k_0=5$. By using these two pieces of calibration information, fatigue constants α, β, a and b in Eqs (2.36) and (2.37) (see section 2.2.3.2) were calculated to be as follows:

$$k_t(\rho_w) = -2 \cdot \rho_w + 5 \quad (4.14)$$

$$\Delta\tau_{Ref}(\rho_w) = -47.5\rho_w + 160 \text{ [MPa]} \quad (4.15)$$

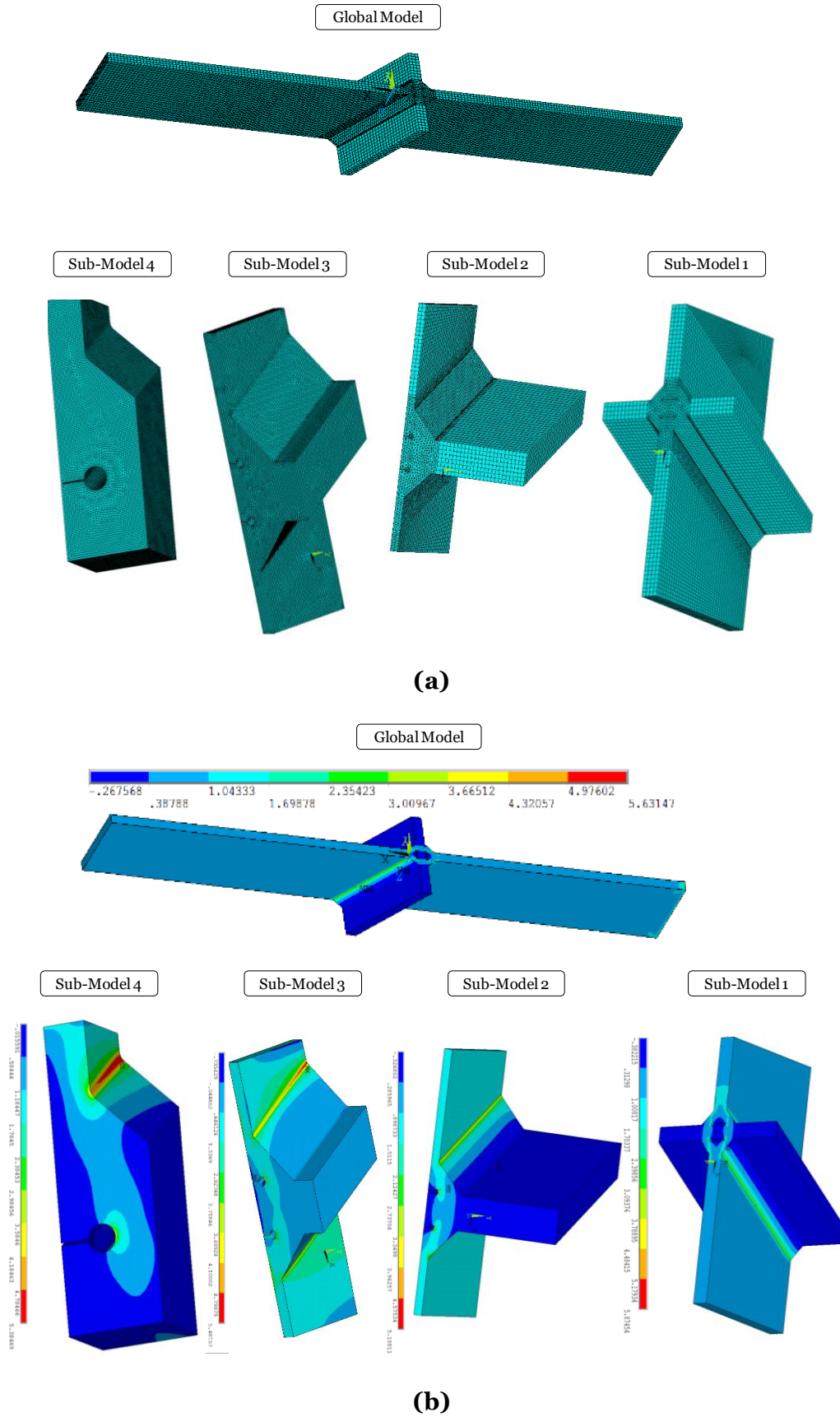


Figure 4.16 Examples of mesh refinement (a); and the linear-elastic FE models solved by following a solid-to-solid sub-modelling procedure (b); using the effective notch stress approach.

4.3 The MWCM to estimate the fatigue lifetime of inclined welds subjected to uniaxial fatigue loading

Independently of the crack initiation location (i.e., either at toes or at roots), the log-log diagram of Figure 4.17 confirms that, as expected, the FAT 225 uniaxial fatigue curves was capable of modelling the fatigue behaviour of the $\theta = 0^\circ$ welded specimens being considering not only with a remarkable level of accuracy but also with a suitable level of conservatism.

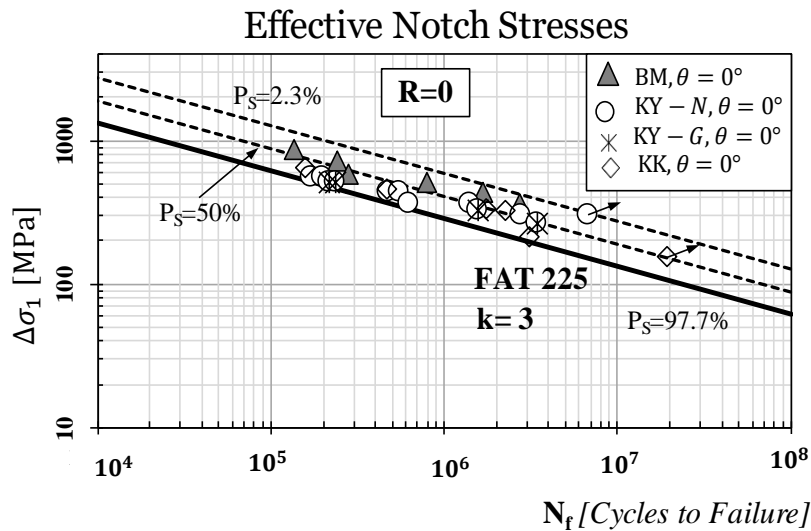


Figure 4.17 Accuracy of the recommended reference design curves in estimating the fatigue strength of the investigated welded joints in terms of 1st principal stresses.

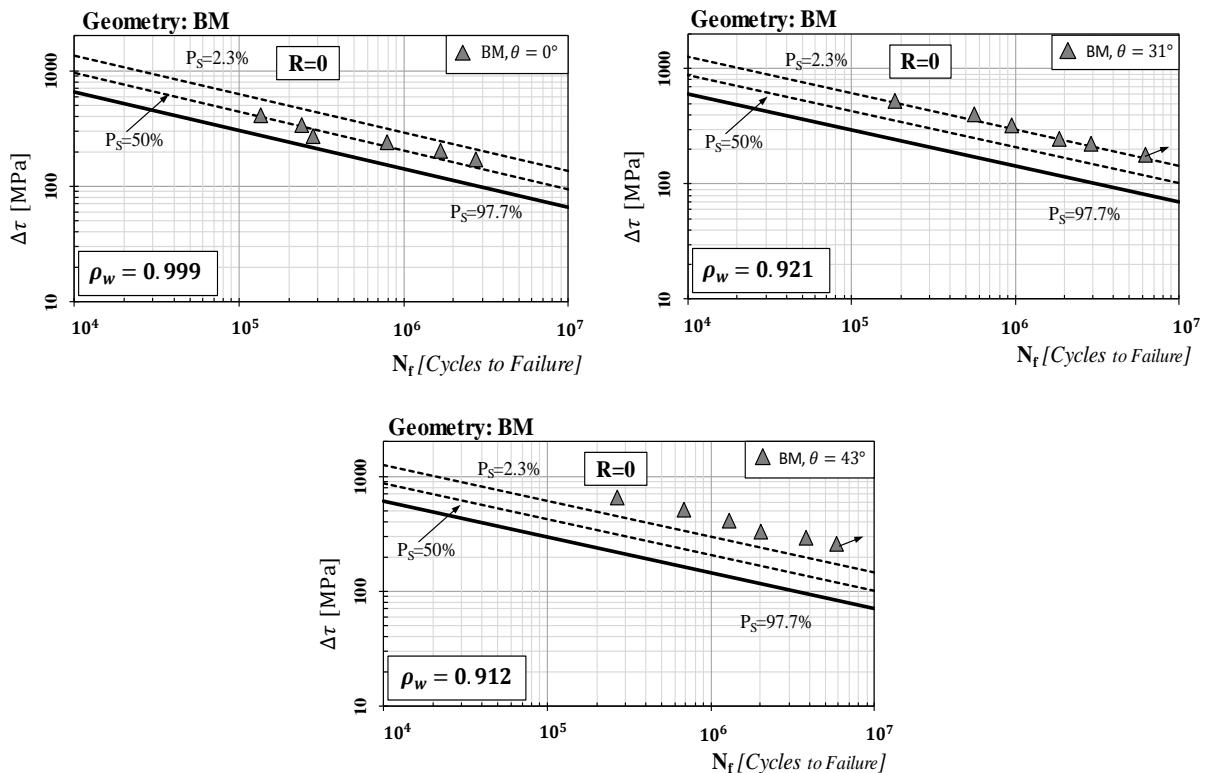


Figure 4.18 Accuracy of the MWCM applied along with effective notch stresses in estimating fatigue strength in the presence of inclined welds (for geometry BM).

Chapter 4: Fatigue assessment of inclined welded joints subjected to uniaxial cyclic loading.

The results obtained by applying the MWCM along with the effective notch stress approach to estimate the fatigue lifetime of the welded specimens with $\theta > 0^\circ$ are summarised in the modified Wöhler diagrams reported in Figure 4.18 to Figure 4.20 (see also Table B.5 to Table B.8, Appendix B).

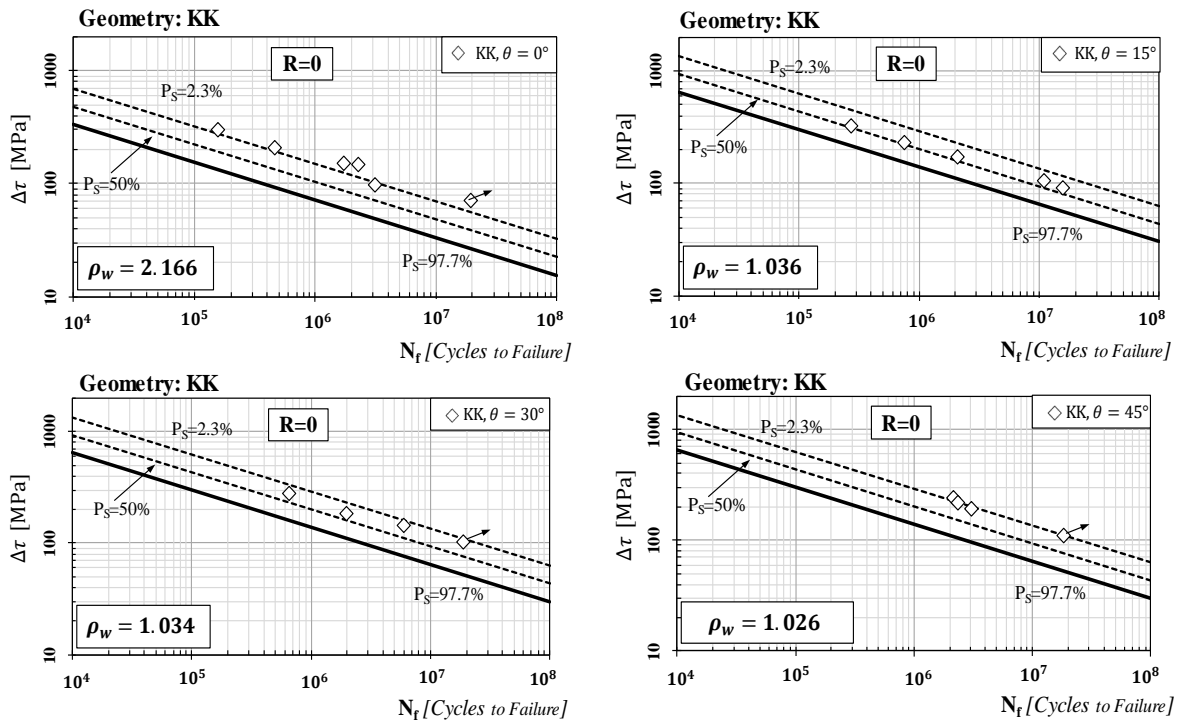


Figure 4.19 Accuracy of the MWCM applied along with effective notch stresses in estimating fatigue strength in the presence of inclined welds (for geometry KK).

These charts demonstrate that the use of the MWCM along with the r_{ref} concept resulted in a very high level of accuracy, with the estimates falling within the corresponding scatter bands calculated for P_S equal to 2.3% and 97.7%. The only exception is represented by geometry BM with $\theta = 43^\circ$ (Figure 4.18) [4] for which the estimates being obtained were seen to be slightly conservative.

To conclude, it is worth observing that such a remarkable level of accuracy was reached when reanalysing not only the results characterised by weld toe failures but also those tests where fatigue cracks were seen to initiate at the weld roots

4.3 The MWCM to estimate the fatigue lifetime of inclined welds subjected to uniaxial fatigue loading

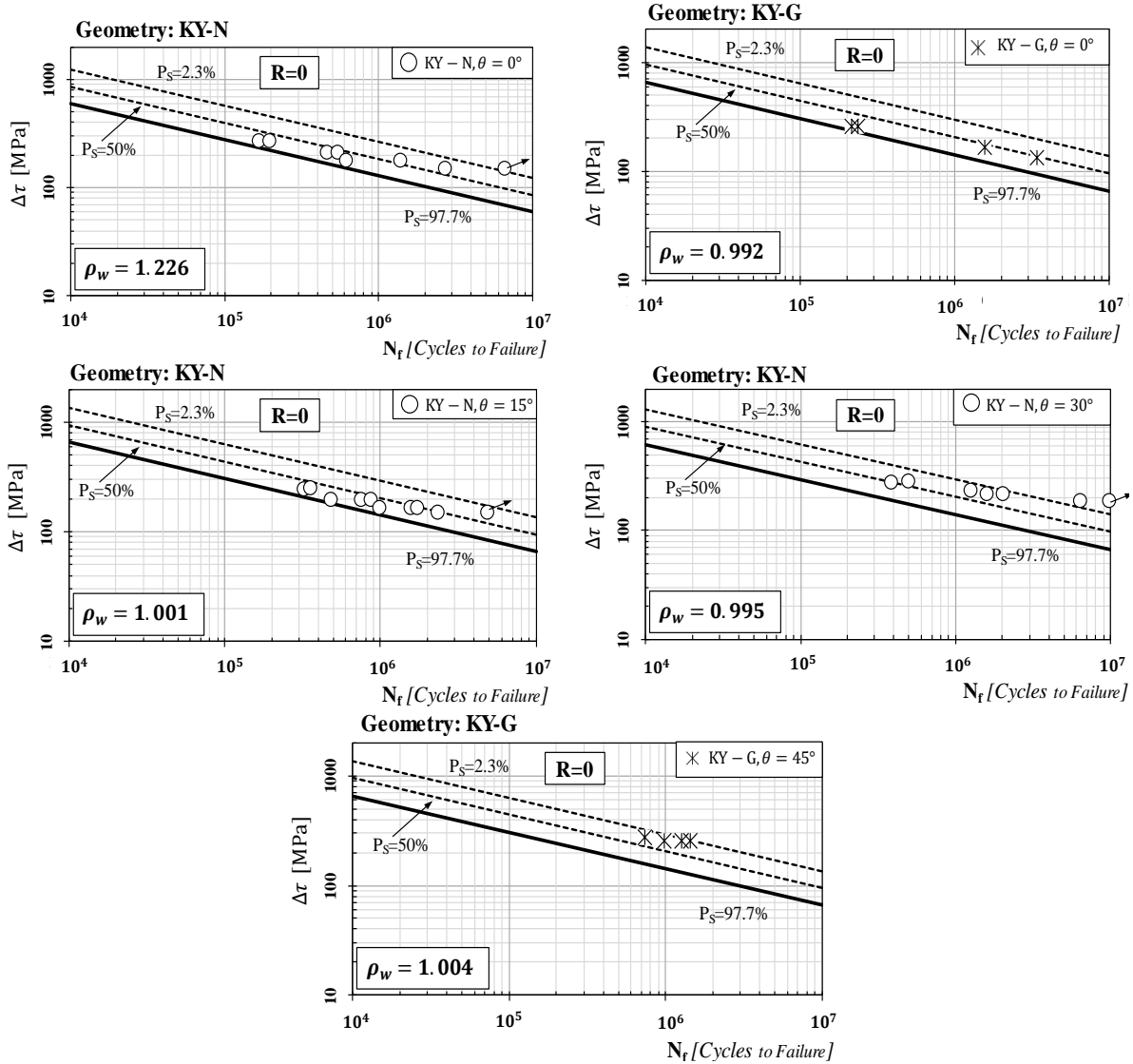


Figure 4.20 Accuracy of the MWCM applied along with effective notch stresses in estimating fatigue strength in the presence of inclined welds (for geometry KY-N and KY-G).

4.3.4 The MWCM applied along with the Point Method

The fundamental concept on which the TCD is based can be formalised in different ways that include the Point Method (PM), the Line Method (LM), the Area Method (AM), and the Volume Method (VM) [22]. Amongst these different formalisations of the same idea, certainly, the PM represents the simplest way to use the TCD in situations of practical interest. In more detail, the PM postulates that the effective stresses to be used to perform fatigue assessment have to be determined at a given distance from the assumed crack initiation location. In this context, the required critical distance is seen to be a material property. In other words, for a given material, the critical distance value is not affected by the sharpness of the geometrical feature being assessed.

Further, as soon as the required length scale parameter is known, effective stresses can be determined by using a simple linear-elastic constitutive law to model the stress-strain behaviour of the material under investigation, with this holding true independently of the actual level of ductility/non-linearity that characterises the material itself [9, 23].

As far as steel welded joints are concerned, to apply the MWCM along with the PM, the local-linear elastic stress components relative to the critical plane have to be determined, along the weld toe/root bisector, at a distance from the assumed crack initiation point equal to 0.5 mm [9, 12, 24]. The range of the normal stress, $\Delta\sigma_n$, as well as the range of the shear stress, $\Delta\tau$, acting on the critical plane are then used to calculate stress ratio ρ_w . The negative inverse slope, $k_\tau(\rho_w)$, of the corresponding modified Wöhler curve is directly derived from the following relationships [12, 24]:

$$k_\tau(\rho_w) = -2\rho_w + 5 \quad \text{for } \rho_w \leq 1 \quad (4.16)$$

$$k_\tau(\rho_w) = 3 \quad \text{for } \rho_w > 1 \quad (4.17)$$

The reference shear stress range, $\Delta\tau_{Ref}(\rho_w)$, extrapolated at $5 \cdot 10^6$ cycles to failure is instead estimated for $P_s=50\%$ from [24]:

$$\Delta\tau_{Ref}(\rho_w) = -32\rho_w + 96 \text{ [MPa]} \quad \text{for } \rho_w \leq 2 \quad (4.18)$$

$$\Delta\tau_{Ref}(\rho_w) = 32 \text{ [MPa]} \quad \text{for } \rho_w > 2 \quad (4.19)$$

And, for P_s equal to 97.7% from [24]:

$$\Delta\tau_{Ref}(\rho_w) = -24\rho_w + 67 \text{ [MPa]} \quad \text{for } \rho_w \leq 2 \quad (4.20)$$

$$\Delta\tau_{Ref}(\rho_w) = 19 \text{ [MPa]} \quad \text{for } \rho_w > 2 \quad (4.21)$$

4.3 The MWCM to estimate the fatigue lifetime of inclined welds subjected to uniaxial fatigue loading

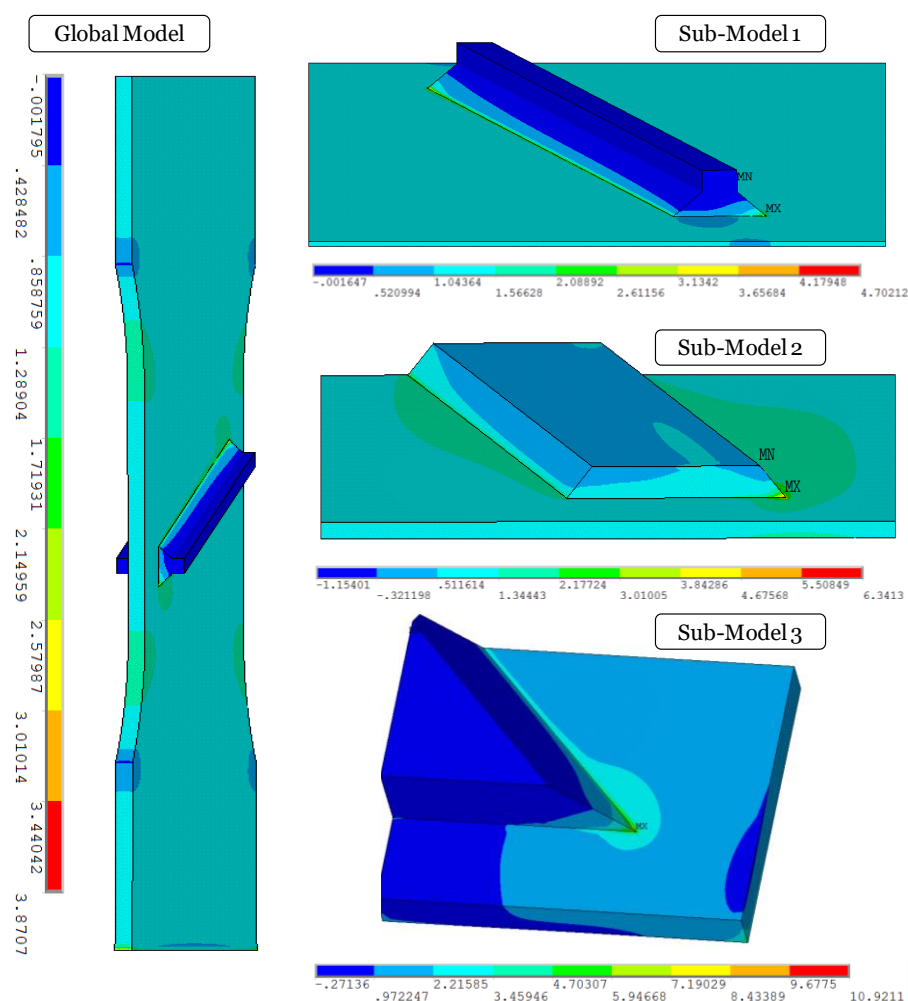


Figure 4.21 Examples of the linear-elastic FE models solved by following a solid-to-solid sub-modelling procedure using the TCD.

In order to check the accuracy of the MWCM applied along with the PM in estimating fatigue strength in the presence of inclined welds, the relevant linear-elastic stress states were determined, along the weld toe/root bisectors and at a distance from the crack initiation point equal to 0.5 mm, by solving three-dimensional models with FE code ANSYS®. In particular, the solutions for the different welded geometries being investigated were obtained by following a standard solid-to-solid sub-modelling procedure (section 4.2.2), with the mesh density being increased gradually until convergence occurred (Figure 4.21). The required linear elastic stress field is determined by setting the weld toe radius invariably equal to zero. The required local stresses along the weld bisector were obtained from the 3D FE models where the weld bisector was rotated for each different inclination angle so that it is always perpendicular to the weld seams (Figure 4.22).

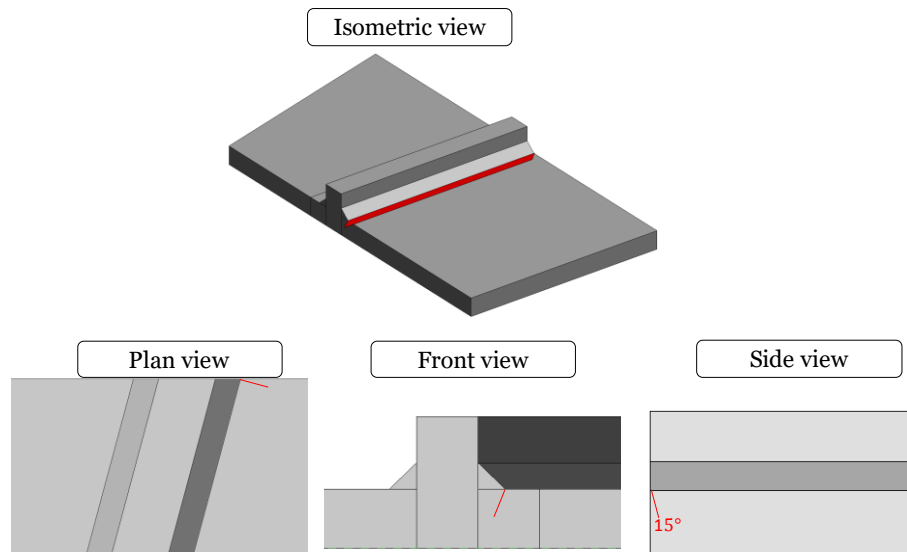


Figure 4.22 Schematic illustration of the focus path used to calculate the effective stresses of 15° inclination angle welded joints using the PM.

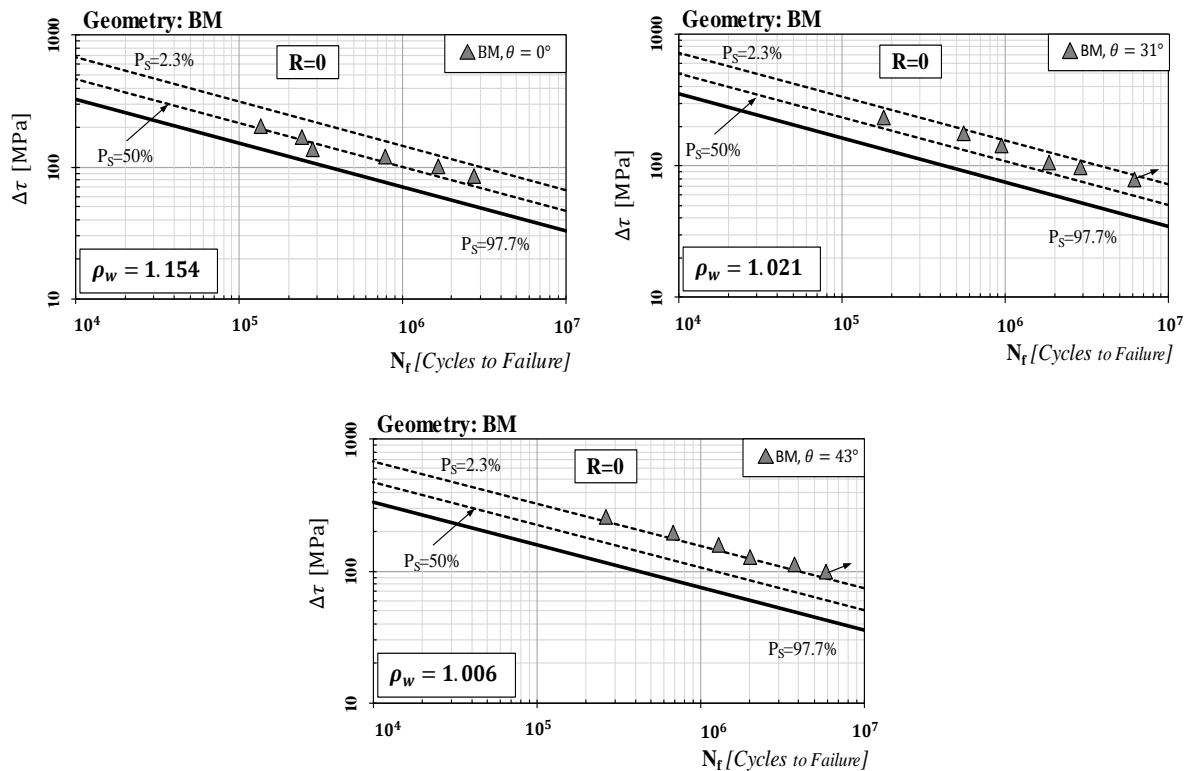


Figure 4.23 Accuracy of the MWCM to estimate the fatigue strength of the inclined welded joints using the Theory of Critical Distances in the form of Point Method (Geometry BM).

4.3 The MWCM to estimate the fatigue lifetime of inclined welds subjected to uniaxial fatigue loading

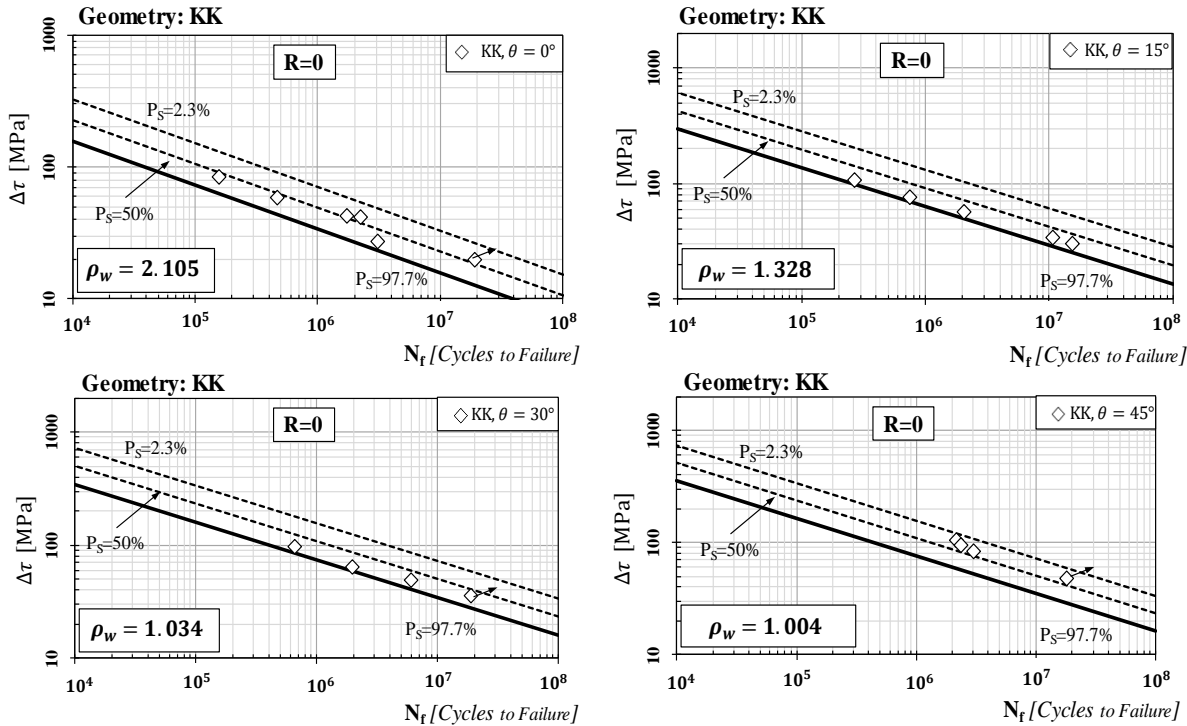


Figure 4.24 Accuracy of the MWCM to estimate the fatigue strength of the inclined welded joints using the Theory of Critical Distances in the form of Point Method (Geometry KK).

The results obtained by applying the MWCM along with the PM are summarised in the modified Wöhler diagrams of Figure 4.23 to Figure 4.25 (see also Table B.5 to Table B.8, Appendix B). These charts demonstrate that this local stress based multiaxial fatigue assessment technique is capable of estimating the fatigue strength of connections containing inclined welds with a remarkable level of accuracy, the advantage being that the required stress analysis can be performed by solving simple linear elastic FE model.

Chapter 4: Fatigue assessment of inclined welded joints subjected to uniaxial cyclic loading.

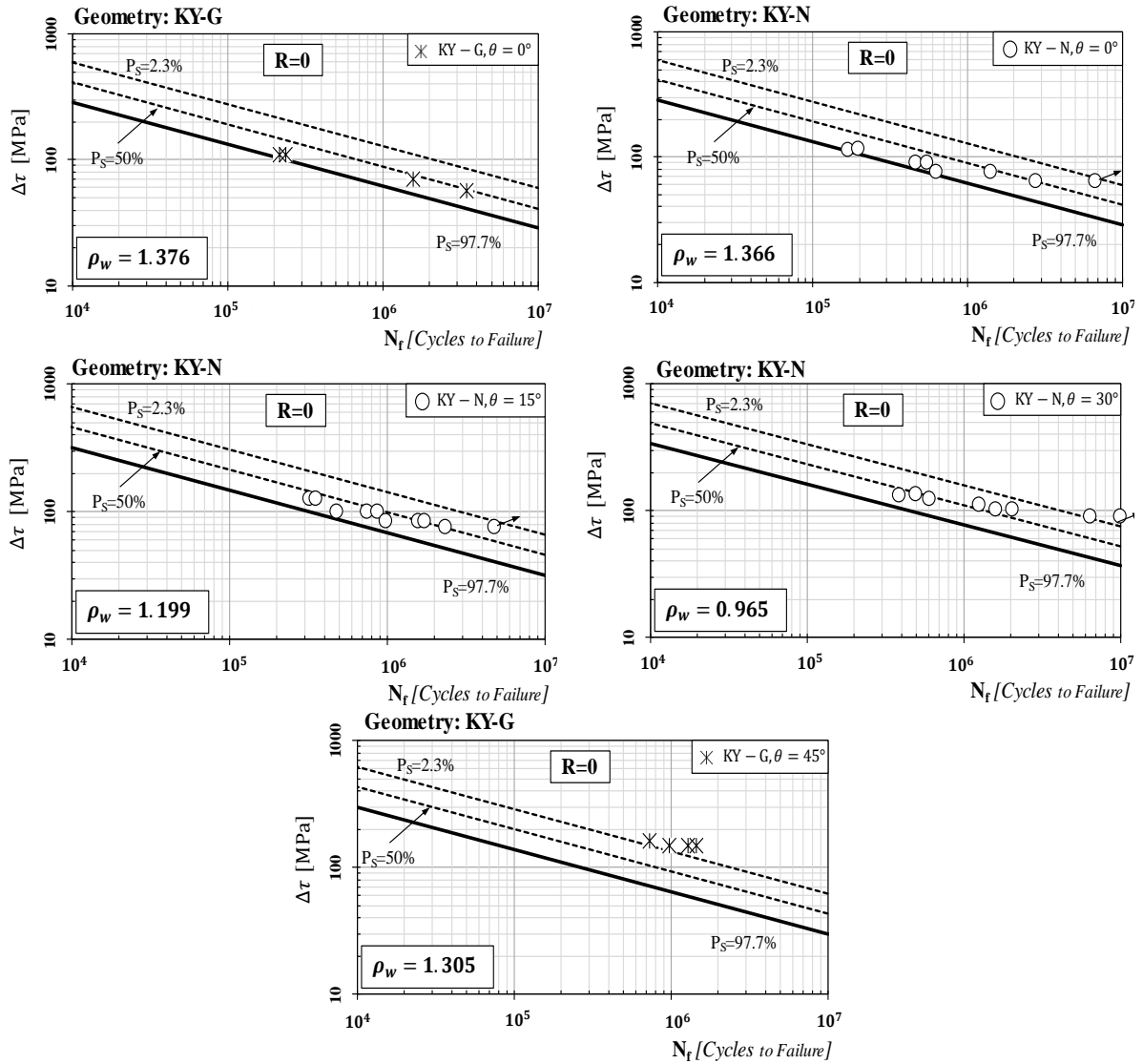


Figure 4.25 Accuracy of the MWCM to estimate the fatigue strength of the inclined welded joints using the Theory of Critical Distances in the form of Point Method (Geometry KY).

4.4 Conclusions

In the present paper, the MWCM was applied along with nominal, hot spot, and local stresses to estimate the fatigue strength of uniaxially loaded steel welded joints containing inclined welds. The accuracy and reliability of these different ways of using the MWCM to address this specific design problem were checked systematically by post-processing a large number of data taken from the technical literature. These experimental results were generated by initiating fatigue cracks not only at the weld toes, but also at the weld roots. According to the outcomes from the present research work, the most important conclusions are summarised in what follows.

- Fatigue strength of uniaxially loaded inclined welds can be assessed successfully by tackling the problem from a multiaxial fatigue angle. In particular, for this particular geometry/loading configuration, weld seams are damaged by proportional multiaxial load histories, with this holding true independently of the strategy that is adopted to perform the stress analysis.
- As far as steel connections are concerned, the MWCM applied in conjunction with nominal, hot-spot, and notch stresses as well as with the TCD is seen to be highly successful in estimating fatigue strength in the presence of uniaxially loaded inclined welds.
- Irrespective of the type of stress analysis being adopted, the MWCM's governing equations can be calibrated accurately by taking full advantage of those uniaxial and torsional reference design curves that are provided by the pertinent Standard Codes and Recommendations.
- More work needs to be done in this area to check whether this multiaxial fatigue-based idea can be extended successfully also to the fatigue assessment of uniaxially loaded aluminium joints containing inclined welds.

4.5 References

- [1] Hobbacher A. Recommendations for fatigue design of welded joints and components. IIW document XIII-2151-07/XV-1254-07; 2007..
- [2] Design of steel structures. ENV 1993-1-1, EUROCODE 3; 1988..
- [3] Eurocode 9: design of aluminium structures – Part 2: structures susceptible to fatigue, prENV; 1999..
- [4] Booth GS, Maddox SJ. Influence of various factors on the fatigue strength of steel plates with fillet welded attachments. TWI Research Report no. 93, Cambridge, UK; 1979..
- [5] Kim I-T, Kainuma S. Fatigue life assessment of load-carrying fillet welded cruciform joints inclined to uniaxial cyclic loading. *Int J Pres Ves Pip* 2005; 82: 807–13..
- [6] Kim I-T, Yamada K. Fatigue behaviour of fillet welded joints inclined to a uniaxial cyclic load. IIW Document XIII-2021-04; 2004..
- [7] Radaj D, Sonsino CM, Fricke W. Fatigue assessment of welded joints by local approaches. Cambridge, UK: Woodhead Publishing Limited; 2007..
- [8] Niemi E, Fricke W, Maddox SJ. Fatigue analysis of welded components: designer's guide to the structural hot-spot stress approach. Cambridge, UK: Woodhead Publishing Limited; 2006..
- [9] Susmel L. Multiaxial notch fatigue: from nominal to local stress–strain quantities. Cambridge, UK: Woodhead Publishing Limited; 2009..
- [10] Susmel L, Tovo R. On the use of nominal stresses to predict the fatigue strength of welded joints under biaxial cyclic loading. *Fatigue Fract Eng Mater Struct* 2004;27:1008–24..
- [11] Susmel L. Three different ways of using the Modified Wöhler Curve Method to perform the multiaxial fatigue assessment of steel and aluminium welded joints. *Eng Fail Anal* 2009; 16: 1074–89..
- [12] Susmel L. Four stress analysis strategies to use the Modified Wöhler Curve Method to perform the fatigue assessment of weldments subjected to constant and variable amplitude multiaxial fatigue loading. *Int J Fatigue* 2014; 64: 38–54..
- [13] Susmel L. Nominal stresses and Modified Wöhler Curve Method to perform the fatigue assessment of uniaxially-loaded inclined welds. *Proc Inst Mech Eng C-J Mech* 2014;228(16):2871–80..

4.5 References

- [14] Maddox SJ. Fatigue assessment of welds not oriented either normal or parallel to the direction of loading. IIW Document JWG XIII/XV-218-10; 2010..
- [15] Lazzarin P, Tovo R. A unified approach to the evaluation of linear elastic stress fields in the neighbourhood of cracks and notches. *Int J Fracture* 1996; 78: 3–19..
- [16] Lazzarin P, Tovo R. A notch intensity factor approach to the stress analysis of welds. *Fatigue Fract Eng Mater Struct* 1998; 21: 1089–103..
- [17] Lazzarin P, Sonsino CM, Zambardi R. A notch stress intensity approach to assess the multiaxial fatigue strength of welded tube-to-flange joints subjected to combined loadings. *Fatigue Fract Eng Mater Struct* 2004; 27: 127–40..
- [18] Haibach E. Service fatigue-strength – methods and data for structural analysis. Düsseldorf: VDI, 1992..
- [19] Susmel L, Tovo R. Local and structural multiaxial stress states in welded joints under fatigue loading. *Int J Fatigue* 2006; 28: 564–75..
- [20] Susmel L, Sonsino CM, Tovo R. Accuracy of the Modified Wöhler Curve Method applied along with the $r_{ref}=1$ mm concept in estimating lifetime of welded joints subjected to multiaxial fatigue loading. *Int J Fatigue* 2011; 33: 1075–91..
- [21] Sonsino CM. A consideration of allowable equivalent stresses for fatigue design of welded joints according to the notch stress concept with the reference radii $r_{ref}=1.00$ and 0.05 mm. *Weld World* 2009;53(3/4):R64–75..
- [22] Taylor D. Geometrical effects in fatigue: a unifying theoretical model. *Int J Fatigue* 1999; 21: 413–20..
- [23] Taylor D. The theory of critical distances: a new perspective in fracture mechanics. Oxford, UK: Elsevier; 2007..
- [24] Susmel L. Modified Wöhler Curve Method, Theory of Critical Distances and EUROCODE 3: a novel engineering procedure to predict the lifetime of steel welded joints subjected to both uniaxial and multiaxial fatigue loading. *Int J Fatigue* 2008; 30:888–907..

Chapter 5

5.Experimental Procedure

In this present study, a systematic experimental programme was designed to:

- 1) Test the capability of the EWM coldArc® technology described in chapter 2 (section 2.1.5) of producing a strong and robust hybrid welded joint.
- 2) Investigate the static strength of aluminium-to-steel thin welded joints manufactured using this welding technology. It is worth mentioning that the design of the specimens is for non-standard tests. However, standards were consulted so that the geometries are suitable to predict the stress fields on the weld toes.
- 3) Extend the use of the existing stress-based approaches and check the accuracy and reliability of those approaches to estimate the fatigue strength of the thin hybrid welded joints.

5.1 Materials

In this investigation aluminium alloy AA1050 (containing 99.5% of aluminium) and a zinc-coated cold-rolled low carbon steel manufactured in accordance with EN 10130:1991. The ultimate tensile strength of these two materials was 120 MPa and 410 MPa, respectively, with Young's modulus equal to 71 GPa for the aluminium alloy and to 210 GPa for the steel. The steel sheets were coated with a layer of zinc having a thickness equal to approximately 25 µm.

The 1 mm diameter filler wire used in the welding process was made of AA4043 aluminium alloy. During welding, pure argon was used as shielding gas. Two different sheet thicknesses (1 mm and 2 mm) were used to manufacture the fatigue specimens to be tested under different fatigue load ratios (i.e., $R=-1$, $R=0.1$ and $R=0.5$). The chemical compositions of the materials used in this investigation are summarised in Table 5.1.

5.2 Welding Process

Table 5.1 Mass chemical composition of the used materials by weight percentage.

Alloy	Chemical composition [wt%]							
	Cu	Mg	Si	Fe	Mn	Zn	Ti	Al
AA1050	0-0.05	0-0.05	0.25	0-0.4	0.05	0.07	0-0.05	Balance
EN10130:199	C	P	S	Mn	Fe			
	0.12	0.045	0.045	0.60	Balance			
AA4043	Cu	Mg	Si	Fe	Mn	Zn	Ti	Al
	0.01	0.05	4.5-6.0	0.80	0.05	0.1	0.2	Balance

5.2 Welding Process

An experienced welding technician using an EWM alpha Q551 pulse machine (Figure 5.1) manufactured various welded joint configurations (see Figure 5.4 and Figure 5.5). The EWM coldArc® welding process is a modified short-arc process that has gap bridge capabilities and it can also provide control over the heat input and the metal transfer (see section 2.1.5 for more details). As far as very thin materials are concerned, the low heat input allows them to be welded without causing burn-through. The coldArc® process is able to weld hybrid sheets with a thickness as thin as 0.3 mm and 0.7 mm using automated and manual machines, respectively.



Figure 5.1 EWM welding machine.

The unique features of the coldArc® process make it suitable for fabricating aluminium-to-steel thin joints, provided that the steel sheet is pre-coated with zinc to prevent the formation of hard and brittle intermetallic phases at the interface between the two materials. EWM provides very detailed welding parameter envelopes for different welding combinations and different thicknesses. For the 1 mm thick sheets, the welding parameters were set as follows: arc voltage equal to 15.3 V, current to 54 A, wire feed to 5 m/min; for the 2 mm thick plates the parameters were: arc voltage equal to 18.2 V, current to 88 A, wire feed to 7.9 m/min.

The specimens were prepared by welding aluminium and steel sheets with a width equal to 70 mm which were neatly cut down to 50 mm to eliminate any undesirable defects formed at the edges during the welding process. It is worth mentioning that the welding parameters are optimised and integrated into the machine programme provided by EWM® welding company. By choosing the correct programme code from the list provided and set the thickness of the material, the machine will set up the corresponding welding parameters accordingly (see Figure 5.2a). If required, the welding parameters can be adjusted manually (Figure 5.2b).

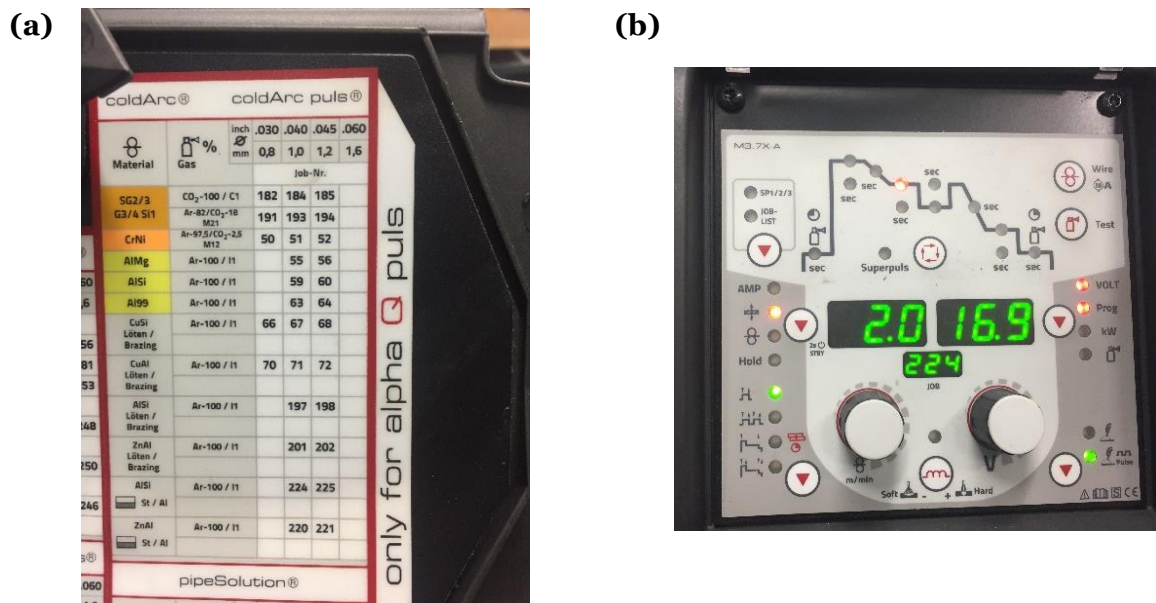


Figure 5.2 EWM alpha Q pul including codes list for various material combination (a) the machine interface showing values for different welding parameters (b).

5.3 Investigated configurations

5.3.1 Static investigation

Figure 5.3a shows the different welded specimens that were tested under tensile static loading to investigate the static strength of aluminium-to-steel welded joints. In particular, Butt-welded joints with different inclination angles ranging between 0° and 60°, cruciform welded and lap welded joints were investigated.

5.3 Investigated configurations

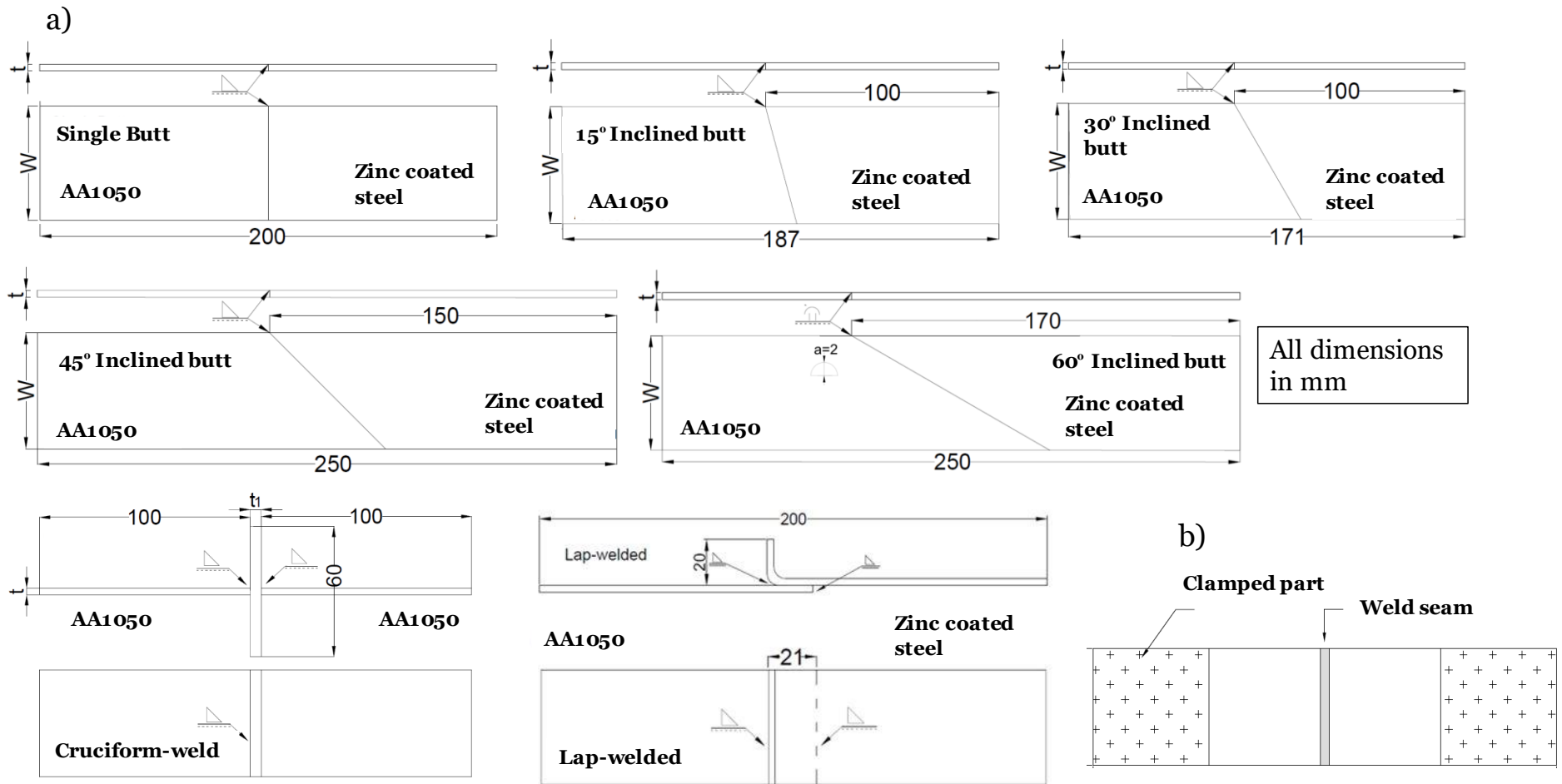


Figure 5.3 Geometry of the investigated aluminium-to-steel welded components (a). Schematisation of the tensile specimens (b).

5.3.2 Fatigue investigation

Four different configurations were manufactured and prepared for fatigue testing including butt, cruciform (Figure 5.4), lap and tee (Figure 5.5) welded joints. As far as the butt-welded joints are concerned, a single weld was applied. It is very important to mention that the galvanised steel sheets are only zinc coated on the top and bottom surfaces, leaving the edges without any zinc. Thus, the butt-welded joints experience a lack of adhesion between the steel and the aluminium. This lack of adhesion results in a gap between the two materials and the weld only acts as a bridge to hold the two materials together.

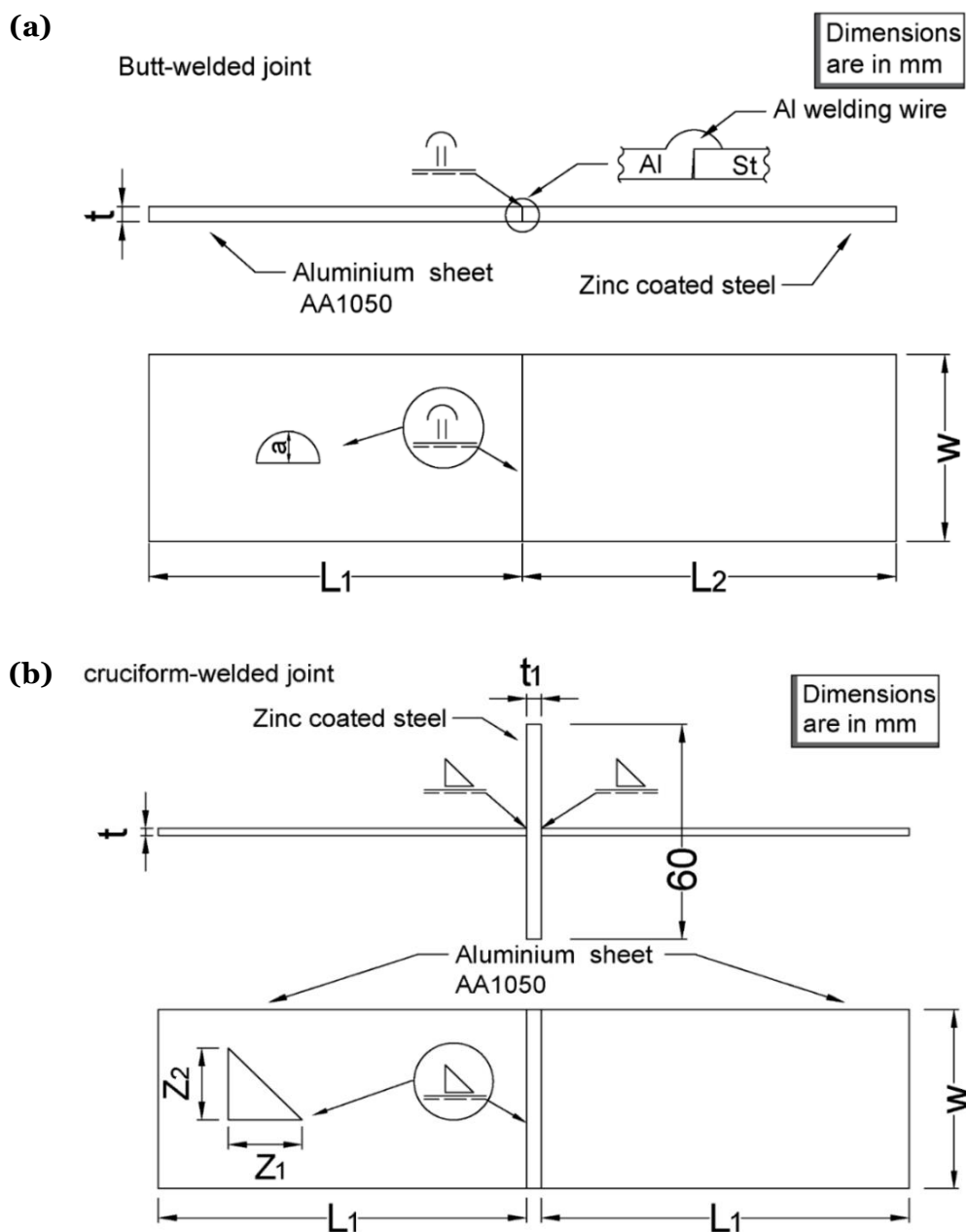
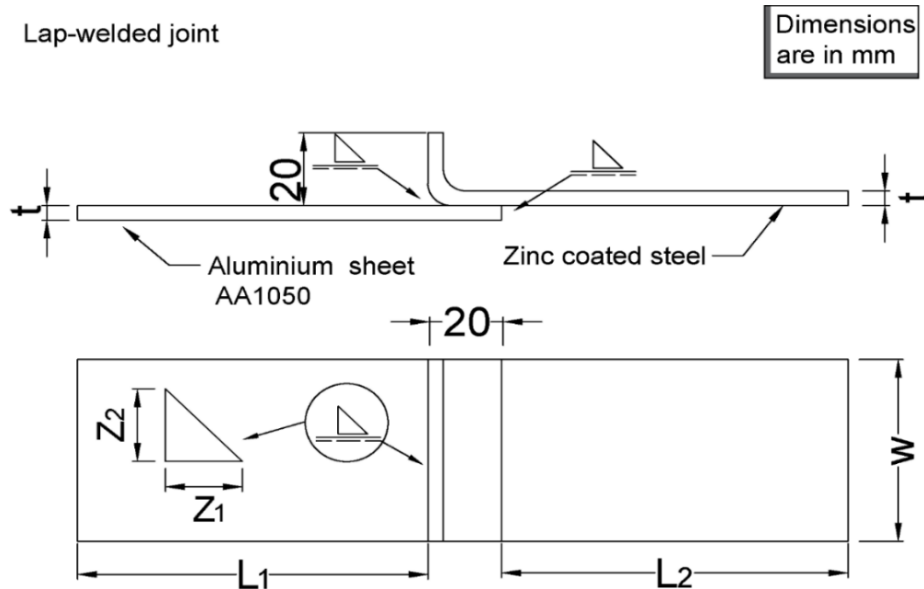


Figure 5.4 Geometry of the investigate aluminium-to-steel welded joints, butt-welded joints (a); and the load carrying cruciform welded joints (b).

5.3 Investigated configurations

The manufacture of the cruciform welded joints was performed using a welding jig designed to ensure the top and bottom stiffeners were aligned and welded as straight as possible, with this allowing us to minimise effectively any detrimental phenomena associated with eccentricity.

(a) Lap-welded joint



(b)

Tee-welded joint

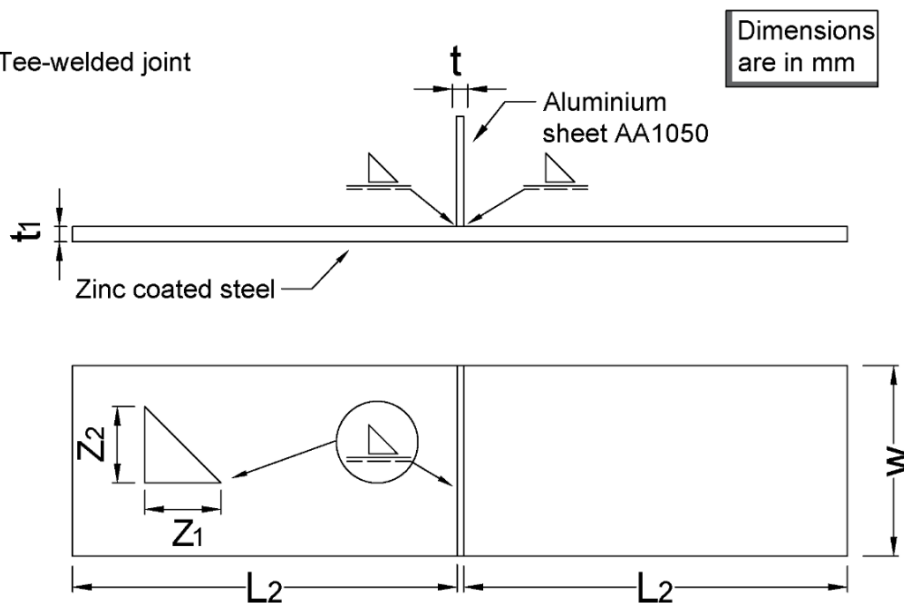


Figure 5.5 Geometry of the investigate aluminium-to-steel welded joints, lap-welded hybrid welded joints (a); and the tee welded joints (b).

Because the steel edges were not galvanised, producing the lap joint in the traditional form was not possible. Accordingly, the lap joints being tested were manufactured by bending the steel sheet at 90°. As it can be seen in Figure 5.5a, this allowed to place the weld seam between the galvanised steel and the aluminium, with this resulting in an adequate level of mechanical strength also for the lap joints.

The tee-welded joints were prepared with the stiffener made of aluminium and the main plate made of steel. To prevent the bending of the main plate during welding, all the tee-welded joints were made with 2 mm thick plates. Prior to the fatigue testing, the clear distance between the weld tip and the hydraulic grips for all the welded configurations was set to approximately 20 mm to avoid any secondary bending effect during the fatigue tests.

5.4 Static test

The tensile tests were run using a 100 kN MAYSE dynamic and static machine. (Figure 5.6). The specimens were prepared as shown in Figure 5.3b and tested at room temperature under a nominal displacement rate of 2 mm/min.

To investigate the aging effect on the aluminium heat affected zone (HAZ), and whether the material would restore its microstructure which were disrupted during the welding process and gain more strength, the investigated geometries illustrated in Figure 5.3a were manufactured in two batches. The first batch was tested straightway after the welding. The second batch was stored in the laboratory at room temperature for 12 months. After 12 months, the same testing procedure is used to run a tensile test for batch two.

5.5 Fatigue test

The fatigue tests were run at room temperature using a 100 kN capacity MAYSE static and dynamic machine (shown in Figure 5.6). The specimens were tested in the as-welded condition (i.e. no heat treatment was applied prior to the fatigue test) at a frequency equal to 10 Hz. For the butt and cruciform welded joints, two different plate thicknesses were used including 1 mm for a load ratio equal to 0.1 and 2 mm for a load ratio equal to -1. For a 95% confidence level and for research and development tests, it is suggested to run 6-12 tests for each series with at least 2 samples per stress level².

² Lee Y, Pan J, Hatmaway R, Barkey M. Fatigue testing and analysis (Theory and Practice). Burlington: Elsevier Butterworth Heinemann, 2005.

5.5 Fatigue test



(a) (b)
Figure 5.6 MAYSE uniaxial fatigue machine (a), hydraulic grips (b).

For the fully reversed loading ($R = -1$), the 2 mm thickness provided extra stiffness and prevented any bending effect under the compression loading. For the lap welded joints, by keeping the 20 mm distance between the weld tip and the grips, the lap specimens were rather long and the excessive bending effect caused while performing fully reverse fatigue loading made it impossible to run fatigue tests under $R = -1$. For this reason, different load ratio is used. The lap joints were tested using a thickness of 1 mm for $R = 0.1$ and 2 mm for $R = 0.5$ to explore different loading levels. The tee welded joints were tested using a thickness of 2 mm for both load ratios ($R = 0.1$ and $R = -1$), because during the manufacturing process of the Tee joints it was important to increase the thickness of the plate to prevent the bending of the plate. The results generated from the fatigue investigation are summarised in Table 5.2 to Table 5.5 these tables provide information about the geometries dimensions, the applied nominal stress ranges, load ratio as well as the number of cycles to failure. In this investigation, if the samples have not failed after $2 \cdot 10^6$ cycles the fatigue test was stopped and the test was considered as a run-out and re-tested at a high-stress range.

Table 5.2 Fatigue results generated by testing butt-welded joints (Figure 5.4a).

Code	R	t	W	a	$\Delta\sigma_{nom}$	$\Delta\sigma_{eff}$	N_f	Run-out
		[mm]	[mm]	[mm]	[MPa]	[MPa]	[cycles to failure]	
Butt_0.1_1	0.1	0.99	49.00	1.88	60	420	15617	
Butt_0.1_2	0.1	1.10	49.80	1.60	50	350	2000000	✓
Butt_0.1_3	0.1	1.00	50.80	1.89	54	378	289490	
Butt_0.1_4	0.1	1.02	49.92	2.10	57	399	89952	
Butt_0.1_5	0.1	1.03	50.05	2.17	57	399	105241	
Butt_0.1_6	0.1	1.01	49.73	2.14	54	378	14380	
Butt_0.1_7	0.1	1.01	50.43	1.92	52	364	23470	
Butt_0.1_8	0.1	1.03	49.85	1.66	50	350	23335	
Butt_0.1_9	0.1	1.01	50.34	1.82	50	350	138007	
Butt_0.1_10	0.1	1.02	49.97	1.96	60	420	15275	
Butt_0.1_11	0.1	1.04	50.67	1.78	50	350	67660	
Butt_0.1_12	0.1	1.03	49.84	1.88	50	350	36631	
Butt_0.1_13	0.1	1.03	49.50	1.97	35	245	837329	
Butt_0.1_14	0.1	1.00	49.41	2.10	40	280	2000000	✓
Butt_0.1_15	0.1	1.01	49.84	1.88	45	315	967279	
Butt_-1_1	-1	1.96	49.21	2.21	35	525	235783	
Butt_-1_2	-1	1.96	49.12	1.92	42	630	2327	
Butt_-1_3	-1	1.95	49.07	1.79	32	480	138731	
Butt_-1_4	-1	1.97	49.27	2.01	35	525	6415	
Butt_-1_5	-1	1.97	49.32	2.13	30	450	162306	
Butt_-1_6	-1	1.98	50.41	1.87	28	420	2000000	✓
Butt_-1_7	-1	1.98	50.41	1.83	40	600	25032	
Butt_-1_8	-1	1.96	50.45	1.83	32	480	2000000	✓
Butt_-1_9	-1	1.96	49.21	1.68	35	525	54914	
Butt_-1_10	-1	1.99	50.24	2.00	28	420	2000000	✓
Butt_-1_11	-1	1.99	50.24	2.13	38	570	9857	
Butt_-1_12	-1	1.98	50.25	2.09	28	420	41366	

5.5 Fatigue test

Table 5.3 Fatigue results generated by testing cruciform welded joints (Figure 5.4b).

Code	R	t	w	Z1	Z2	L1	$\Delta\sigma_{nom}$	$\Delta\sigma_{eff}$	ΔK_I	N_f	Run-out
		[mm]	[mm]	[mm]	[mm]	[mm]	[mm]	[MPa]	[MPa·mm ^{0.326}]	[cycles to failure]	
Cr_0.1_1	0.1	1.02	49.83	5.07	7.43	25.07	60	256	103	1656	
Cr_0.1_2	0.1	1.02	50.73	5.27	7.84	25.27	55	235	95	52093	
Cr_0.1_3	0.1	1.02	49.73	5.21	7.67	25.21	50	214	86	51492	
Cr_0.1_4	0.1	1.03	49.78	4.66	7.51	24.66	50	214	86	327683	
Cr_0.1_5	0.1	1.04	48.98	5.13	7.33	25.13	60	256	103	21171	
Cr_0.1_6	0.1	1.01	48.56	5.18	7.62	25.18	55	235	95	564736	
Cr_0.1_7	0.1	1.02	50.62	5.56	8.10	25.56	40	171	69	564974	
Cr_0.1_8	0.1	1.01	50.60	5.23	7.20	25.23	40	171	69	279615	
Cr_0.1_9	0.1	1.01	50.58	5.49	7.95	25.49	45	192	78	86145	
Cr_0.1_10	0.1	1.01	50.49	5.66	7.58	25.66	45	192	78	2456047	
Cr_-1_1	-1	1.97	48.19	4.04	4.65	24.04	60	256	120	44535	
Cr_-1_2	-1	1.97	48.49	3.97	5.14	23.97	60	256	120	122917	
Cr_-1_3	-1	1.98	48.09	4.30	4.96	24.3	55	235	110	289083	
Cr_-1_4	-1	1.99	47.63	3.77	4.62	23.77	55	235	110	220433	
Cr_-1_5	-1	1.97	48.27	2.89	5.38	22.89	50	214	100	417151	
Cr_-1_6	-1	1.99	48.39	3.58	4.75	23.58	50	214	100	242154	
Cr_-1_7	-1	1.99	47.70	3.84	4.96	23.84	45	192	90	2000000	✓
Cr_-1_8	-1	1.99	47.70	3.25	5.07	23.25	55	235	110	297435	
Cr_-1_9	-1	1.99	48.16	3.66	4.95	23.66	48	205	96	188002	
Cr_-1_10	-1	1.98	48.76	3.68	4.50	23.68	48	205	96	699617	
Cr_-1_11	-1	1.98	48.10	3.33	5.55	23.33	48	205	96	2000000	✓
Cr_-1_12	-1	1.98	48.10	3.33	5.55	23.33	58	248	116	89987	

Table 5.4 Fatigue results generated by testing lap welded joints (Figure 5.5a).

Code	R	t	w	Z1	Z2	L1	L2	$\Delta\sigma_{nom}$	$\Delta\sigma_{eff}$	ΔK_I	N_f	Run-out
		[mm]	[mm]	[mm]	[mm]	[mm]	[mm]	[MPa]	[MPa]	[MPa.mm ^{0.32}]	[cycles to failure]	
Lap_0.1_1	0.1	1.02	50.11	2.92	2.83	22.92	22.83	60	234	96	31581	
Lap_0.1_2	0.1	1.01	50.21	3.03	3.15	23.03	23.15	60	234	96	102426	
Lap_0.1_3	0.1	1.01	50.20	2.42	2.37	22.42	22.37	65	253	104	94739	
Lap_0.1_4	0.1	1.03	50.14	2.73	2.44	22.73	22.44	65	253	104	55703	
Lap_0.1_5	0.1	1.01	50.09	2.53	2.63	22.53	22.63	55	214	88	86888	
Lap_0.1_6	0.1	1.02	50.29	3.02	2.80	23.02	22.8	55	214	88	94390	
Lap_0.1_7	0.1	0.98	50.17	2.79	2.55	22.79	22.55	50	195	80	367625	
Lap_0.1_8	0.1	1.00	50.28	2.61	2.97	22.61	22.97	45	175	72	191873	
Lap_0.1_9	0.1	1.01	50.17	2.53	2.64	22.53	22.64	45	175	72	1131920	
Lap_0.1_10	0.1	1.00	50.10	2.66	2.70	22.66	22.7	50	195	80	496799	
Lap_0.5_1	0.5	1.98	51.73	4.89	5.15	24.89	25.15	30	147	67	1093169	
Lap_0.5_2	0.5	1.97	50.34	4.36	5.46	24.36	25.46	35	172	79	275251	
Lap_0.5_3	0.5	1.98	51.82	4.58	5.60	24.58	25.6	35	172	79	209757	
Lap_0.5_4	0.5	1.97	51.75	4.11	6.28	24.11	26.28	30	147	67	929710	
Lap_0.5_5	0.5	1.97	51.73	6.13	4.10	26.13	24.1	32	157	72	467257	
Lap_0.5_6	0.5	1.98	50.48	5.40	3.98	25.4	23.98	32	157	72	531450	
Lap_0.5_7	0.5	1.97	51.76	6.27	4.83	26.27	24.83	28	137	63	2000000	✓
Lap_0.5_8	0.5	1.97	50.50	5.04	4.35	25.04	24.35	38	186	85	247044	
Lap_0.5_9	0.5	1.97	51.57	4.14	4.99	24.14	24.99	38	186	85	253922	
Lap_0.5_10	0.5	1.98	50.32	4.81	5.91	24.81	25.91	28	137	63	1037289	

5.5 Fatigue test

Table 5.5 Fatigue results generated by testing tee welded joints (Figure 5.5b).

Code	R	t	t1	w	Z1	Z2	L	$\Delta\sigma_{nom}$	N_f	Run-out
		[mm]	[mm]	[mm]	[mm]	[mm]	[mm]	[mm]	[cycles to failure]	
Tee_0.1_1	0.1	0.99	1.94	50.14	5.75	9.26	25.75	200	634101	
Tee_0.1_2	0.1	1.01	1.93	50.14	5.66	8.85	25.66	200	357228	
Tee_0.1_3	0.1	1.00	1.94	49.97	5.75	8.42	25.75	180	1001833	
Tee_0.1_4	0.1	0.98	1.95	49.88	5.24	7.85	25.24	180	1074989	
Tee_0.1_5	0.1	1.00	1.92	49.66	6.09	8.77	26.09	210	545593	
Tee_0.1_6	0.1	0.98	1.92	50.13	5.15	7.51	25.15	210	2000000	✓
Tee_0.1_7	0.1	1.00	1.92	50.13	5.15	7.51	25.15	240	731154	
Tee_0.1_8	0.1	1.00	1.94	50.13	5.72	8.25	25.72	220	429920	
Tee_0.1_9	0.1	0.98	1.94	49.70	5.57	8.89	25.57	220	534240	
Tee_0.1_10	0.1	1.00	1.95	49.99	5.25	8.54	25.25	230	348954	
Tee_0.1_11	0.1	1.02	1.94	49.77	5.77	8.04	25.77	230	269310	
Tee_0.1_12	0.1	1.08	1.93	49.58	5.67	8.02	25.67	210	419127	
Tee_-1_1	-1	1.03	1.96	50.01	5.47	8.11	25.47	220	498691	
Tee_-1_2	-1	1.04	1.96	49.89	5.67	9.33	25.67	220	562767	
Tee_-1_3	-1	1.01	1.96	50.21	5.51	8.52	25.51	210	426377	
Tee_-1_4	-1	1.06	1.95	50.13	5.75	8.42	25.75	190	994315	
Tee_-1_5	-1	1.08	1.95	49.90	5.81	7.41	25.81	200	1074229	
Tee_-1_6	-1	1.02	1.97	49.98	6.02	8.43	26.02	190	1651181	
Tee_-1_7	-1	1.08	1.95	50.01	5.09	7.54	25.09	240	260375	
Tee_-1_8	-1	1.00	1.96	49.98	5.18	8.66	25.18	240	257386	
Tee_-1_9	-1	1.03	1.95	50.27	5.83	7.94	25.83	230	847412	
Tee_-1_10	-1	1.02	1.95	48.67	5.79	8.15	25.79	230	400377	
Tee_-1_11	-1	1.01	1.97	50.00	5.60	8.52	25.60	210	694024	

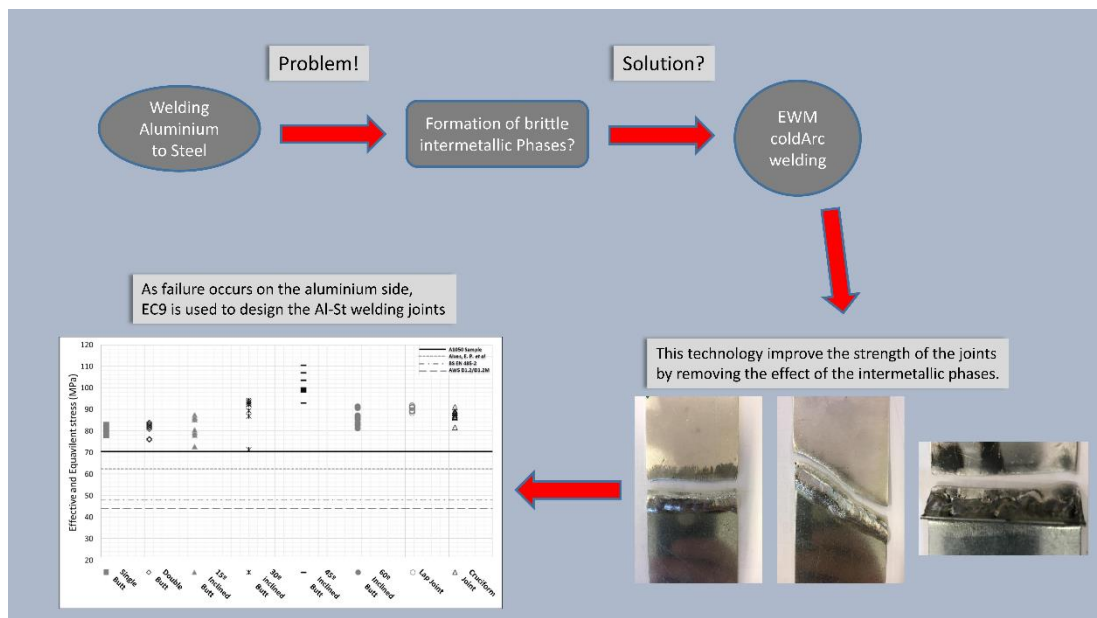
Chapter 6

6.Static strength and design of aluminium-to-steel thin welded joints

The work presented in this chapter was published in Welding in the World Journal with the following title:

Al Zamzami I, Cocco V.Di, Davison J.B, Iacoviello F, Susmel L. Static strength and design of aluminium-to-steel thin welded joints. Welding in the World 2018; 62: 1255-1272.

<https://doi.org/10.1007/s40194-018-0634-2>.



6.1 Introduction

To increase their competitiveness in the market, one of the most difficult challenges faced by companies designing and manufacturing metallic components and structures of all kinds is improving their performance by reducing not only the weight but also the associated production, energy and maintenance costs. In this context, driven by tightening legislation, customer demands and competitive pressures, it is necessary to reduce carbon emissions and the use of natural resources. For instance, many governments established policies to lower the carbon dioxide emissions from land transportation, resulting in a challenge to reduce the fuel consumption by the transport industry. In addition to fuel-efficient engines, mass-efficient structural materials are required to reduce the total weight of the vehicles [1-2].

In recent years, there has been extensive research on the possibilities of replacing the use of steel in the automotive industry and instead use lightweight materials such as aluminium to reduce the overall weight of the vehicles and hence reducing the carbon dioxide emission. Welding together dissimilar materials, and, in particular, aluminium alloys to steel, has always been a challenge because of the significant differences in their mechanical, thermo-physical and metallurgical properties which causes the formations of hard and brittle intermetallic phases in the welding region. Recently, EWM® has developed a welding process known as coldArc®, where the heat input and arc stability are precisely controlled.

In this complex and challenging scenario, the goal of the present chapter is to investigate the static strength of hybrid welded joints manufactured using the EWM coldArc® welding technology with the aim of understanding the static behaviour of such joints. Hence, proposing safe assessment rules to apply in situations of practical interest to design aluminium-to-steel welded joints against static loading. For the purpose of this chapter, butt-welded joints with various inclination angles, lap, and cruciform welded joints were prepared to study the tensile strength and failure mode of the hybrid-welded joints.

6.2 Experimental Results

The aluminium-to-steel thin welded joints were tested under a tensile static loading in the as-welded condition. As mentioned in Chapter 5, all the specimens were replicated to run two sets of experiments. This exercise was performed to investigate the mechanical performance of the HAZ of the aluminium alloys being investigated

Chapter 6: Static strength and design of aluminium-to-steel thin welded joints

straightaway after the weld (short-term aging) and one year after welding (long-term aging). Three aluminium alloys samples were tested following the standards procedure to predict the Ultimate Tensile strength (UTS) of the parent material. The average UTS of the parent material was measured as 120 MPa.

For each welded configuration being considered, at least nine specimens were tested. The experimental results generated for the short-term specimens are illustrated in Table 6.1 to Table 6.4; these tables provide the geometry dimension, the maximum tensile load in kN and the corresponding (UTS). These tables also provide information about the failure mode of each specimen. The results obtained for batch two (long-term ageing) are summarised in Appendix C (Table C.1 to Table C.4). It is apparent from the tables that the ultimate tensile strengths show no significant variation and consistent results are achieved by using EMW coldArc welding technology.

Table 6.1 Ultimate tensile strength of plain, single and double-sided butt-welded joints (short term).

Code	Angle	Width (mm)	Thickness (mm)	Max tensile load (kN)	UTS (MPa)	Failure mode
Plain 1	-	50.2	1.12	6.53	118.31	-
Plain 2	-	50.06	1.14	6.63	120.32	-
Plain 3	-	50.03	1.13	6.70	121.72	-
Average					120.1	
butt-single-1	0	50.70	1.14	4.68	81.28	AH, WS
butt-single-2	0	50.64	1.13	4.70	82.06	AH
butt-single-3	0	50.58	1.14	4.57	79.57	AH
butt-single-4	0	50.47	1.14	4.66	81.29	AH
butt-single-5	0	50.34	1.14	3.49	60.56	WS
butt-single-6	0	50.57	1.14	4.73	81.77	AH
butt-single-7	0	50.28	1.14	4.68	81.91	AH
butt-single-8	0	50.35	1.14	4.72	82.30	AH
butt-single-9	0	49.54	1.14	4.67	82.84	AH
butt-single-10	0	50.38	1.13	4.59	80.36	AH
-2 SD					75.38	
Average					79.39	
+2 SD					83.41	
butt-double-1	0	49.24	1.15	4.64	82.10	AH
butt-double-2	0	49.92	1.15	4.67	81.61	AH
butt-double-3	0	50.49	1.14	4.79	83.43	AH
butt-double-4	0	50.55	1.15	4.73	81.60	AH
butt-double-5	0	50.56	1.14	4.39	75.98	AH
butt-double-6	0	50.35	1.14	4.82	83.93	AH
butt-double-7	0	50.68	1.14	4.68	80.85	AH
butt-double-8	0	50.34	1.14	4.39	76.25	AH
butt-double-9	0	50.85	1.14	4.80	82.74	AH
butt-double-10	0	50.31	1.14	4.74	82.87	AH
-2 SD					79.45	
Average					81.14	
+2 SD					82.82	

Short term Specimens

* WS=weld seam; AH= Aluminium HAZ

6.2 Experimental Results

Table 6.2 Ultimate tensile strength of single-sided butt-welded joints with various inclination angles (short term).

Code	Angle	Width (mm)	Thickness (mm)	Max tensile load (kN)	UTS (MPa)	Failure mode
butt-single-1	15	50.07	1.14	4.82	84.14	AH
butt-single-2	15	50.27	1.15	4.77	82.83	AH
butt-single-3	15	50.28	1.14	4.88	84.97	AH
butt-single-4	15	50.11	1.15	3.83	66.71	WS
butt-single-5	15	50.06	1.14	4.43	77.41	AH, WS
butt-single-6	15	50.48	1.14	4.07	70.74	WS
butt-single-7	15	50.47	1.14	4.82	83.54	AH
butt-single-8	15	50.14	1.14	2.81	48.97	WS
butt-single-9	15	50.22	1.13	3.28	57.59	WS
butt-single-10	15	50.21	1.14	4.47	78.30	AH, WS
				-2 SD	66.10	
				Average	73.52	
				+2 SD	80.95	
butt-single-1	30	50.35	1.15	3.88	67.27	AH, WS
butt-single-2	30	50.13	1.14	5.04	87.89	AH
butt-single-3	30	50.32	1.14	5.08	88.21	AH
butt-single-4	30	50.15	1.14	5.10	88.89	AH
butt-single-5	30	50.47	1.14	5.02	87.26	AH
butt-single-6	30	50.34	1.14	5.00	86.93	AH
butt-single-7	30	49.89	1.14	4.67	81.85	AH
butt-single-8	30	50.27	1.15	4.86	84.29	AH, WS
butt-single-9	30	50.17	1.14	5.06	88.18	AH
				-2 SD	104.07	
				Average	84.53	
				+2 SD	69.30	
butt-single-1	45	50.55	0.98	5.15	103.56	AH
butt-single-2	45	49.83	0.99	4.95	99.97	AH
butt-single-3	45	50.66	0.99	4.66	92.96	AH
butt-single-4	45	50.76	1.00	5.43	106.92	AH
butt-single-5	45	50.63	1.00	5.58	110.53	AH
butt-single-6	45	50.32	0.99	4.92	98.32	AH
butt-single-7	45	50.81	0.98	4.92	98.45	AH
butt-single-8	45	50.62	0.99	5.03	99.97	AH
butt-single-9	45	50.15	0.99	4.94	99.23	AH
				-2 SD	104.04	
				Average	101.10	
				+2 SD	98.16	
butt-single-1	60	50.46	0.99	5.24	104.83	AH
butt-single-2	60	49.76	0.99	5.64	114.81	AH
butt-single-3	60	50.59	1.00	5.56	109.60	AH
butt-single-4	60	50.64	0.99	5.82	115.74	AH
butt-single-5	60	50.68	0.99	5.32	105.98	AH
butt-single-6	60	50.37	0.99	5.53	110.51	AH
butt-single-7	60	50.53	0.99	5.22	104.68	AH
butt-single-8	60	50.55	0.99	5.46	108.69	AH
butt-single-9	60	50.28	0.99	5.10	102.83	AH
butt-single-10	60	50.48	0.98	5.35	107.85	AH
				-2 SD	111.0	
				Average	108.55	
				+2 SD	106.11	

Short term Specimens

* W=weld seam; AH= Aluminium HAZ

Table 6.3 Ultimate tensile strength of lab welded joints (short term).

Code	Angle	Width (mm)	Thickness (mm)	Max tensile load (kN)	UTS (MPa)	Failure mode
Lap-1	0	48.72	1.00	4.48	91.89	AH
Lap-2	0	49.35	0.99	4.45	91.02	AH
Lap-3	0	49.27	1.01	4.45	89.43	AH
Lap-4	0	49.49	1.01	4.48	89.55	AH
Lap-5	0	49.37	1.01	4.41	88.50	AH
Lap-6	0	49.49	1.02	4.50	89.21	AH
Lap-7	0	49.75	1.00	4.46	89.68	AH
Lap-8	0	49.26	1.00	4.47	90.69	AH
Lap-9	0	49.55	0.99	4.38	89.19	AH
Lap-10	0	49.43	1.01	4.47	89.56	AH
Lap-11	0	49.45	1.00	4.51	91.20	AH
Lap-12	0	49.68	1.00	4.56	91.73	AH
Lap-13	0	49.59	1.01	4.48	89.45	AH
				-2 SD	90.62	
				Average	90.08	
				+2 SD	89.55	

Short term Specimens

* WS=weld seam; AH= Aluminium HAZ

Table 6.4 Ultimate tensile strength of cruciform welded joints (short term).

Code	Angle	Width (mm)	Thickness (mm)	Max tensile load (kN)	UTS (MPa)	Failure mode
Cr-1	0	50.28	1.03	4.46	86.07	AH
Cr-2	0	48.99	1.02	4.35	87.14	AH
Cr-3	0	49.80	1.03	4.44	86.52	AH
Cr-4	0	50.11	1.02	4.18	81.70	AH
Cr-5	0	49.28	1.00	4.40	89.32	AH
Cr-6	0	49.63	1.01	4.37	87.21	AH
Cr-7	0	49.42	1.00	4.41	89.24	AH
Cr-8	0	49.37	1.01	4.42	88.60	AH
Cr-9	0	49.30	1.01	4.38	88.05	AH
Cr-10	0	49.89	1.01	4.59	91.10	AH
Cr-11	0	51.14	1.02	4.52	86.61	AH
				-2 SD	88.69	
				Average	87.41	
				+2 SD	86.14	

Short term Specimens

* WS=weld seam; AH= Aluminium HAZ

Figure 6.1 shows the measured force (kN) versus extension (mm) data for the different hybrid welded joint geometries. These graphs illustrate how the different types of welded configurations featured a similar behaviour under a tensile static loading. This Figure records the maximum forces sustained by the various welded joints. It was noticeable that the force vs. extension response of the hybrid-welded joints follows the same force vs. extension behaviour of the typical aluminium alloys. All the samples show similar behaviour (see Appendix C).

6.2 Experimental Results

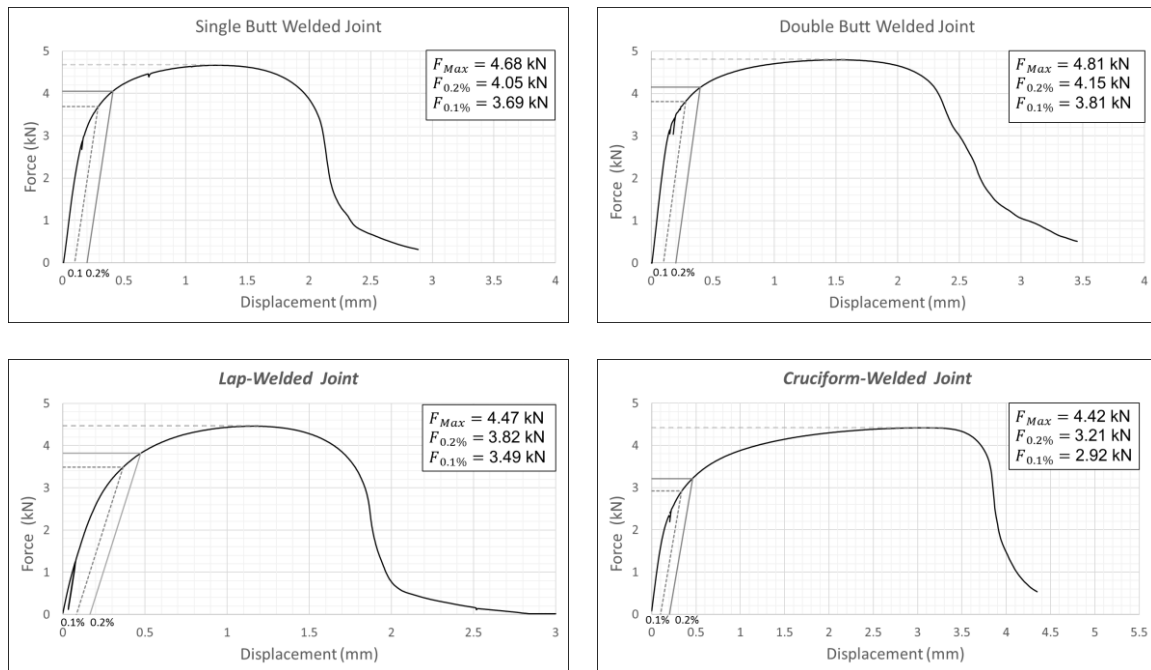


Figure 6.1 Force vs extension for different aluminium-to-steel welded joints.

Figure 6.2a and Figure 6.2b display the fracture surface of the single-butt, 15° inclined-butt, 30° inclined-butt and lap welded joints. For the lap, cruciform, double butt and 45° and 60° inclined butt welded joints, all the samples follow the same fracture behaviour, and the rupture occurs on the aluminium alloys HAZ (Figure 6.2a). However, for the single-butt, 15° and 30° inclined-butt welded joints there were three different failure modes, including a fracture in the aluminium HAZ, fracture through the weld seam and a combination of both failures (Figure 6.2b). The fracture surfaces for all the geometries are presented in Appendix C.

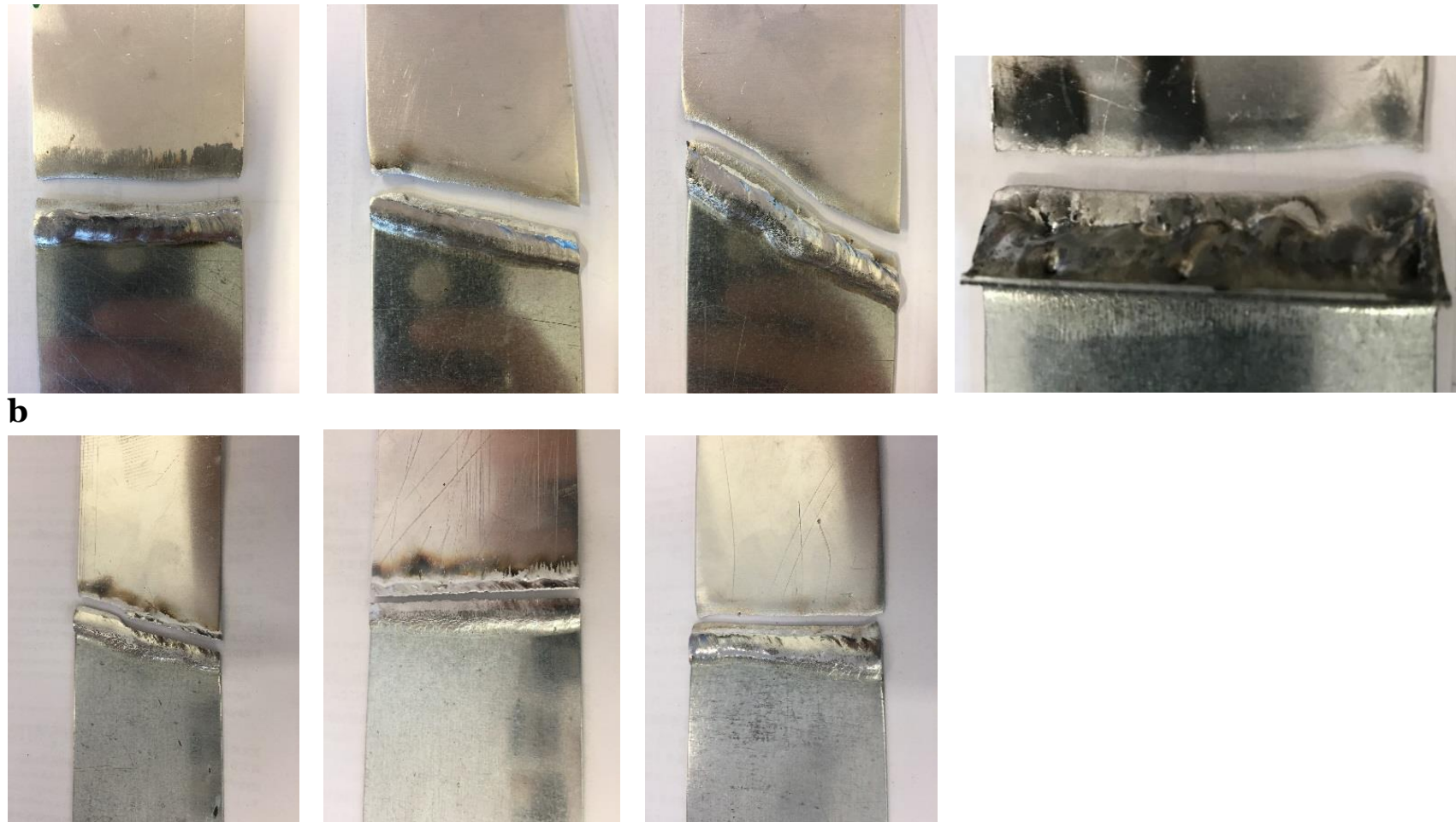


Figure 6.2 Tensile static failure of double butt, 45°, and 60 ° inclined butt, cruciform and lap hybrid welded joints (a) Tensile static failure modes of single butt, 15° and 30° inclined butt hybrid welded joints (b).

Figure 6.3 and Figure 6.4 present the short-term ageing experimental results obtained from this investigation. These Figures present the ultimate tensile strength (UTS) for each welded configuration. In particular Figure 6.3 displays the UTS for butt, lap and cruciform welded joints with \pm two standard deviations from the mean, whereas Figure 6.4 shows the UTS for the single, double and inclined butt-welded joints with various inclination angles including 15° , 30° , 45° and 60° . It can be seen from the results in Figure 6.4 that as the weld angle of the hybrid-welded joints increased the static strength increased.

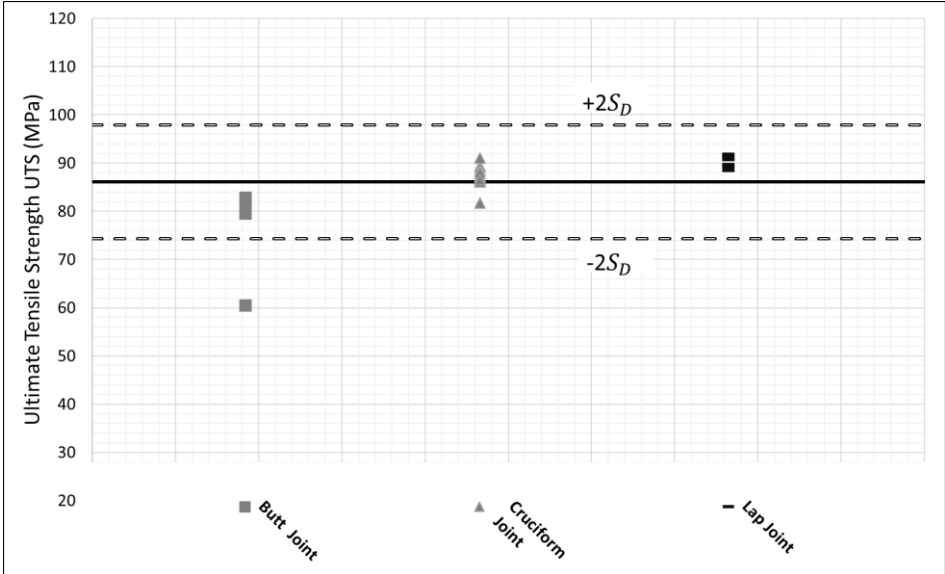


Figure 6.3 the average tensile strength results of Al-St butt, lap and cruciform Welded Joints ((short-term ageing).

Table 6.5 Ultimate tensile strength comparison of the short-term and long-term experiments.

configuration type	Angle	Average UTS (MPa)	
		Short term	Long term
butt-single	0	79.39	77.50
butt-double	0	81.14	84.42
butt-single	15	73.52	77.91
butt-single	30	84.53	89.44
butt-single	45	101.10	103.21
butt-single	60	108.55	109.01
Lap	0	90.08	90.33
Cruciform	0	87.41	92.50

Figure 6.5 compares the results obtained from the short-term and long-term experiments for the single butt, double butt, cruciform and lap welded joints. This figure shows the consistency in the strength of the short-term and long-term specimens. Furthermore, Table 6.5 compares the average UTS for each configuration. There is a small difference between the two sets of experiments, and the effect of long-term ageing can be neglected.

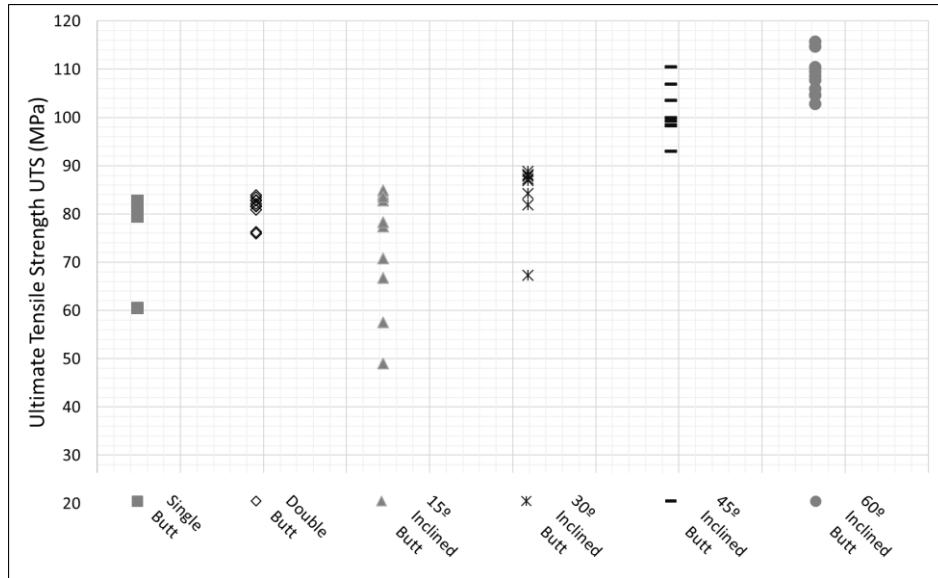


Figure 6.4 the average tensile strength results of Al-St butt Welded Joints with various inclination angles (short-term ageing).

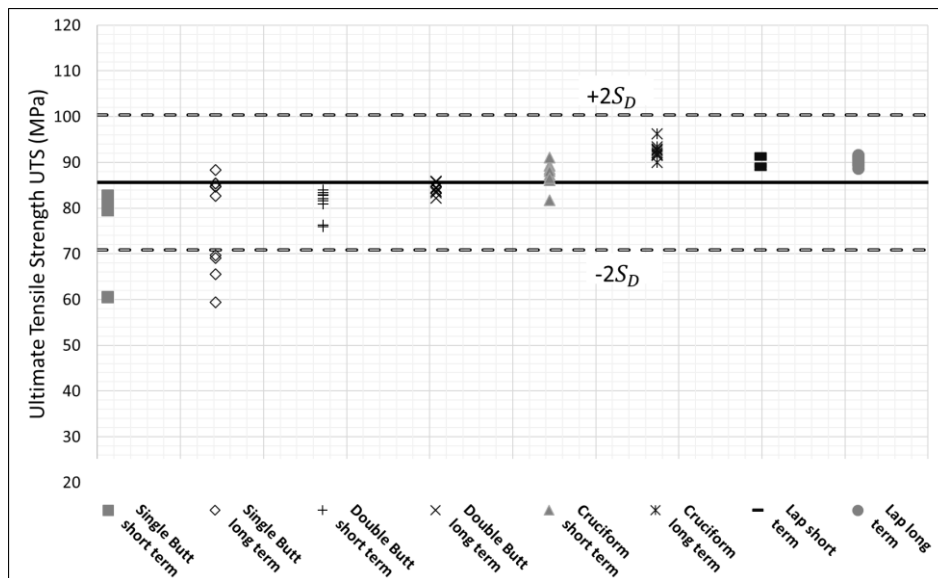


Figure 6.5 Comparison between the short term and long-term tensile static strength of butt-welded, cruciform-welded and lap-welded aluminium-to-steel hybrid joints.

6.3 Design against static loading

In general, to design any structural component attention must be paid to the weakest part of the structural chain. Therefore, the design resistance of the hybrid-welded joints should be taken as equal to the design resistance of the weakest part of the connection, in this case, aluminium alloys.

According to the above experimental findings, EC9 was then used to estimate the static strength of the aluminium-to-steel hybrid welded joint. By using EC9 to design the butt-welded and fillet-welded joints, the combined stresses and direct stress on the weld throat must be checked and compared with different limiting stresses, as shown in equation (6.2) and (6.3). Equation (6.4) is used to design the fillet welds.

$$\text{Normal Stress} \quad \sigma_{Ed} \leq \frac{f_w}{\gamma_{Mw}} \quad (6.1)$$

$$\text{Shear Stress} \quad \tau_{Ed} \leq \frac{1}{\sqrt{3}} \cdot \frac{f_w}{\gamma_{Mw}} \quad (6.2)$$

$$\text{Normal + Shear Stress} \quad \sigma_{eq} : \sqrt{\sigma_{Ed}^2 + 3\tau_{Ed}^2} \leq \frac{f_w}{\gamma_{Mw}} \quad (6.3)$$

$$\text{Design Stress} \quad \sigma_{eq,fillet} = \sqrt{\sigma_{\perp}^2 + 3(\tau_{\perp}^2 + \tau_{\parallel}^2)} \leq \frac{f_w}{\gamma_{Mw}} \quad (6.4)$$

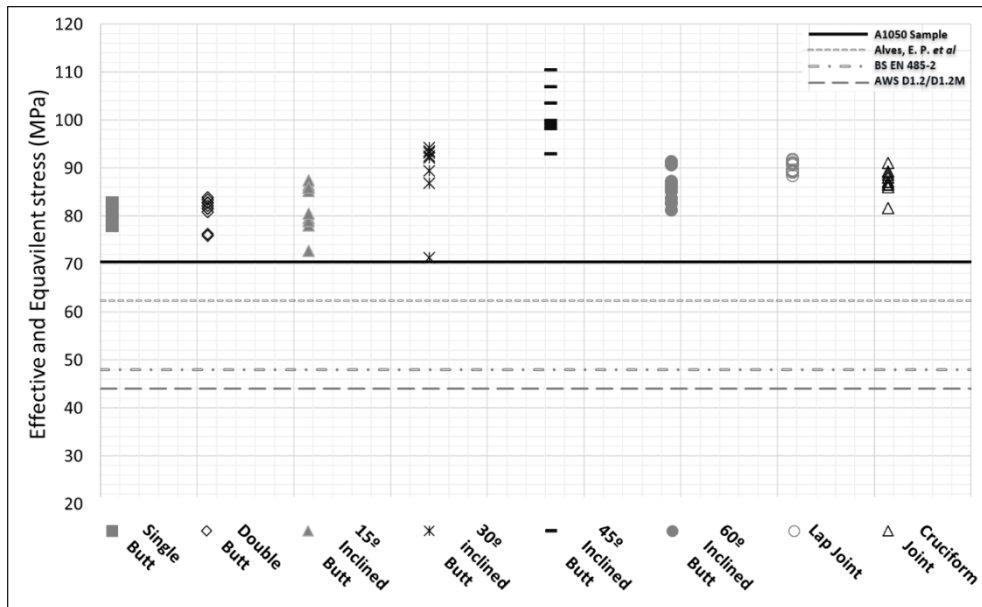


Figure 6.6 Effective and equivalent design stresses of aluminium-to-steel welded joints compared with standard design codes.

According to British Standard [9], the American society of Welding [10] and Alves, E. P. *et al* [11], the characteristic strength (f_w) of the welded joints made of aluminium alloys AA1050 ranges from 55 MPa to 78 MPa. Figure 6.6 displays the results obtained by using equations (6.1) to (6.4) to design the butt-welded (with various weld inclination angles) and the fillet-welded joints and compares them with standard design codes.

The results are well above the values suggested by the standard design codes, and conservative results were obtained by using EC9 [12]. This fully supports the idea that aluminium-to-steel welded joints can safely and effectively be designed against static loading by following the assessment procedure recommended by EC9 for aluminium-welded joints.

6.4 Discussion

The results of this study indicate that for the single butt, 15° and 30° inclined butt hybrid joints (reported in Table 6.1, Table 6.2, Table C.1 and Table C.2) there are three different failure modes: failure occurs in the aluminium HAZ, weld seam fracture and a combination of both failures (Figure 6.2b). There are several explanations for these results. A plausible reason for this might be that there is a lack of weld penetration between the aluminium and steel, as the steel edges are not galvanized. There is already a gap between the two materials, and the weld acts as a bridge between aluminium and steel resulting in the formation of a weak weld. Another explanation for this behaviour is that the weld seam is not thick enough in some specimens resulting in an inadequate weld, which can be seen in the second failure mode.

There are, however, other explanation, which is that for some specimens the quality of the weld is inadequate. This can be seen clearly in the third failure mode where the crack initiates and start propagating from the weld seams until it hits a strong weld then it diverges its path and starts propagating on the aluminium HAZ. There are ways to solve this problem, either by galvanizing the edges of the steel sheet or by using different geometry where the edges of the steel are galvanized. Another solution is to use an automated welding machine to perform consistent weld thickness along the weld path.

The results reported in Table 6.1 and Table C.1 for the double butt joints indicate that the fracture of the joints always took place in the aluminium HAZ. These results confirm the association between the thickness of the weld seams and the strength of the weld. Although there is still a gap between the two materials, having weld on both sides have increased the strength of the weld. This overcomes the problem of having a fracture on the weld seam.

For double butt, 45°, 60° inclined butt, cruciform and lap welded joints, the fracture always took place in the aluminium HAZ away from the weld seam (see Figure 6.2a). These findings demonstrated that the use of the EWM® coldArc technology improved the strength of the

6.4 Discussion

aluminium-to-steel hybrid welded joints significantly and successfully dealt with the problem of having a brittle phase in the welding zone. The use of low heat input reduced the size of the intermetallic phase at the weld interface, which resulted in a stronger weld.

From Figure 6.4, it is worth mentioning that the same static strength was achieved for both single butt and double butt-welded joints. This finding further confirms that, for the combination of materials being investigated (steel and aluminium), the welded joints manufactured using the EWM® coldArc welding technology were stronger than the heat-affected zone in the aluminium alloys. In particular, the UTS of the aluminium HAZ of the butt, lap, and cruciform welded joints was seen to be larger than 70% of the parent aluminium UTS. These findings showed that aluminium-to-steel hybrid welded joints have excellent mechanical performance.

The results in Figure 6.6 confirms that EC9 recommendations along with a characteristic strength value for the welded aluminium alloys provide a suitable design approach for aluminium-to-steel hybrid welded joints against static loading. Finally, by performing the short-term and long-term ageing experiments, it is evidently clear from the findings that ageing has little or no effect on the tensile strength of the welded joints. These results suggested that the strength of the heat-affected zone of the aluminium alloys has already recovered from the welding process and therefore leaving the specimens for a longer period would lead to similar results.

6.5 Conclusion

This study provides the first comprehensive assessment of the static strength of aluminium-to-steel thin welded joints using the EWM coldArc® welding technology. The key findings of this chapter have been the following:

- The use of the EWM coldArc® welding technology results in efficient and robust aluminium-to-steel welded joints, with the manufacturing requiring minimum effort;
- Irrespective of the configuration or inclination angle of the hybrid welded joints, the fracture failure will always occur on the aluminium side;
- The results generated by testing our specimens confirm that aluminium-to-steel welded joints can be designed against static loading by focussing attention solely on the aluminium part, i.e., on the weakest link in the structural chain of the joint.

6.6 References

- [1] K. Kimapong and T. Watanabe , Lap Joint of A5083 Aluminium Alloy and SS400 Steel by Friction Welding, *Materials Transactions*, vol. 46, no. 4 (2005) 835-841. .
- [2] S. Meco, G. Pardal, S. Ganguly , S. Williams, N. McPherson, Application of laser in seam welding of dissimilar steel to aluminium joints for thick structural components, *Optics and Laser in Engineering*, vol. 67 (2015) 22-30. .
- [3] T. Era, A Isw, T Uezono, T. Ueyama and Y Hitata, Controlled bridge transfer (CBT) gas metal arc process for steel sheets joining, *Welding International*, vol. 27, no. 4, (2013) 268-273. .
- [4] R. Cao, J. H. Sun, J. H. Chen and P. Wang, Cold metal transfer joining aluminum alloys-togalvanized mild steel, *Journal of Manufacturing Science and Engineering*, vol. 136, (2014) 051015-1 to 051015-10. .
- [5] J. Goldstein, *Scanning Electron Microscopy and X-Ray Microanalysis*, Springer, May 26 2003, ISBN 978-0-306-47292-3. .
- [6] V.D. Scott, G. Love, *Quantitative Electron Probe Microanalysis*, (1994) 2nd edn. Ellis Horwood, Chichester. .
- [7] S.J.B. Reed, *Electron Microprobe Analysis*, (1993) 2nd ed. Cambridge University Press, Cambridge..
- [8] B.K. Agarwal, *X-ray Spectroscopy*, (1991) 2nd edn, Springer-verlag, Berlin. .
- [9] BS EN 485-2:2016, Aluminium and aluminium alloys - Sheet, strip and plate - Part 2: Mechanical properties, (2016) EUROPEAN COMMITTEE FOR STANDARDIZATION. .
- [10] AWS D1.2/D1.2M:2014, *Structural Welding Code-Aluminium*, American Welding Society, (2014) USA. .
- [11] E. P. Alves, F. P. Neto and C.Y. An, Welding of AA1050 aluminum with AISI 304 stainless steel by rotary friction welding process, *Journal of Aerospace Technology and Management*, vol. 2, no. 3, (2010) 301-306. .
- [12] Eurocode 9: Design of aluminium structures – Part 1-1: General structural rules, (1998) prENV.

Chapter 7

7. Fatigue behaviour of aluminium-to-steel thin welded joints

The work presented in this chapter was published in the International Journal of Fatigue with the following title:

Al Zamzami I, Davison J.B, Susmel L. Nominal and local stress quantities to design aluminium-to-steel thin welded joints against fatigue. Int J Fatigue 2019; 279-295.

<https://doi.org/10.1016/j.ijfatigue.2019.02.018>.

7.1 Introduction

For more than a century, engineers have been developing welding technologies in a systematic way as an economical and versatile joining process to replace the use of mechanical fasteners where appropriate [1]. Avoidance of fatigue failure associated with the welding process was identified as important from the outset so that a considerable amount of literature has been published on the effect of the welding process on the durability of weldments subject to fatigue loading.

There is a large volume of published studies describing the fatigue behaviour of welded structural details made of either steel or aluminium. These studies considered different fatigue

7.2 Lifetime estimation in terms of nominal stress approach

design approaches to estimate the fatigue lifetime of structural components. The available Standards and Codes of Practice [2, 3, 4] suggest different design methods including those based on the use of nominal stress as well as the effective notch stresses.

Understanding the fatigue behaviour of welded joints made using dissimilar materials (and, in particular, aluminium alloys and steel) is very limited. Before investigating the fatigue behaviour of aluminium-to-steel welded joints it was important to understand the static behaviour of such joints. In this context, chapter 6 provided a full experimental investigation of the static strength of aluminium-to-steel thin welded joints with various welded configurations - including butt-welded joints (with weld seam inclination angles ranging between 0° and 60°), cruciform connections, and lap joints. This study highlighted that, regardless of the joint configuration or the angle of inclination, the fracture of the joints always took place in the aluminium heat affected zone and confirmed that Eurocode 9 (EC9) [5] can be used to design aluminium-to-steel welded joints with a high level of accuracy.

There are two main primary aims of the study presented in this chapter:

1. Experimentally investigate the fatigue strength of aluminium-to-steel welded joints subjected to uniaxial cyclic loading. Each geometry will be tested under two different load ratios to define appropriate fatigue design curves.
2. Extend the use of the nominal stresses and the local stresses (i.e. the effective notch stresses, the N-SIFs approaches and the TCD) to design the hybrid welded joints with an adequate level of conservatism.

7.2 Lifetime estimation in terms of nominal stress approach

Currently, (As mentioned in section 7.1), there is no guidance for the static and fatigue assessment of these hybrid welded connections. As far as static failures are concerned, examination of the state of the art demonstrates that, so far, the international scientific community has focused their attention mainly on studying the existing interactions amongst welding technologies, material microstructural features and ultimate tensile strength [6-13].

From the experimental work presented in chapter 6, it has been demonstrated that the static fracture of aluminium-to-steel welded joints always occurs in the heat-affected zone on the aluminium side. In contrast, the direct inspection of the fracture surfaces generated under fatigue loading revealed that the fatigue breakage of the aluminium-to-steel welded joints always took place at the interface between the weld toe and aluminium plate ((Figure 7.1). This strongly supports the idea that in the investigated aluminium-to-steel welded connections the

crack initiation process was favoured by localised stress concentration phenomena occurring in the weld seam region.

According to the above experimental evidence, the hypothesis was formed that aluminium-to-steel welded joints behave like conventional aluminium-to-aluminium welded connections. so that, in situations of practical interest they can be designed against fatigue by directly using the nominal stress approach along with the design curves being recommended by EC9 [3], EC3 [4] (only for the tee joints) and the IIW [2].

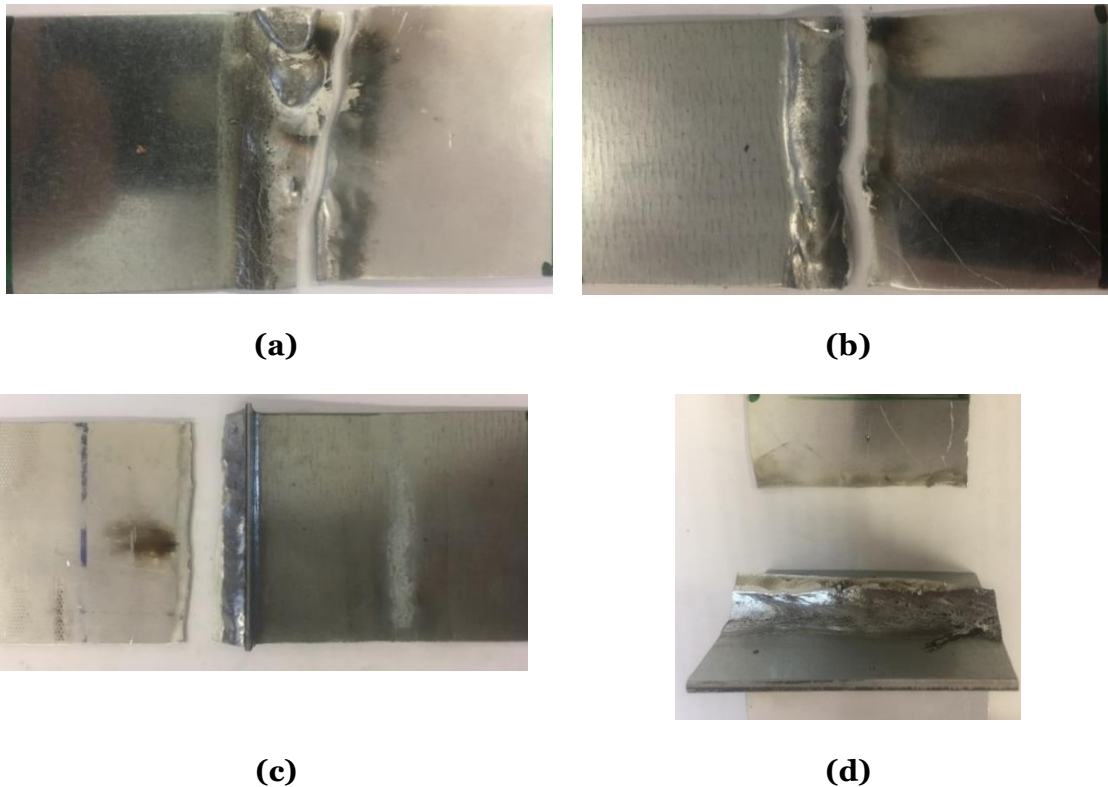


Figure 7.1 Fatigue Failure of butt, lap and cruciform welded joints.

The results of the re-analyses done in terms of nominal stresses are summarised in Table 5.2 to Table 5.5 (chapter 5, section 5.5). In more detail, these tables were populated by post-processing the experimental results, expressed in terms of nominal stress ranges, under the hypothesis of a log-log normal distribution of the number of cycles to failure for each stress level, with the confidence level being set equal to 95% [14]. The ranges of the endurance limits listed in Table 7.1 were extrapolated at $2 \cdot 10^6$ cycles to failure for a probability of survival, P_s , equal to 50% and 97.7% according to the statistical procedure reviewed in chapter 2 section 2.2.1.2.

7.2 Lifetime estimation in terms of nominal stress approach

Figure 7.2 presents the same results in log-log Wöhler diagrams, where, for the different welded configurations being investigated, the nominal stress ranges, $\Delta\sigma_{nom}$, are plotted against the number of cycles to failure, N_f . In addition, the design curves recommended by EC9 and the IIW for each welded geometry are also plotted in the charts of Figure 7.2, with this allowing the experimental results generated in this investigation to be compared directly with the standard design curves (see Figure 7.2).

Table 7.1 Summary of the statistical re-analyses for the different welded geometries in terms of nominal stress approach (the experimental results are presented in chapter 5).

Series	No. of Data	R	t [mm]	a [mm]	Z [mm]	k	T_σ	Nominal stress	
								$\Delta\sigma_{A,50\%}$	$\Delta\sigma_{A,97.7\%}$
								[MPa]	[MPa]
Butt-joint	12	-1	1.97	1.96	-	7.52	3.39	20.11	10.93
	15	0.1	1.02	1.92	-	6.98	2.75	31.92	19.26
Cruciform-joint	10	-1	1.98	-	3.66	6.82	1.72	38.43	29.27
	12	0.1	1.02	-	5.25	8.99	3.37	36.17	19.47
Lap-joint	10	0.1	1.01	-	2.72	6.31	2.12	36.15	24.86
	10	0.5	1.97	-	4.97	5.79	1.33	25.49	21.72
Tee-joint	11	-1	1.96	-	5.61	2.89	2.27	132.38	87.88
	12	0.1	1.94	-	5.56	5.90	1.45	175.60	145.66

Table 7.1 and the Wöhler diagrams of Figure 7.2 make it evident that the values of the negative inverse slope, k , determined for the investigated welded configurations were much larger not only than the value of 3 recommended by the IIW, but also larger than the value of 3.4 suggested by EC9. In a way, this fact is not at all surprising, since the negative inverse slopes provided by the available design codes were determined by re-analysing a large number of experimental results generated by testing welded joints that were thick and stiff - i.e., welded connections with a thickness larger than 5 mm. In contrast, the experimental fatigue curves experimentally determined by testing thin and flexible welded connections are seen to be characterised by a negative inverse slope that varies in the range 3-6 [15]. This is the reason why Sonsino et al. [15] have recommended to perform the fatigue assessment of thin welded joints via fatigue curves that have the same endurance limit (at 2 million cycles) as the one recommended by the pertinent standard codes, but negative inverse slope invariably equal to 5.

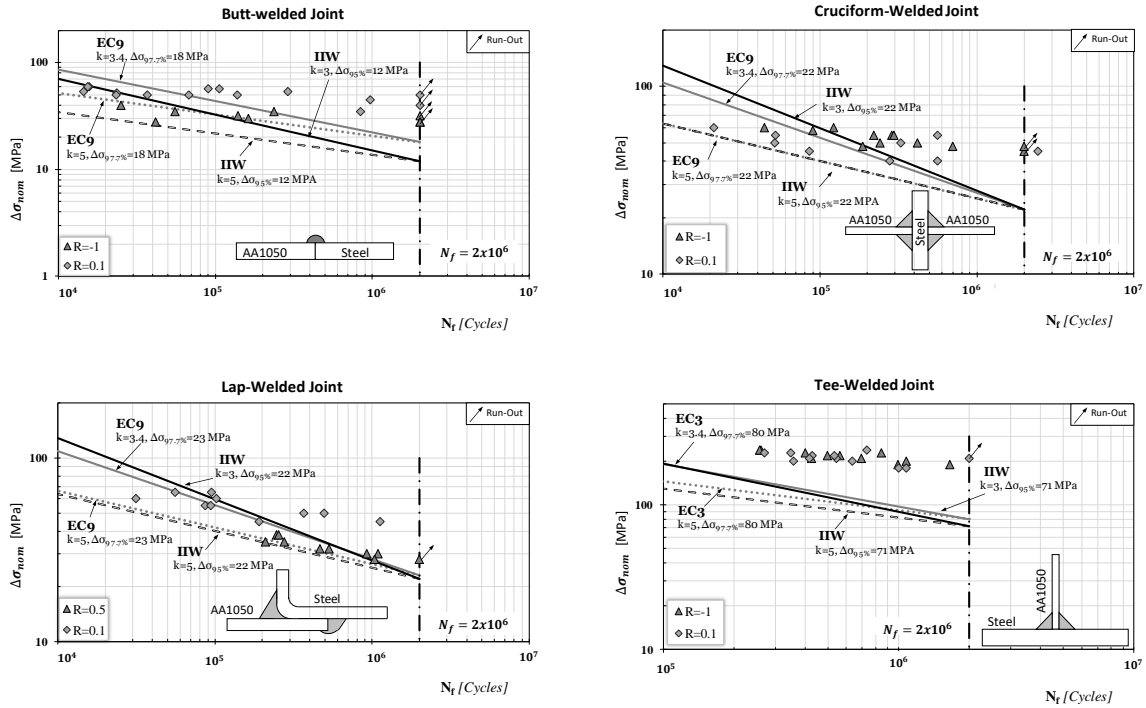


Figure 7.2 Accuracy of the nominal stress approach to estimate the fatigue strength of the thin hybrid welded joints.

By applying the strategy recommended by Sonsino and co-workers to assess the fatigue strength of thin welded joints [15], it is apparent that the modified EC9 design curve (grey dotted line in Figure 7.2) and the modified IIW design curve (black dashed line) curves lead to a more conservative estimation of the fatigue lifetime of the investigated aluminium-to-steel welded joints. In particular, as per the Wöhler diagrams of Figure 7.2, the modified design curves suggested by the IIW were seen to provide conservative fatigue lifetime estimations for all the welded configurations. In contrast, the modified EC9 curves were seen to result in conservative fatigue strength predictions in all cases except for butt joints.

Turning to the non-load carrying fillet tee-welded joint (Figure 5.5b), the steel plate was subjected to fatigue loading whereas the aluminium plate acted solely as a stiffener. Looking at Figure 7.2, although the tee-welded joint was 2mm thick which is classified as a thin joint, it is worth mentioning that the negative inverse slope was kept the same as suggested by the design codes for plates ≥ 5 mm but this still results in a conservative fatigue life estimation of the hybrid welded joints. Use of the k value suggested by Sonsino for thin plates results in an even higher level of conservatism in estimating the fatigue lifetime of the tee-welded joint.

To summarise, using the nominal stress approach and the fatigue design curves for aluminium-welded joints with a modified negative inverse slope value, the fatigue behaviour of aluminium-to-steel butt, lap and cruciform welded joints (Figure 5.4 and Figure 5.5a) can be estimated by considering the joints as all aluminium-welded joints. In the case of tee-welded

7.3 Lifetime estimation in terms of the effective notch stress approach

configuration (Figure 5.5b), the hybrid welded joints can be considered as steel welded joints without altering the negative inverse slope value.

7.3 Lifetime estimation in terms of the effective notch stress approach

As far as aluminium welded joints with a thickness larger than 5 mm are concerned, the IIW recommends to assess their fatigue strength by using a design curve having a notch stress endurance limit range, $\Delta\sigma_{A,97.7}$, equal to 71 MPa (extrapolated at $2 \cdot 10^6$ cycles to failure for a probability of survival, P_s , equal 97.7%) and negative inverse slope, k , equal to 3. In contrast, aluminium welded detail with a thickness lower than 5 mm should be designed against fatigue by using the FAT180 design curve, i.e., a fatigue curve having k equal to 5 and $\Delta\sigma_{A,97.7}$ equal to 180 MPa (with this endurance limit being again determined at $2 \cdot 10^6$ cycles to failure for a P_s equal 97.7%) [15].

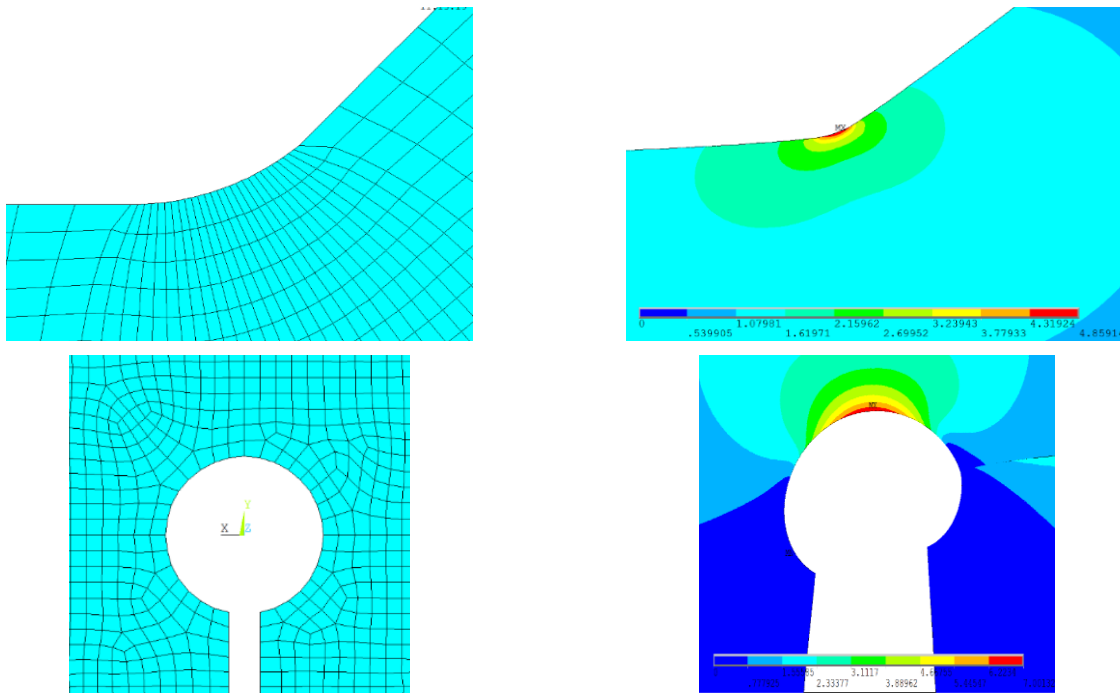


Figure 7.3 Examples of linear elastic 2D FE models solved using effective notch stress approach.

In order to post-process the experimental data according to the effective notch stress approach, the stress analysis was carried out by using FE code ANSYS ® to solve linear-elastic bi-dimensional models (Figure 7.3). Since the welded joints, being investigated had thickness lower than 5 mm, the design notch stresses were calculated by rounding the weld toes of the lap and cruciform joints and the roots of the butt joints by setting the reference radius, r_{ref} , equal to 0.05 mm. The mesh density in the vicinity of the fictitious fillet radii was gradually refined until convergence occurred.

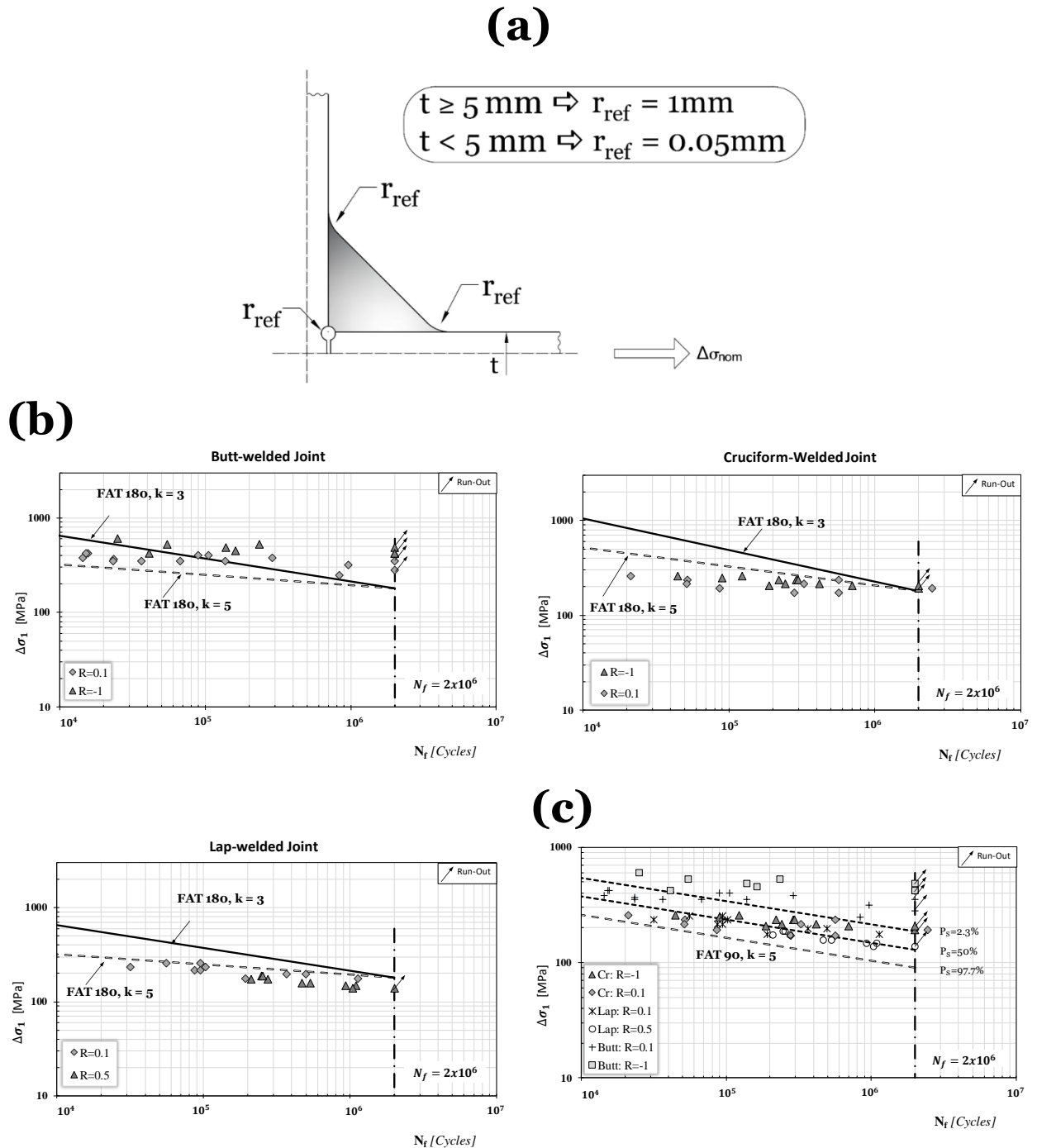


Figure 7.4 Weld toe and root rounded according to the reference radius concept (a); accuracy of the effective notch stress approach to estimate the fatigue strength of the thin hybrid welded joints (b); results generated for the whole data and FAT90 design curve (c).

The experimental results post-processed according to the effective notch stress approach, for the butt-welded (Figure 5.4a), cruciform welded (Figure 5.4b) and lap-welded joints (Figure 5.5a), are listed in Table 5.2 to Table 5.5. The same results are also plotted in the log-log Wöhler diagrams of Figure 7.4b. Table 7.2. summarises the results from the statistical reanalysis in terms of negative inverse slope and endurance limit range, $\Delta\sigma_A$, extrapolated at $2 \cdot 10^6$ cycles to

7.3 Lifetime estimation in terms of the effective notch stress approach

failure for a probability of survival, P_s , equal to 50% and to 97.7%. As far as the tee joint is concerned, the maximum stress was instead occurred at the interface between the aluminium weld and the steel plate rather than at the weld toe (Figure 7.5). A possible explanation is that the tensile loading results in a significant stress concentration at the interface location between the two materials. Therefore, the tee-welded joints (Figure 5.5b) were excluded from this re-analysis.

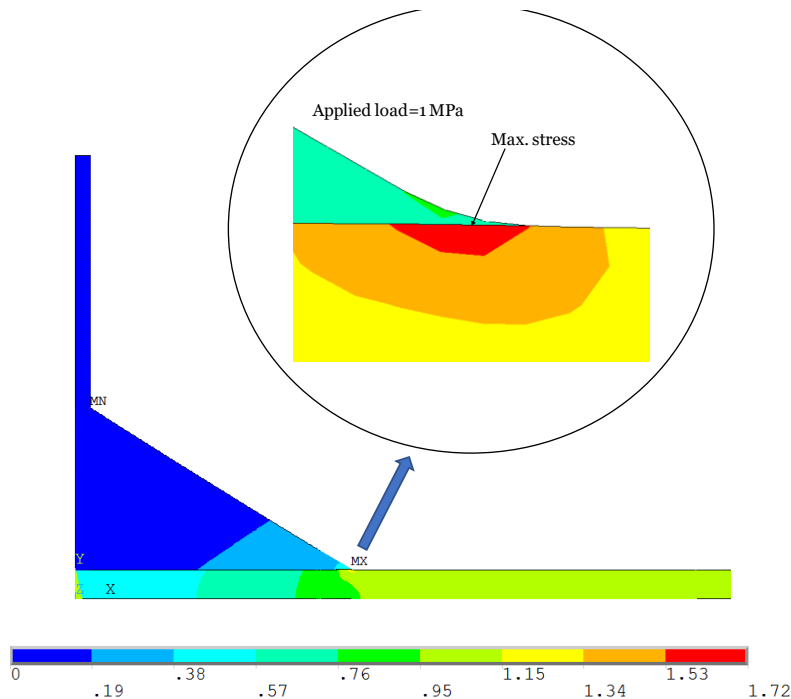


Figure 7.5 FE model for the tee welded joints

The SN charts of Figure 7.4b demonstrate that the use of the FAT180 curve recommended by Sonsino to design aluminium-to-aluminium welded joints [15] is not suitable for modelling the fatigue behaviour of the hybrid-welded specimens being tested, which results in a large degree of non-conservatism. However, the diagrams of Figure 7.4c fully support the idea that the notch stress approach can still be used to assess the fatigue strength of aluminium-to-steel welded joints provided that a fatigue curve with a lower FAT class is used. Accordingly, as per the Wöhler diagrams of Figure 7.4b, the most appropriate design curve to be used to model the fatigue strength of the aluminium-to-steel thin welded specimens, was seen to be the one having endurance fatigue limit range equal to 90 MPa (at $2 \cdot 10^6$ cycles to failure for P_s equal to 97.7%) and inverse negative slope equal to 5. In particular, the value for the endurance limit was derived in accordance with the IIW numeric system [3], whereas the value for the negative slope was chosen according to the value that is recommended by Sonsino et al. to design thin and flexible welded joints [15].

Table 7.2 Summary of the statistical re-analyses for the different welded geometries in terms of effective notch stress and the N-SIFs approaches (the experimental data are presented in chapter 5).

Series	No. of Data	R	k	T_{σ}	Effective notch stress		The N-SIF	
					$\Delta\sigma_{A,50\%}$	$\Delta\sigma_{A,97.7\%}$	$\Delta K_{I,50\%}$	$\Delta K_{I,97.7\%}$
					[MPa]	[MPa]	[MPa.mm ^{0.326}]	[MPa.mm ^{0.326}]
Butt-joint	12	-1	7.52	3.39	301.71	163.97	-	-
	15	0.1	6.98	2.75	223.43	134.83	-	-
Cruciform-joint	10	-1	6.82	1.72	164.48	125.37	76.85	58.52
	12	0.1	8.99	3.37	154.60	83.20	62.40	33.58
Lap-joint	10	0.1	6.31	2.12	140.61	96.50	57.84	39.77
	10	0.5	5.79	1.33	125.00	107.03	57.27	48.82

7.4 Lifetime estimation in terms of the N-SIFs approach

In the present investigation, the experimental results were re-analysed using the N-SIFs approach (Chapter 2, section 2.2.2.4.). The master curve to be used to design against fatigue steel weldments is characterised by a Mode I N-SIF range at $5 \cdot 10^6$ cycles to failure, ΔK_I , equal to 155 MPa·mm^{0.326} ($P_S=97.7\%$) and a negative inverse slope, k, equal to 3.2. In contrast, the reference curve recommended to be used to design aluminium welded connections against fatigue has ΔK_I , at $5 \cdot 10^6$ cycles to failure, equal to 74 MPa·mm^{0.326} (for $P_S=97.7\%$) and k value equal to 4 (section 2.2.2.4, Figure 2.22) . The experimental results generated by testing the lap and cruciform aluminium-to-steel welded joints were post-processed in terms of Mode I N-SIF ranges. The butt joints were instead excluded from this re-analysis, since the master curve proposed by Lazzarin and Livieri [16] is only suitable for estimating the fatigue strength of fillet-welded joints with an open angle of 135°.

As to the numerical stress analysis done using commercial software ANSYS®, the weld seams of the hybrid joints were all modelled by setting the weld toe radius equal to zero, with the weld leg attached to the steel stiffener being equal to the weld leg attached to the aluminium plate (see Figure 7.6). The numerical procedure proposed by Tovo and Lazzarin was followed to mesh the FE models as well as to calculate the associated N-SIF values [17, 18].

7.4 Lifetime estimation in terms of the N-SIFs approach

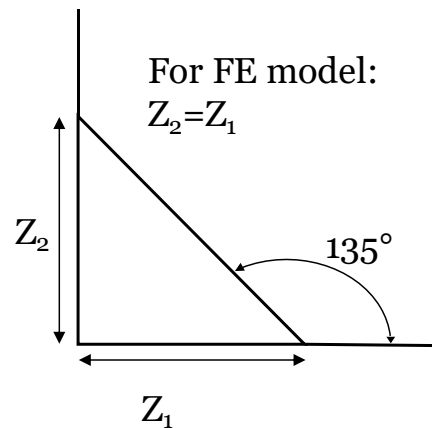


Figure 7.6 schematization of the weld details used in the FE model for the NSIF approach.

The results obtained from the statistical re-analysis by post-processing the lap and cruciform welded configurations according to the N-SIFs approach are listed in Table 5.3 and Table 5.4 and plotted in Figure 7.7 in the form of ΔK_I vs. N_f log-log Wöhler diagrams. Table 7.2 summarises the values of the negative inverse slope, k , and the Mode I N-SIF ranges (for P_s equal to 50% and 97.7%) determined at $5 \cdot 10^6$ cycles to failure.

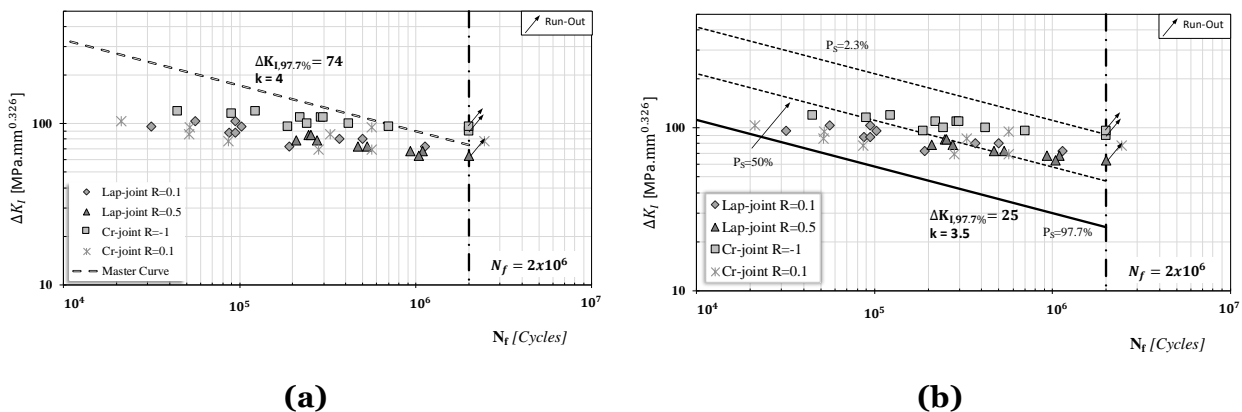


Figure 7.7 Accuracy of the N-SIF approach to estimate the fatigue strength of the thin hybrid welded joints (a); statistical reanalysis for the data with a proposed design curve (b).

Figure 7.7a makes it evident that Lazzarin and Livieri's master curve was not suitable for modelling the fatigue strength of the aluminium-to-steel hybrid joints being tested, with its use resulting in non-conservative estimates. This may be ascribed to the fact that, since the aluminium alloy used to manufacture the welded specimens belonged to the 1000 series, its fatigue strength was much lower than the one characterising the aluminium-to-aluminium welded joints that were used by Lazzarin and Livieri themselves to construct their master curve. Furthermore, the parent material's thickness used in the present investigation was equal either to 1 mm or to 2 mm. In contrast, the welded joints used to build the master curve had a thickness ranging between 3 mm and 24 mm [16]. All these differences could then explain the

reason why the fatigue strength of our hybrid-welded connections was seen to be slightly lower than the one predicted by Lazzarin and Livieri's master curve.

In order to propose a design curve suitable for estimating, in terms of Mode I N-SIF ranges, the fatigue strength of the thin aluminium-to-steel welded joints, the full set of data for the lap and cruciform welded joints were reanalysed together. The results from this re-analysis are summarised in the chart of Figure 7.7b. According to this figure, the fatigue strength of the hybrid welded joints manufactured by employing aluminium alloy AA1050 can effectively be modelled via a master curve having Mode I N-SIF range, at $5 \cdot 10^6$ cycles to failure, equal to $25 \text{ MPa} \cdot \text{mm}^{0.326}$ (for $P_s = 97.7\%$) and negative inverse slope equal to 3.5.

To conclude, examination of the state of the art certainly demonstrates that the N-SIFs approach is a very powerful tool suitable for estimating the fatigue strength of welded joints by systematically reaching an adequate level of accuracy [19-24]. However, to successfully extend the usage of this design methodology also to those situations involving not only very small thicknesses but also very low strength aluminium alloys, a different master curve should be derived by post-processing a large number of appropriate experimental results.

7.5 Lifetime estimation in terms of the MWCM along with the Point Method

As defined by David Taylor [25], the Theory of Critical Distances (TCD) is a theoretical framework grouping together different methods that all make use of a length scale parameter, commonly known as the critical distance, to estimate fatigue strength in the presence of stress concentrators [26, 27].

The TCD can be formalised in different ways that include the Point Method (PM), the Line Method (LM), the Area Method (AM) and the Volume Method (VM) [27, 28]. The PM [28] represents the simplest version of the TCD and it can be used to estimate the fatigue strength of either notched, cracked or welded structural components. Accordingly, this formalisation of the TCD will be attempted to be used in what follows to assess the fatigue strength of the aluminium-to-steel hybrid-welded joints. In particular, this will be done by applying the PM along with the Modified Wöhler Curve Method (MWCM) (chapter 2, section 2.2.3.2) which is a bi-parametrical critical plane approach assuming that fatigue damage reaches its maximum value on those materials planes experiencing the maximum shear stress amplitude.

7.5 Lifetime estimation in terms of the MWCM along with the Point Method

In real structures, the stress state generated at the critical locations is always multiaxial. So that the three-dimensional FE analysis would solve the governing equations in the three axes, resulting in a more accurate estimation of the fatigue lifetime of the structure. However, the 3D analysis requires too many elements and therefore more computational effort and time-consuming to achieve a very fine mesh. In some cases, where the load applied, the geometry, and the material being investigated are symmetrical at least in one axis, the 3D problem can be simplified to an axisymmetric 2D problem. As long as the structure is symmetrical, the 2D FE model is capable of analysing the structure with less computational effort and results in an adequate level of conservatism solution. In this investigation, the accuracy of the 2D and 3D FE analysis will be investigated to estimate the fatigue lifetime of the aluminium-to-steel welded joints using the MWCM along with the PM.

7.5.1 Method formalisation

To perform the fatigue assessment of the aluminium-to-steel thin welded joints using the MWCM in conjunction with the PM, the first step is to calibrate the MWCM governing equations (Eqs. (7.1) and (7.2)).

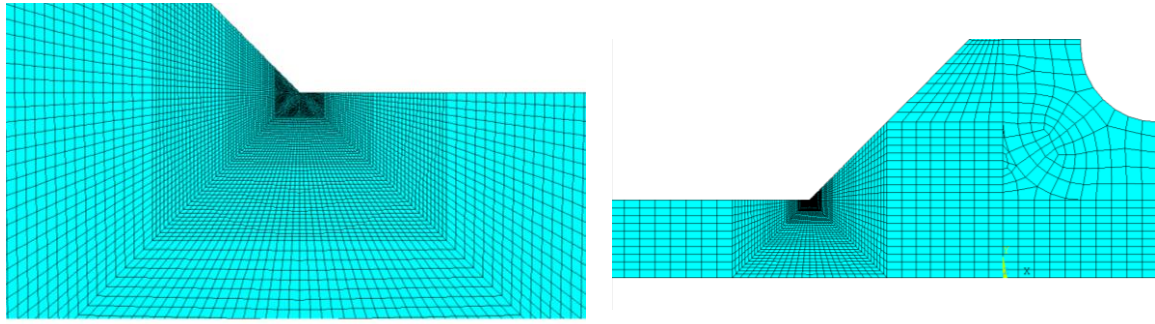
$$k_t(\rho_w) = (k - k_0) \cdot \rho_w + k_0 \quad (7.1)$$

$$\Delta\tau_{Ref}(\rho_w) = \left(\frac{\Delta\sigma_A}{2} - \Delta\tau_A\right) \cdot \rho_w + \Delta\tau_A \quad (7.2)$$

The following procedure is used to calibrate the required MWCM constants:

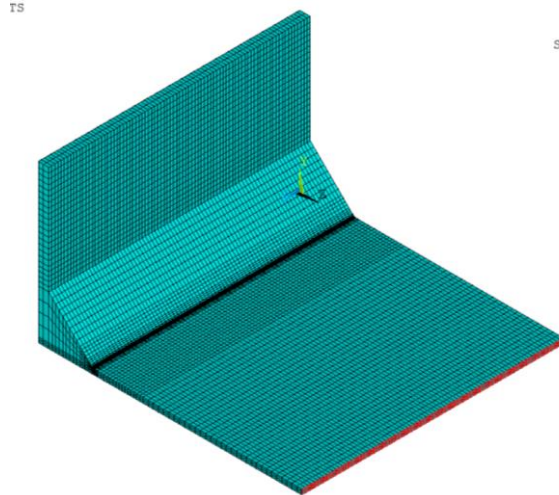
- Linear-elastic bi-dimensional and tri-dimensional FE models were solved via a commercial software ANSYS® (Figure 7.8). The 3D FE models for the different welded configurations were obtained by following a standard solid-to-solid sub-modelling procedure (chapter 4 section 4.2.2). The mesh density for the 2D and 3D models was increased gradually until convergence was achieved.

(a) 2D FE Models



(b) 3D FE Models

Complete model



Sub-model

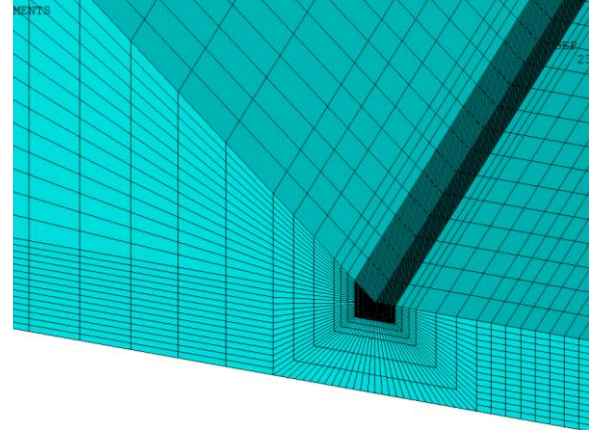


Figure 7.8 Examples of linear elastic FE models (a) solved using a 2-dimensional models (b) solved using a 3-dimensional models following the standard solid-solid sub-modelling procedure.

- For the 2D models, the corresponding local stress distributions $[\Delta\sigma]$ were determined along the bisector from the weld apex at a distance equal to 0.075 mm. However, for the 3D models, the local stresses were extrapolated at a distance equal to 0.075 mm along the bisector from the weld toe (obtained for the entire width of the specimen). Subsequently, the effective stresses are determined at a distance equal to 0.075 mm away from the edge of the weld (Figure 7.9). From Figure 7.9, the linear elastic stress distributions obtained from the 2D models are lower than those obtained from the 3D models, resulting in a more conservative solution. The effective stresses for the butt-welded and lap-welded joints are determined following the same procedure (see Figure D.9 and Figure D.10).

7.5 Lifetime estimation in terms of the MWCM along with the Point Method

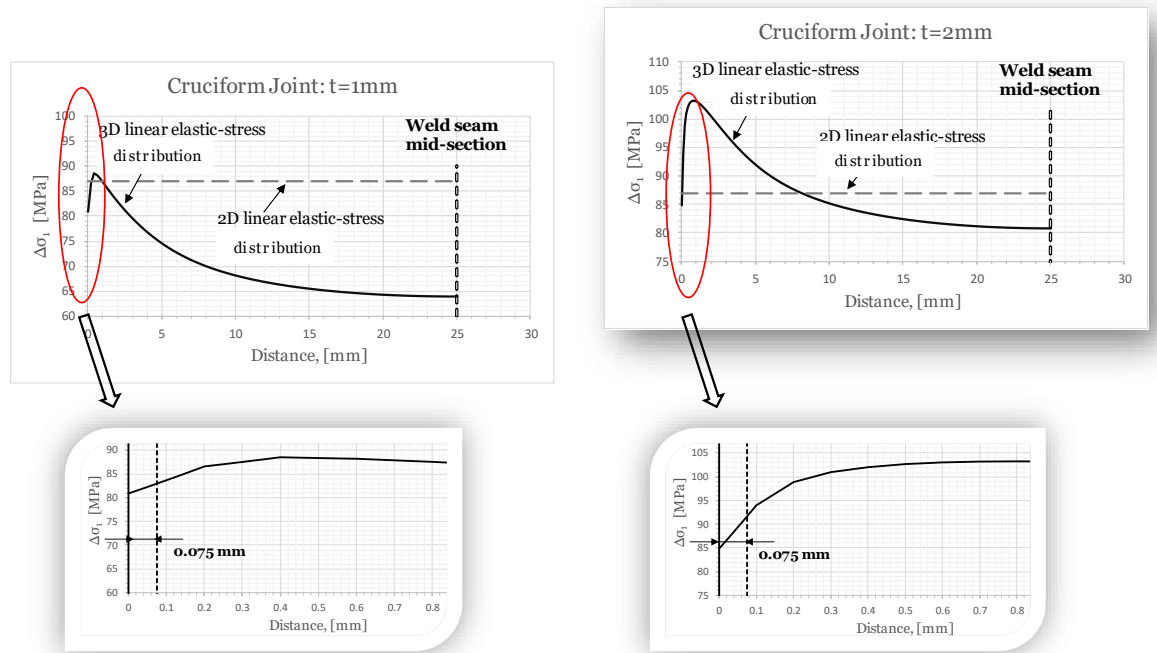


Figure 7.9 2D and 3D linear elastic stress distribution along the weld seam for the cruciform welded joints.

- Subsequently, the nominal stress range, $\Delta\sigma_n$ and the shear stress range, $\Delta\tau$ relative to the critical plane were calculated (Figure 7.10b).
- The shear stress range, $\Delta\tau$ for each configuration were post-processed, according to the statistical procedure reviewed in in chapter 2 section 2.2.1.2, to calculate the endurance limit range $\Delta\tau_{A,50\%}$, extrapolated at $5 \cdot 10^6$ cycles to failure for P_s equal to 50%.
- The maximum and minimum ρ_w were selected to characterise the MWCM constant, in particular, $\Delta\tau_{Ref}(\rho_w)$.

By following the procedure described above, the reference shear stress ranges, $\Delta\tau_{Ref}(\rho_w)$, extrapolated at $5 \cdot 10^6$ cycles to failure for P_s equal to 50% is estimated as (Figure 7.10d):

$$\Delta\tau_{Ref}(\rho_w) = -1.7 \cdot \rho_w + 16.4 \text{ [MPa]} \quad \text{for } \rho_w \leq 2 \quad (7.3)$$

$$\Delta\tau_{Ref}(\rho_w) = 13 \text{ [MPa]} \quad \text{for } \rho_w > 2 \quad (7.4)$$

and for P_s equal to 97.7% is estimated as:

$$\Delta\tau_{Ref}(\rho_w) = -1.2 \cdot \rho_w + 11.4 \text{ [MPa]} \quad \text{for } \rho_w \leq 2 \quad (7.5)$$

$$\Delta\tau_{Ref}(\rho_w) = 9 \text{ [MPa]} \quad \text{for } \rho_w > 2 \quad (7.6)$$

- The modified Wöhler curve's negative inverse slope k_τ was determined by using the k values recommended by Sonsino [15] for thin and flexible welded joints (i.e. 7 under torsion and 5 under axial loading).

The k_τ of the corresponding modified Wöhler curve required to estimate the fatigue life of aluminium-to-steel welded joints is derived from the following relationships (Figure 7.10d):

$$k_\tau(\rho_w) = -2 \cdot \rho_w + 7 \quad \text{for } \rho_w \leq 1 \quad (7.7)$$

$$k_\tau(\rho_w) = 5 \quad \text{for } \rho_w > 1 \quad (7.8)$$

7.5 Lifetime estimation in terms of the MWCM along with the Point Method

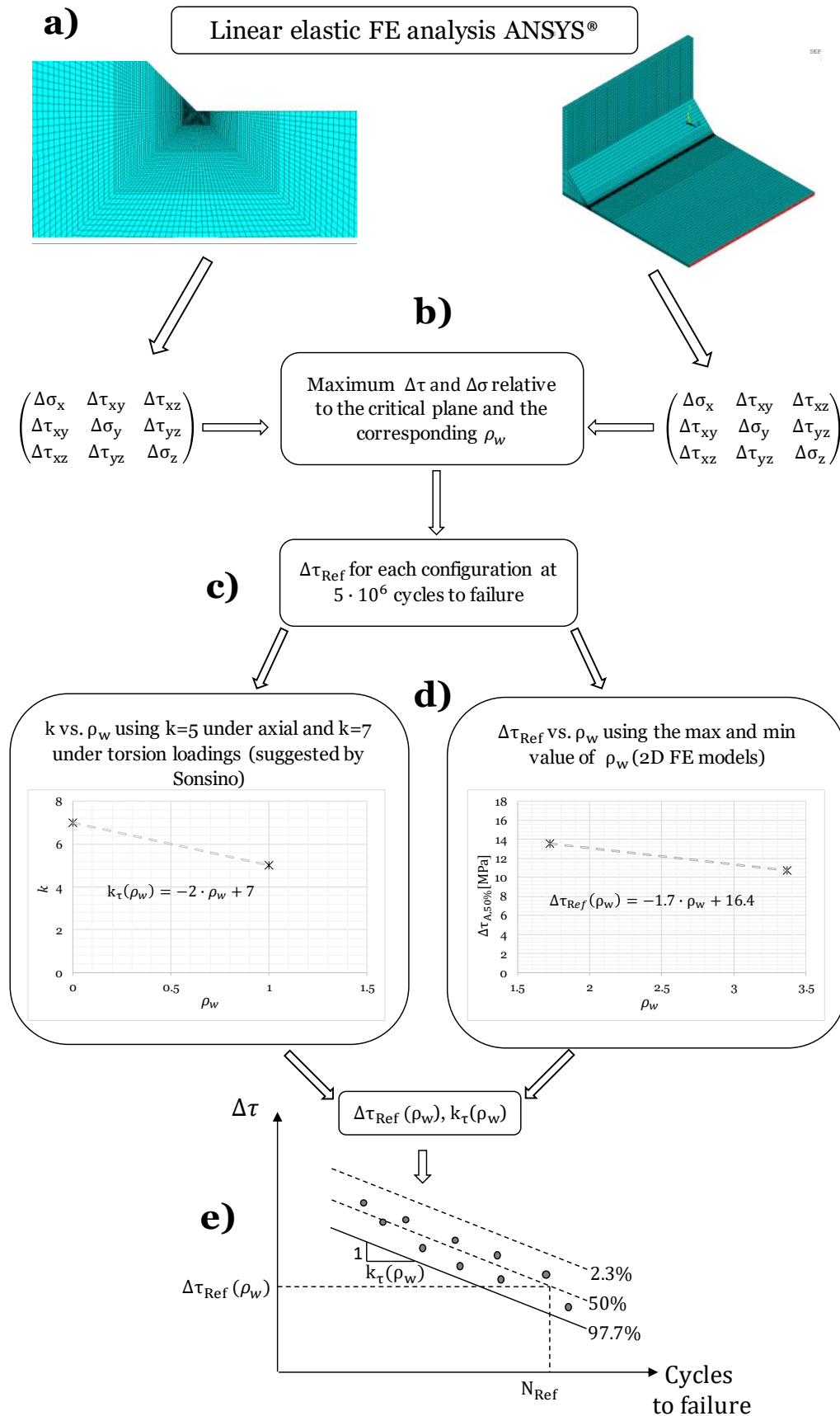


Figure 7.10 the procedure used to calibrate the MWCM constants and estimate the fatigue strength of hybrid welded joint according to the PM.

7.5.2 Method validation

The accuracy and consistency of the procedure presented above were checked by reanalysing the experimental data for various hybrid-welded joints using the 2D and the 3D FE models. (Note, the data used to form the proposed procedure are excluded from the validation exercise). Figure 7.11 and Figure 7.12 report the results obtained by using the MWCM along with PM in the modified Wöhler diagrams. As can be seen from the diagrams, by performing simple linear-elastic FE models the MWCM along with the PM was capable of providing a remarkable level of accuracy in estimating the fatigue behaviour of very thin and hybrid welded joints.

To summarise, the 3D FE analysis was able to capture the stress state at the critical location for the three axes, achieving an accurate fatigue lifetime estimation of the hybrid welded joint. In contrast, it is worth mentioning that, with much less time and computational effort, the 2D FE analysis was capable of estimating the fatigue strength of the hybrid-welded joints with an adequate level of conservatism. As long as the hybrid welded joints being analysed have a symmetrical feature at least in one axis, it is highly recommended to use the 2D FE analysis to perform the fatigue assessment.

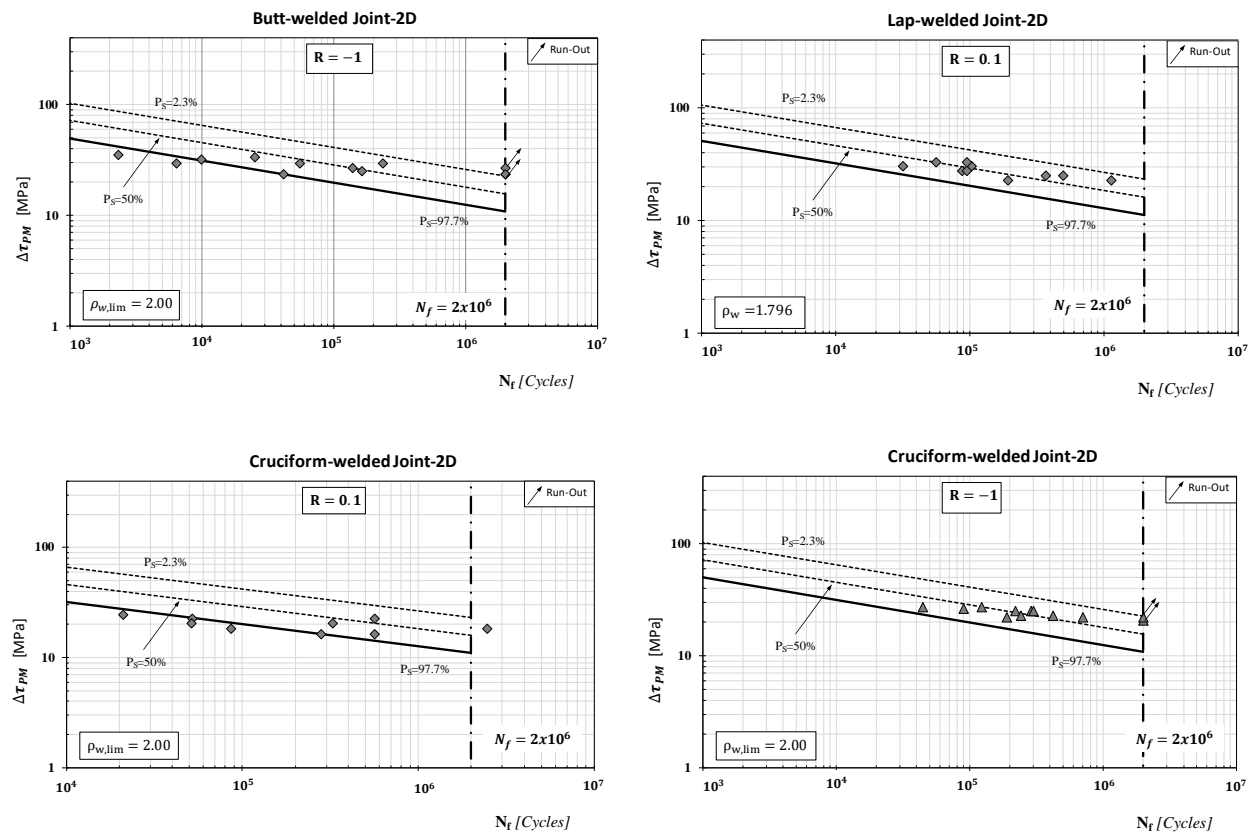


Figure 7.11 Accuracy of the MWCM applied along with the Point Method in estimating fatigue strength of thin hybrid welded components (2D FE models).

7.5 Lifetime estimation in terms of the MWCM along with the Point Method

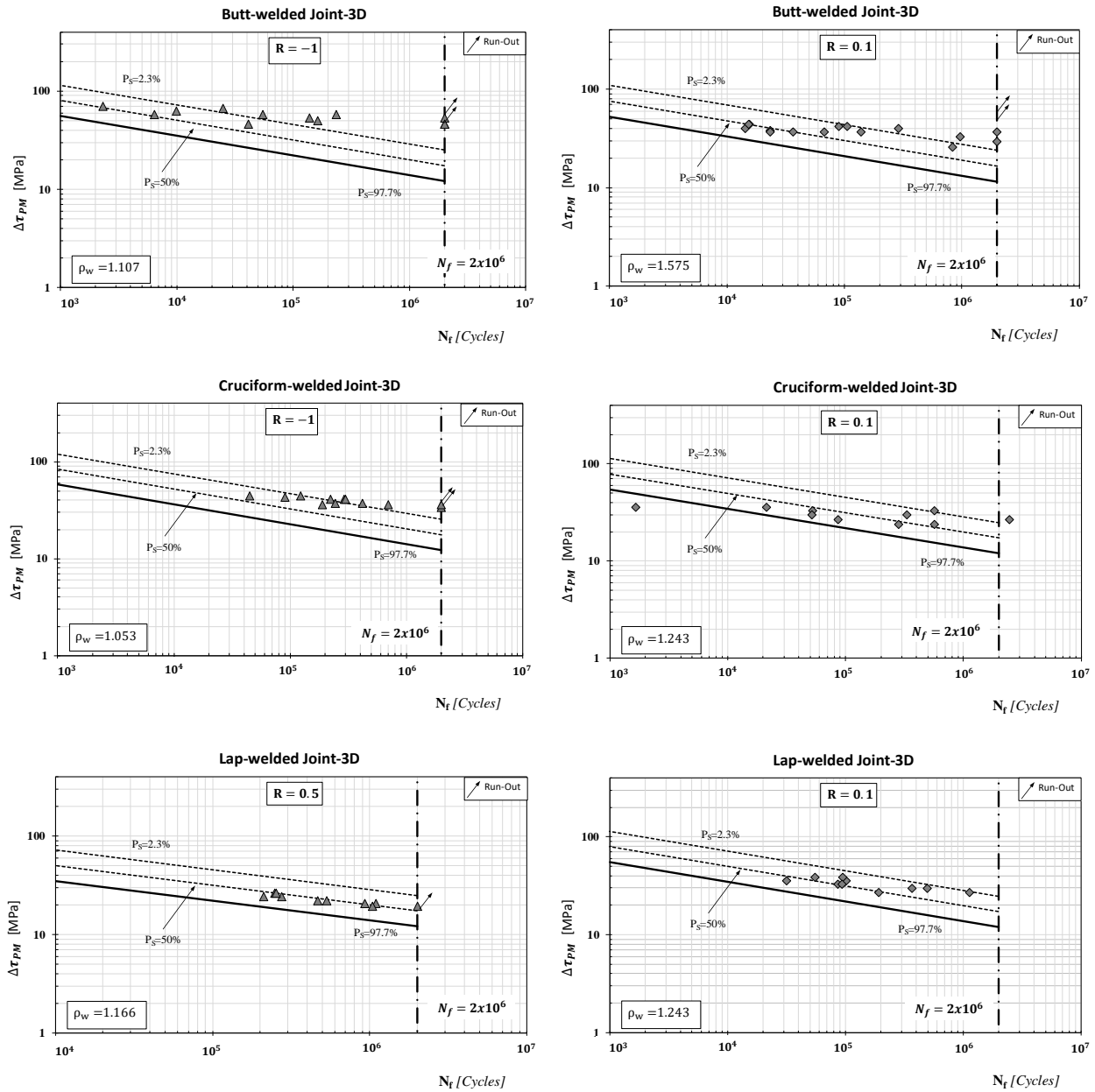


Figure 7.12 Accuracy of the MWCM applied along with the Point Method in estimating fatigue strength of thin hybrid welded components (3D FE models).

7.6 Conclusions

The present chapter provided a comprehensive assessment of the fatigue strength of aluminium-to-steel thin welded joints using different stress-based approaches. The key findings of the present investigations are the following:

- The visual examination of the fatigue failure of the hybrid-welded joints revealed that the crack initiates at the weld toe on the aluminium side. Therefore, the hybrid joint can be designed against fatigue loading by treating it as aluminium only.
- The negative inverse slope, k , suggested by Sonsino [15] for thin materials was seen to provide a conservative fatigue strength estimation of the aluminium-to-steel welded joints using the nominal stress approach.
- The effective notch stresses and the N-SIFs approaches indicated that the fatigue strength of the structural details being investigated was very low compared to the aluminium alloys used in structural applications.
- A fatigue design curve (FAT90) is proposed to be used to estimate the fatigue strength of thin hybrid welded joints according to the effective notch stress approach.
- When using the N-SIFs approach a master curve $\Delta K_{1,97.9\%} = 25 \text{ MPa}\cdot\text{mm}^{0.326}$, at $5 \cdot 10^6$ cycles to failure) is recommended to estimate the fatigue life of aluminium-to-steel thin welded joints with a high level of conservatism.
- The MWCM along with the PM was seen to be highly accurate in providing an estimation of fatigue lifetime of thin hybrid welded joints

7.7 References

- [1] Schijve J. Fatigue predictions of welded joints and the effective notch stress concept. *Int J Fatigue* 2012; 45:31-38 .
- [2] Hobbacher A. Recommendations For Fatigue Design of Welded Joints and Components. International Institute of Welding, Paris, 2007..
- [3] EuroCode 9: Design of aluminium structures- Part 1-3: Structures susceptible to fatigue. 2011..
- [4] EuroCode 3: Design of steel structures- Part 1-9: Fatigue. 2005..
- [5] Eurocode 9: Design of aluminium structures – Part 1-1: General structural rules, (1998) prENV..
- [6] Okamura H, Aota K. Joining of dissimilar materials with friction stir welding. *Welding International* 2004; 18(11): 852-860. .
- [7] Goecke S.F. Low Energy Arc Joining Process for Materials Sensitive to Heat. EWM Mündersbach, Germany, 2005..
- [8] Kah P, Suoranta R, Martikainen J. Advanced gas metal arc welding processes. *Int J Adv Manuf Technol* 2013; 67:655-674..
- [9] Elrefaey A, Gouda M, Takahashi M, Ikeuchi K. Characterization of Aluminium/Steel Lap Joint by Friction Stir Welding. *J Mate Eng Perf* 2005;14(1):12-17. .
- [10] Liu H, Maeda M, Fujii H, Nogi K. Tensile properties and fracture locations of friction-stir welded joints of 1050-H24 aluminum alloy. *J Mate Sci Letters* 2003;22:41-43. .
- [11] Meco S, Pardal G, Ganguly S, Williams S, McPherson N. Application of laser in seam welding of dissimilar steel to aluminium joints for thick structural components. *Optics and Laser in Engineering* 2015: 22-30..
- [12] Katayama S. Laser welding of aluminium alloys and dissimilar metals. *Welding International* 2004; 18(8): 618-625. .
- [13] Wang P, Chen X , Pan Q, Madigan B, Long J. Laser welding dissimilar materials of aluminum to steel: an overview. *Int J Adv Manuf Tech* 2016;87:3081-3090..
- [14] Susmel L. Multiaxial notch fatigue- From nominal to local stress/strain quantities, Cambridge: Woodhead Publishing Limited, 2009. .
- [15] Sonsino C. M, Bruder T, Baumgartner J, “S-N Lines for welded thin joints- suggested slopes and FAT values for applying the notch stress concept with various reference radii. *Welding World* 2010; 54(11/12): R375-392. .

- [16] Gurney TR. The Fatigue strength of transverse fillet welded joints: a study of the influence of the joint geometry. Cambridge: Abington Publishing, 1991. .
- [17] Lazzarin P, Tovo R. A notch Intensity Factor Approach to the Stress Analysis of Welds. *Fatigue & Fract of Eng Mate & Struct* 1998;21:1089-1103. .
- [18] Lazzarin P, Livieri P. Notch stress intensity factors and fatigue strength of aluminium and steel welded joints. *Int J Fatigue* 2001; 23:225-232. .
- [19] Fischer C, Fricke W, Rizzo C.M. Review of the fatigue strength of welded joints based on the notch stress intensity factor and SED approaches. *Int J Fatigue* 2016;84:59-66. .
- [20] Atzori B, Lazzarin P, Meneghetti G, Ricotta M. Fatigue design of complex welded structures. *Int J Fatigue* 2009;31:59-69..
- [21] Susmel L, Lazzarin P. A bi-parametric modified Wöhler curve for high cycle multiaxial fatigue assessment. *Fatigue Fract Engng Mater Struct* 2002;25:63-78. .
- [22] Susmel L, Tovo R. Local and structural multiaxial stress states in welded joints under fatigue loading. *Int J Fatigue* 2006;28:564-575. .
- [23] Susmel L. Estimating fatigue lifetime of steel weldments locally damaged by variable amplitude multiaxial stress fields. *Int J Fatigue* 2010;32:1057-1080. .
- [24] Al Zamzami I, Susmel L. On the accuracy of nominal, structural, and local stress based approaches in designing aluminium welded joints against fatigue. *Int J Fatigue* 2017;101:137-158. .
- [25] Taylor D. The theory of critical distances- a new perspective in fracture mechanics, Oxford, UK: Elsevier, 2007. .
- [26] Taylor D, Barrett N, Lucano G. Some new methods for predicting fatigue in welded joints. *Int J Faigue* 2002; 24:509-518..
- [27] Crupi G, Crupi V, Guglielmino E, Taylor D. Fatigue assessment of welded joints using critical distance and other methods. *Eng Fail Anal* 2005; 12:129-142. .
- [28] Taylor D. Geometrical effects in fatigue: a unifying theoretical model. *Int J Fatigue* 1999; 21(5): 413-420..

Chapter 8

8. Conclusions and recommendation for future work

8.1 Conclusion

The main purpose of this research project was to investigate the static and fatigue strength of aluminium-to-steel thin welded joints. Accordingly, theoretical and experimental activities were carried out with the aim of 1) Investigating the static strength of this type of joints using the coldArc® welding technology and hence design them accurately against static loading; 2) Extending the use of the global and local stress-based approaches to estimate the fatigue lifetime of the aluminium-to-steel thin hybrid welded joints. At the end of this project, all the objectives were fulfilled, and the main aims of this thesis were achieved, and the main conclusions drawn from this project are summarised below:

- Currently aluminium as structural material plays a significant role in the construction and automotive industries. Surprisingly in the technical literature, there is much less investigation on the fatigue behaviour of aluminium-welded joints in a comparison with the fatigue behaviour of steel.
- The Standards and Codes of Practice have recommended design curves for structures experiencing both uniaxial and/or torsional loading, and recommend equations for combined loading. There is no proper investigation of structures experiencing inclined loading except the work done by the Japanese research group.
- To date, the static behaviour of hybrid-welded joints has still not yet been comprehensively examined. The existing literature on the hybrid-welded joints is focused extensively on the microstructure of the hybrid joints and the welding technology to optimise the welding parameters and hence eliminate the presence of IMC that deteriorate the strength of the joint.

- Unexpectedly there is a very limited investigation of the fatigue behaviour of the hybrid-welded joints, and yet there is no any guideline or codes to design these joints against fatigue loading.
- From chapter 3, the use of the EC9 and the IIW to estimate the fatigue strength of aluminium-welded joints, using the nominal stresses, hot-spot stresses and effective notch stresses, is seen to provide an accurate estimation with an adequate level of conservatism with the effective notch stress being the most precise method. This investigation presented in chapter 3 further confirms the accuracy of the N-SIFs approach in designing aluminium-welded components. Finally, the TCD in the form of PM was calibrated to assess the fatigue strength of aluminium-welded joints. From this analysis, the TCD is seen to be accurate, and it can be used to design aluminium-welded joints against uniaxial fatigue loading by taking the critical distance equal to 0.5 mm.
- Chapter 4 presented a detailed study on the MWCM in estimating the fatigue strength of steel inclined welded joints subjected to uniaxial loading. The MWCM was not only capable of determining the fatigue lifetime of the steel inclined welded joints, but also provided a high level of accuracy.
- From Chapter 6, the static tensile tests were conducted with various hybrid-welded configurations. The fracture surface revealed that irrespective to the type of configurations or the inclination angle the static failure mainly occurs in the aluminium HAZ for the short-term and long-term tests. This conclusion makes it evident that the coldArc® welding process has improved the static strength of the hybrid welded joints and succeed in eliminating the formation of the intermetallic phase. From this investigation, the EC9 (used to design aluminium-welded joints) was also able to accurately design the aluminium-to-steel hybrid welded joints.
- The aim of chapter 7 was to investigate the fatigue behaviour of the hybrid-welded joints and use the existing stress-based approach to perform fatigue assessment of these hybrid joints. The nominal stress approach was seen to provide a conservative estimation on one condition that the negative inverse slope of 5 suggested by Sonsino for a thin material is used. Reanalysing the experimental data generated in Chapter 5 using the effective notch stresses and the N-SIFs has shown that the fatigue strength of the aluminium alloys used in the investigation was considerably low. In this investigation, the author has proposed a FAT90 to be used with the effective notch stresses and $\Delta K_{I, 97.7\%} = 25 \text{ MPa}\cdot\text{mm}^{0.326}$ to be used while using the N-SIFs approach. The work presented in chapter 7 further confirms the high accuracy of MWCM to assess the fatigue behaviour of any design components regardless of the complexity of the load applied neither the stress state damaging the component.

8.1 Conclusion

- It is worth recalling that the aluminium alloy used in this investigation is AA1050, which is considered to have the lowest static and fatigue strength amongst the rest of the aluminium series. As a result, the findings from this investigation would be suitable and safe to be used for any type of aluminium series. However, the degree of conservatism would be higher for a different series of aluminium alloys. The Outcome of this research can be used in any particular of interest where the weight of the structure is important and replacing part of the heavy steel structure is essential in particular in the automated, offshore and railway structures.

A summary of the contribution achieved in this investigation as shown in the table below:

Objective	Why is it novel?	Why is it scientifically sound?	To whom is it of value?
Manufacture of Al-to-St welded joints using coldArc technology.	The coldArc technology is able to eliminate the IMC which deteriorate the strength of the welded joints.	It forms a strong and robust welded joints that can be used in many structural applications	Scientists who are interested in reducing the presence of IMC and increasing the strength of the hybrid welded joints.
Investigation the fatigue behaviour of the hybrid welded joints experimentally	Al-St joints were never been examined systematically and structurally.	It provides valuable experimental information about the fatigue behaviour of this type of joints. Also, provide fatigue design curves to design this type of joints against cyclic loading.	Researchers. The experimental outcome of this thesis is the foundation that researchers can build on to investigate further different parameters associated with hybrid joints (i.e. different materials, thickness, load ratios, etc...)
Numerical procedure for using the Theory of Critical Distances	The numerical procedure developed is capable of analysing the structure with less computational effort using just a linear elastic FE analysis. It results in an adequate level of conservatism solution.	It provides a numerical model that can be used to perform fatigue assessment of the hybrid welded joints using linear elastic FE analysis	Structural designer in offshore, railway and automated industries. The outcome provides a numerical procedure that can be easily followed to design and validity of any structural parts.

8.2 Recommendation for future work

Based on the work carried out as part of this thesis, recommendations for future work are given below:

- Use different aluminium alloys such as 4000 and 6000 series to experimentally investigate the static behaviour and compare it with the static behaviour of AA1000 series. This would give a better understanding of the joints strength.
- An experimental programme is also needed to investigate further the fatigue behaviour of the aluminium-to-steel welded joints using materials with a thickness equal to or greater than 5 mm. It is important to understand the thickness effect and whether the recommended design codes are still valid.
- Investigate the fatigue behaviour of the aluminium-to-steel thin welded joints subjected to variable amplitude to determine the allowable damage sum to be used to design these joints against variable loading.
- Experimentally investigating the existing interaction between non-zero mean stresses and residual stresses in aluminium-to-steel hybrid welded joints subjected to fatigue loading

A Appendix A Fatigue results generated by testing aluminium alloys (Chapter 3)

Table A.1 The ultimate tensile strength (UTS) of different parent aluminium alloys

Parent material	UTS (MPa)	Parent material	UTS (MPa)
5083	317	Al Mg5	300
5083-0	310	Al Mg5 F28	300
5083 a 6061	310	Al Mg Si	289
5083-H112	340	Al Zn Mg1	384
5083-H113	340	Al Zn4 Mg1	350
5086-H32	340	D54 S M	306
5456-H321	317	NP 5/6	294
5456-H343	345	NP 5/6 M	336
6061-T6	260	S-ALMg4.5MnF28	317
6061-T651	310	S-ALMg4.5MnF30	300

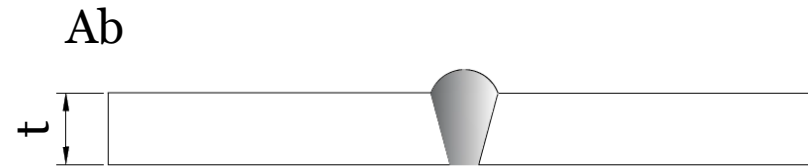


Table A.2 Fatigue results generated by testing butt-welded joints (geometry Ab) statistically re-analysed in terms of nominal stresses.

Series	Ref.	No of Data	Load Type ⁽¹⁾	R	t [mm]	k	T _σ	Nominal Stress		Parent material	Filler material
								Δσ _{A,50%} [MPa]	Δσ _{A,97.7%} [MPa]		
Ab-1	[39]	15	Ax	0	9.5	4.4	2.90	56.8	33.4	5083 a 6061	5356
Ab-2	[39]	15	Ax	0	9.5	4.3	2.32	57.9	38.0	5083-H113	5356
Ab-3	[28]	30	Be	-1	4.0	7.1	1.69	191.2	146.9	Al Mg5	Al Mg5
Ab-4	[27]	32	Be	-1	6.4	5.5	1.92	124.6	89.9	NP 5/6	NG 6
Ab-5	[27]	16	Be	-1	6.4	8.8	1.46	182.3	150.9	NP 5/6	NG 6
Ab-6	[27]	13	Be	-1	6.4	5.5	2.06	128.3	89.3	NP 5/6	NG 6
Ab-7	[27]	8	Be	-1	6.4	3.6	1.85	108.7	79.8	NP 5/6	NG 6
Ab-8	[27]	11	Be	-1	6.4	4.6	2.14	147.8	101.0	NP 5/6	NG 6
Ab-9	[27]	11	Be	-1	6.4	4.9	2.68	122.1	74.6	NP 5/6	NG 6
Ab-10	[26]	14	Be	-1	9.5	5.4	1.72	136.8	104.3	5083-H113	5183
Ab-11	[26]	14	Be	-1	6.4	4.7	1.82	121.6	90.2	5456-H321	5556
Ab-12	[38]	12	Ax	-1	2.5	7.5	2.44	251.5	161.1	5456-H321	5556
Ab-13	[38]	12	Ax	-1	2.5	6.0	1.69	164.8	126.8	5456-H343	5556
Ab-14	[38]	12	Ax	-1	2.5	6.0	1.80	135.3	100.8	5456-H343	5556
Ab-15	[36]	13	Be	-1	9.5	5.5	2.84	189.0	112.1	5083-H113	5183
Ab-16	[36]	13	Be	-1	9.5	5.4	1.80	136.2	101.4	5083-H113	5183
Ab-17	[36]	13	Be	-1	9.5	5.4	2.02	165.4	116.5	n/a	n/a
Ab-18	[28]	30	Ax	-1	4.0	4.0	2.47	64.4	41.0	Al Mg5	Al Mg5
Ab-19	[28]	18	Ax	-1	4.0	4.6	2.53	106.7	67.0	Al Mg5	Al Mg5
Ab-20	[28]	20	Ax	-1	4.0	5.7	1.88	121.8	88.9	Al Mg5	Al Mg5

Table A.2 (continued)

Series	Ref.	No of Data	Load Type ⁽¹⁾	R	t [mm]	k	T _σ	Nominal Stress		Parent material	Filler material
								Δσ _{A,50%} [MPa]	Δσ _{A,97.7%} [MPa]		
Ab-21	[28]	12	Ax	-1	4.0	2.0	13.31	41.9	11.5	Al Mg5	Al Mg5
Ab-22	[28]	12	Ax	-1	4.0	4.4	3.21	104.2	58.1	Al Mg5	Al Mg5
Ab-23	[28]	12	Ax	-1	4.0	5.5	1.87	104.1	76.1	Al Mg5	Al Mg5
Ab-24	[28]	12	Ax	-1	4.0	4.5	2.86	95.2	56.3	Al Mg5	Al Mg5
Ab-25	[28]	12	Ax	-1	4.0	4.5	2.08	99.8	69.3	Al Mg5	Al Mg5
Ab-26	[28]	12	Ax	-1	4.0	6.2	2.19	100.5	68.0	Al Mg5	Al Mg5
Ab-27	[28]	13	Ax	-1	4.0	4.6	3.72	90.8	47.1	Al Mg5	Al Mg5
Ab-28	[28]	14	Ax	-1	4.0	3.1	9.43	60.4	19.7	Al Mg5	Al Mg5
Ab-29	[28]	15	Ax	-1	6.4	10.1	2.18	126.3	85.5	D54 S M	A 56 S
Ab-30	[28]	18	Ax	-1	5.0	5.1	1.85	86.5	63.6	S-AlMg4.5MnF30	S-Al Mg5
Ab-31	[28]	30	Ax	0	4.0	3.9	2.51	46.0	29.0	Al Mg5	Al Mg5
Ab-32	[26]	9	Ax	0	9.5	6.3	2.65	83.4	51.2	5083-H113	5183
Ab-33	[26]	17	Ax	0	9.5	5.1	1.83	65.6	48.5	5083-H113	5356
Ab-34	[26]	10	Ax	0	9.5	4.7	1.58	74.3	59.2	5086-H32	5356
Ab-35	[34]	30	Ax	0	12.0	4.4	2.06	52.0	36.2	Al Mg5 F28	S-Al Mg5
Ab-36	[31]	15	Ax	0	6.4	4.8	2.88	73.1	43.1	D54 S M	A 56 S
Ab-37	[31]	50	Ax	0	10.0	5.8	1.47	86.4	71.4	S-AlMg4.5MnF28	S-AlMg4.5Mn
Ab-38	[32]	17	Ax	0	6.4	6.3	2.42	100.3	64.6	NP 5/6 M	NG 6
Ab-39	[32]	10	Ax	0	6.4	4.6	2.03	71.1	49.8	NP 5/6 M	NG 6
Ab-40	[30]	15	Ax	0	4.8	5.4	1.95	84.1	60.2	5083-H113	5356
Ab-41	[30]	12	Ax	0	6.4	10.6	1.59	112.1	88.9	5083-H113	5356
Ab-42	[30]	21	Ax	0	9.5	8.4	1.83	102.9	75.9	5083-H113	5356
Ab-43	[30]	18	Ax	0	9.5	4.1	1.39	60.8	51.6	5083-H113	5356
Ab-44	[30]	14	Ax	0	6.4	3.1	5.58	58.3	24.7	5083-H113	5356
Ab-45	[30]	15	Ax	0	6.4	3.2	2.53	51.9	32.6	5083-H113	5356
Ab-46	[31]	9	Ax	-0.4	6.4	5.4	4.10	105.3	52.0	D54 S M	A 56 S
Ab-47	[31]	16	Ax	-0.2	6.4	6.6	3.16	96.6	54.3	D54 S M	A 56 S

Appendix A Fatigue results generated by testing aluminium alloys (Chapter 3)

Table A.2 (continued)

Series	Ref.	No of Data	Load Type ⁽¹⁾	R	t [mm]	k	T _σ	Nominal Stress		Parent material	Filler material
								Δσ _{A,50%} [MPa]	Δσ _{A,97.7%} [MPa]		
Ab-48	[31]	11	Ax	0.2	6.4	6.0	1.59	72.3	57.4	D54 S M	A 56 S
Ab-49	[30]	14	Ax	0.25	4.8	7.0	1.36	75.9	65.0	5083-H113	5356
Ab-50	[30]	12	Ax	0.25	6.4	8.2	1.40	89.1	75.2	5083-H113	5356
Ab-51	[30]	18	Ax	0.25	9.5	9.0	1.47	87.1	71.9	5083-H113	5356
Ab-52	[30]	21	Ax	0.25	9.5	5.0	1.53	60.3	48.8	5083-H113	5356
Ab-53	[31]	16	Ax	0.4	6.4	4.3	1.84	61.1	45.1	D54 S M	A 56 S
Ab-54	[34]	7	Ax	0.5	4.8	5.8	1.38	63.6	54.1	5083-H113	5356
Ab-55	[30]	14	Ax	0.5	6.4	10.9	1.42	75.9	63.7	5083-H113	5356
Ab-56	[30]	12	Ax	0.5	9.4	6.4	1.67	66.8	51.6	5083-H113	5356
Ab-57	[30]	21	Ax	0.5	9.5	5.2	1.93	56.3	40.5	5083-H113	5356
Ab-58	[30]	17	Ax	0.6	6.4	6.6	2.11	65.4	45.0	D54 S M	A 56 S
Ab-59	[40]	48	Ax	0	4.0	6.6	1.71	97.6	74.7	Al Mg Si	Al Si5
Ab-60	[40]	9	Ax	0	4.0	7.4	2.17	101.6	68.9	Al Mg Si	Al Mg5
Ab-61	[40]	43	Be	0	4.0	4.4	1.72	149.6	114.0	Al Mg Si	Al Si5
Ab-62	[40]	57	Ax	-1	4.0	7.7	1.89	135.7	98.7	Al Mg Si	Al Si5
Ab-63	[40]	12	Ax	-1	4.0	6.6	1.59	125.2	99.4	Al Mg Si	Al Mg5
Ab-59	[40]	48	Ax	0	4.0	6.6	1.71	97.6	74.7	Al Mg Si	Al Si5
Ab-60	[40]	9	Ax	0	4.0	7.4	2.17	101.6	68.9	Al Mg Si	Al Mg5
Ab-61	[40]	43	Be	0	4.0	4.4	1.72	149.6	114.0	Al Mg Si	Al Si5
Ab-62	[40]	57	Ax	-1	4.0	7.7	1.89	135.7	98.7	Al Mg Si	Al Si5
Ab-63	[40]	12	Ax	-1	4.0	6.6	1.59	125.2	99.4	Al Mg Si	Al Mg5
Ab-64	[40]	18	Ax	-1	4.0	5.0	1.66	111.1	86.2	Al Mg Si	Al Si5
Ab-65	[40]	12	Ax	-1	8.0	4.4	1.45	136.8	113.6	Al Mg Si	Al Si5
Ab-66	[40]	10	Ax	-1	8.0	5.6	2.16	140.3	95.4	Al Mg Si	Al Si5
Ab-67	[40]	55	Be	-1	4.0	5.7	1.56	169.6	135.9	Al Mg Si	Al Si5
Ab-68	[40]	22	Be	-1	4.0	4.4	1.70	159.6	122.5	Al Mg Si	Al Si5
Ab-69	[40]	27	Be	-1	8.0	5.1	1.48	167.3	137.4	Al Mg Si	Al Si5

Table A.2 (continued)

Series	Ref.	No of Data	Load Type ⁽¹⁾	R	t [mm]	k	T _σ	Nominal Stress		Parent material	Filler material
								Δσ _{A,50%} [MPa]	Δσ _{A,97.7%} [MPa]		
Ab-70	[40]	22	Be	-1	4.0	4.4	1.47	166.1	137.2	Al Mg Si	Al Si5
Ab-71	[40]	30	Be	-1	4.0	3.2	1.86	152.5	111.9	Al Mg Si	Al Si5
Ab-72	[34]	21	Ax	0.08	12.0	5.2	1.55	74.2	59.5	Al Zn Mg1	Al Mg7
Ab-73	[34]	23	Ax	0.08	12.0	6.1	1.74	89.1	67.5	Al Zn Mg1	S-Al Mg5
Ab-74	[42]	82	Ax	0.1	6.0	3.9	2.43	57.1	36.7	Al Zn Mg1	Al Mg5
Ab-75	[42]	33	Ax	0.1	6.0	2.9	3.07	52.0	29.7	Al Zn Mg1	Al Mg5
Ab-76	[41]	26	Ax	0.1	10.0	3.8	2.02	61.0	43.0	Al Zn Mg1	Al Mg5
Ab-77	[40]	50	Ax	-1	4.0	4.6	3.42	137.5	74.4	Al Zn4 Mg1	Al Mg5
Ab-78	[40]	18	Ax	-1	4.0	3.8	2.05	125.8	87.8	Al Zn4 Mg1	Al Mg5
Ab-79	[40]	18	Ax	-1	8.0	2.8	2.72	105.9	64.2	Al Zn4 Mg1	Al Mg5

⁽¹⁾Ax= axial cyclic loading; Be=cyclic bending.

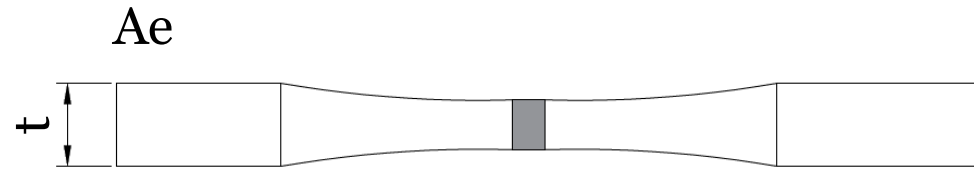


Table A.3 Fatigue results generated by testing ground butt-welded joints (geometries Ae) statistically re-analysed in terms of nominal stresses.

Series	Ref.	No of Data	Load Type ⁽¹⁾	R	t [mm]	k	T _σ	Nominal Stress		Parent material	Filler material
								Δσ _{A,50%} [MPa]	Δσ _{A,97.7%} [MPa]		
Ae-1	[37]	9	Ax	0	7.6	10.2	3.08	139.7	79.6	5086-H32	5356
Ae-2	[37]	9	Ax	0	7.6	12.9	1.45	199.6	165.8	5456-H321	5556
Ae-3	[37]	10	Ax	0	7.6	12.3	1.91	162.9	117.8	5456-H321	5556
Ae-4	[37]	8	Ax	0	7.6	9.8	1.89	171.1	124.6	5083-H113	5556
Ae-5	[37]	6	Ax	0	7.6	12.7	3.25	181.3	100.6	5086-H32	5356
Ae-6	[37]	29	Be	-1	7.6	6.7	2.62	229.9	142.0	5083-H112	5556
Ae-7	[37]	28	Be	-1	7.6	8.4	1.74	242.7	184.1	5083-0	5183
Ae-8	[37]	24	Be	-1	7.6	6.9	1.66	221.5	171.8	5083-H112	5183

⁽¹⁾Ax= axial cyclic loading; Be=cyclic bending.

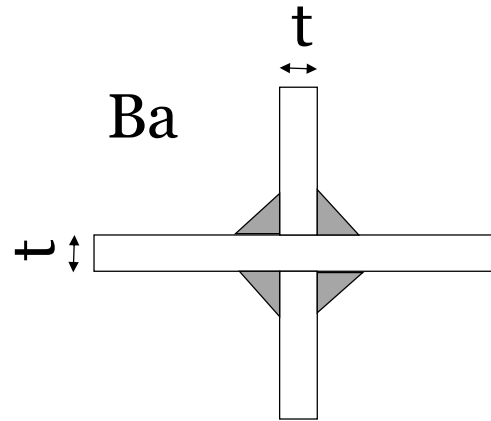


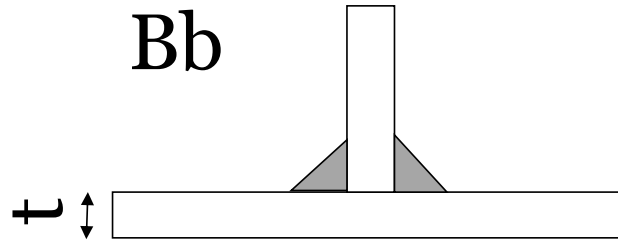
Table A.4 Fatigue results generated by testing non-load carrying fillet welded joints (geometries Ba, Bd and Be) statistically re-analysed in terms of nominal stresses.

Series	Ref.	No of Data	Load Type ⁽¹⁾	R							Nominal Stress		Parent material	Filler material
					t	L	Z	k	T _σ	Δσ _{A,50%}	Δσ _{A,97.7%}			
					[mm]	[mm]	[mm]			[MPa]	[MPa]			
Ba-1	[28]	10	Be	-1	8.0	8.0	7.7	4.7	1.48	104.4	85.9	Al Mg5	Al Mg5	
Ba-2	[28]	10	Ax	-1	8.0	8.0	-	3.5	3.44	88.9	47.9	Al Mg5	Al Mg5	
Ba-3	[33]	16	Ax	-1	6.4	12.7	-	3.1	3.74	75.6	39.1	D54 S M	A 56 S	
Ba-4	[28]	10	Ax	0	8.0	8.0	-	5.5	2.23	82.5	55.3	Al Mg5	Al Mg5	
Ba-5	[33]	17	Ax	0	6.4	12.7	-	3.4	6.37	57.8	22.9	D54 S M	A 56 S	
Ba-6	[33]	10	Ax	0.7	6.4	12.7	-	2.9	6.39	32.9	13.0	D54 S M	A 56 S	
Ba-7	[40]	11	Ax	0	8.0	8.0	7.7	2.9	7.01	66.4	25.1	Al Mg Si	Al Si5	
Ba-8	[40]	10	Be	0	8.0	8.0	7.7	5.8	1.45	124.0	102.8	Al Mg Si	Al Si5	
Ba-9	[40]	15	Ax	-1	8.0	8.0	7.7	3.7	1.84	70.2	51.8	Al Mg Si	Al Si5	
Ba-10	[40]	10	Be	-1	8.0	8.0	7.7	5.2	1.36	160.7	137.6	Al Mg Si	Al Si5	
Ba-11	[41]	29	Ax	0.1	6.0	6.0	-	3.5	2.05	65.3	45.6	Al Zn Mg1	Al Mg5	
Ba-12	[41]	27	Ax	0.1	10.0	10.0	-	3.5	2.12	53.5	36.7	Al Zn Mg1	Al Mg5	
Ba-13	[40]	18	Ax	0	8.0	8.0	7.7	5.3	1.37	101.8	87.0	Al Zn4 Mg1	Al Mg5	
Ba-14	[40]	18	Ax	-1	8.0	8.0	7.7	5.0	1.36	145.1	124.6	Al Zn4 Mg1	Al Mg5	

Table A.4 (continued)

Series	Ref.	No of Data	Load Type ⁽¹⁾	R	Nominal Stress							Parent material	Filler material
					t [mm]	L [mm]	Z [mm]	k	T _σ	Δσ _{A,50%} [MPa]	Δσ _{A,97.7%} [MPa]		
Ba-15	[44]	6	Ax	0.1	3.0	3.0	4.5	4.3	2.19	58.2	39.3	6061-T6	6061-T6
Ba-16	[44]	6	Ax	0.1	6.0	6.0	7.0	4.2	2.18	41.0	27.8	6061-T6	6061-T6
Ba-17	[44]	4	Ax	0.1	12.0	12.0	10.0	3.8	2.27	37.5	24.9	6061-T6	6061-T6
Ba-18	[44]	8	Ax	0.1	24.0	24.0	20.5	3.7	1.54	29.6	23.8	6061-T6	6061-T6
Ba-19	[44]	7	Ax	0.1	24.0	6.0	7.0	3.8	1.48	39.0	32.1	6061-T6	6061-T6
Ba-20	[44]	9	Ax	0.1	12.0	6.0	7.0	3.7	1.56	30.4	24.3	6061-T6	6061-T6
Bd-1	[35]	8	Ax	0	9.5	9.5	-	3.4	3.69	28.1	14.7	NP 5/6 M	NG 6
Bd-2	[35]	6	Ax	0	9.5	9.5	-	3.3	2.47	32.5	20.7	NP 5/6 M	NG 6
Bd-3	[35]	8	Ax	0	9.5	9.5	-	3.8	3.55	64.6	53.6	NP 5/6 M	NG 6
Be-1	[29]	6	Be	0	10.0	-	-	-	-	-	-	Al Zn Mg1	S-ALMg4.5 Mn
Be-2	[29]	25	Be	-1	10.0	-	-	4.5	1.28	156.2	133.6	Al Zn Mg1	S-ALMg4.5 Mn

⁽¹⁾Ax= axial cyclic loading; Be=cyclic bending.

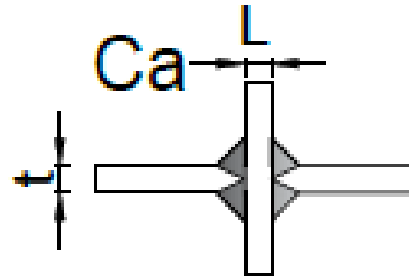

Table A.5 Fatigue results generated by testing non-load carrying fillet welded T-joints (geometry Bb) statistically re-analysed in terms of nominal stresses.

Series	Ref.	No of Data	Load Type ⁽¹⁾	R	Nominal Stress							Parent material	Filler material
					t [mm]	L [mm]	Z [mm]	k	T _σ	Δσ _{A,50%} [MPa]	Δσ _{A,97.7%} [MPa]		
Bb-1	[28]	30	Be	0	4.0	4.0	4.2	4.6	1.70	79.1	60.7	Al Mg5	Al Mg5
Bb-2	[28]	30	Be	0	8.0	8.0	7.7	4.1	1.98	73.5	52.2	Al Mg5	Al Mg5
Bb-3	[28]	30	Be	-1	4.0	4.0	4.2	4.5	2.06	94.8	66.1	Al Mg5	Al Mg5
Bb-4	[28]	30	Be	-1	8.0	8.0	7.7	5.1	1.22	103.3	93.7	Al Mg5	Al Mg5
Bb-5	[28]	10	Ax	-1	4.0	4.0	-	6.5	1.83	141.3	104.4	Al Mg5	Al Mg5
Bb-6	[28]	29	Ax	-1	8.0	8.0	-	6.6	1.66	125.7	97.5	Al Mg5	Al Mg5
Bb-7	[28]	10	Ax	-1	8.0	4.0	-	7.1	1.68	132.7	102.5	Al Mg5	Al Mg5
Bb-8	[28]	28	Ax	0	4.0	4.0	-	8.8	1.51	102.5	83.5	Al Mg5	Al Mg5
Bb-9	[28]	27	Ax	0	8.0	8.0	-	7.5	1.46	91.2	75.4	Al Mg5	Al Mg5
Bb-10	[28]	10	Ax	0	8.0	4.0	-	7.8	1.88	111.7	81.6	Al Mg5	Al Mg5
Bb-11	[40]	27	Ax	0	4.0	4.0	4.2	7.3	1.36	105.2	90.4	Al Mg Si	Al Si5
Bb-12	[40]	29	Ax	0	8.0	8.0	7.7	7.0	1.62	79.3	62.2	Al Mg Si	Al Si5
Bb-13	[40]	15	Ax	0	8.0	4.0	7.7	6.7	1.91	85.2	61.6	Al Mg Si	Al Si5
Bb-14	[40]	28	Be	0	4.0	4.0	4.2	6.0	1.36	143.4	122.8	Al Mg Si	Al Si5
Bb-15	[40]	36	Be	0	8.0	8.0	7.7	4.6	1.72	94.7	72.2	Al Mg Si	Al Si5
Bb-16	[40]	27	Ax	-1	4.0	4.0	4.2	7.1	1.48	146.0	120.1	Al Mg Si	Al Si5
Bb-17	[40]	9	Ax	-1	4.0	4.0	4.2	8.9	1.23	147.0	132.4	Al Mg Si	Al Si5
Bb-18	[40]	34	Ax	-1	8.0	8.0	7.7	6.0	1.79	115.3	86.2	Al Mg Si	Al Si5

Table A.5 (continued)

Series	Ref.	No of Data	Load Type ⁽¹⁾	R	Nominal Stress							Parent material	Filler material
					t [mm]	L [mm]	Z [mm]	k	T _σ	Δσ _{A,50%} [MPa]	Δσ _{A,97.7%} [MPa]		
Bb-19	[40]	21	Ax	-1	8.0	4.0	7.7	5.1	2.56	111.7	69.9	Al Mg Si	Al Si5
Bb-20	[40]	30	Be	-1	4.0	4.0	4.2	5.8	1.56	176.0	140.8	Al Mg Si	Al Si5
Bb-21	[40]	9	Be	-1	4.0	4.0	4.2	6.8	1.28	153.7	135.6	Al Mg Si	Al Si5
Bb-22	[40]	30	Be	-1	8.0	8.0	7.7	5.3	1.51	143.3	116.8	Al Mg Si	Al Si5
Bb-23	[29]	7	Be	0	10.0	10.0	-	8.0	2.13	152.6	104.5	Al Zn Mg1	S-ALMg4.5Mn
Bb-24	[29]	9	Ax	0	10.0	-	-	4.8	1.27	85.3	75.6	Al Zn Mg1	S-ALMg4.5Mn
Bb-25	[29]	33	Be	-1	10.0	10.0	-	5.5	1.29	142.1	125.2	Al Zn Mg1	S-ALMg4.5Mn
Bb-26	[29]	9	Ax	-1	10.0	10.0	-	5.0	1.83	114.6	84.8	Al Zn Mg1	S-ALMg4.5Mn
Bb-27	[40]	27	Ax	0	8.0	8.0	7.7	7.6	1.39	134.0	113.6	Al Zn4 Mg1	Al Mg5
Bb-28	[40]	18	Ax	0	8.0	4.0	7.7	7.6	1.26	139.2	123.9	Al Zn4 Mg1	Al Mg5
Bb-29	[40]	26	Ax	-1	8.0	8.0	7.7	5.5	4.43	170.8	81.2	Al Zn4 Mg1	Al Mg5
Bb-30	[40]	18	Ax	-1	8.0	4.0	7.7	6.6	1.35	195.9	168.5	Al Zn4 Mg1	Al Mg5
Bb-31	[45]	11	Be	0.1	10.0	10.0	7.0	3.9	1.64	41.3	32.3	5083-H11	5183
Bb-32	[45]	15	Be	0.5	10.0	10.0	7.0	3.3	1.64	36.6	28.6	5083-H11	5183
Bb-33	[46]	11	Ax	0.1	12.0	10.0	8.0	4.2	1.46	45.7	37.8	5083-H3	5083-H3
Bb-34	[46]	13	Ax	0.1	12.0	10.0	8.0	4.0	1.38	42.0	35.8	5083-H3	5083-H3
Bb-35	[34]	7	Ax	0.1	12.0	12.0	8.0	4.6	3.78	53.0	27.3	6061-T651	6061-T652

⁽¹⁾Ax= axial cyclic loading; Be=cyclic bending.


Table A.6 Fatigue results generated by testing cruciform full-penetration welded joints (geometry Ca) statistically re-analysed in terms of nominal stresses.

Series	Ref.	No of Data	Load Type ⁽¹⁾	R	t [mm]	L [mm]	Z [mm]	k	T _σ	Nominal Stress		Parent material	Filler material
										Δσ _{A,50%} [MPa]	Δσ _{A,97.7%} [MPa]		
Ca-1	[28]	30	Be	0	8.0	4.0	7.7	4.0	1.67	75.5	58.5	Al Mg5	Al Mg5
Ca-2	[28]	30	Be	-1	8.0	4.0	7.7	3.7	1.52	87.5	71.0	Al Mg5	Al Mg5
Ca-3	[28]	9	Be	-1	8.0	8.0	7.7	4.0	1.59	95.9	76.0	Al Mg5	Al Mg5
Ca-4	[28]	10	Be	-1	8.0	4.0	7.7	2.7	2.28	93.6	62.0	Al Mg5	Al Mg5
Ca-5	[28]	29	Ax	-1	8.0	4.0	-	4.0	1.94	57.6	41.4	Al Mg5	Al Mg5
Ca-6	[28]	10	Ax	-1	8.0	4.0	-	2.6	3.09	67.9	38.6	Al Mg5	Al Mg5
Ca-7	[28]	10	Ax	-1	8.0	4.0	-	3.9	1.66	52.7	40.8	Al Mg5	Al Mg5
Ca-8	[28]	29	Ax	0	8.0	4.0	-	4.3	2.81	30.3	18.1	Al Mg5	Al Mg5
Ca-9	[40]	30	Ax	0	8.0	4.0	7.7	4.9	1.74	50.7	38.5	Al Mg Si	Al Si5
Ca-10	[40]	32	Be	0	8.0	4.0	7.7	5.3	2.01	123.5	87.1	Al Mg Si	Al Si5
Ca-11	[40]	31	Ax	-1	8.0	4.0	7.7	4.6	2.07	76.4	53.1	Al Mg Si	Al Si5
Ca-12	[40]	13	Ax	-1	8.0	4.0	7.7	4.6	7.61	61.8	22.4	Al Mg Si	Al Mg5
Ca-13	[40]	12	Ax	-1	8.0	4.0	7.7	3.5	4.03	95.0	47.4	Al Mg Si	Al Si5
Ca-14	[40]	12	Ax	-1	8.0	4.0	7.7	3.9	4.57	48.3	22.6	Al Mg Si	Al Si5
Ca-15	[40]	27	Be	-1	8.0	4.0	7.7	5.1	1.39	148.6	126.0	Al Mg Si	Al Si5
Ca-16	[40]	9	Be	-1	8.0	4.0	7.7	6.3	1.75	151.5	114.4	Al Mg Si	Al Si5
Ca-17	[40]	9	Be	-1	8.0	4.0	7.7	7.2	1.55	152.7	122.7	Al Mg Si	Al Si5
Ca-18	[40]	9	Be	-1	8.0	4.0	7.7	6.6	1.49	163.0	133.8	Al Mg Si	Al Mg5

Table A.6 (continued)

Series	Ref.	No of Data	Load Type ⁽¹⁾	R	t [mm]	L [mm]	Z [mm]	k	T _σ	Nominal Stress		Parent material	Filler material
										Δσ _{A,50%} [MPa]	Δσ _{A,97.7%} [MPa]		
Ca-19	[34]	16	Ax	0.08	12.0	12.0	-	4.8	1.36	61.9	53.0	Al Zn Mg1	Al Si5
Ca-20	[34]	8	Ax	0.08	12.0	12.0	-	4.6	2.47	53.5	34.0	Al Zn Mg1	Al Si5
Ca-21	[40]	27	Ax	-1	8.0	4.0	-	4.9	1.80	112.0	83.5	Al Zn4 Mg1	Al Mg5
Ca-22	[40]	18	Ax	-1	8.0	8.0	-	5.4	1.45	153.0	126.9	Al Zn4 Mg1	Al Mg5
Ca-23	[40]	18	Ax	-1	8.0	4.0	-	2.9	3.78	93.1	47.9	Al Zn4 Mg1	Al Mg5
Ca-24	[40]	18	Ax	-1	8.0	4.0	-	4.9	1.40	119.1	100.6	Al Zn4 Mg1	Al Si5

⁽¹⁾Ax=axial cyclic loading; Be=cyclic bending.

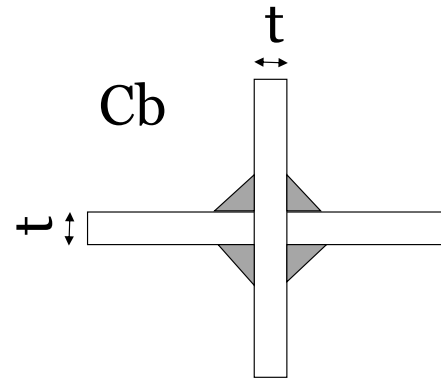


Table A.7 Fatigue results generated by testing load carrying fillet cruciform welded joints (geometries Cb and Cc) statistically re-analysed in terms of nominal stresses.

Series	Ref.	No of Data	Load Type ⁽¹⁾	R	t [mm]	L [mm]	Z [mm]	k	T _σ	Nominal Stress		Parent material	Filler material
										Δσ _{A,50%} [MPa]	Δσ _{A,97.7%} [MPa]		
Cb-1	[28]	27	Ax	-1	4.0	4.0	-	4.8	1.86	84.8	62.2	Al Mg5	Al Mg5
Cb-2	[28]	29	Ax	-1	8.0	8.0	-	3.8	1.77	69.3	52.1	Al Mg5	Al Mg5
Cb-3	[33]	9	Ax	-1	6.4	12.7	-	4.5	2.41	75.9	48.9	D54 S M	A 56 S
Cb-4	[28]	27	Ax	0	4.0	4.0	-	4.8	2.16	54.3	37.0	Al Mg5	Al Mg5
Cb-5	[28]	30	Ax	0	8.0	8.0	-	4.3	1.88	39.5	28.8	Al Mg5	Al Mg5
Cb-6	[33]	20	Ax	0	6.4	12.7	-	5.0	4.61	49.6	23.1	D54 S M	A 56 S
Cb-7	[33]	25	Ax	0	10.0	10.0	-	3.4	1.26	28.6	25.5	Al Mg5 F28	S-AlMg4.5Mn
Cb-8	[33]	10	Ax	0.6	6.4	12.7	-	5.0	1.83	42.5	31.4	D54 S M	A 56 S
Cb-9	[33]	6	Ax	0.75	6.4	12.7	-	2.9	2.38	33.7	21.9	D54 S M	A 56 S
Cb-10	[40]	31	Ax	0	4.0	4.0	4.2	6.0	1.84	72.0	53.1	Al Mg Si	Al Si5
Cb-11	[40]	23	Ax	0	8.0	8.0	7.7	6.0	1.49	50.2	41.1	Al Mg Si	Al Si5
Cb-12	[40]	25	Ax	0	8.0	8.0	7.7	5.9	1.51	42.9	34.9	Al Mg Si	Al Si5
Cb-13	[40]	27	Ax	-1	4.0	4.0	4.2	6.5	1.76	114.2	86.0	Al Mg Si	Al Si5
Cb-14	[40]	11	Ax	-1	4.0	8.0	4.2	5.8	2.47	105.1	66.9	Al Mg Si	Al Si5
Cb-15	[40]	28	Ax	-1	8.0	8.0	7.7	4.4	1.98	66.9	47.5	Al Mg Si	Al Si5
Cb-16	[34]	12	Ax	0.08	12.0	12.0	6.3	5.8	1.40	38.9	32.9	Al Zn Mg1	Al Si5

Table A.7 (continued)

Series	Ref.	No of Data	Load Type ⁽¹⁾	R								Nominal Stress		Parent material	Filler material
					t [mm]	L [mm]	Z [mm]	k	T _σ	Δσ _{A,50%} [MPa]	Δσ _{A,97.7%} [MPa]				
Cb-17	[34]	14	Ax	0.08	12.0	12.0	6.3	4.6	1.36	36.2	31.0	Al Zn Mg1	Al Si5		
Cb-18	[41]	29	Ax	0.1	6.0	6.0	-	5.3	1.77	54.9	41.2	Al Zn Mg1	Al Si5		
Cb-19	[40]	27	Ax	0	4.0	4.0	4.2	3.5	1.86	65.9	48.3	Al Zn4 Mg1	Al Mg5		
Cb-20	[40]	27	Ax	0	8.0	8.0	7.7	4.2	2.14	50.0	34.2	Al Zn4 Mg1	Al Mg5		
Cb-21	[40]	18	Ax	0	8.0	-	-	4.1	2.32	43.5	28.6	Al Zn4 Mg1	Al Mg5		
Cb-22	[40]	27	Ax	-1	8.0	8.0	7.7	3.5	3.43	92.3	49.8	Al Zn4 Mg1	Al Mg5		
Cb-23	[43]	12	Ax	0.1	12.0	12.0	8.0	5.3	2.17	29.5	20.0	6061-T651	6061-T652		
Cb-24	[43]	18	Ax	0.1	12.0	12.0	6.4	4.4	1.47	27.4	22.6	Al Zn Mg1	Al Zn Mg2		
Cc-1	[40]	30	Be	0	4.0	8.0	-	4.7	1.83	119.4	88.3	Al Mg Si	Al Si5		
Cc-2	[40]	11	Be	0	4.0	8.0	-	5.5	1.78	133.8	100.3	Al Mg Si	Al Si5		
Cc-3	[40]	28	Be	0	8.0	8.0	-	3.9	1.66	92.8	72.0	Al Mg Si	Al Si5		
Cc-4	[40]	29	Be	-1	4.0	8.0	-	4.1	1.55	144.4	116.1	Al Mg Si	Al Si5		
Cc-5	[40]	12	Be	-1	4.0	8.0	-	6.5	1.42	165.1	138.6	Al Mg Si	Al Si5		

⁽¹⁾Ax= axial cyclic loading; Be=cyclic bending.

Appendix A Fatigue results generated by testing aluminium alloys (Chapter 3)

Table A.8 Fatigue results generated by testing non-load carrying fillet cruciform welded joints (geometry Ba) and non-load carrying fillet welded T-joints (geometry Bb) statistically re-analysed in terms of hot-spot stresses and effective notch stresses approaches.

Series	No of Data	Load Type ⁽¹⁾	R	k	T _σ	Hot-Spot Stress		Effective Notch Stress	
						Δσ _{A,50%} [MPa]	Δσ _{A,97.7%} [MPa]	Δσ _{A,50%} [MPa]	Δσ _{A,97.7%} [MPa]
Ba-1	10	Be	-1	4.7	1.48	129.8	106.8	244.3	200.9
Ba-7	11	Ax	0	2.9	7.01	76.4	28.9	155.3	58.6
Ba-8	10	Be	0	5.8	1.45	142.6	118.3	290.0	240.5
Ba-9	15	Ax	-1	3.7	1.84	80.8	59.6	164.3	121.1
Ba-10	10	Be	-1	5.2	1.36	184.9	158.3	375.9	321.9
Ba-13	18	Ax	0	5.3	1.37	126.6	108.2	238.2	203.6
Ba-14	18	Ax	-1	5.0	1.36	180.4	154.9	339.4	291.4
Ba-15	6	Ax	0.1	4.3	2.19	81.9	55.3	124.1	83.8
Ba-16	6	Ax	0.1	4.2	2.18	58.4	39.6	110.6	75.0
Ba-17	4	Ax	0.1	3.8	2.27	55.1	36.6	125.9	83.6
Ba-18	8	Ax	0.1	3.7	1.54	43.6	35.0	124.5	100.2
Ba-19	7	Ax	0.1	3.8	1.48	56.2	46.3	125.0	102.9
Ba-20	9	Ax	0.1	3.7	1.56	45.2	36.2	94.9	75.9
Bb-1	30	Be	0	4.6	1.70	91.5	70.3	171.6	131.7
Bb-2	30	Be	0	4.1	1.98	81.1	57.6	191.8	136.2
Bb-3	30	Be	-1	4.5	2.06	109.7	76.5	205.7	143.4
Bb-4	30	Be	-1	5.1	1.22	119.6	108.4	224.2	203.2
Bb-11	27	Ax	0	7.3	1.36	138.0	118.6	258.8	222.3
Bb-12	29	Ax	0	7.0	1.62	104.6	82.0	235.7	184.9
Bb-13	15	Ax	0	6.7	1.91	112.5	81.4	250.1	180.9
Bb-14	28	Be	0	6.0	1.36	193.3	165.6	362.3	310.3
Bb-15	36	Be	0	4.6	1.72	133.8	102.1	301.6	230.0
Bb-16	27	Ax	-1	7.1	1.48	192.4	158.3	360.7	296.7
Bb-17	9	Ax	-1	8.9	1.23	188.6	169.8	353.5	318.3
Bb-18	34	Ax	-1	6.0	1.79	155.5	116.3	350.4	262.1
Bb-19	21	Ax	-1	5.1	2.56	153.9	96.3	342.2	214.1
Bb-20	30	Be	-1	5.8	1.56	238.7	190.9	447.4	357.9
Bb-21	9	Be	-1	6.8	1.28	203.4	179.5	381.3	336.5
Bb-22	30	Be	-1	5.3	1.51	197.1	160.5	444.2	361.8
Bb-27	27	Ax	0	7.6	1.39	147.9	125.3	349.4	296.2
Bb-28	18	Ax	0	7.6	1.26	160.3	142.7	356.4	317.3
Bb-29	26	Ax	-1	5.5	4.43	188.5	89.6	445.4	211.6
Bb-30	18	Ax	-1	6.6	1.35	225.6	194.1	501.7	431.5
Bb-31	11	Be	0.1	3.9	1.64	60.0	46.8	137.2	107.1
Bb-32	15	Be	0.5	3.3	1.64	55.4	43.3	126.7	99.1
Bb-33	11	Ax	0.1	4.2	1.46	65.2	53.9	155.4	128.6
Bb-34	13	Ax	0.1	4.0	1.38	60.4	51.4	144.1	122.7
Bb-35	7	Ax	0.1	4.6	3.78	74.0	38.1	176.6	90.9

⁽¹⁾Ax=axial cyclic loading; Be=cyclic bending; ⁽²⁾T_σ=ΔK_{I,90%}/ΔK_{I,10%} for the N-SIF approach.

Appendix A Fatigue results generated by testing aluminium alloys (Chapter 3)

Table A.9 Fatigue results generated by testing cruciform full-penetration welded joints (geometry Ca) and load carrying fillet cruciform welded joints (geometry Cb) statistically re-analysed in terms of hot-spot stresses and effective notch stress approaches.

Series	No of Data	Load Type ⁽¹⁾	R	K	T_{σ}	Hot-Spot Stress		Effective Notch Stress	
						$\Delta\sigma_{A,50\%}$	$\Delta\sigma_{A,97.7\%}$	$\Delta\sigma_{A,50\%}$	$\Delta\sigma_{A,97.7\%}$
						[MPa]	[MPa]	[MPa]	[MPa]
Ca-1	30	Be	0	4.0	1.67	86.7	67.1	172.3	133.5
Ca-2	30	Be	-1	3.7	1.52	100.5	81.5	199.9	162.1
Ca-3	9	Be	-1	4.0	1.59	109.6	86.9	221.3	175.4
Ca-4	10	Be	-1	2.7	2.28	107.5	71.3	213.7	141.7
Ca-9	30	Te	0	4.9	1.74	58.3	44.2	115.8	87.8
Ca-10	32	Be	0	5.3	2.01	141.8	100.0	281.9	198.9
Ca-11	31	Te	-1	4.6	2.07	87.8	61.0	174.5	121.2
Ca-12	13	Te	-1	4.6	7.61	70.9	25.7	141.1	51.1
Ca-13	12	Te	-1	3.5	4.03	108.7	54.2	219.3	109.3
Ca-14	12	Te	-1	3.9	4.57	55.5	25.9	110.3	51.6
Ca-15	27	Be	-1	5.1	1.39	170.7	144.7	339.3	287.7
Ca-16	9	Be	-1	6.3	1.75	173.2	130.8	349.5	263.9
Ca-17	9	Be	-1	7.2	1.55	175.4	140.9	348.7	280.1
Ca-18	9	Be	-1	6.6	1.49	187.2	153.6	372.2	305.4
Cb-10	31	Te	0	6.0	1.84	83.1	61.3	610.3	450.2
Cb-11	23	Te	0	6.0	1.49	58.7	48.1	171.3	140.2
Cb-12	25	Te	0	5.9	1.51	50.2	40.8	146.4	119.0
Cb-13	27	Te	-1	6.5	1.76	131.8	99.2	967.8	729.0
Cb-14	11	Te	-1	5.8	2.47	155.3	98.9	555.1	353.4
Cb-15	28	Te	-1	4.4	1.98	78.3	55.6	228.5	162.3
Cb-16	12	Te	0.08	5.8	1.40	57.5	48.6	234.5	198.2
Cb-17	14	Te	0.08	4.6	1.36	53.5	45.9	218.1	187.0
Cb-19	27	Te	0	3.5	1.86	76.0	55.7	556.3	407.4
Cb-20	27	Te	0	4.2	2.14	58.6	40.0	170.7	116.6
Cb-21	18	Te	0	4.1	2.32	50.9	33.5	148.3	97.5
Cb-22	27	Te	-1	3.5	3.43	108.2	58.4	315.0	170.0
Cb-23	12	Te	0.1	5.3	2.17	45.9	31.1	206.3	140.0
Cb-24	18	Te	0.1	4.4	1.47	49.2	40.6	239.0	197.0

⁽¹⁾Ax=axial cyclic loading; Be=cyclic bending; ⁽²⁾ $T_{\sigma}=\Delta K_{I,90\%}/\Delta K_{I,10\%}$ for the N-SIF approach.

Appendix A Fatigue results generated by testing aluminium alloys (Chapter 3)

Table A.10 Fatigue results generated by testing non-load carrying fillet cruciform welded joints (geometry Ba) and non-load carrying fillet welded T-joints (geometry Bb) statistically re-analysed in terms of N-SIFs and the TCD.

Series	No of Data	Load Type ⁽¹⁾	R	k	T _σ	N-SIF		TCD	
						ΔK _{I,50%}	ΔK _{I,97.7%}	Δσ _{A,50%}	Δσ _{A,97.7%}
						[MPa·mm ^{0.326}]	[MPa·mm ^{0.326}]	[MPa]	[MPa]
Ba-1	10	Be	-1	4.7	1.48	184.8	152.0	124.6	102.5
Ba-7	11	Ax	0	2.9	7.01	156.4	59.1	105.5	39.8
Ba-8	10	Be	0	5.8	1.45	219.7	182.2	148.1	122.9
Ba-9	15	Ax	-1	3.7	1.84	165.5	122.0	111.6	82.3
Ba-10	10	Be	-1	5.2	1.36	284.8	243.9	192.0	164.4
Ba-13	18	Ax	0	5.3	1.37	240.0	205.1	161.8	138.3
Ba-14	18	Ax	-1	5.0	1.36	342.0	293.6	230.6	197.9
Ba-15	6	Ax	0.1	4.3	2.19	124.7	84.2	84.4	57.0
Ba-16	6	Ax	0.1	4.2	2.18	110.2	74.7	75.1	49.1
Ba-17	4	Ax	0.1	3.8	2.27	127.5	84.7	86.0	57.1
Ba-18	8	Ax	0.1	3.7	1.54	126.7	101.9	85.6	68.9
Ba-19	7	Ax	0.1	3.8	1.48	127.4	104.9	85.9	70.7
Ba-20	9	Ax	0.1	3.7	1.56	96.7	77.3	63.5	50.8
Bb-1	30	Be	0	4.6	1.70	175.8	134.9	118.5	91.0
Bb-2	30	Be	0	4.1	1.98	198.3	140.8	128.4	91.2
Bb-3	30	Be	-1	4.5	2.06	210.7	146.9	142.1	99.1
Bb-4	30	Be	-1	5.1	1.22	287.9	260.9	194.1	175.9
Bb-11	27	Ax	0	7.3	1.36	259.9	223.3	178.7	153.5
Bb-12	29	Ax	0	7.0	1.62	243.5	191.1	164.3	128.9
Bb-13	15	Ax	0	6.7	1.91	263.1	190.3	172.2	124.6
Bb-14	28	Be	0	6.0	1.36	363.9	311.7	250.2	214.3
Bb-15	36	Be	0	4.6	1.72	311.6	237.7	210.2	160.3
Bb-16	27	Ax	-1	7.1	1.48	362.3	298.0	249.1	204.9
Bb-17	9	Ax	-1	8.9	1.23	355.1	319.8	244.2	219.9
Bb-18	34	Ax	-1	6.0	1.79	362.1	270.8	244.2	182.7
Bb-19	21	Ax	-1	5.1	2.56	360.0	225.2	235.6	147.4
Bb-20	30	Be	-1	5.8	1.56	449.4	359.5	309.0	247.2
Bb-21	9	Be	-1	6.8	1.28	383.0	338.0	263.4	232.4
Bb-22	30	Be	-1	5.3	1.51	459.0	373.9	309.6	252.2
Bb-27	27	Ax	0	7.6	1.39	361.3	306.3	243.6	206.5
Bb-28	18	Ax	0	7.6	1.26	364.0	324.0	245.4	218.5
Bb-29	26	Ax	-1	5.5	4.43	460.5	218.8	310.5	147.5
Bb-30	18	Ax	-1	6.6	1.35	512.3	440.7	345.4	297.1
Bb-31	11	Be	0.1	3.9	1.64	99.3	77.5	65.2	50.9
Bb-32	15	Be	0.5	3.3	1.64	91.7	71.7	60.2	47.1
Bb-33	11	Ax	0.1	4.2	1.46	147.9	122.4	79.9	66.1
Bb-34	13	Ax	0.1	4.0	1.38	137.2	116.8	74.0	63.0
Bb-35	7	Ax	0.1	4.6	3.78	170.2	87.6	90.7	46.7

⁽¹⁾Ax=axial cyclic loading; Be=cyclic bending; ⁽²⁾T_σ=ΔK_{I,90%}/ΔK_{I,10%} for the N-SIF approach.

Appendix A Fatigue results generated by testing aluminium alloys (Chapter 3)

Table A.11 Fatigue results generated by testing cruciform full-penetration welded joints (geometry Ca) and load carrying fillet cruciform welded joints (geometry Cb) statistically re-analysed in terms of N-SIFs and the TCD.

Series	No of Data	Load Type ⁽¹⁾	R	K	T _σ ⁽²⁾	N-SIF		TCD	
						$\Delta K_{I,50\%}$ [MPa·mm ^{0.326}]	$\Delta K_{I,50\%}$ [MPa·mm ^{0.326}]	$\Delta\sigma_{A,50\%}$ [MPa]	$\Delta\sigma_{A,97.7\%}$ [MPa]
Ca-1	30	Be	0	4.0	1.67	175.7	136.1	118.5	91.8
Ca-2	30	Be	-1	3.7	1.52	203.8	165.3	137.4	111.5
Ca-3	9	Be	-1	4.0	1.59	226.2	179.2	152.7	121.0
Ca-4	10	Be	-1	2.7	2.28	218.0	144.5	147.0	97.4
Ca-9	30	Te	0	4.9	1.74	118.2	89.6	79.7	60.4
Ca-10	32	Be	0	5.3	2.01	287.5	202.8	193.9	136.8
Ca-11	31	Te	-1	4.6	2.07	178.0	123.6	120.0	83.3
Ca-12	13	Te	-1	4.6	7.61	143.9	52.2	97.0	35.2
Ca-13	12	Te	-1	3.5	4.03	224.1	111.7	151.3	75.4
Ca-14	12	Te	-1	3.9	4.57	112.5	52.6	75.8	35.5
Ca-15	27	Be	-1	5.1	1.39	346.1	293.4	233.3	197.8
Ca-16	9	Be	-1	6.3	1.75	588.7	444.4	241.1	182.0
Ca-17	9	Be	-1	7.2	1.55	355.6	285.7	239.8	192.6
Ca-18	9	Be	-1	6.6	1.49	379.6	311.5	256.0	210.0
Cb-10	31	Te	0	6.0	1.84	159.7	117.8	107.6	79.4
Cb-11	23	Te	0	6.0	1.49	144.9	118.6	97.7	79.9
Cb-12	25	Te	0	5.9	1.51	123.8	100.6	83.5	67.8
Cb-13	27	Te	-1	6.5	1.76	253.2	190.7	170.7	128.6
Cb-14	11	Te	-1	5.8	2.47	279.5	177.9	188.4	119.9
Cb-15	28	Te	-1	4.4	1.98	193.2	137.3	130.3	92.5
Cb-16	12	Te	0.08	5.8	1.40	185.9	157.1	125.3	105.9
Cb-17	14	Te	0.08	4.6	1.36	172.9	148.2	116.6	99.9
Cb-19	27	Te	0	3.5	1.86	146.1	107.0	98.5	72.1
Cb-20	27	Te	0	4.2	2.14	144.3	98.6	97.3	66.5
Cb-21	18	Te	0	4.1	2.32	125.4	82.4	84.6	55.6
Cb-22	27	Te	-1	3.5	3.43	266.4	143.8	179.6	96.9
Cb-23	12	Te	0.1	5.3	2.17	136.7	92.8	92.2	62.6
Cb-24	18	Te	0.1	4.4	1.47	156.9	129.3	105.8	87.2

⁽¹⁾Ax=axial cyclic loading; Be=cyclic bending; ⁽²⁾T_σ=ΔK_{I,90%}/ΔK_{I,10%} for the N-SIF approach.

B Appendix Fatigue results generated by testing steel inclined welded joints (chapter 4)

Table B.1 Experimental data and stress components relative to the critical plane calculated in terms of nominal stresses and hot-spot stresses (Geometry BM).

Code	θ	$\Delta\sigma_{nom}$	$N_f (\cdot 10^3)$ [Cycles to Failure]	Nominal Stress			Hot-spot stress			Run-out
				$\Delta\tau$ [MPa]	$\Delta\sigma_n$ [MPa]	ρ_w	$\Delta\tau$ [MPa]	$\Delta\sigma_n$ [MPa]	ρ_w	
BM0-01	0	240	134	119.6	119.6		129.0	126.8		
BM0-02	0	200	240	99.8	99.8		107.6	105.8		
BM0-03	0	160	281	79.6	79.6		85.8	84.4		
BM0-04	0	140	787	69.9	69.9	1.000	75.4	74.2		
BM0-05	0	120	1667	59.8	59.8		64.6	63.4		
BM0-06	0	100	2728	49.9	49.9		53.8	53.0		
BM31-01	31	260	181	149.1	95.4		216.4	173.2		
BM31-02	31	200	554	114.6	73.3		166.4	133.2		
BM31-03	31	160	950	91.7	58.6	0.640	133.0	106.4		
BM31-04	31	120	1848	68.9	44.0		100.0	80.0		
BM31-05	31	110	2872	63.3	40.5		91.8	73.6		
BM31-06	31	90	6170	51.2	32.7		74.2	59.4		✓
BM43-01	43	260	268	147.4	69.6		244.2	155.4		
BM43-02	43	200	684	113.6	53.7		188.2	119.8		
BM43-03	43	160	1306	90.6	42.8	0.473	150.0	95.4		
BM43-04	43	130	2040	73.5	34.7		121.6	77.4		
BM43-05	43	115	3806	65.2	30.8		108.0	68.8		
BM43-06	43	100	5887	56.9	26.9		94.4	60.0		✓

Table B.2 Experimental data and stress components relative to the critical plane calculated in terms of nominal stresses and hot-spot stresses (Geometry KK).

Code	θ	$\Delta\sigma_{nom}$	$N_f (\cdot 10^3)$ [Cycles to Failure]	Nominal Stress			Hot-spot stress			Run-out
				$\Delta\tau$ [MPa]	$\Delta\sigma_n$ [MPa]	ρ_w	$\Delta\tau$ [MPa]	$\Delta\sigma_n$ [MPa]	ρ_w	
KK-0-01	0	111	158	55.4	55.4		-	-	-	
KK-0-02	0	77	466	38.6	38.6		-	-	-	
KK-0-03	0	56	1740	28.2	28.2		-	-	-	
KK-0-04	0	55	2250	27.7	27.7	1.000	-	-	-	
KK-0-05	0	36	3100	18.2	18.2		-	-	-	
KK-0-06	0	26	19200	13.1	13.1		-	-	-	
KK-15-01	15	103	270	58.2	51.3		-	-	-	
KK-15-02	15	72	756	41.1	36.2		-	-	-	
KK-15-03	15	54	2060	30.7	27.1	0.881	-	-	-	
KK-15-04	15	33	10900	18.7	16.5		-	-	-	
KK-15-05	15	29	15700	16.3	14.4		-	-	-	
KK-30-01	30	83	664	63.0	41.3		-	-	-	
KK-30-02	30	55	1980	41.9	27.4		-	-	-	
KK-30-03	30	42	6010	32.3	21.1	0.655	-	-	-	
KK-30-04	30	30	19000	23.2	15.2		-	-	-	
KK-45-01	45	60	2160	66.5	29.8		-	-	-	
KK-45-02	45	54	2360	60.4	27.0		-	-	-	
KK-45-03	45	48	3030	53.3	23.9	0.447	-	-	-	
KK-45-04	45	28	18200	30.6	13.7		-	-	-	

Appendix Fatigue results generated by testing steel inclined welded joints (chapter 4)

Table B.3 Experimental data and stress components relative to the critical plane calculated in terms of nominal stresses and hot-spot stresses (Geometry KN-G).

Code	θ	$\Delta\sigma_{nom}$	$N_f (\cdot 10^3)$ [Cycles to Failure]	Nominal Stress			Hot-spot stress			Run-out
				$\Delta\tau$ [MPa]	$\Delta\sigma_n$ [MPa]	ρ_w	$\Delta\tau$ [MPa]	$\Delta\sigma_n$ [MPa]	ρ_w	
KY-G-0-01	0	190	216	95.0	95.0	1.000	102.3	101.9	0.996	
KY-G-0-02	0	190	237	95.0	95.0		102.3	101.9		
KY-G-0-03	0	120	1564	60.0	60.0		64.6	64.3		
KY-G-0-04	0	98	3428	49.0	49.0		52.8	52.6		
KY-G-45-01	45	190	394	106.2	47.5	0.447	135.1	62.7	0.464	
KY-G-45-02	45	190	702	106.2	47.5		135.1	62.7		
KY-G-45-03	45	152	623	85.0	38.0		108.1	50.2		
KY-G-45-04	45	152	1200	85.0	38.0		108.1	50.2		
KY-G-45-05	45	190	1447	106.2	47.5		135.1	62.7		
KY-G-45-06	45	204	735	114.0	51.0		145.0	67.3		
KY-G-45-07	45	190	1278	106.2	47.5		135.1	62.7		
KY-G-45-08	45	190	982	106.2	47.5		135.1	62.7		
KY-G-45-09	45	152	2270	85.0	38.0		108.1	50.2		✓

Table B.4 Experimental data and stress components relative to the critical plane calculated in terms of nominal stresses and hot-spot stresses (Geometry KY-N).

Code	θ	$\Delta\sigma_{nom}$	$N_f (\cdot 10^3)$ [Cycles to Failure]	Nominal Stress			Hot-spot stress			Run-out
				$\Delta\tau$ [MPa]	$\Delta\sigma_n$ [MPa]	ρ_w	$\Delta\tau$ [MPa]	$\Delta\sigma_n$ [MPa]	ρ_w	
KY-N-0-01	0	206	198	103.0	103.0	1.000	120.2	120.2	1.000	
KY-N-0-02	0	203	170	101.5	101.5		118.5	118.5		
KY-N-0-03	0	160	470	80.0	80.0		93.4	93.4		
KY-N-0-04	0	160	556	80.0	80.0		93.4	93.4		
KY-N-0-05	0	136	1415	68.0	68.0		79.4	79.4		
KY-N-0-06	0	136	630	68.0	68.0		79.4	79.4		
KY-N-0-07	0	136	990	68.0	68.0		79.4	79.4		
KY-N-0-08	0	113	2788	56.5	56.5		66.0	66.0		
KY-N-0-09	0	113	6764	56.5	56.5		66.0	66.0		✓
KY-N-15-01	15	206	360	109.0	96.1	0.881	127.1	105.3	0.828	
KY-N-15-02	15	203	324	107.4	94.7		125.3	103.7		
KY-N-15-03	15	161	479	85.2	75.1		99.3	82.3		
KY-N-15-04	15	160	867	84.7	74.6		98.7	81.8		
KY-N-15-05	15	160	760	84.7	74.6		98.7	81.8		
KY-N-15-06	15	136	1577	72.0	63.4		83.9	69.5		
KY-N-15-07	15	136	1739	72.0	63.4		83.9	69.5		
KY-N-15-08	15	136	984	72.0	63.4		83.9	69.5		
KY-N-15-09	15	123	2366	65.1	57.4		75.9	62.8		
KY-N-15-10	15	123	4860	65.1	57.4		75.9	62.8		✓
KY-N-30-01	30	206	502	118.0	77.3	0.655	116.4	76.2	0.655	
KY-N-30-02	30	203	389	116.3	76.1		118.2	77.4		
KY-N-30-03	30	174	1264	99.7	65.3		108.8	71.2		
KY-N-30-04	30	159	2053	91.1	59.6		99.4	65.2		
KY-N-30-05	30	159	1620	91.1	59.6		91.2	59.8		
KY-N-30-06	30	138	6449	79.0	51.8		91.2	59.8		
KY-N-30-07	30	138	10000	79.0	51.8		79.0	51.8		✓
KY-N-30-08	30	123	10000	70.5	46.1		79.0	51.8		✓

Appendix Fatigue results generated by testing steel inclined welded joints
(chapter 4)

Table B.5 Experimental data and stress components relative to the critical plane calculated in terms of notch stresses and Point Method (Geometry BM).

Code	θ	$\Delta\sigma_{nom}$	$N_f (\cdot 10^3)$ [Cycles to Failure]	Effective notch stress			Point Method			Run-out
				$\Delta\tau$	$\Delta\sigma_n$	ρ_w	$\Delta\tau$	$\Delta\sigma_n$	ρ_w	
				[MPa]	[MPa]		[MPa]	[MPa]		
BM0-01	0	240	134	410.0	409.6		204.4	235.8		
BM0-02	0	200	240	342.2	341.8		170.5	196.7		
BM0-03	0	160	281	273.0	272.6		136.0	156.9		
BM0-04	0	140	787	239.6	239.4	0.999	119.4	137.7	1.154	
BM0-05	0	120	1667	205.0	204.8		102.2	117.9		
BM0-06	0	100	2728	171.0	170.8		85.2	98.3		
BM31-01	31	260	181	523.6	482.2		233.8	238.8		
BM31-02	31	200	554	402.6	370.6		179.8	183.6		
BM31-03	31	160	950	321.8	296.4		143.8	146.8		
BM31-04	31	120	1848	242.0	222.8	0.921	108.0	110.4	1.021	
BM31-05	31	110	2872	222.2	204.6		99.2	101.4		
BM31-06	31	90	6170	179.4	165.2		80.2	81.8	✓	
BM43-01	43	260	268	663.0	604.2		257.2	258.6		
BM43-02	43	200	684	511.2	466.0		198.2	199.4		
BM43-03	43	160	1306	407.5	371.4		158.0	158.8		
BM43-04	43	130	2040	330.4	301.2	0.912	128.2	129.0	1.006	
BM43-05	43	115	3806	293.2	267.4		113.8	114.4		
BM43-06	43	100	5887	256.2	233.4		99.4	100.0	✓	

Table B.6 Experimental data and stress components relative to the critical plane calculated in terms of notch stresses and Point Method (Geometry KK).

Code	θ	$\Delta\sigma_{nom}$	$N_f (\cdot 10^3)$ [Cycles to Failure]	Effective notch stress			Point Method			Run-out
				$\Delta\tau$	$\Delta\sigma_n$	ρ_w	$\Delta\tau$	$\Delta\sigma_n$	ρ_w	
				[MPa]	[MPa]		[MPa]	[MPa]		
KK-0-01	0	111	158	302.0	654.2		84.0	176.7		
KK-0-02	0	77	466	209.5	453.8		58.5	123.1		
KK-0-03	0	56	1740	152.4	330.1		42.8	90.0		
KK-0-04	0	55	2250	149.6	324.2	2.166	42.1	88.4	2.103	
KK-0-05	0	36	3100	98.0	212.2		27.6	58.0		
KK-0-06	0	26	19200	70.7	153.2		19.9	41.9		
KK-15-01	15	103	270	305.4	316.3		107.3	142.6		
KK-15-02	15	72	756	213.5	221.1		75.7	100.5		
KK-15-03	15	54	2060	160.1	165.8		56.6	75.2		
KK-15-04	15	33	10900	97.9	101.3	1.036	34.4	45.8	1.328	
KK-15-05	15	29	15700	86.0	89.1		30.1	39.9		
KK-30-01	30	83	664	212.5	219.7		96.6	99.9		
KK-30-02	30	55	1980	140.8	145.6		64.2	66.4		
KK-30-03	30	42	6010	107.5	111.2	1.034	49.5	51.2	1.034	
KK-30-04	30	30	19000	76.8	79.4		35.6	36.8		
KK-45-01	45	60	2160	121.6	128.9		105.4	105.8		
KK-45-02	45	54	2360	109.5	116.0		95.7	96.0		
KK-45-03	45	48	3030	97.3	103.1	1.060	84.5	84.8	1.004	
KK-45-04	45	28	18200	56.8	60.1		48.4	48.6		

Appendix Fatigue results generated by testing steel inclined welded joints (chapter 4)

Table B.7 Experimental data and stress components relative to the critical plane calculated in terms of notch stresses and Point Method (Geometry KN-G).

Code	θ	$\Delta\sigma_{nom}$	$N_f (\cdot 10^3)$ [Cycles to Failure]	Effective notch Stress			Point Method			Run-out
				$\Delta\tau$	$\Delta\sigma_n$	ρ_w	$\Delta\tau$	$\Delta\sigma_n$	ρ_w	
				[MPa]	[MPa]		[MPa]	[MPa]		
KY-G-0-01	0	190	216	258.7	256.7	0.992	221.8	305.3	1.376	
KY-G-0-02	0	190	237	258.7	256.7		221.8	305.3		
KY-G-0-03	0	120	1564	163.4	162.1		140.1	192.8		
KY-G-0-04	0	98	3428	133.4	132.4		114.4	157.5		
KY-G-45-01	45	190	394	253.1	254.0	1.004	296.5	387.1	1.305	
KY-G-45-02	45	190	702	253.1	254.0		296.5	387.1		
KY-G-45-03	45	152	623	202.5	203.2		237.2	309.6		
KY-G-45-04	45	152	1200	202.5	203.2		237.2	309.6		
KY-G-45-05	45	190	1447	253.1	254.0		296.5	387.1		
KY-G-45-06	45	204	735	271.7	272.7		318.4	415.6		
KY-G-45-07	45	190	1278	253.1	254.0		296.5	387.1		
KY-G-45-08	45	190	982	253.1	254.0		296.5	387.1		
KY-G-45-09	45	152	2270	253.1	254.0		237.2	309.6		✓

Table B.8 Experimental data and stress components relative to the critical plane calculated in terms of notch stresses and Point Method (Geometry KY-N).

Code	θ	$\Delta\sigma_{nom}$	$N_f (\cdot 10^3)$ [Cycles to Failure]	Effective notch Stress			Point Method			Run-out
				$\Delta\tau$	$\Delta\sigma_n$	ρ_w	$\Delta\tau$	$\Delta\sigma_n$	ρ_w	
				[MPa]	[MPa]		[MPa]	[MPa]		
KY-N-0-01	0	206	198	265.4	325.4	1.226	227.1	310.1	1.366	
KY-N-0-02	0	203	170	269.5	330.5		223.8	305.6		
KY-N-0-03	0	160	470	248.0	304.1		176.4	240.9		
KY-N-0-04	0	160	556	248.0	304.1		176.4	240.9		
KY-N-0-05	0	136	1415	208.7	255.9		149.9	204.7		
KY-N-0-06	0	136	630	209.4	256.7		149.9	204.7		
KY-N-0-07	0	136	990	177.3	217.4		149.9	204.7		
KY-N-0-08	0	113	2788	177.9	218.1		124.6	170.1		
KY-N-0-09	0	113	6764	157.3	192.8		124.6	170.1		✓
KY-N-15-01	15	206	360	244.6	245.0	1.002	249.8	299.2	1.199	
KY-N-15-02	15	203	324	248.4	248.8		246.1	294.8		
KY-N-15-03	15	161	479	228.6	229.0		195.2	233.8		
KY-N-15-04	15	160	867	228.6	229.0		194.0	232.4		
KY-N-15-05	15	160	760	192.4	192.7		194.0	232.4		
KY-N-15-06	15	136	1577	193.0	193.3		164.9	197.5		
KY-N-15-07	15	136	1739	163.4	163.7		164.9	197.5		
KY-N-15-08	15	136	984	163.9	164.2		164.9	197.5		
KY-N-15-09	15	123	2366	144.9	145.2		149.1	178.6		
KY-N-15-10	15	123	4860	136.3	136.5		149.1	178.6		✓
KY-N-30-01	30	206	502	274.4	273.0	0.995	262.7	252.6	0.965	
KY-N-30-02	30	203	389	278.7	277.2		258.9	248.9		
KY-N-30-03	30	174	1264	256.4	255.1		221.9	213.4		
KY-N-30-04	30	159	2053	256.4	255.1		202.8	195.0		
KY-N-30-05	30	159	1620	215.8	214.7		202.8	195.0		
KY-N-30-06	30	138	6449	216.5	215.4		176.0	169.2		
KY-N-30-07	30	138	10000	183.3	182.4		176.0	169.2		✓
KY-N-30-08	30	123	10000	183.9	183.0		156.9	150.8		✓

C Appendix C Static data of aluminium-to-steel welded joints (chapter 6)

Static experimental data of the hybrid joints (Long-term).

Table C.1 Ultimate tensile strength of single and double sided butt-welded joints (long term).

Code	Angle	Width (mm)	Thickness (mm)	Max tensile load (kN)	UTS (MPa)	Failure mode	Long term Specimens	
butt-single-1	0	50.76	1.14	3.99	69.10	WS		
butt-single-2	0	60.00	1.13	4.44	65.54	WS		
butt-single-3	0	50.60	1.14	4.87	84.63	AH		
butt-single-4	0	50.65	0.98	4.37	88.38	WS		
butt-single-5	0	51.11	1.14	4.95	84.76	AH		
butt-single-6	0	50.71	1.14	4.95	85.43	WS		
butt-single-7	0	50.96	1.14	3.44	59.45	WS		
butt-single-8	0	50.25	1.14	4.73	82.61	AH/WS		
butt-single-9	0	50.45	1.14	4.90	85.42	AH		
butt-single-10	0	50.49	1.13	3.99	69.67	WS		
					-2 SD	71.82		
					Average	77.50		
					+2 SD	83.17		
butt-double-1	0	53.15	1.15	5.23	85.78	AH		
butt-double-2	0	50.34	1.15	4.77	82.16	AH		
butt-double-3	0	50.68	1.13	4.84	84.30	AH		
butt-double-4	0	50.47	1.14	4.95	85.82	AH		
butt-double-5	0	49.98	1.15	4.81	83.73	AH		
butt-double-6	0	49.12	1.15	4.76	84.29	AH		
butt-double-7	0	49.10	1.14	4.80	85.82	AH		
butt-double-8	0	50.63	1.15	4.84	83.33	AH		
butt-double-9	0	53.15	1.15	4.90	84.57	AH		
					-2 SD	83.71		
					Average	84.42		
					+2 SD	85.13		

* WS=weld seam; AH= Aluminium HAZ

Table C.2 Ultimate tensile strength of single-sided butt-welded joints with various inclination angles (long term)

Code	Angle	Width (mm)	Thickness (mm)	Max tensile load (kN)	UTS (MPa)	Failure mode
butt-single-1	15	50.33	1.14	5.05	87.76	AH
butt-single-2	15	50.31	1.15	3.58	62.06	WS
butt-single-3	15	50.49	1.15	3.77	65.05	WS
butt-single-4	15	48.15	1.15	4.76	86.16	AH
butt-single-5	15	50.21	1.15	3.71	64.25	WS
butt-single-6	15	50.26	1.15	4.70	81.28	AH/WS
butt-single-7	15	50.38	1.15	4.54	78.58	WS
butt-single-8	15	50.04	1.14	4.94	86.34	AH
butt-single-9	15	50.57	1.14	4.16	71.95	AH/WS
butt-single-10	15	50.12	1.15	4.99	86.57	AH
butt-single-11	15	50.26	1.14	5.00	87.01	AH
				-2 SD	72.52	
				Average	77.91	
				+2 SD	83.30	
butt-single-1	30	50.65	1.12	5.33	93.68	AH
butt-single-2	30	50.29	1.14	5.23	90.91	AH
butt-single-3	30	50.26	1.14	5.25	91.41	AH
butt-single-4	30	50.09	1.15	5.17	89.72	AH
butt-single-5	30	50.33	1.14	5.11	88.80	AH/WS
butt-single-6	30	50.76	1.15	4.88	83.84	AH/WS
butt-single-7	30	50.65	1.15	4.99	85.93	AH/WS
butt-single-8	30	50.13	1.15	4.85	84.45	AH
butt-single-9	30	50.47	1.15	5.24	90.35	AH/WS
butt-single-10	30	49.44	1.15	5.33	93.75	WS
butt-single-11	30	50.41	1.15	5.26	90.95	AH
				-2 SD	87.65	
				Average	89.44	
				+2 SD	91.22	
butt-single-1	45	50.66	0.98	4.97	99.75	AH
butt-single-2	45	50.76	0.99	5.27	104.53	AH
butt-single-3	45	50.93	0.99	5.37	106.46	AH
butt-single-4	45	50.92	0.99	5.25	104.14	AH
butt-single-5	45	50.25	0.99	5.16	104.08	AH
butt-single-6	45	50.83	0.99	5.14	101.78	AH
butt-single-7	45	50.89	1.00	4.95	97.30	AH
butt-single-8	45	50.10	1.00	5.52	110.56	AH
butt-single-9	45	50.59	0.99	5.11	101.67	AH
butt-single-10	45	50.69	0.98	5.08	101.83	AH
				-2 SD	101.21	
				Average	103.21	
				+2 SD	105.21	
butt-single-1	60	50.65	1.00	5.59	110.80	AH
butt-single-2	60	50.26	1.00	5.81	115.18	AH
butt-single-3	60	50.59	1.00	5.35	106.21	AH
butt-single-4	60	50.59	1.00	5.59	110.45	AH

Long term Specimens

Appendix C Static data of aluminium-to-steel welded joints (chapter 6)

butt-single-5	60	50.53	1.00	4.97	98.67	AH
butt-single-6	60	50.08	1.00	5.23	104.39	AH
butt-single-7	60	50.57	1.00	5.51	109.37	AH
butt-single-8	60	50.24	1.00	5.69	112.80	AH
butt-single-9	60	50.77	0.99	5.69	113.21	AH
				-2 SD	106.10	
				Average	109.01	
				+2 SD	111.92	

* W=weld seam; AH= Aluminium HAZ

Table C.3 Ultimate tensile strength of lap welded joints (long term).

Code	Angle	Width (mm)	Thickness (mm)	Max tensile load (kN)	UTS (MPa)	Failure mode	Long term Specimens
Lap-1	0	49.83	1.00	4.48	89.57	AH	
Lap-2	0	49.24	1.01	4.45	89.88	AH	
Lap-3	0	49.20	1.00	4.45	90.40	AH	
Lap-4	0	49.38	0.99	4.49	91.69	AH	
Lap-5	0	49.42	1.00	4.42	89.63	AH	
Lap-6	0	49.46	1.00	4.51	91.18	AH	
Lap-7	0	49.24	1.00	4.48	91.19	AH	
Lap-8	0	49.42	1.00	4.48	91.11	AH	
Lap-9	0	49.37	1.00	4.39	88.67	AH	
Lap-10	0	49.98	1.00	4.48	89.63	AH	
Lap-11	0	50.17	0.99	4.51	90.66	AH	
				-2 SD	89.84		
				Average	90.33		
				+2 SD	90.82		

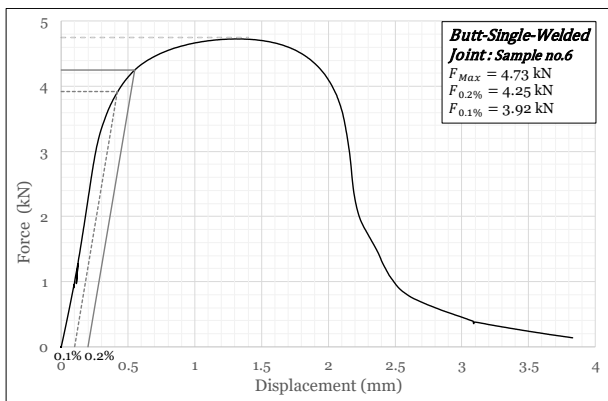
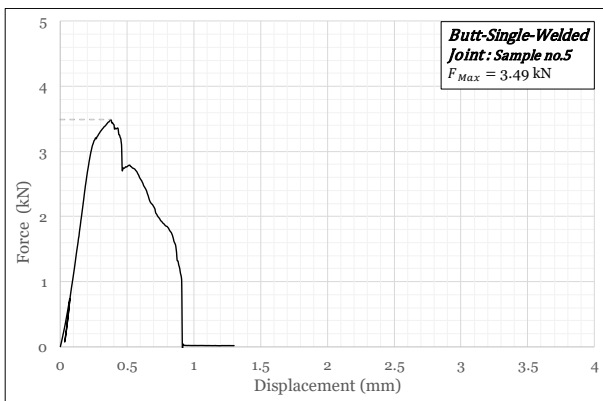
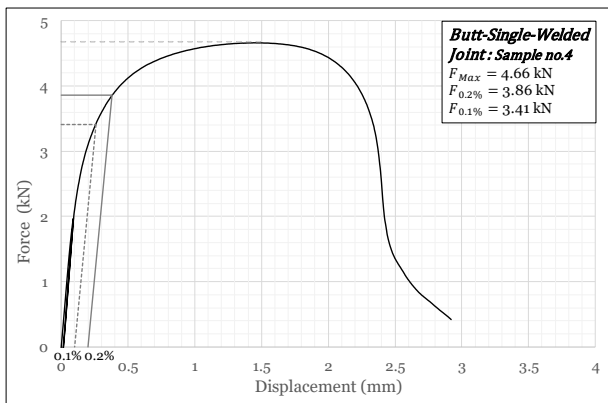
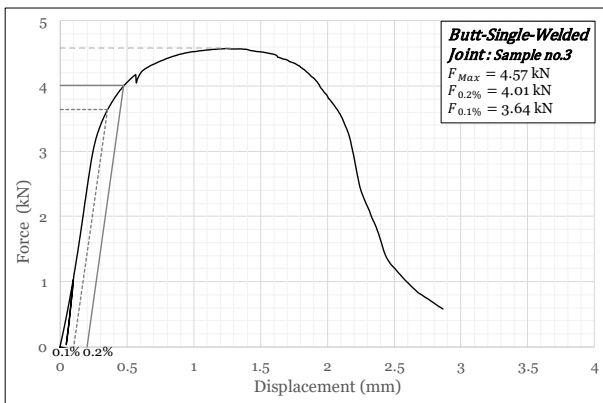
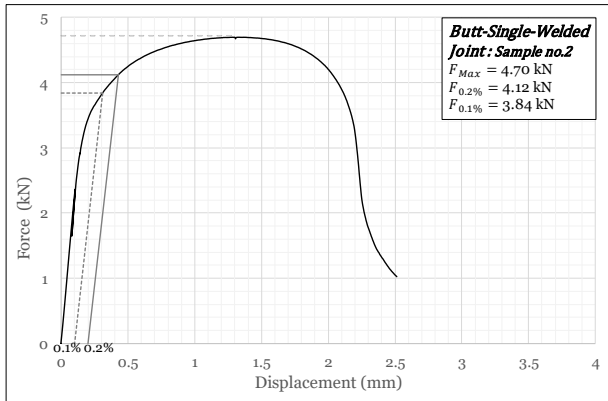
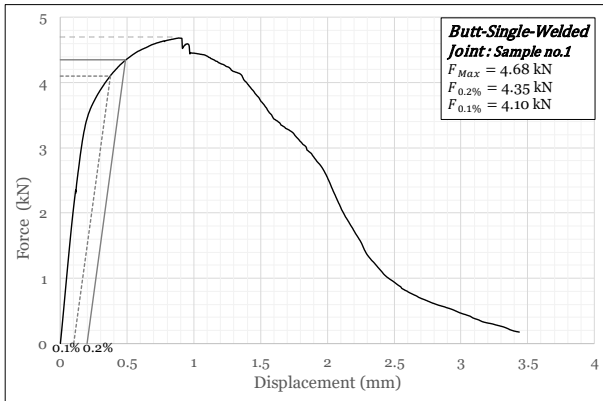
* WS=weld seam; AH= Aluminium HAZ

Table C.4 Ultimate tensile strength of cruciform welded joints (long term).

Code	Angle	Width (mm)	Thickness (mm)	Max tensile load (kN)	UTS (MPa)	Failure mode	Long term Specimens
Cr-1	0	50.06	1.00	4.80	96.30	AH	
Cr-2	0	50.55	1.00	4.62	91.66	AH	
Cr-3	0	50.11	1.00	4.60	91.72	AH	
Cr-4	0	50.31	1.00	4.67	92.80	AH	
Cr-5	0	50.75	0.99	4.66	92.98	AH	
Cr-6	0	49.91	1.01	4.65	92.59	AH	
Cr-7	0	50.90	1.00	4.57	90.01	AH	
Cr-8	0	50.00	1.00	4.56	91.56	AH	
Cr-9	0	49.96	1.00	4.66	93.37	AH	
Cr-10	0	50.60	1.00	4.64	92.06	AH	
				-2 SD	91.61		
				Average	92.51		
				+2 SD	93.40		

* WS=weld seam; AH= Aluminium HAZ

Force vs. displacement curves of the hybrid joints.



Appendix C Static data of aluminium-to-steel welded joints (chapter 6)

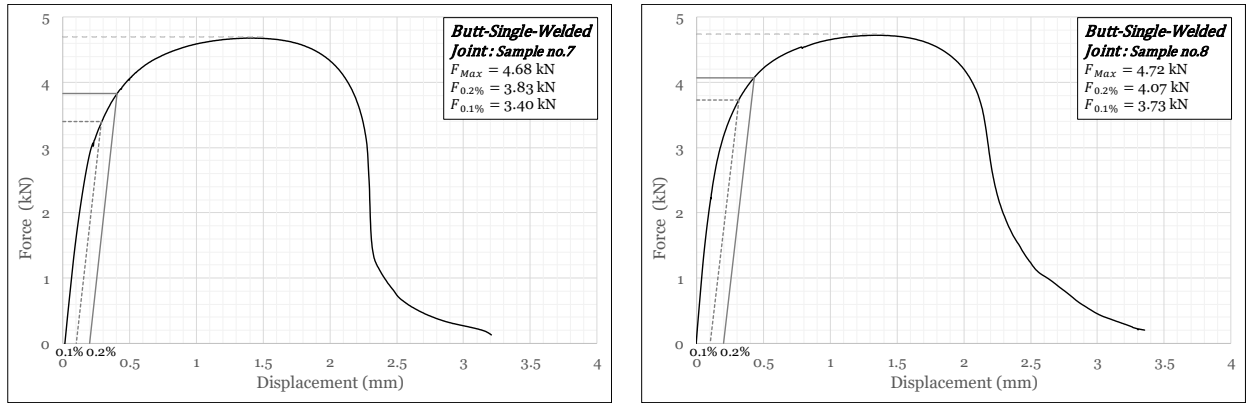


Figure C.1 Force vs. displacement curve for single sided Butt-welded joints (short term).

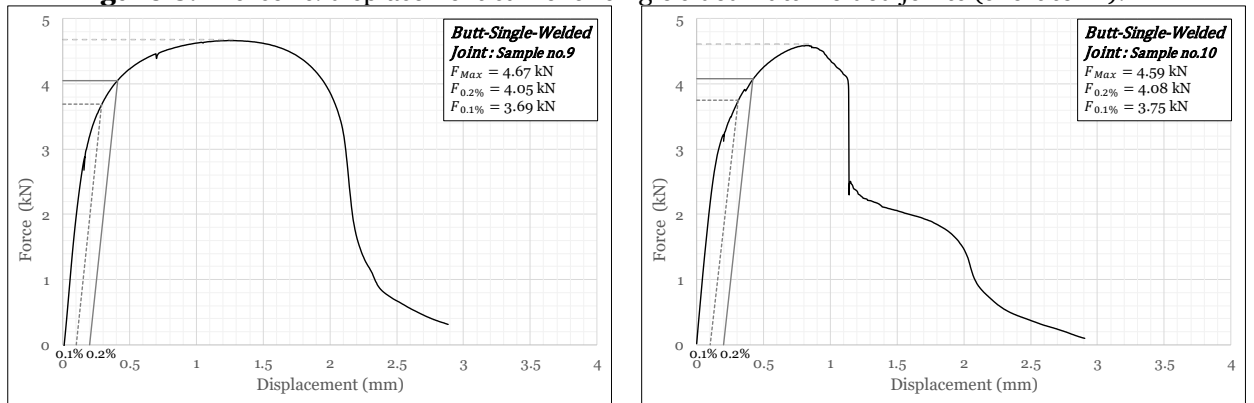
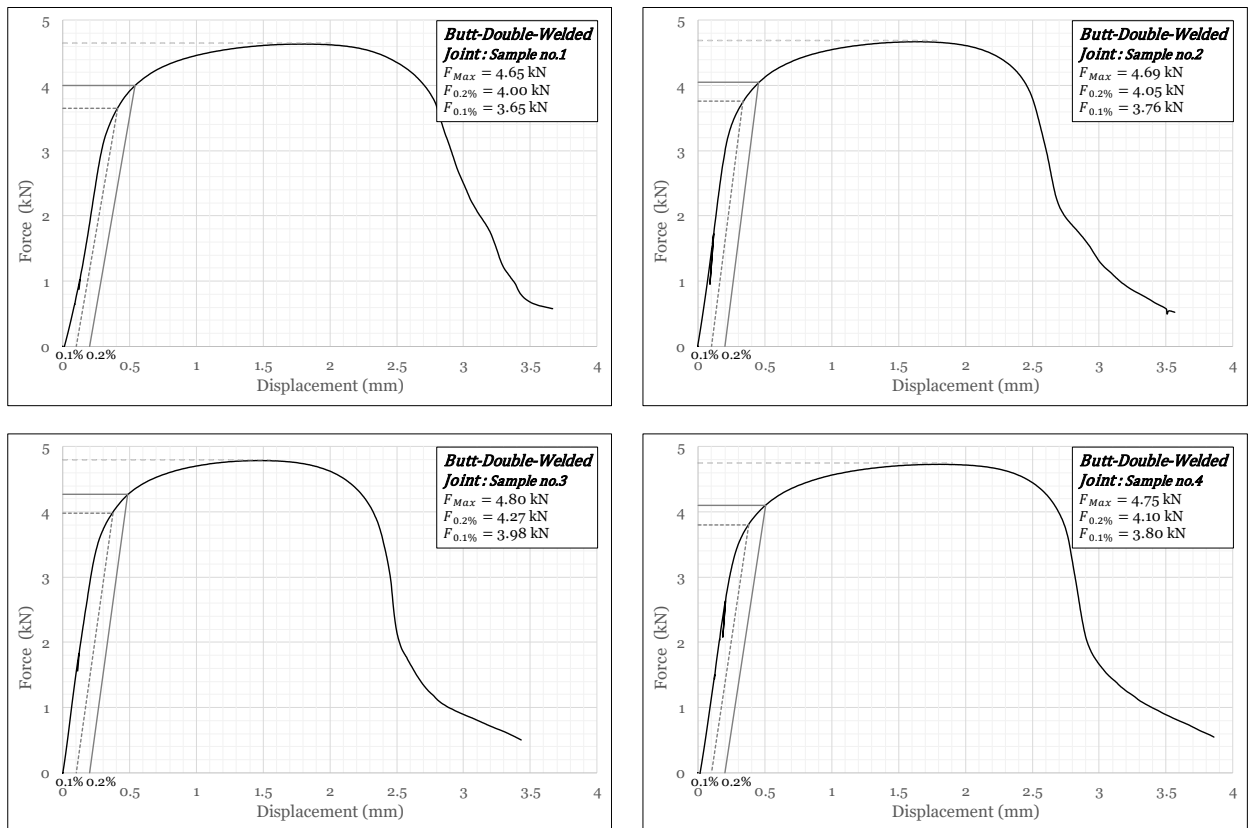


Figure C.1 Force vs. displacement curve for single sided Butt-welded joints (short term) (continue).



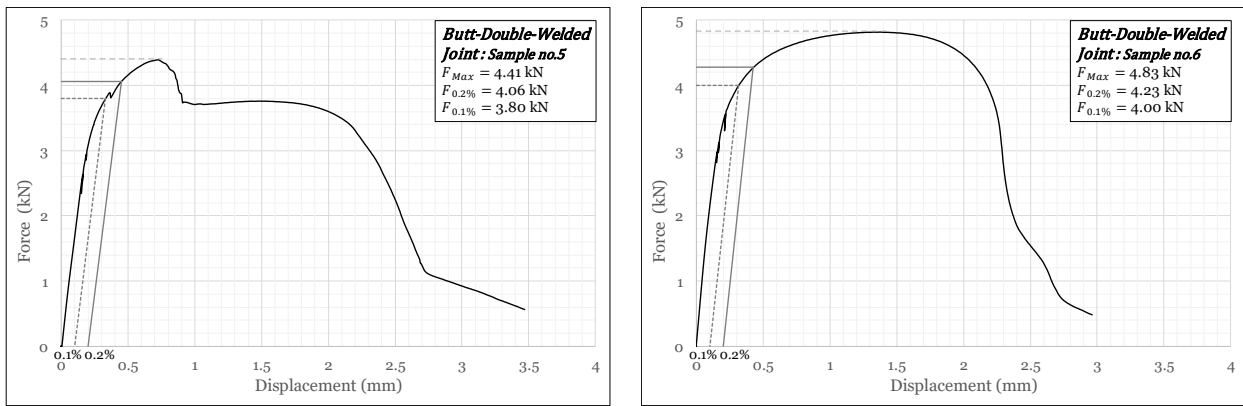


Figure C.2 Force vs. displacement curve for double sided Buttt-welded joints (short term).

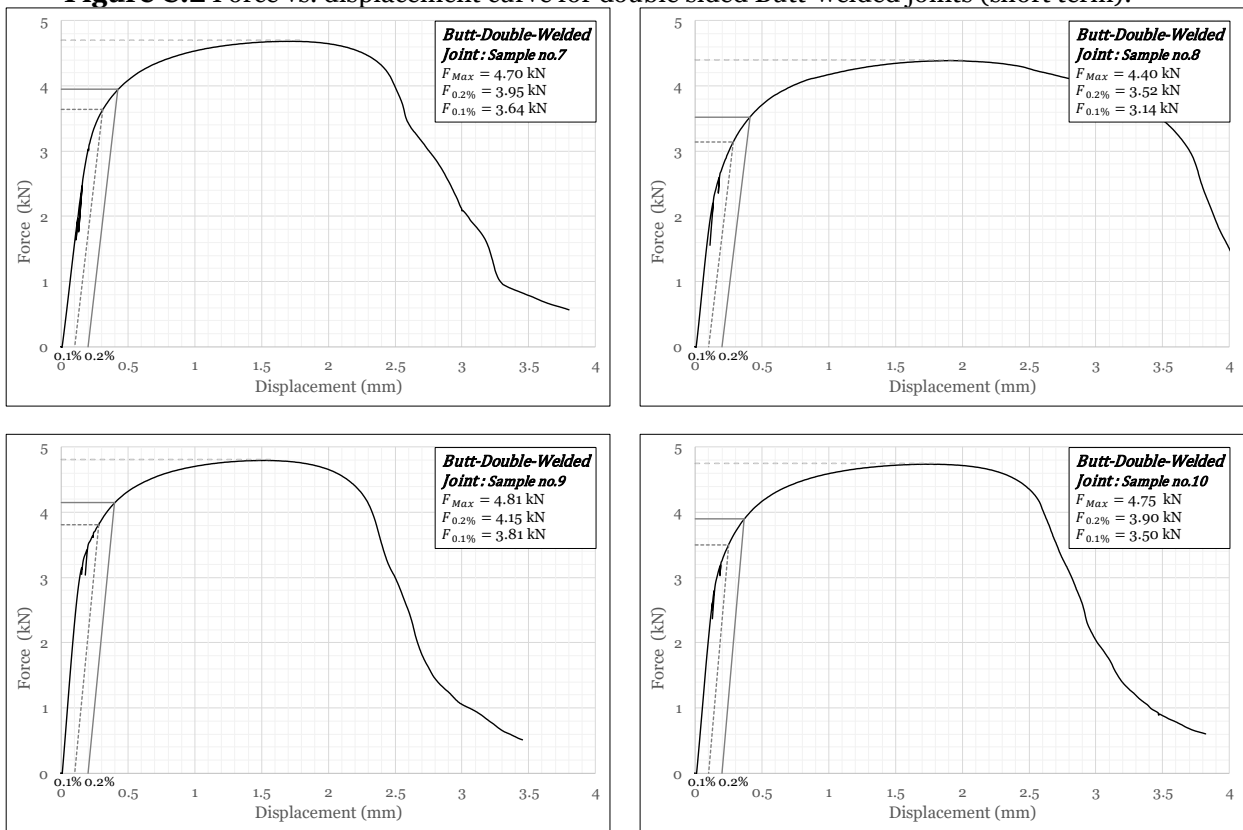
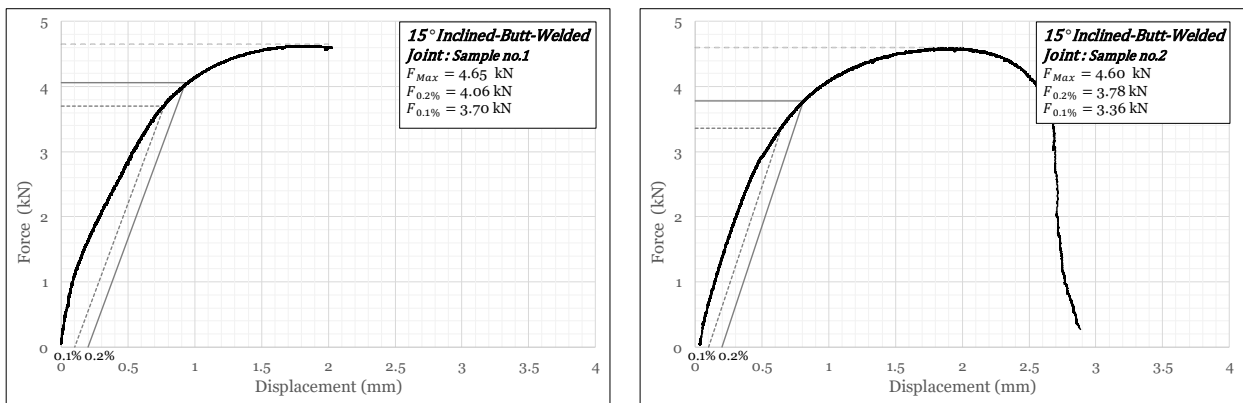


Figure C.2 Force vs. displacement curve for double sided Buttt-welded joints (short term) (continue).



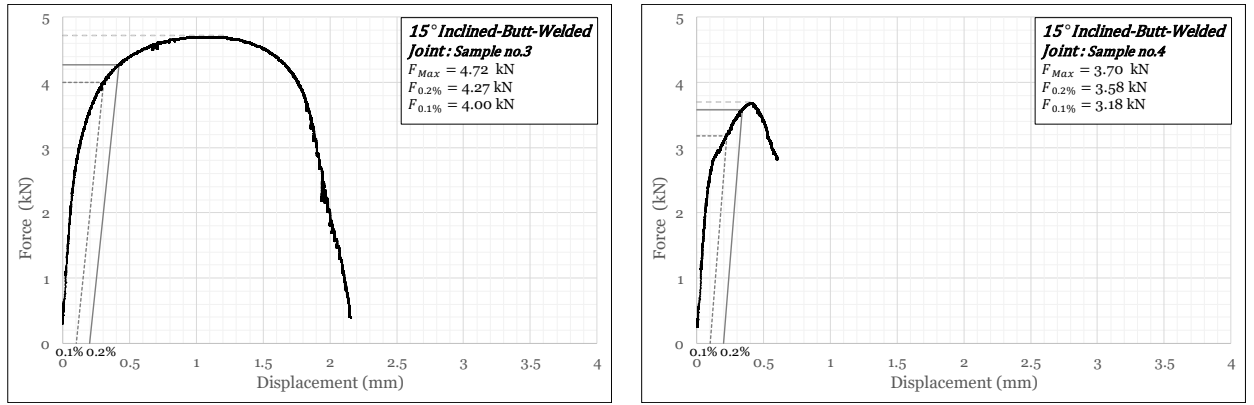


Figure C.3 Force vs. displacement curve for 15° inclined butt-welded joints (short term).

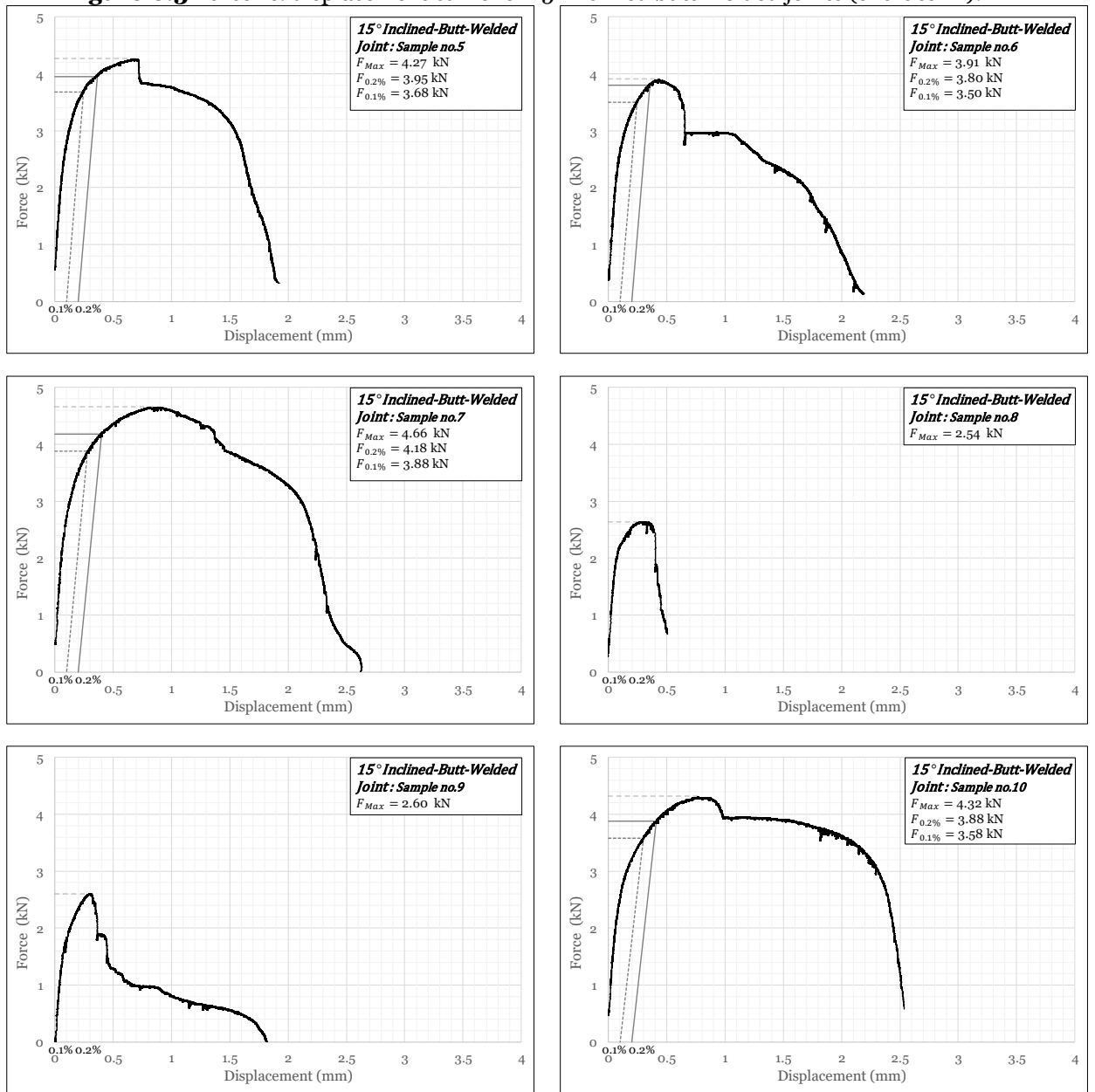


Figure C.3 Force vs. displacement curve for 15° inclined butt-welded joints (short term) (continue).

Appendix C Static data of aluminium-to-steel welded joints (chapter 6)

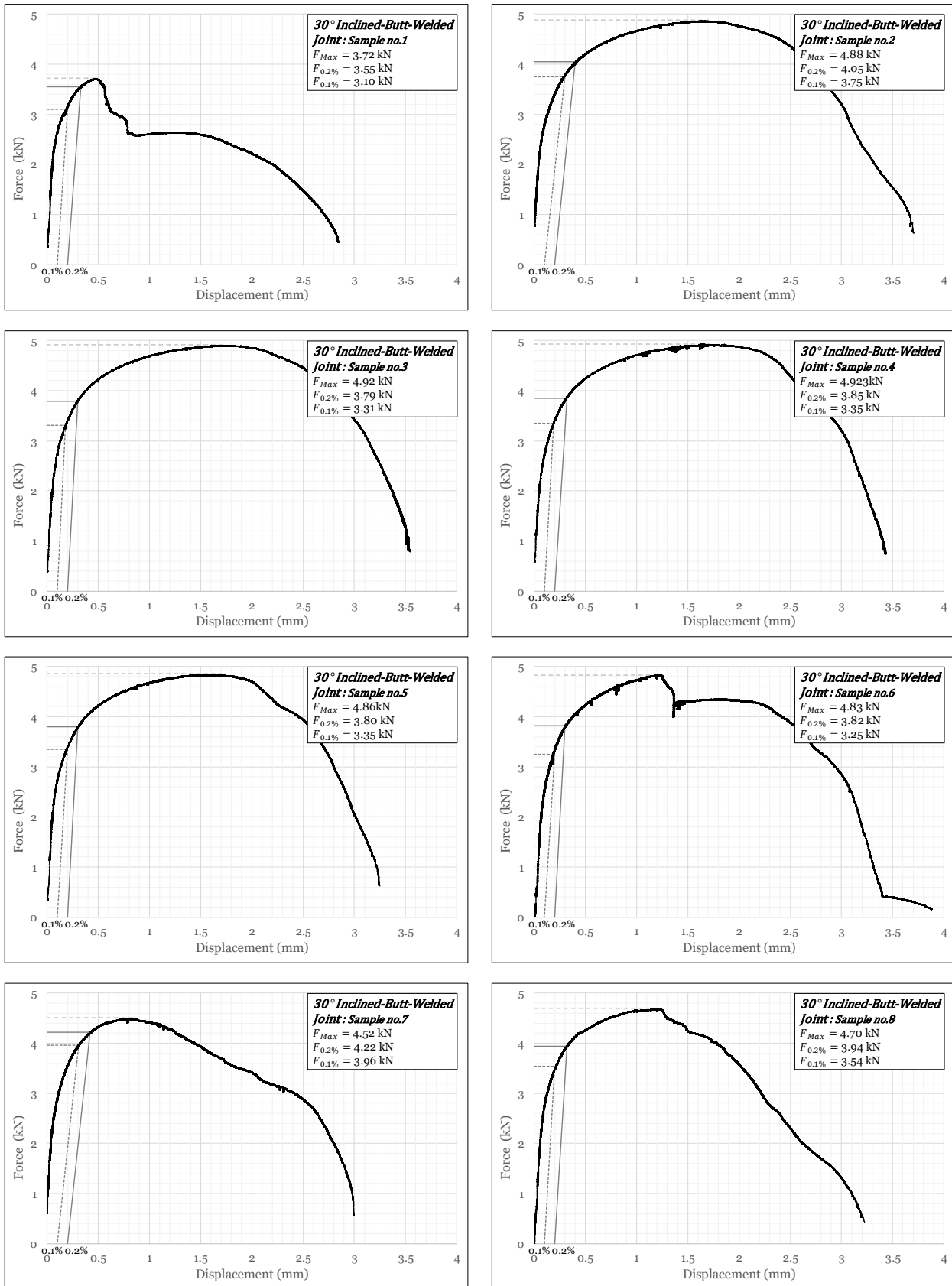


Figure C.4 Force vs. displacement curve for 30° inclined butt-welded joints (short term).

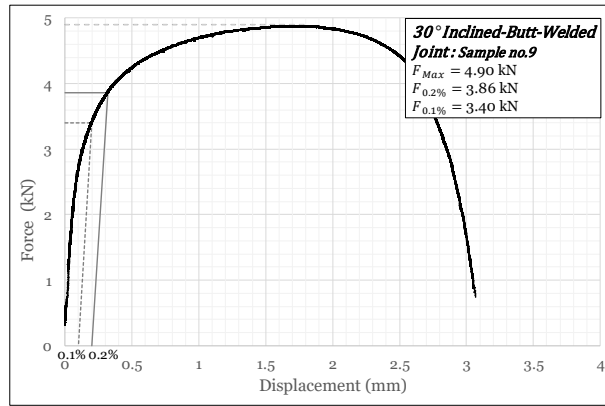


Figure C.4 Force vs. displacement curve for 30° inclined butt-welded joints (short term) (continue).

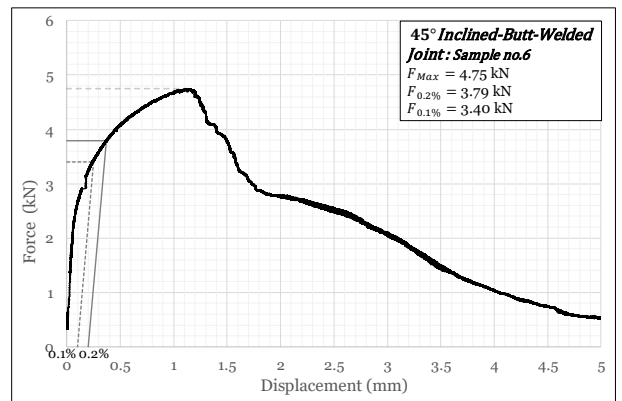
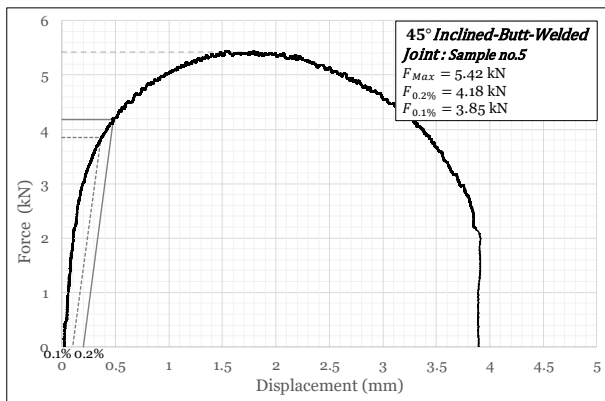
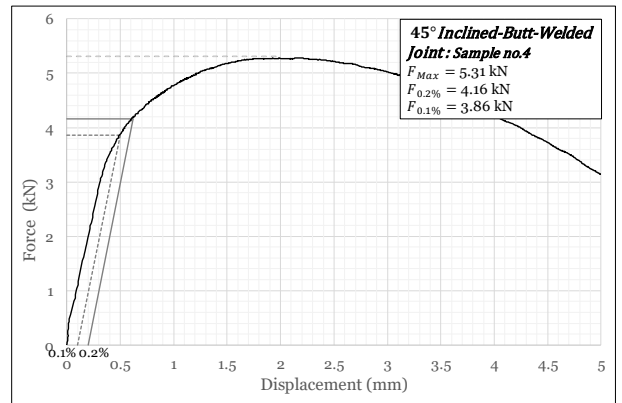
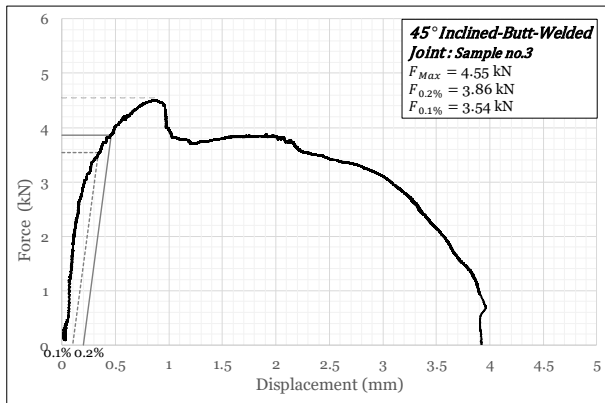
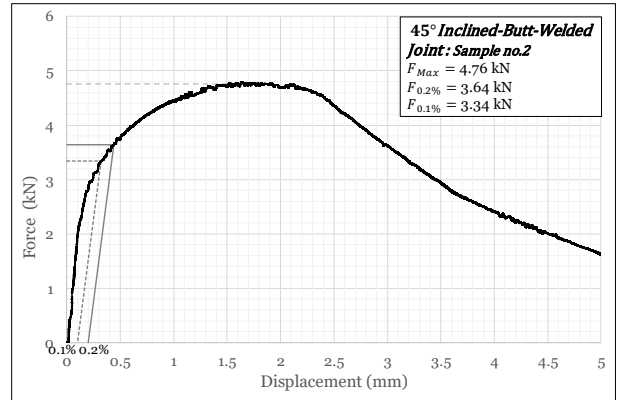
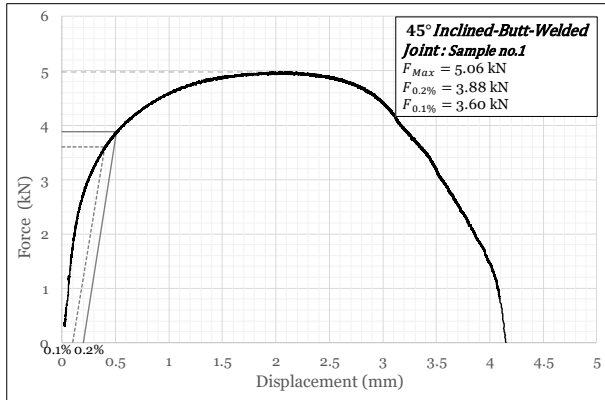


Figure C.5 Force vs. displacement curve for 45° inclined butt-welded joints (short term).

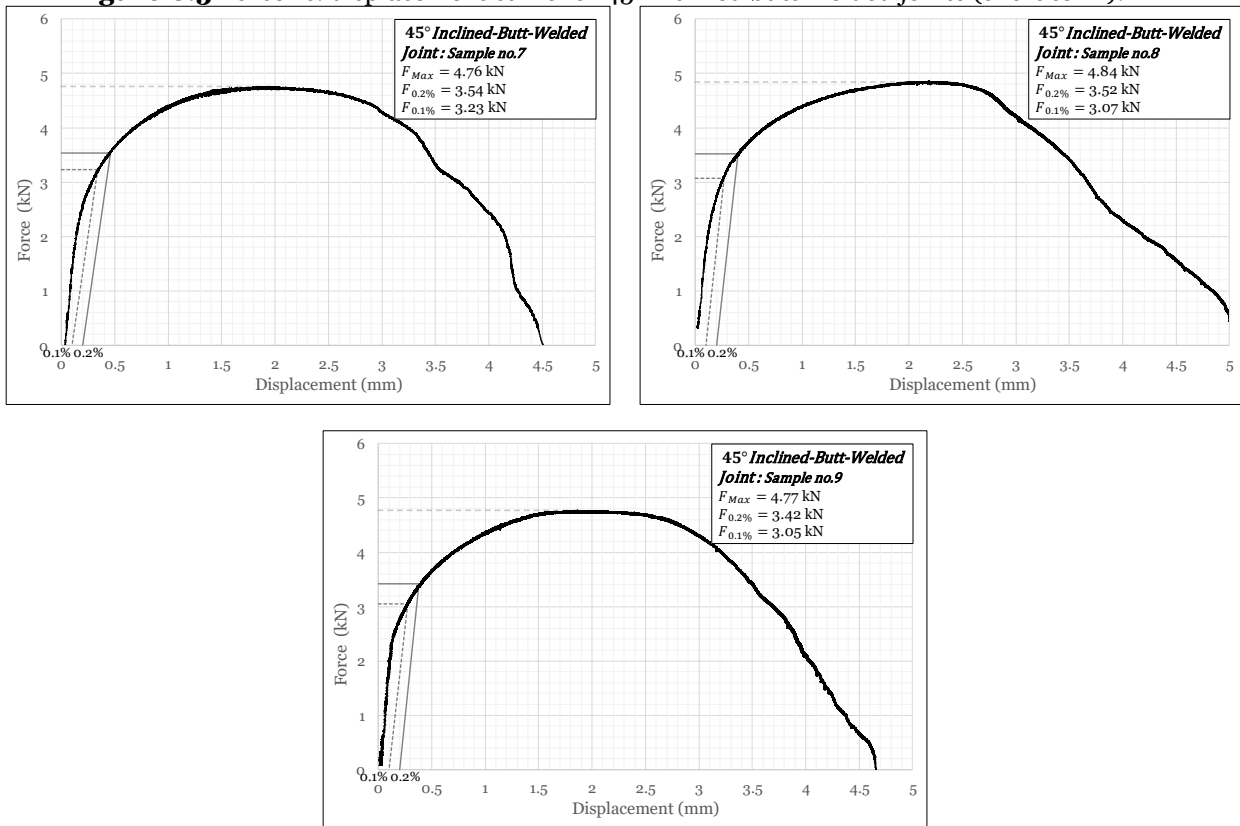
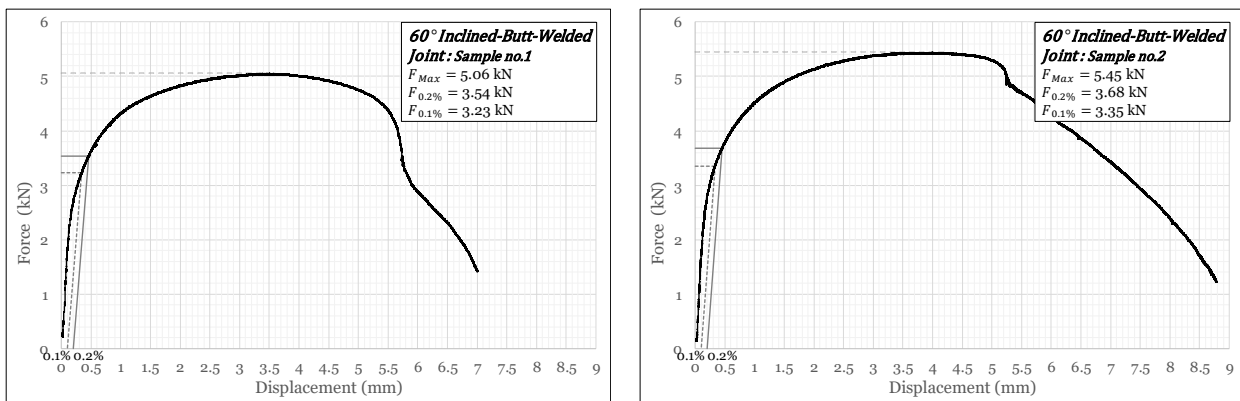


Figure C.5 Force vs. displacement curve for 45° inclined butt-welded joints (short term) (continue).



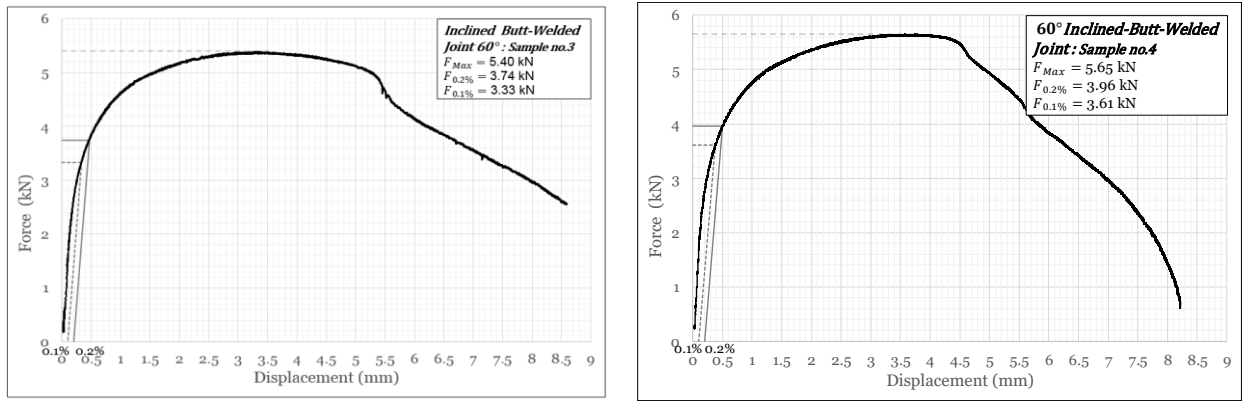


Figure C.6 Force vs. displacement curve for 60° inclined butt-welded joints (short term).

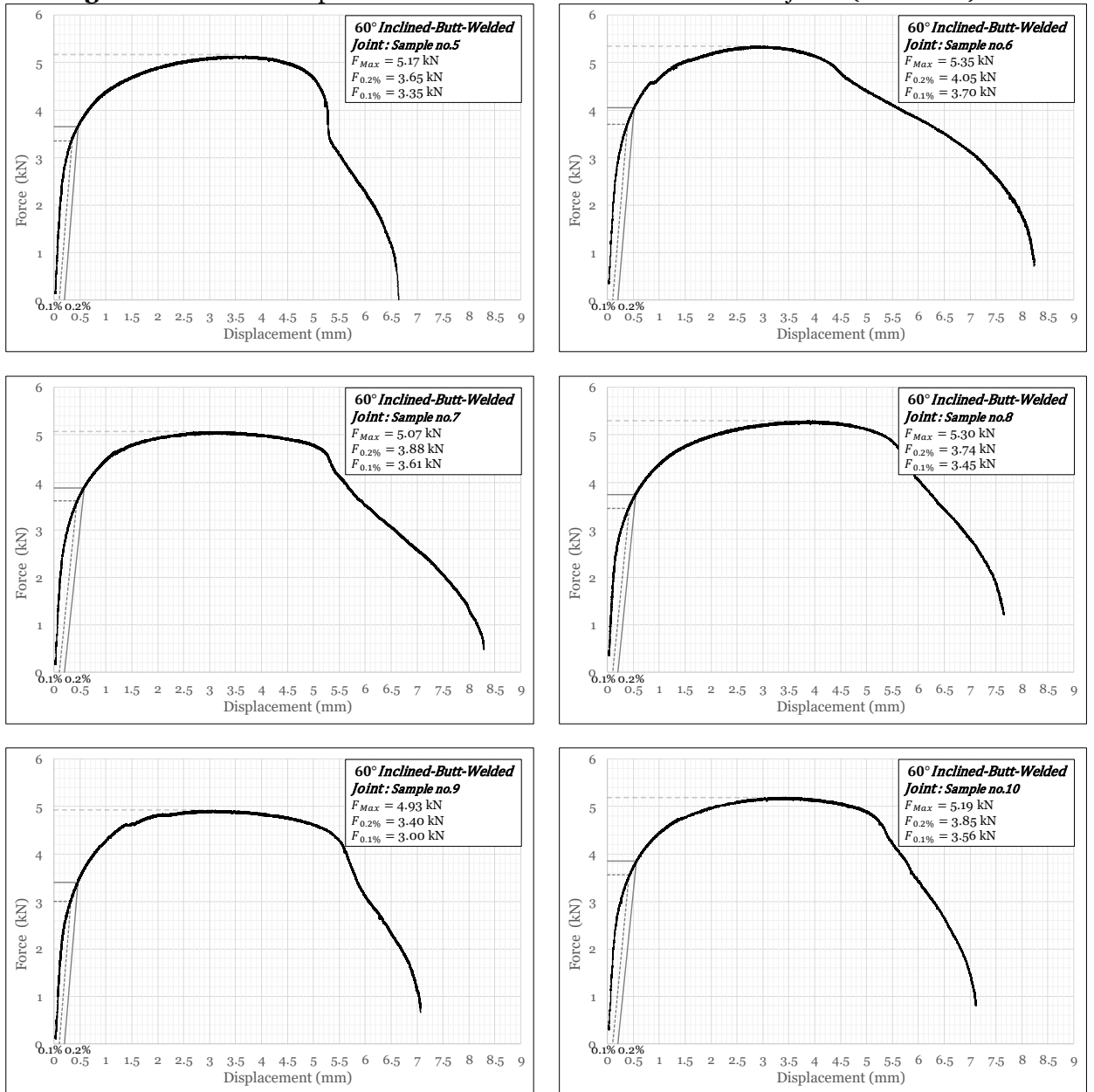
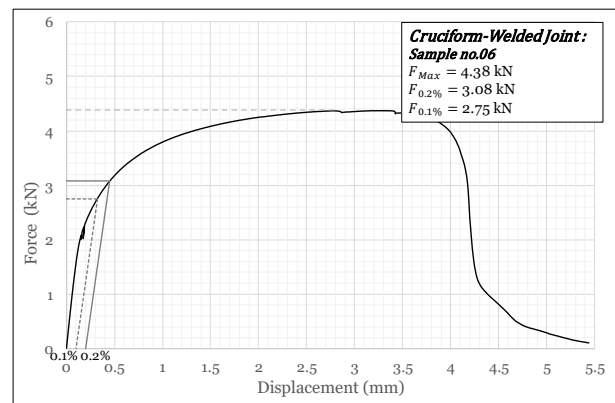
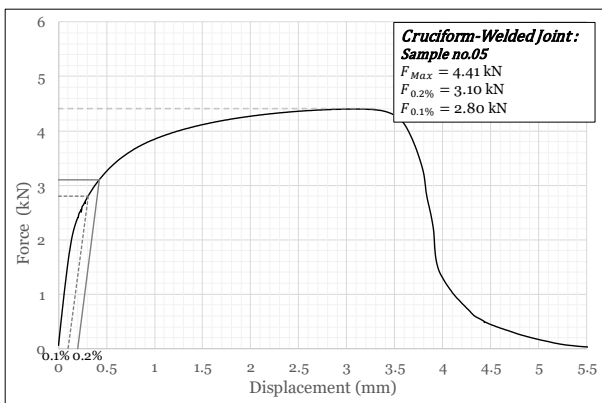
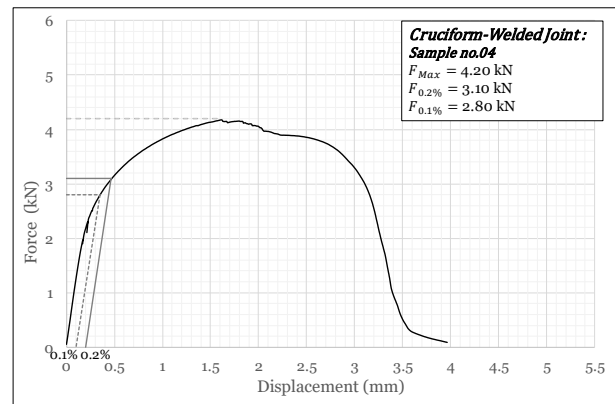
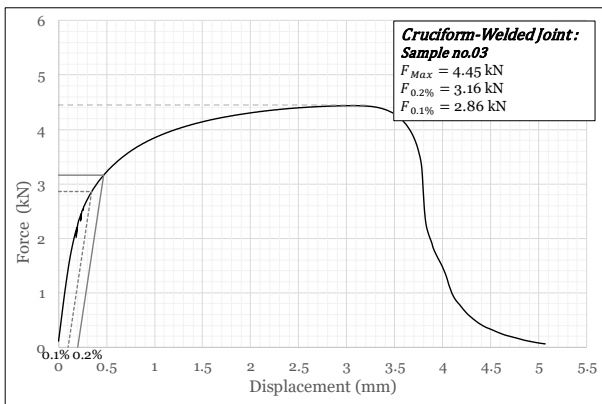
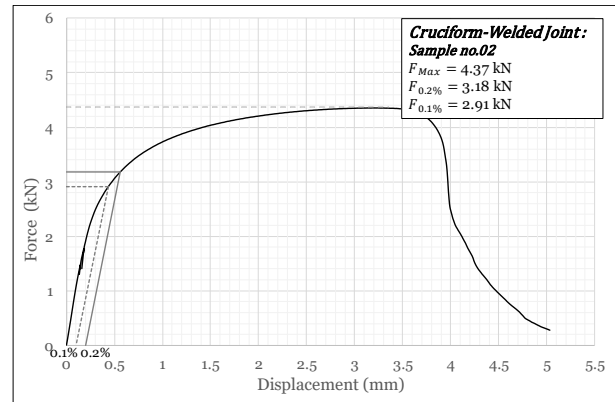
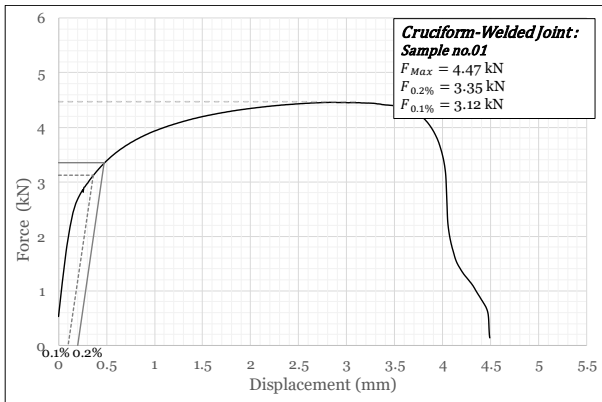




Figure C.6 Force vs. displacement curve for 60° inclined butt-welded joints (short term) (continue)



Appendix C Static data of aluminium-to-steel welded joints (chapter 6)

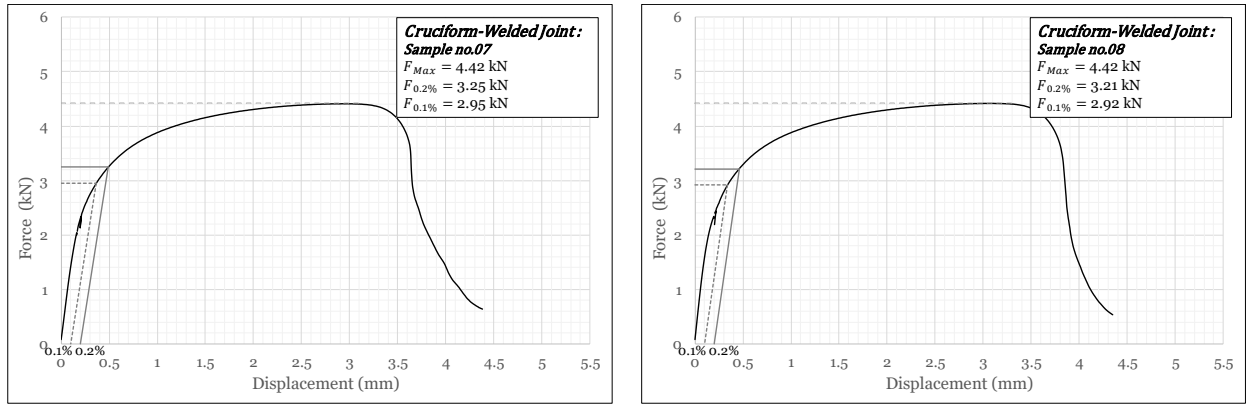


Figure C.7 Force vs. displacement curve for cruciform-welded joints (short term)

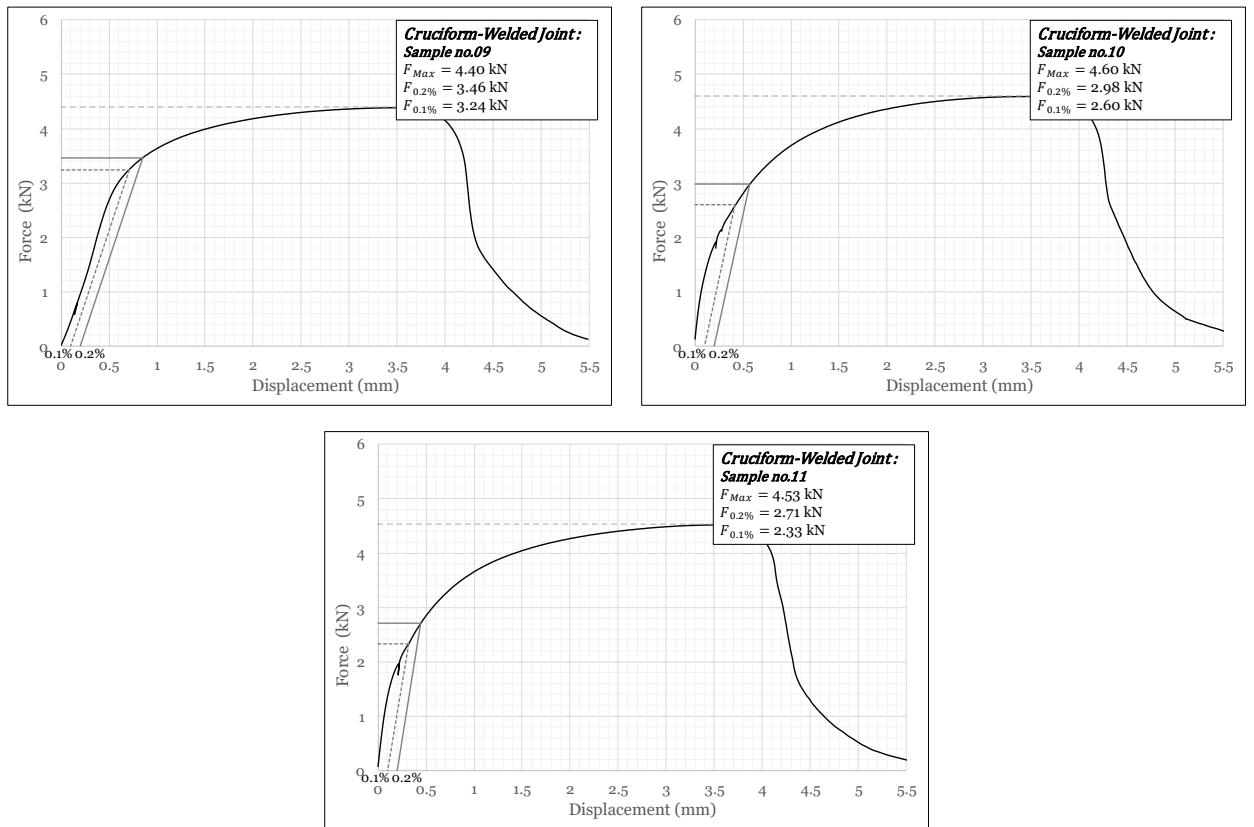


Figure C.7 Force vs. displacement curve for cruciform-welded joints (short term) (continue)

Appendix C Static data of aluminium-to-steel welded joints (chapter 6)

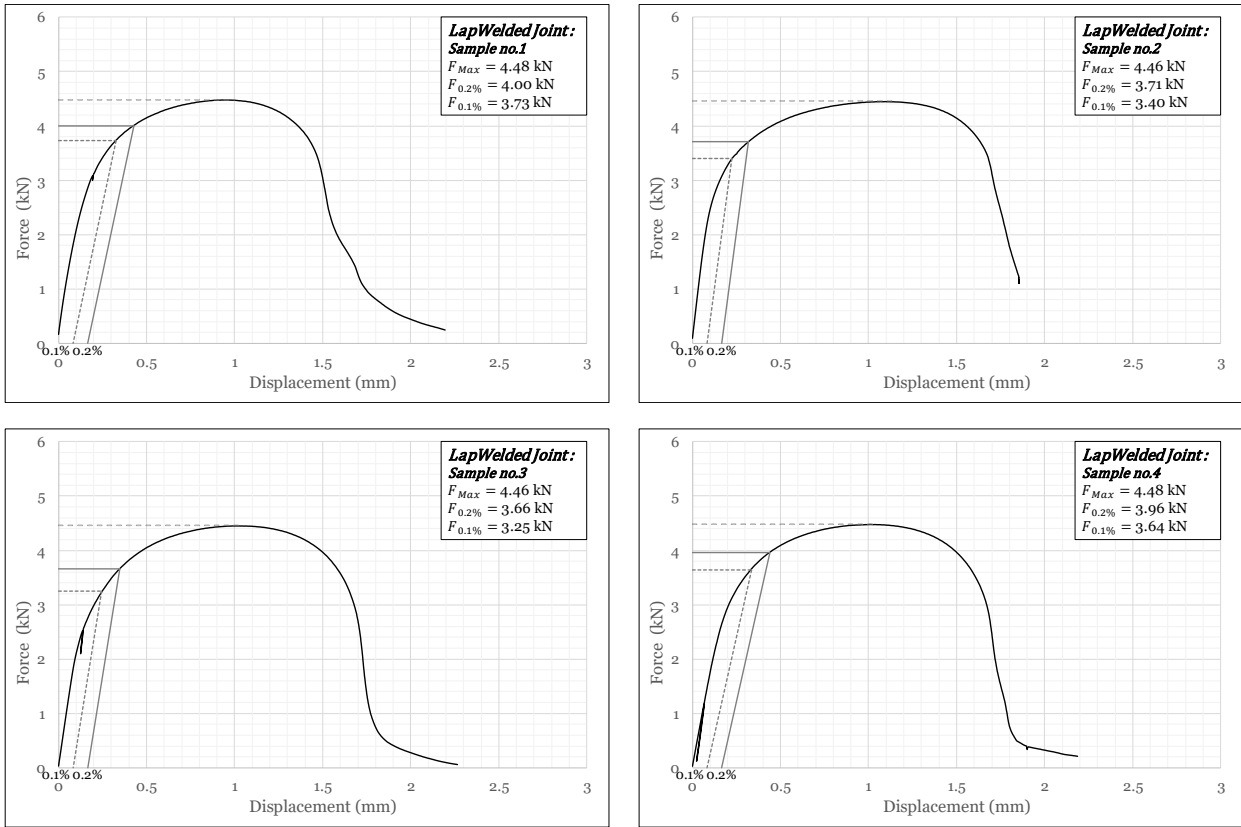
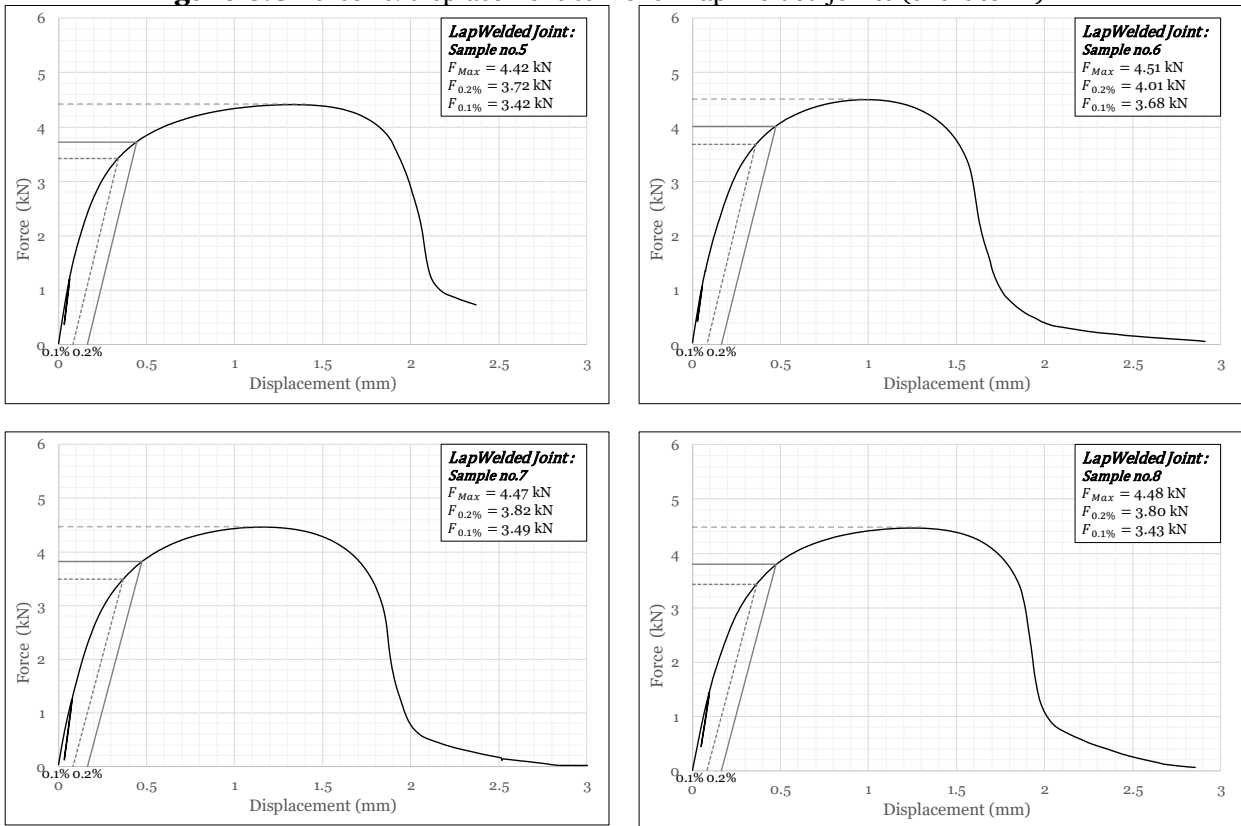


Figure C.8 Force vs. displacement curve for Lap-welded joints (short term)



Appendix C Static data of aluminium-to-steel welded joints (chapter 6)

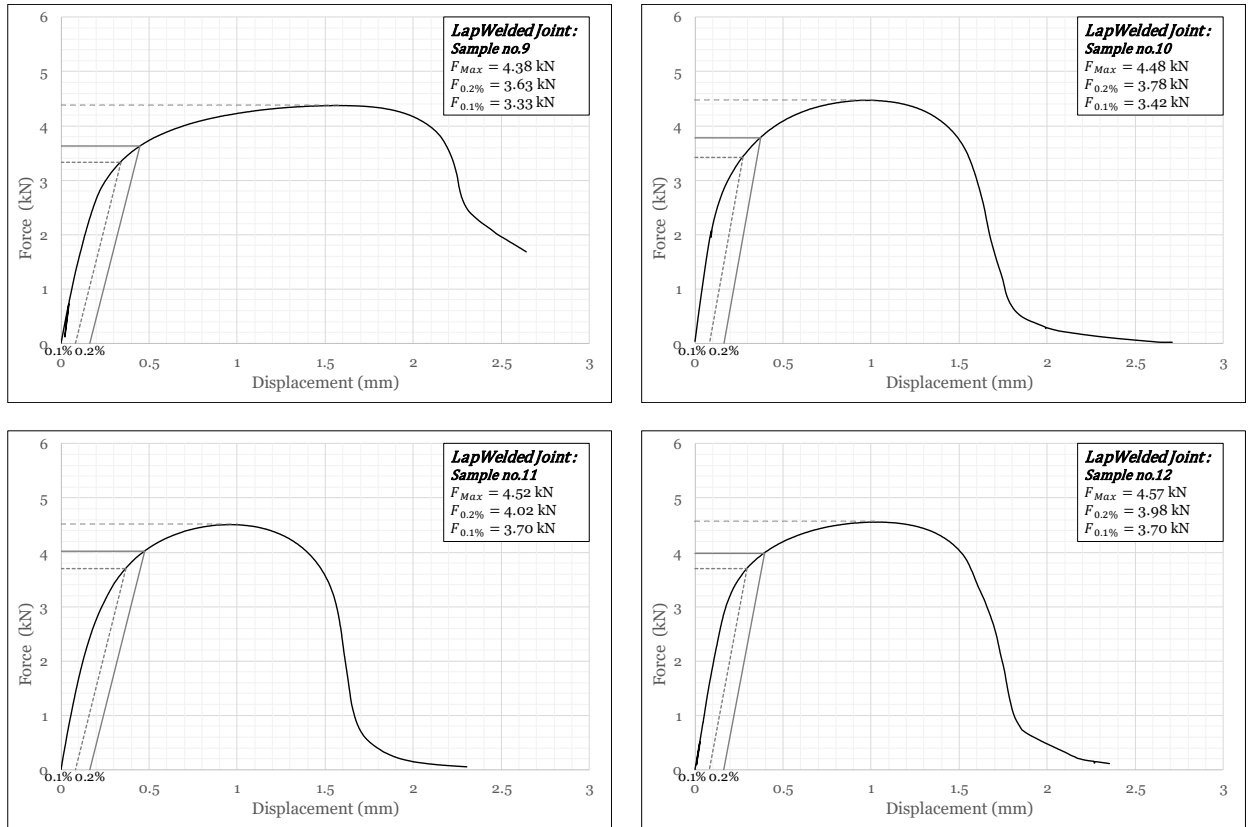


Figure C.8 Force vs. displacement curve for Lap-welded joints (short term) (continue).

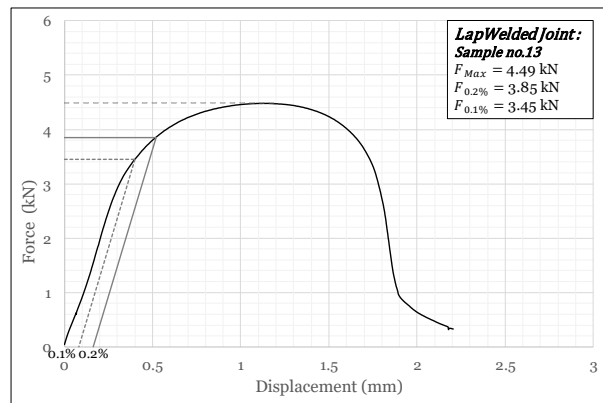


Figure C.8 Force vs. displacement curve for Lap-welded joints (short term) (continue).

Static fracture surface of the hybrid joints (Short-term)



- Butt-single-01
- $F_{max}=4.68$ kN
- Failure mode: WS, AH



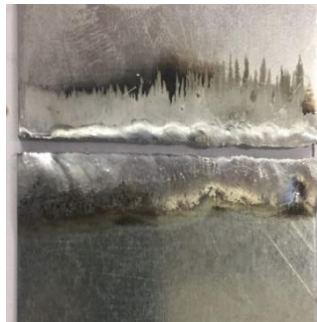
- Butt-single-02
- $F_{max}=4.70$ kN
- Failure mode: AH



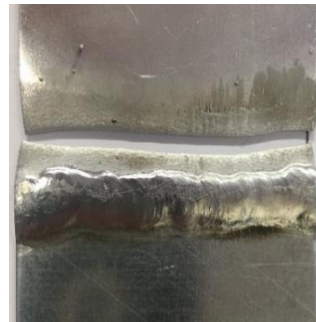
- Butt-single-03
- $F_{max}=4.57$ kN
- Failure mode: AH



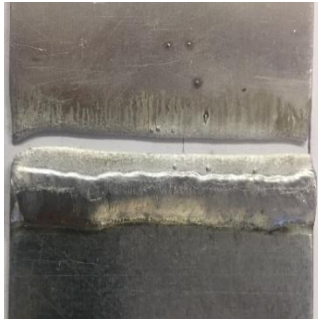
- Butt-single-04
- $F_{max}=4.66$ kN
- Failure mode: AH



- Butt-single-05
- $F_{max}=3.49$ kN
- Failure mode: WS



- Butt-single-06
- $F_{max}=4.73$ kN
- Failure mode: AH



- Butt-single-07
- $F_{max}=4.68$ kN
- Failure mode: AH



- Butt-single-08
- $F_{max}=4.72$ kN
- Failure mode: AH



- Butt-single-09
- $F_{max}=4.67$ kN
- Failure mode: AH



- Butt-single-10
- $F_{max}=4.59$ kN
- Failure mode: WS, AH

Figure C.9 Tensile static failure of single-butt-welded joints (short-term).

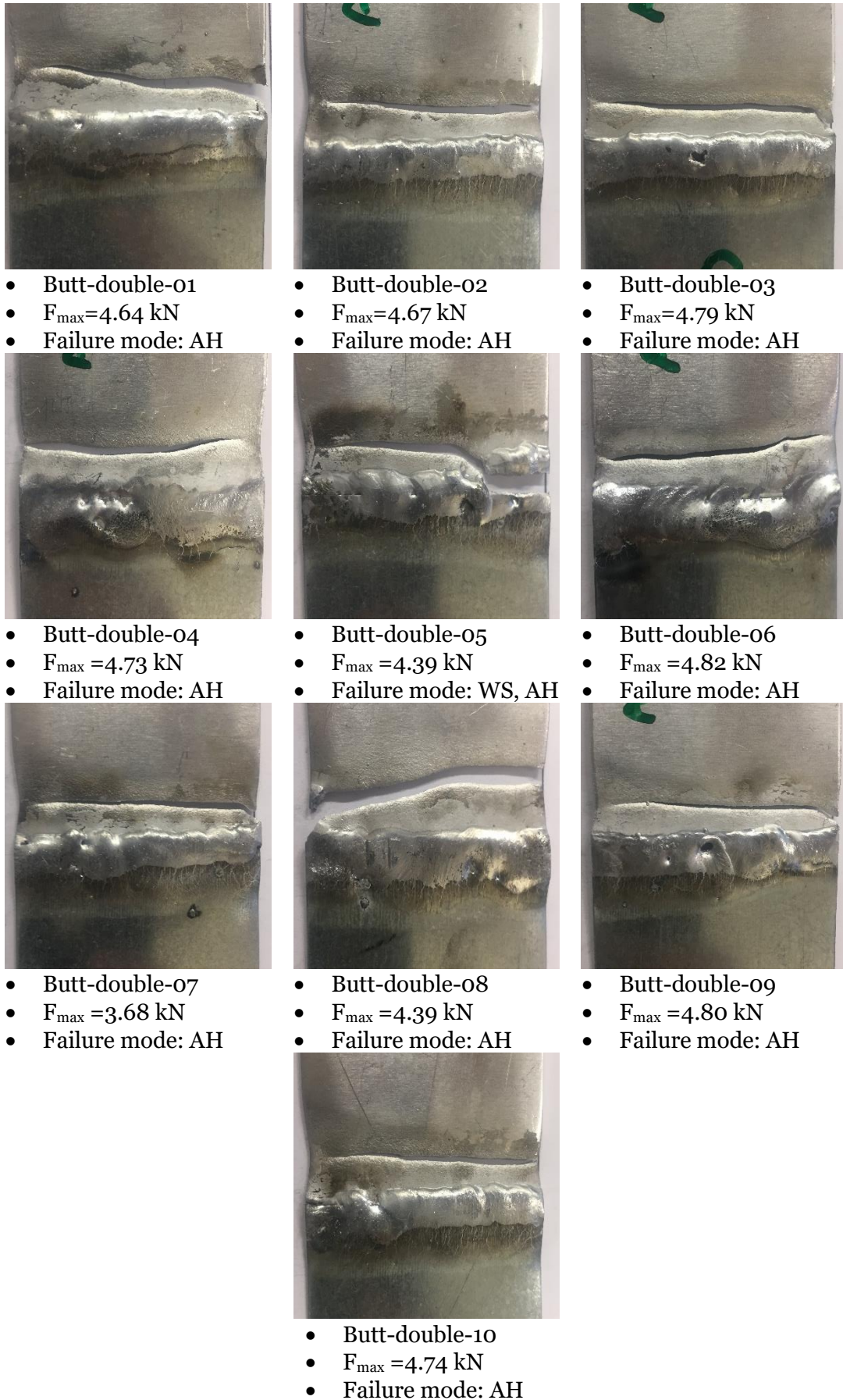


Figure C.10 Tensile static failure of double-butt-welded joints (short-term).



- 15° inclined-butt-01
- $F_{\max} = 4.82$ kN
- Failure mode: AH



- 15° inclined-butt-02
- $F_{\max} = 4.77$ kN
- Failure mode: AH



- 15° inclined-butt-03
- $F_{\max} = 4.88$ kN
- Failure mode: AH



- 15° inclined-butt-04
- $F_{\max} = 4.82$ kN
- Failure mode: WS



- 15° inclined-butt-05
- $F_{\max} = 4.43$ kN
- Failure mode: WS, AH



- 15° inclined-butt-06
- $F_{\max} = 4.07$ kN
- Failure mode: WS



- 15° inclined-butt-07
- $F_{\max} = 4.82$ kN
- Failure mode: AH



- 15° inclined-butt-08
- $F_{\max} = 2.81$ kN
- Failure mode: WS



- 15° inclined-butt-09
- $F_{\max} = 3.28$ kN
- Failure mode: WS



- 15° inclined-butt-10
- $F_{\max} = 4.47$ kN
- Failure mode: WS, AH

Figure C.11 Tensile static failure of 15° inclined butt-welded joints (short-term).

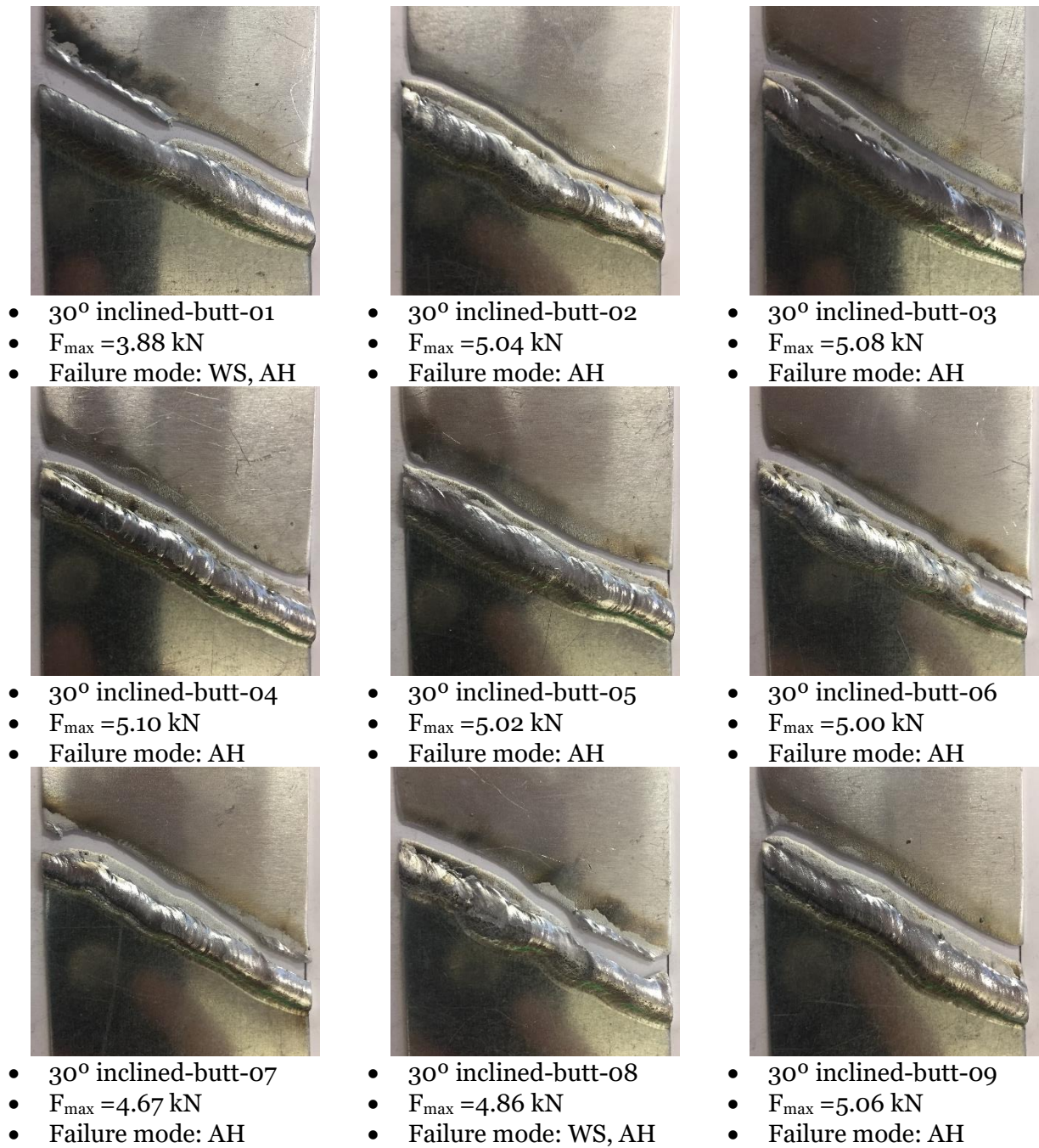


Figure C.12 Tensile static failure of 30° inclined butt-welded joints (short-term).



- 45° inclined-01
- $F_{\max} = 5.15$ kN
- Failure mode: AH



- 45° inclined-02
- $F_{\max} = 4.95$ kN
- Failure mode: AH



- 45° inclined-03
- $F_{\max} = 4.66$ kN
- Failure mode: AH



- 45° inclined-04
- $F_{\max} = 5.43$ kN
- Failure mode: AH



- 45° inclined-05
- $F_{\max} = 5.58$ kN
- Failure mode: AH



- 45° inclined-06
- $F_{\max} = 4.92$ kN
- Failure mode: AH



- 45° inclined-07
- $F_{\max} = 4.92$ kN
- Failure mode: AH



- 45° inclined-08
- $F_{\max} = 5.03$ kN
- Failure mode: AH



- 45° inclined-09
- $F_{\max} = 4.94$ kN
- Failure mode: AH

Figure C.13 Tensile static failure of 45° inclined butt-welded joints (short-term).

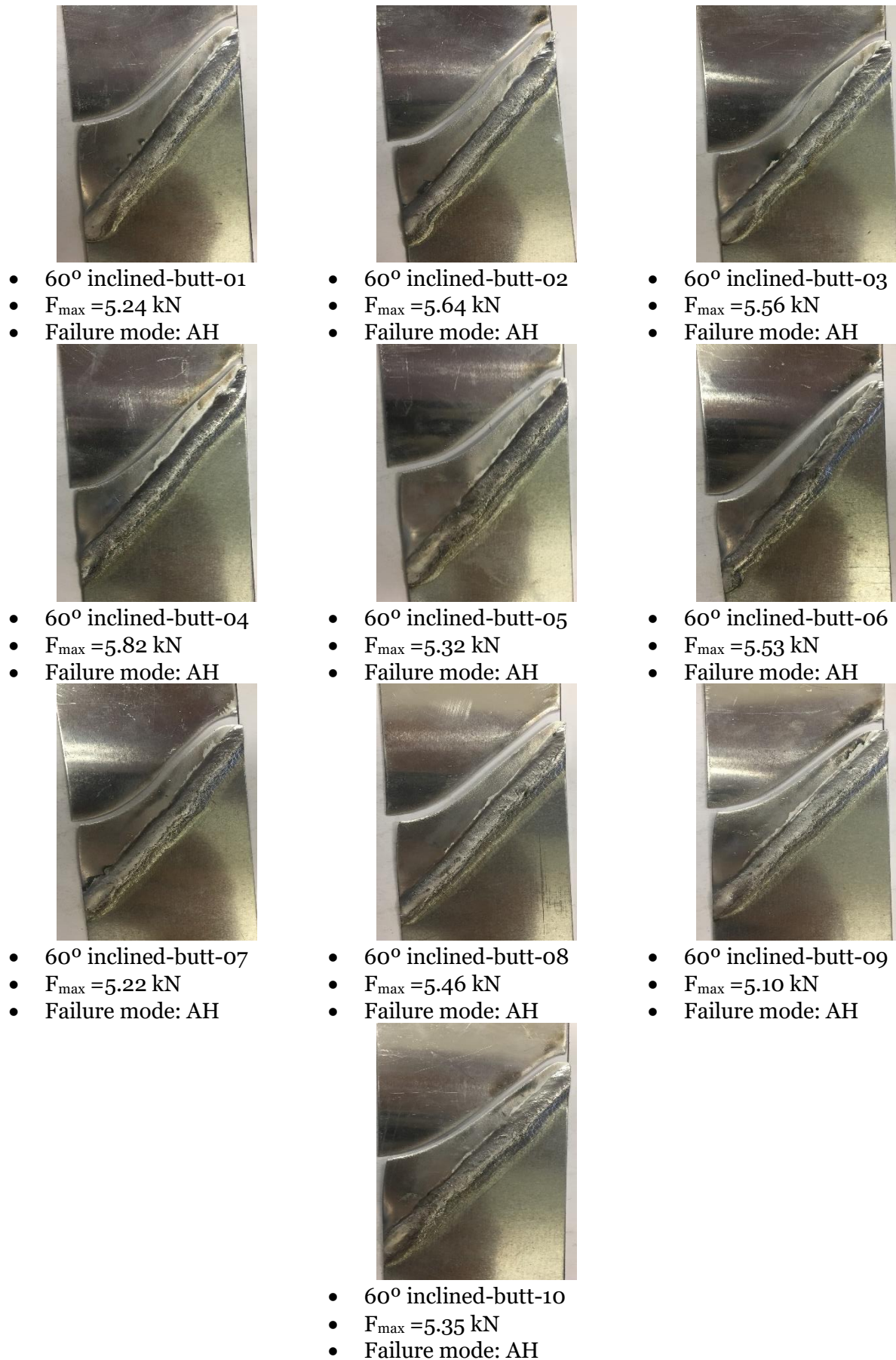


Figure C.14 Tensile static failure of 60° inclined butt-welded joints (short-term).

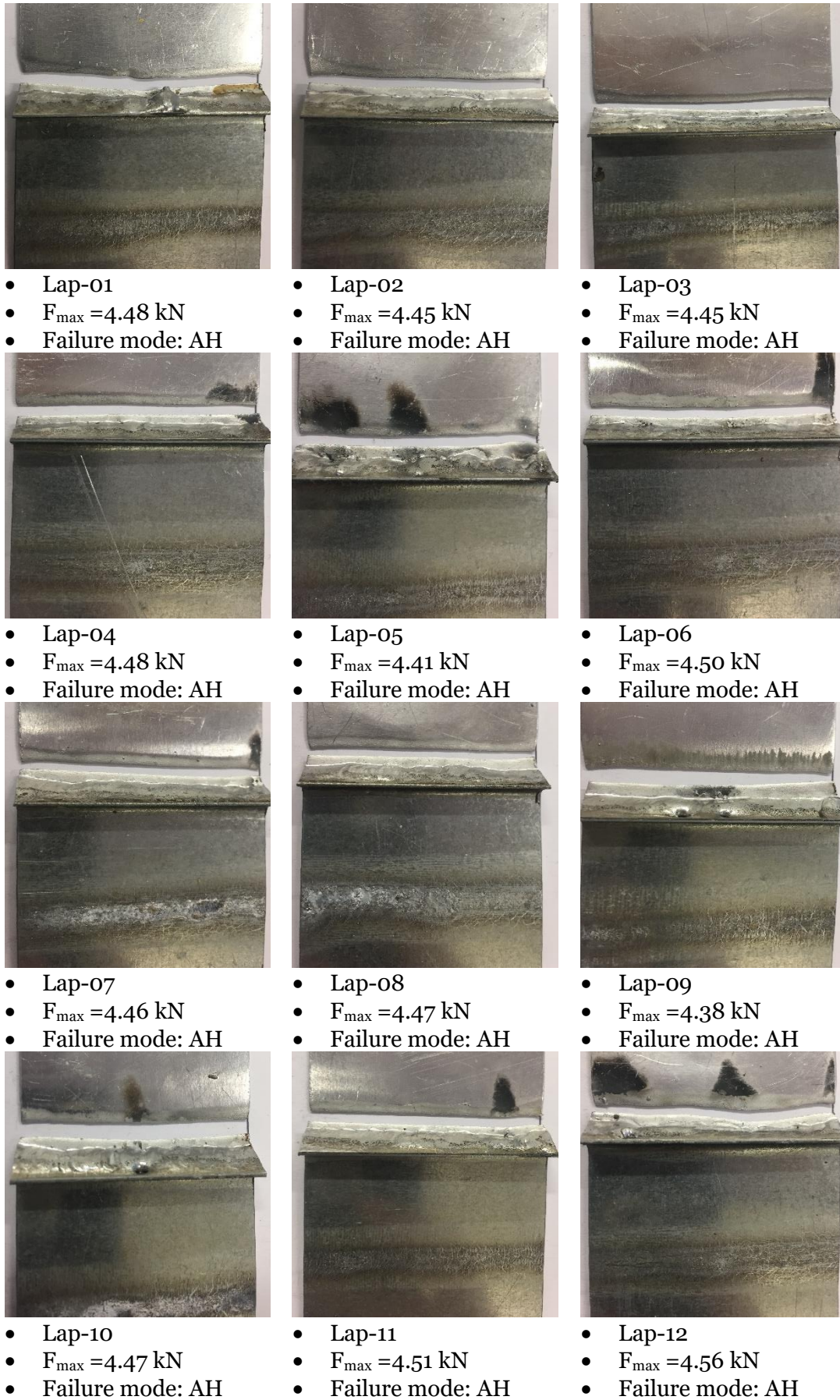


Figure C.15 Tensile static failure of lap-welded joints (short-term).



- Lap-13
 - $F_{\max} = 4.48 \text{ kN}$
- Failure mode: AH

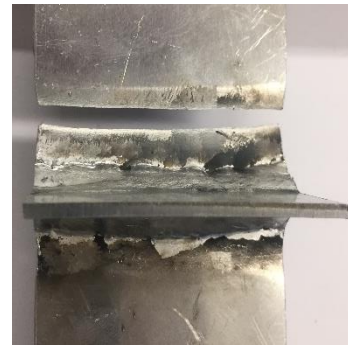
Figure C.15 Tensile static failure of lap-welded joints (short-term) (continue).



- Cr-01
- $F_{\max} = 4.46 \text{ kN}$
- Failure mode: AH



- Cr-02
- $F_{\max} = 4.35 \text{ kN}$
- Failure mode: AH



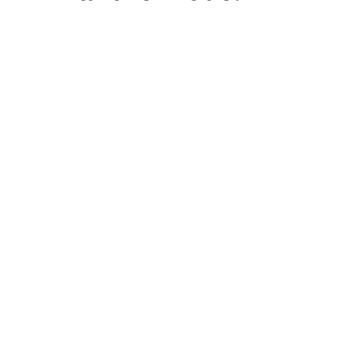
- Cr-03
- $F_{\max} = 4.44 \text{ kN}$
- Failure mode: AH



- Cr-04
- $F_{\max} = 4.18 \text{ kN}$
- Failure mode: AH

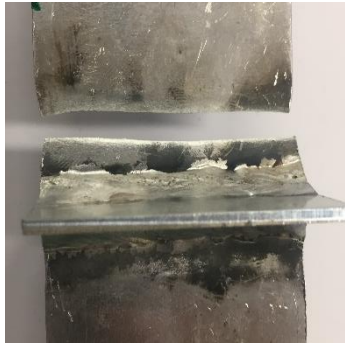


- Cr-05
- $F_{\max} = 4.40 \text{ kN}$
- Failure mode: AH



- Cr-06
- $F_{\max} = 4.37 \text{ kN}$
- Failure mode: AH

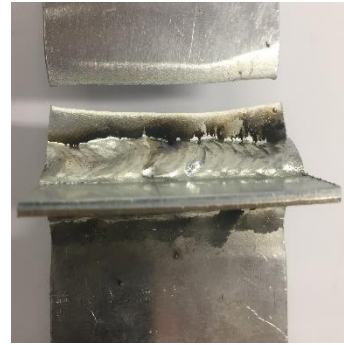
Figure C.16 Tensile static failure of cruciform-welded joints (short-term).



- Cr-07
- $F_{\max} = 4.41 \text{ kN}$
- Failure mode: AH



- Cr-08
- $F_{\max} = 4.42 \text{ kN}$
- Failure mode: AH



- Cr-09
- $F_{\max} = 4.38 \text{ kN}$
- Failure mode: AH



- Cr-10
- $F_{\max} = 4.59 \text{ kN}$
- Failure mode: AH



- Cr-11
- $F_{\max} = 4.52 \text{ kN}$
- Failure mode: AH

Figure C.16 Tensile static failure of cruciform-welded joints (short-term) (continue).

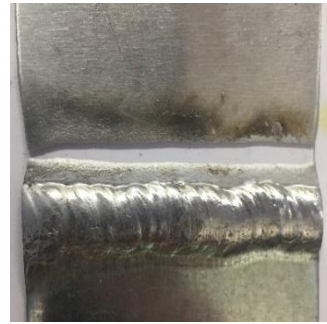
Static fracture surface of the hybrid joints (Long-term)



- Butt-single-01
- $F_{max}=3.99$ kN
- Failure mode: WS, AH



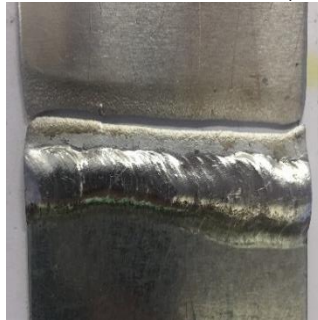
- Butt-single-02
- $F_{max}=4.44$ kN
- Failure mode: WS, AH



- Butt-single-03
- $F_{max}=4.87$ kN
- Failure mode: AH



- Butt-single-04
- $F_{max}=4.37$ kN
- Failure mode: WS



- Butt-single-05
- $F_{max}=4.95$ kN
- Failure mode: AH



- Butt-single-06
- $F_{max}=4.95$ kN
- Failure mode: WS, AH



- Butt-single-07
- $F_{max}=3.44$ kN
- Failure mode: WS, AH



- Butt-single-08
- $F_{max}=4.73$ kN
- Failure mode: WS, AH



- Butt-single-09
- $F_{max}=4.90$ kN
- Failure mode: AH



- Butt-single-10
- $F_{max}=3.99$ kN
- Failure mode: WS

Figure C.17 Tensile static failure of single-butt-welded joints (long-term).



- 15° inclined-butt-01
- $F_{\max} = 5.05$ kN
- Failure mode: AH



- 15° inclined-butt-02
- $F_{\max} = 3.58$ kN
- Failure mode: WS



- 15° inclined-butt-03
- $F_{\max} = 3.77$ kN
- Failure mode: WS



- 15° inclined-butt-04
- $F_{\max} = 4.76$ kN
- Failure mode: AH



- 15° inclined-butt-05
- $F_{\max} = 3.71$ kN
- Failure mode: WS, AH



- 15° inclined-butt-06
- $F_{\max} = 4.70$ kN
- Failure mode: WS, AH



- 15° inclined-butt-07
- $F_{\max} = 4.54$ kN
- Failure mode: WS



- 15° inclined-butt-08
- $F_{\max} = 4.94$ kN
- Failure mode: AH



- 15° inclined-butt-09
- $F_{\max} = 4.16$ kN
- Failure mode: WS, AH

Figure C.18 Tensile static failure of 15° inclined butt-welded joints (long-term).



- 30° inclined-butt-01
- $F_{max} = 5.33$ kN
- Failure mode: AH



- 30° inclined-butt-02
- $F_{max} = 5.23$ kN
- Failure mode: AH



- 30° inclined-butt-03
- $F_{max} = 5.25$ kN
- Failure mode: AH



- 30° inclined-butt-04
- $F_{max} = 5.17$ kN
- Failure mode: AH



- 30° inclined-butt-05
- $F_{max} = 5.11$ kN
- Failure mode: WS, AH



- 30° inclined-butt-06
- $F_{max} = 4.88$ kN
- Failure mode: WS, AH



- 30° inclined-butt-07
- $F_{max} = 4.99$ kN
- Failure mode: WS, AH



- 30° inclined-butt-08
- $F_{max} = 4.85$ kN
- Failure mode: AH



- 30° inclined-butt-09
- $F_{max} = 5.24$ kN
- Failure mode: WS, AH



- 30° inclined-butt-10
- $F_{max} = 5.33$ kN
- Failure mode: WS



- 30° inclined-butt-11
- $F_{max} = 5.26$ kN
- Failure mode: AH

Figure C.19 Tensile static failure of 30° inclined butt-welded joints (long-term).



- 45° inclined-butt-01
- $F_{max} = 4.97$ kN
- Failure mode: AH



- 45° inclined-butt-02
- $F_{max} = 5.27$ kN
- Failure mode: AH



- 45° inclined-butt-03
- $F_{max} = 5.37$ kN
- Failure mode: AH



- 45° inclined-butt-04
- $F_{max} = 5.25$ kN
- Failure mode: AH



- 45° inclined-butt-05
- $F_{max} = 5.16$ kN
- Failure mode: AH



- 45° inclined-butt-06
- $F_{max} = 5.14$ kN
- Failure mode: AH



- 45° inclined-butt-07
- $F_{max} = 4.95$ kN
- Failure mode: AH



- 45° inclined-butt-08
- $F_{max} = 5.52$ kN
- Failure mode: AH



- 45° inclined-butt-09
- $F_{max} = 5.11$ kN
- Failure mode: AH



- 45° inclined-butt-10
- $F_{max} = 5.08$ kN
- Failure mode: AH

Figure C.20 Tensile static failure of 45° inclined butt-welded joints (long-term).

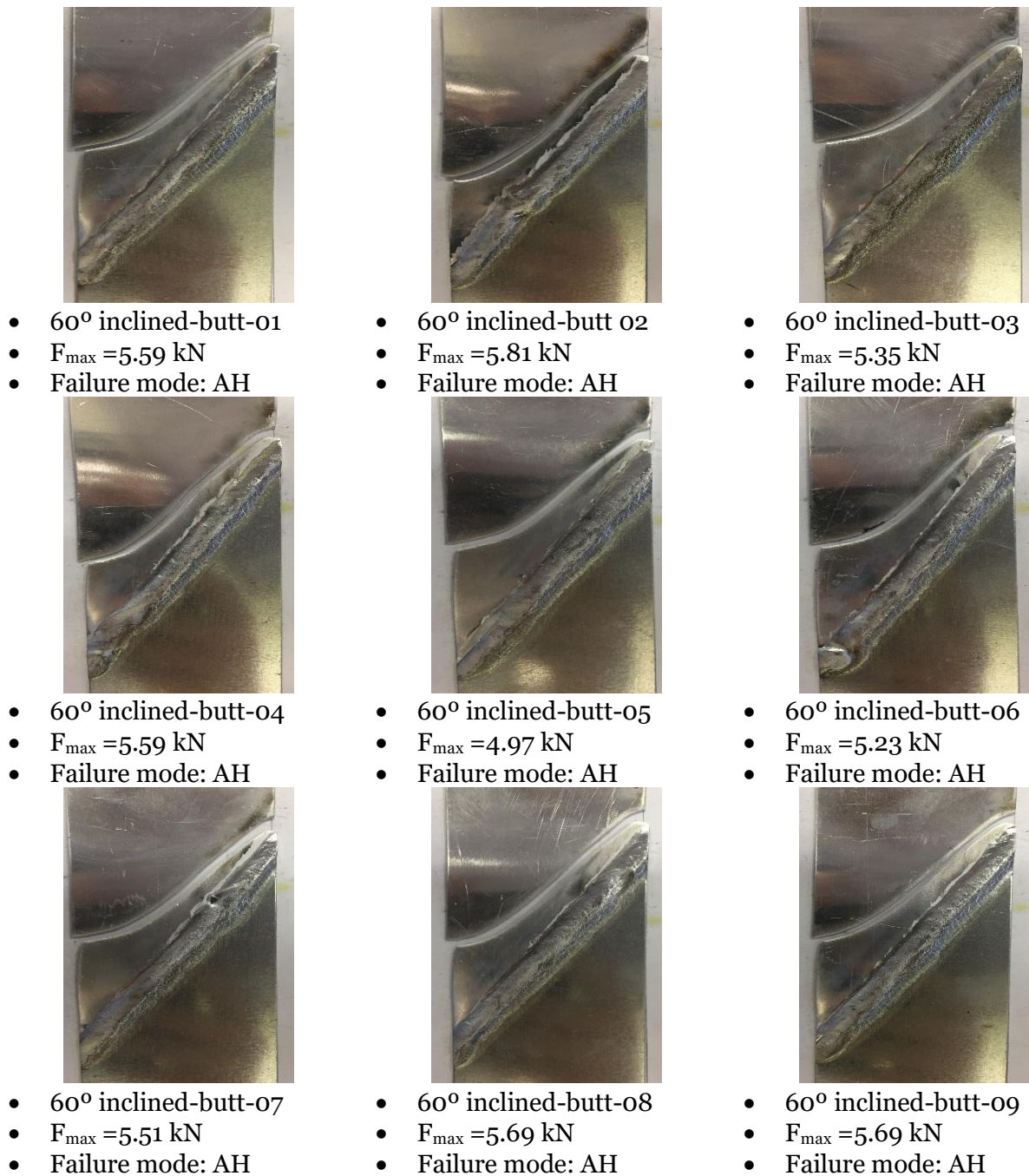


Figure C.21 Tensile static failure of 60° inclined butt-welded joints (long-term).

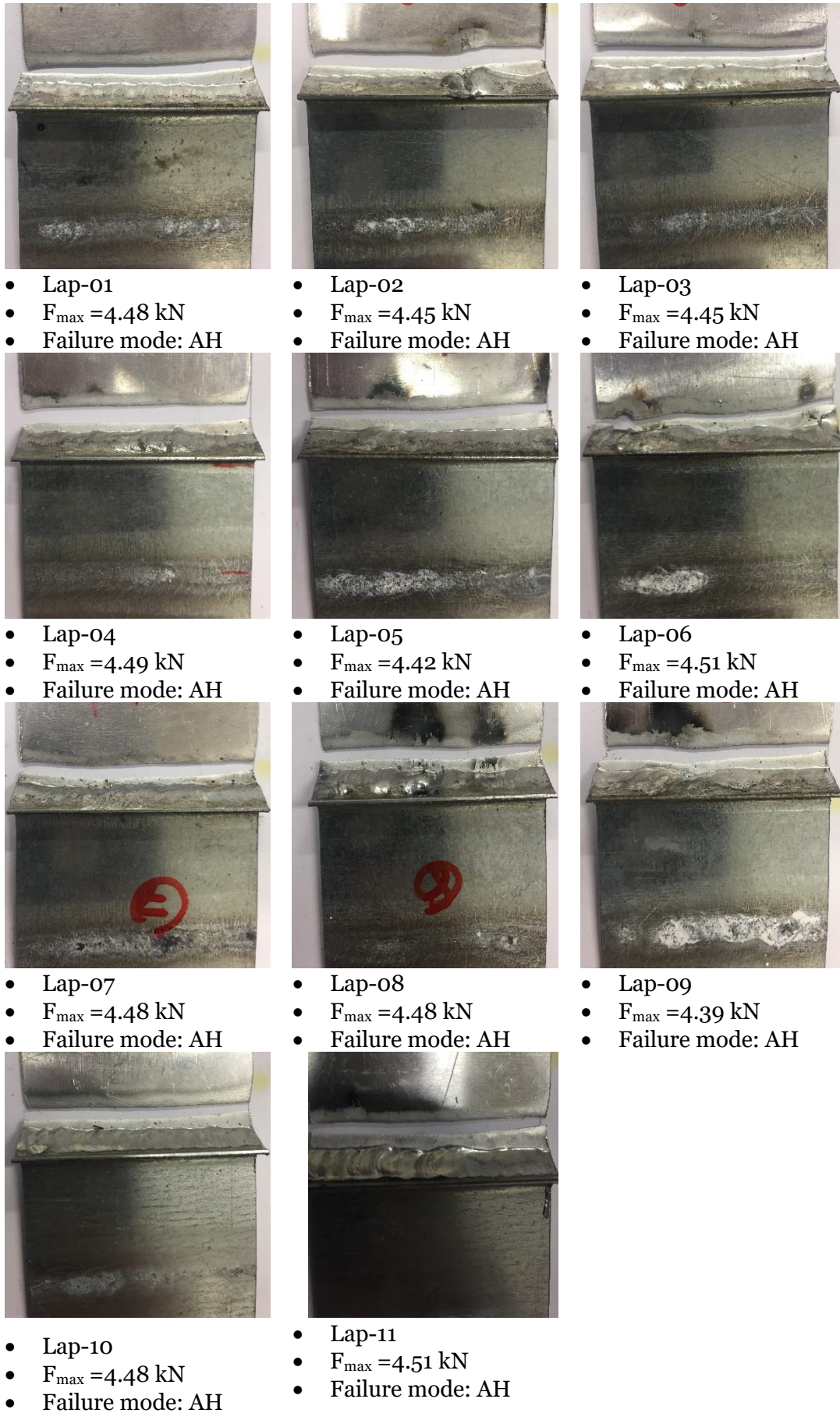


Figure C.22 Tensile static failure of lap-welded joints (long-term).

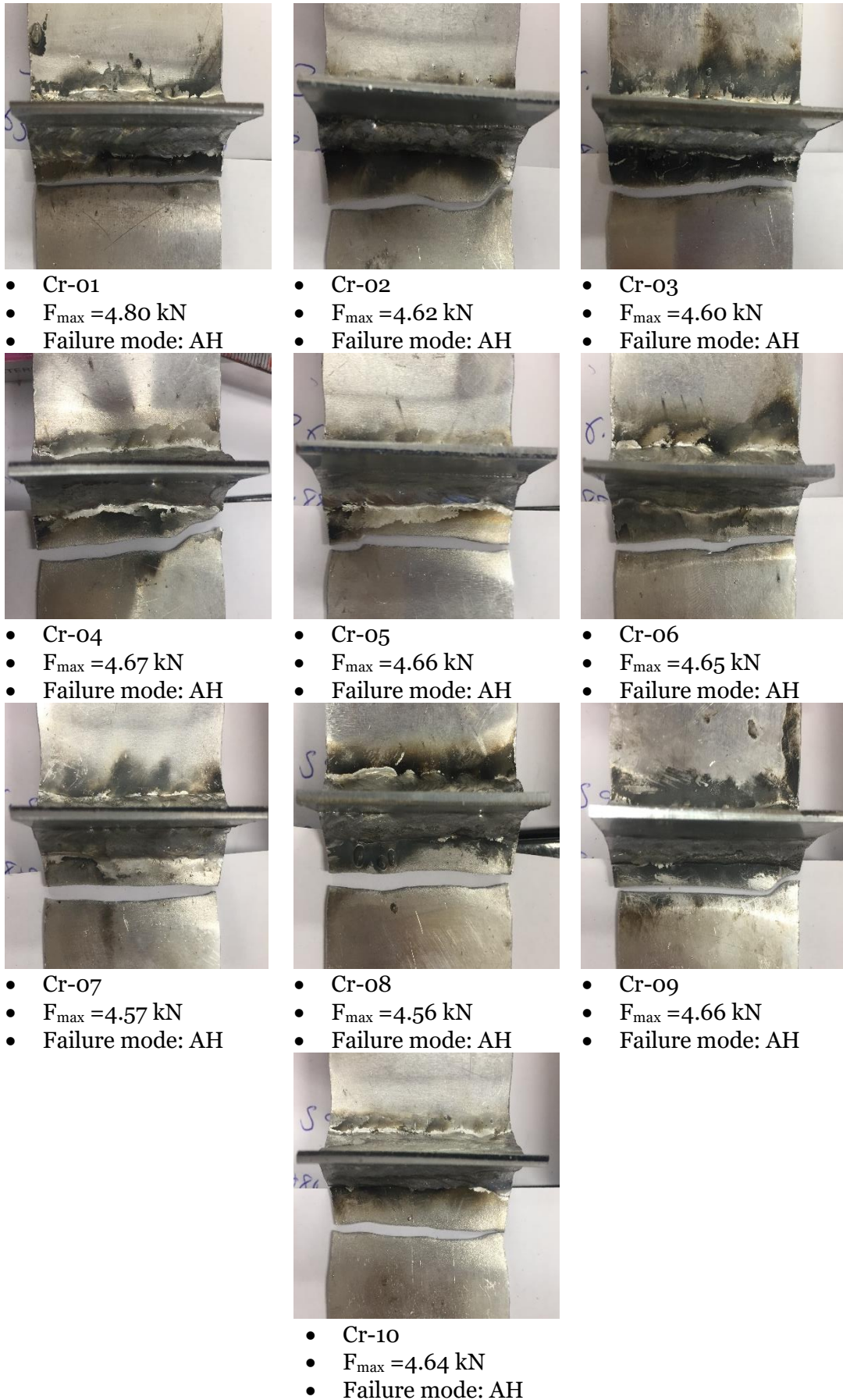


Figure C.23 Tensile static failure of cruciform-welded joints (long-term).

Metallurgical Analysis

A metallurgical investigation of the aluminium-to-steel welded joints was carried out to understand the microstructural behaviour of the joints by performing Scanning Electron Microscopy (SEM) and Energy Dispersive X-ray (EDX) analyses [5-8]. Figure C.24 shows the joint morphology and the position of the investigated sections in the welding zone. The investigated zones were selected to explore different aspects as follow:

- Position a, and position b were localized far from the weld zone to analyse the mechanical behaviour and the interaction between the different metallic layers.
- Position c was localized across the joint to analyse the effect of melting at the interface between aluminium, steel sheets and the filler.
- Position d was localized at the weld and aluminium sheet interface.

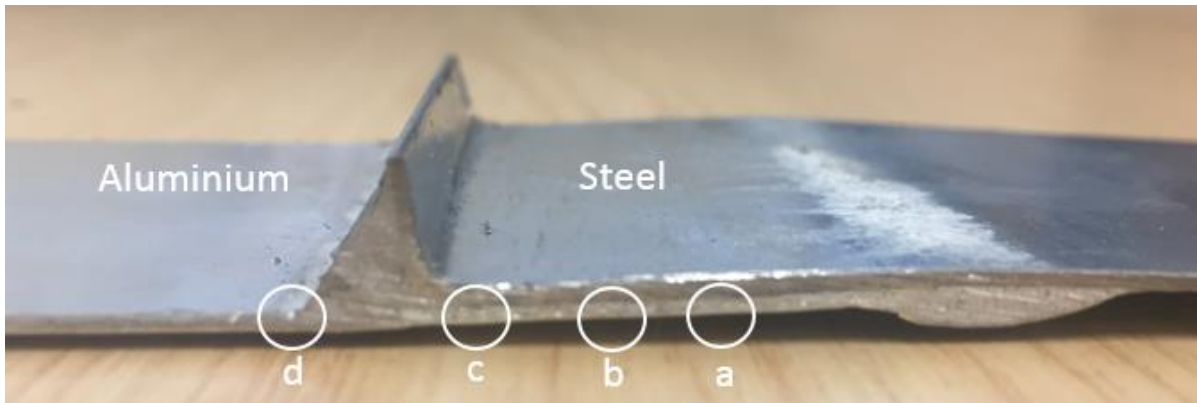


Figure C.24 the position of the investigated sections in the aluminium-to-steel welded joints for the metallurgical analysis.

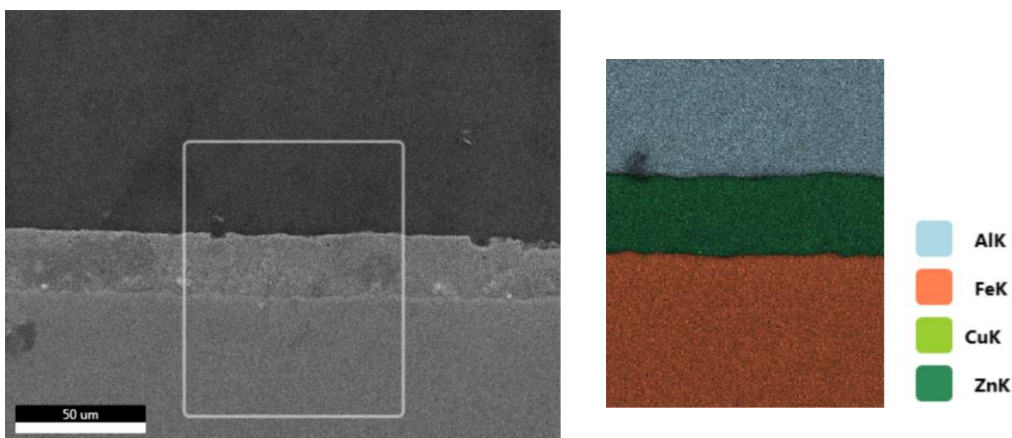


Figure C.25 Map of main metallic elements taken further from melting zone.

The specimens used in the metallurgical analysis were prepared by using a metallographic cutting machine at room temperature. After that, an ultrasonic device was used to clean the specimens in pure alcoholic solution. Figure C.25 explores what happens during welding at the interface between the aluminium sheet and the galvanized steel sheet (position a, in Figure C.24). Aluminium, steel, and zinc layers are presented with a negligible amount of copper found in the zinc layer. By focusing attention on the zinc layer, it is clear that some pores formed within this layer.

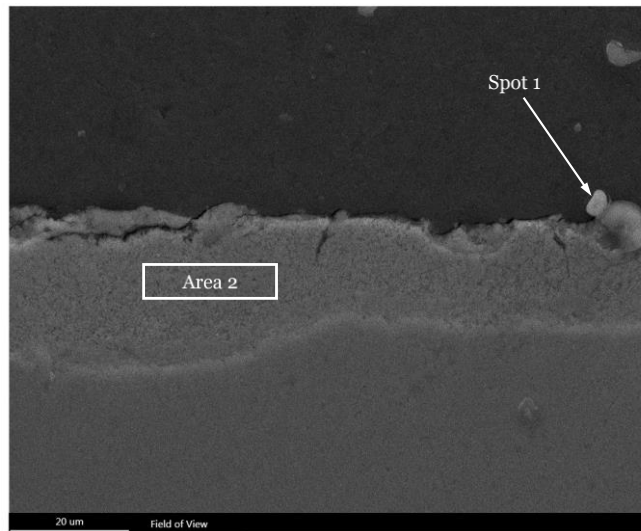


Figure C.26 Zinc –aluminium interface.

Table C.5 Weight and atomic percentages of elements found in Spot 1 and Area2 (Figure C.26).

Element	Weight (%)		Atomic (%)		Error (%)	
	Spot 1	Area 2	Spot 1	Area 2	Spot 1	Area 2
AlK	77.22	2.95	89.05	6.84	6.75	15.38
FeK	1.34	1.07	0.74	1.19	25.98	11.67
CuK	0.14	1.17	0.07	1.15	62.13	18.97
ZnK	21.30	94.82	10.14	90.82	4.96	1.76

Looking at Figure C.26, it is apparent that by moving closer to the melting zone (i.e. position b, in Figure C.24), the pores found in the zinc layer have developed into cracks (Area 1) and round phases (spot 1) at the interface between the aluminium and the zinc layers. Table C.5 presents the chemical compositions of the round particles (spot 1) and around the cracks found in area 1 (Figure C.26). What stands out in this table is the presence of high amounts of zinc (21.3 Wt. %) in the aluminium alloys that implies the initiation of solid diffusions of the zinc atoms in the aluminium alloys layer. Furthermore, the presence of aluminium particles in the

zinc layer (2.95 Wt. %) suggests that the aluminium atoms have diffused into the zinc layer. The solid diffusion of aluminium and zinc atoms in both layers suggests that, although position **a**, and position **b** are far from the melting zone, there is an improvement of adhesion between the welding sheets.

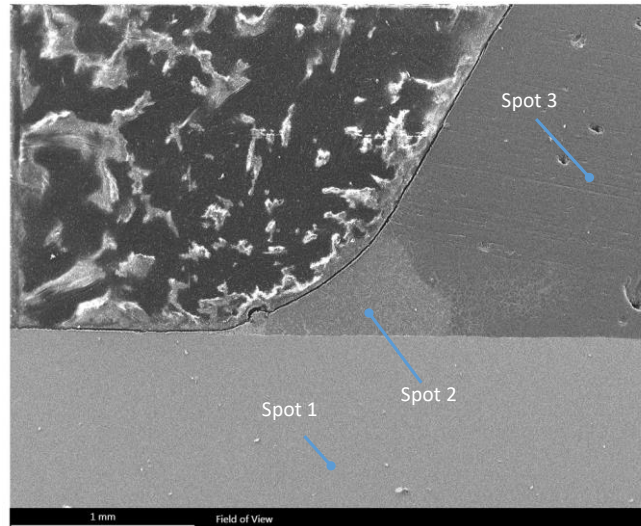


Figure C.27 Steel –filler interface.

Figure C.27 explores the interface between the aluminium and the filler. Spot 1 refers to the aluminium sheet, spot 3 refers to the filler and spot 2 is at the interface between the two layers. As expected spot 1 and 3 contain 97.80% and 98.62% of aluminium particles respectively. However, spot 2 contains 48.41% and 48.59% of aluminium and zinc particles respectively. This finding suggests that during the welding process the zinc particles from the galvanized steel sheet have spread and reacted with the aluminium particles at the interface between the aluminium and filler as seen in Figure C.28.

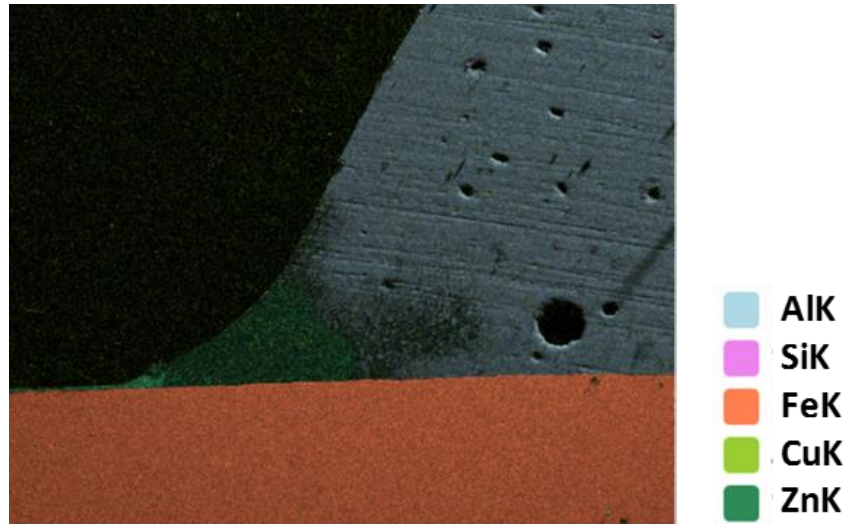


Figure C.28 Distribution of Zinc in the Filler.

Table C.6 Weight percentages of elements found in Spot 1, 2 and 3 (Figure C.27).

Element (wt%)	Spot 1	Spot 2	Spot 3
AlK	1.39	48.41	98.62
SiK	0.25	1.54	–
FeK	97.80	1.46	0.47
CuK	0.21	–	0.47
ZnK	0.35	48.59	0.45

The area characterized by the presence of all three layers (aluminium, steel, and filler) is shown in Figure C.29 and the composition at different places within this area is reported in Table C.7. Spot 3 and spot 6 (Figure C.29) are characterized by the presence of high amounts of aluminium and zinc which determine the start of the joining process between the layers by the metallic inter-diffusion process. However, further away from the interface of aluminium and filler layers, the presence of zinc content becomes negligible (spot 2, 4 and 5). By looking at Figure C.30, the presence of zinc in the filler confirms the occurrence of the diffusion mechanism of the zinc particles into the filler.

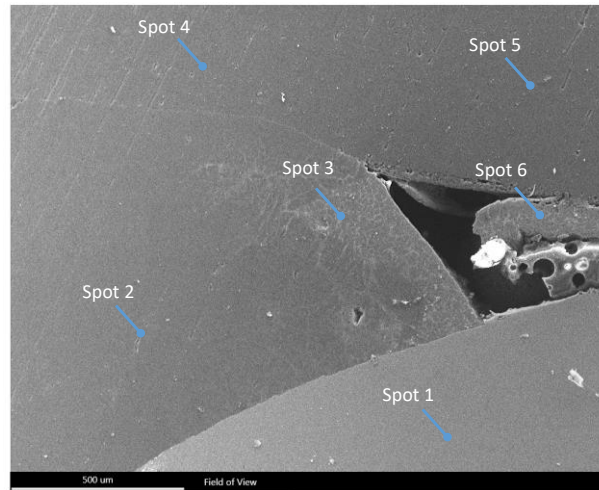


Figure C.29 Steel – Filler – Aluminium interfaces.

Table C.7 Weight percentages of elements found in Spot 1, 2, 3, 4, 5 and 6 (Figure C.29).

Element (wt%)	Spot 1	Spot 2	Spot 3	Spot 4	Spot 5	Spot 6
AlK	0.97	91.56	41.64	98.65	98.62	45.91
SiK	0.19	7.22	6.01	0.56	0.48	2.07
FeK	98.35	0.23	0.43	0.52	0.35	0.24
CuK	0.22	0.26	0.08	0.14	0.28	0.35
ZnK	0.26	0.73	51.84	0.14	0.27	51.43

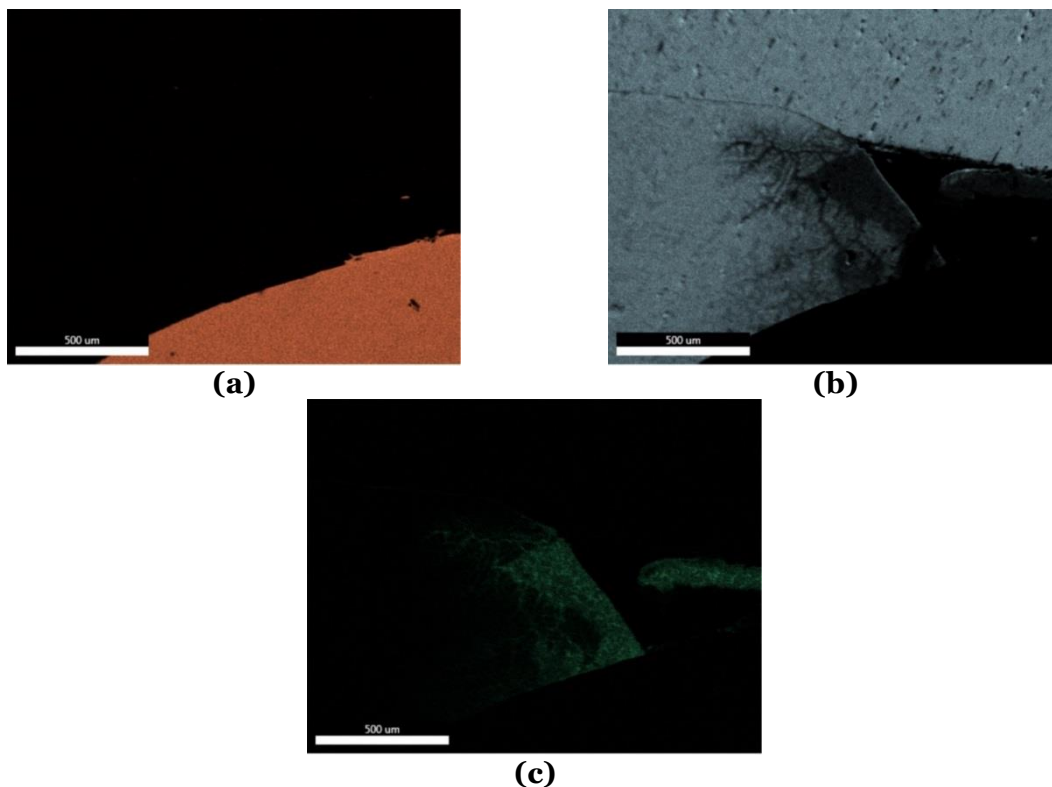


Figure C.30 Map of the main metallic elements in the welding zone: a) Steel, b) Aluminium and c) Zinc.

D Appendix D Fatigue data of aluminium-to-steel welded joints (chapter 7)



- Butt-0.1-01
- $N_f = 15617$ cycles to failure
- $\Delta\sigma_{nom} = 60$ MPa



- Butt-0.1-03
- $N_f = 289490$ cycles to failure
- $\Delta\sigma_{nom} = 54$ MPa



- Butt-0.1-04
- $N_f = 89952$ cycles to failure
- $\Delta\sigma_{nom} = 57$ MPa



- Butt-0.1-05
- $N_f = 105241$ cycles to failure
- $\Delta\sigma_{nom} = 57$ MPa



- Butt-0.1-06
- $N_f = 14380$ cycles to failure
- $\Delta\sigma_{nom} = 54$ MPa



- Butt-0.1-07
- $N_f = 23470$ cycles to failure
- $\Delta\sigma_{nom} = 52$ MPa



- Butt-0.1-08
- $N_f = 23335$ cycles to failure
- $\Delta\sigma_{nom} = 50$ MPa



- Butt-0.1-09
- $N_f = 138007$ cycles to failure
- $\Delta\sigma_{nom} = 50$ MPa



- Butt-0.1-10
- $N_f = 15275$ cycles to failure
- $\Delta\sigma_{nom} = 60$ MPa

Figure D.1 Fatigue failure of butt-welded joints with load ratio, $R=0.1$.



- Butt-0.1-11
- $N_f = 67660$ cycles to failure
- $\Delta\sigma_{nom} = 50$ MPa



- Butt-0.1-12
- $N_f = 36631$ cycles to failure
- $\Delta\sigma_{nom} = 50$ MPa



- Butt-0.1-13
- $N_f = 837329$ cycles to failure
- $\Delta\sigma_{nom} = 35$ MPa



- Butt-0.1-15
- $N_f = 967279$ cycles to failure
- $\Delta\sigma_{nom} = 45$ MPa

Figure D.1 Fatigue failure of butt-welded joints with load ratio, $R=0.1$ (continued).

Appendix D Fatigue data of aluminium-to-steel welded joints (chapter 7)

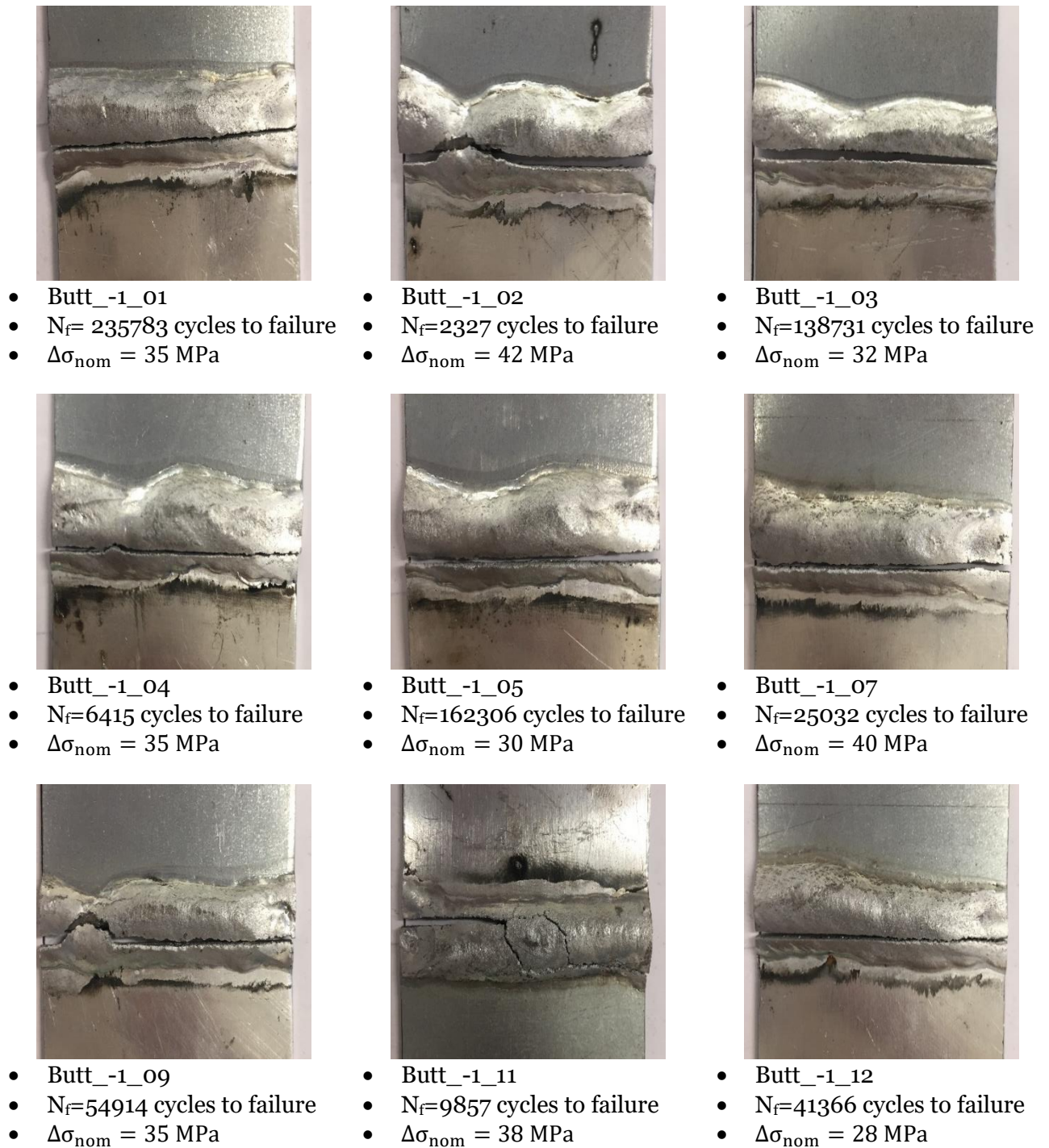


Figure D.2 Fatigue failure of butt-welded joints with load ratio, $R=-1$.

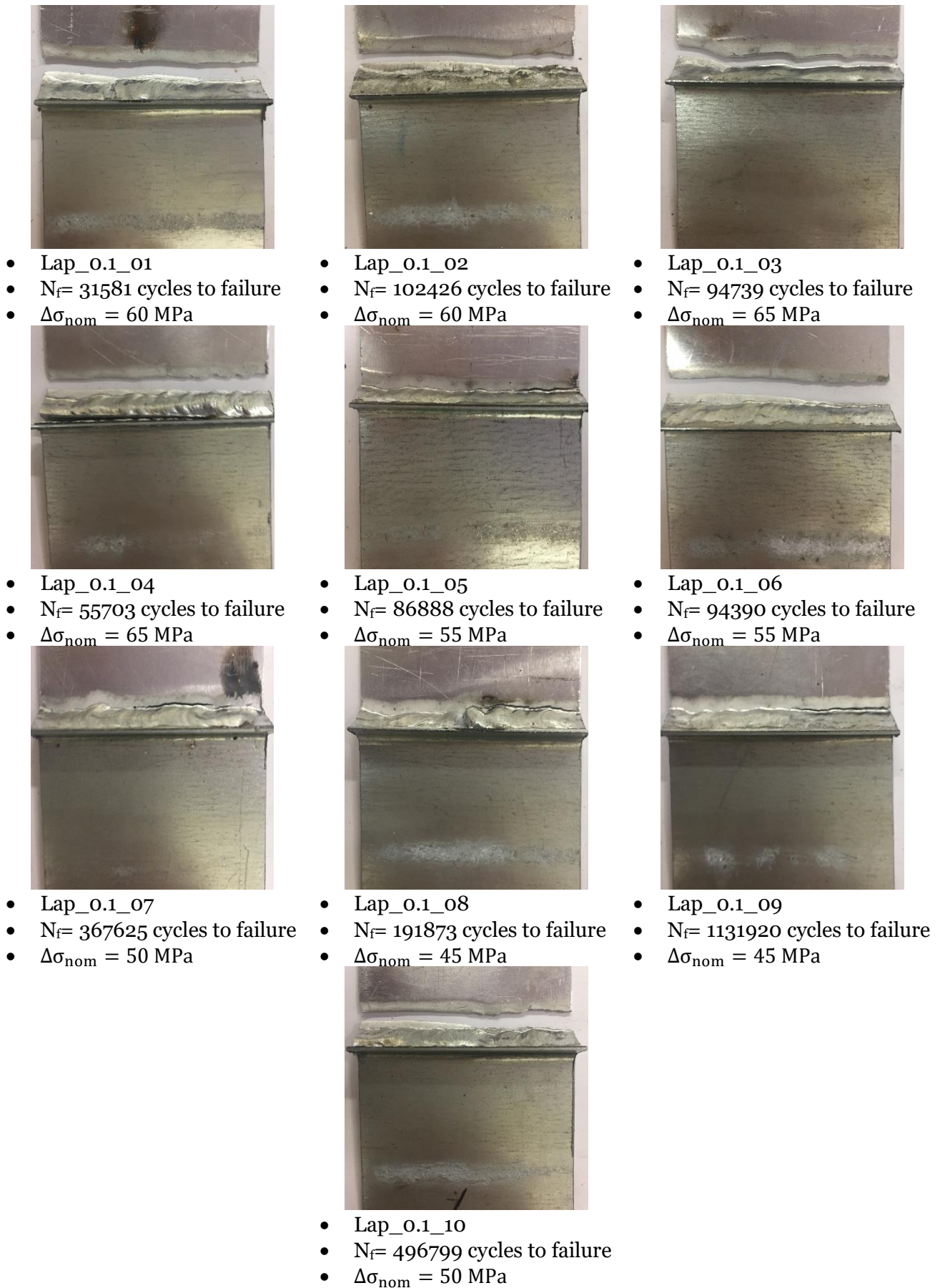


Figure D.3 Fatigue failure of lap-welded joints with load ratio, $R=0.1$.

Appendix D Fatigue data of aluminium-to-steel welded joints (chapter 7)



- Lap_0.5_01
- $N_f=1093169$ cycles to failure
- $\Delta\sigma_{nom} = 30$ MPa



- Lap_0.5_02
- $N_f=275251$ cycles to failure
- $\Delta\sigma_{nom} = 35$ MPa



- Lap_0.5_03
- $N_f=209757$ cycles to failure
- $\Delta\sigma_{nom} = 35$ MPa



- Lap_0.5_04
- $N_f=929710$ cycles to failure
- $\Delta\sigma_{nom} = 30$ MPa



- Lap_0.5_05
- $N_f=467257$ cycles to failure
- $\Delta\sigma_{nom} = 32$ MPa



- Lap_0.5_06
- $N_f=531450$ cycles to failure
- $\Delta\sigma_{nom} = 32$ MPa



- Lap_0.5_08
- $N_f=247044$ cycles to failure
- $\Delta\sigma_{nom} = 38$ MPa



- Lap_0.5_09
- $N_f=253922$ cycles to failure
- $\Delta\sigma_{nom} = 38$ MPa



- Lap_0.5_10
- $N_f=1037289$ cycles to failure
- $\Delta\sigma_{nom} = 28$ MPa

Figure D.4 Fatigue failure of lap-welded joints with load ratio, $R=0.5$.

Appendix D Fatigue data of aluminium-to-steel welded joints (chapter 7)

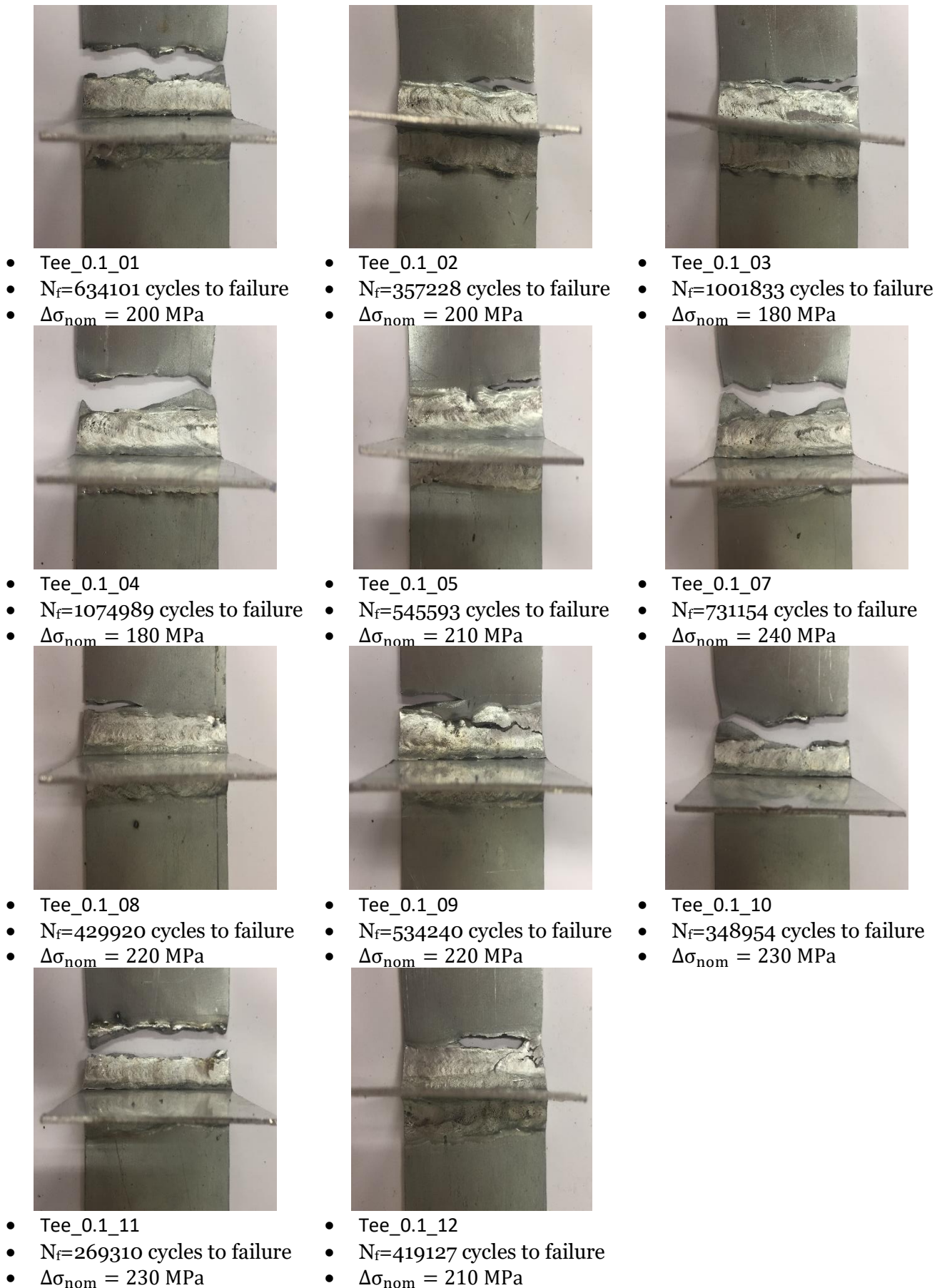


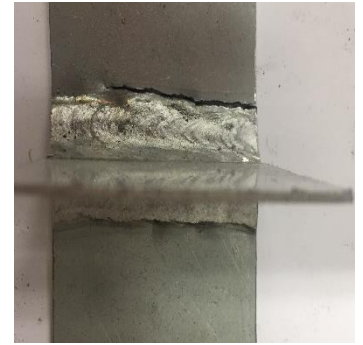
Figure D.5 Fatigue failure of tee-welded joints with load ratio, $R=0.1$



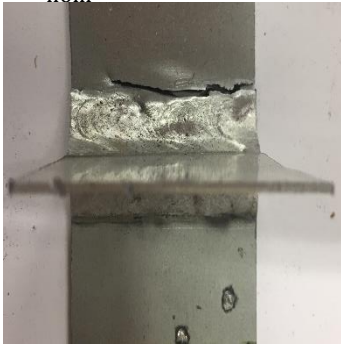
- Tee_-1_01
- $N_f=498691$ cycles to failure
- $\Delta\sigma_{nom} = 220$ MPa



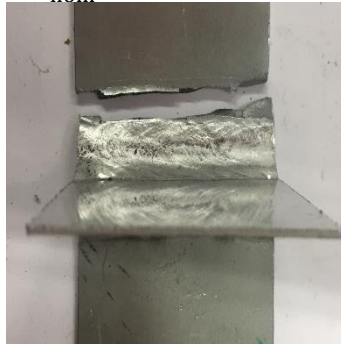
- Tee_-1_02
- $N_f=562767$ cycles to failure
- $\Delta\sigma_{nom} = 220$ MPa



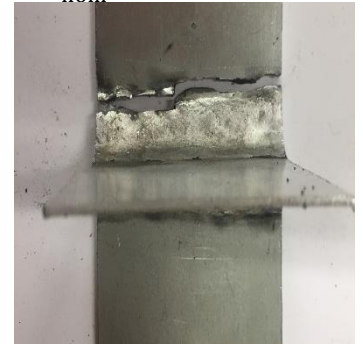
- Tee_-1_03
- $N_f=426377$ cycles to failure
- $\Delta\sigma_{nom} = 210$ MPa



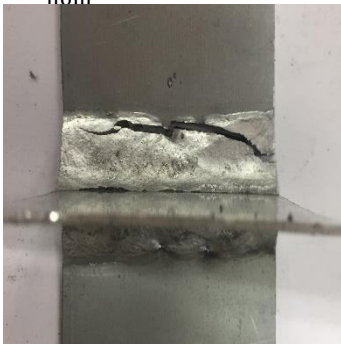
- Tee_-1_04
- $N_f=994315$ cycles to failure
- $\Delta\sigma_{nom} = 190$ MPa



- Tee_-1_05
- $N_f=1074229$ cycles to failure
- $\Delta\sigma_{nom} = 200$ MPa



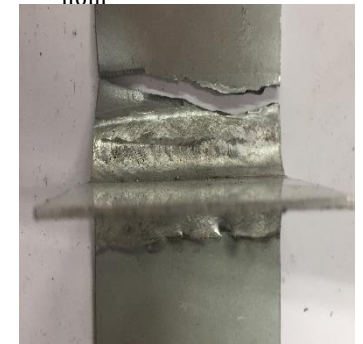
- Tee_-1_06
- $N_f=1651181$ cycles to failure
- $\Delta\sigma_{nom} = 190$ MPa



- Tee_-1_07
- $N_f=260375$ cycles to failure
- $\Delta\sigma_{nom} = 240$ MPa



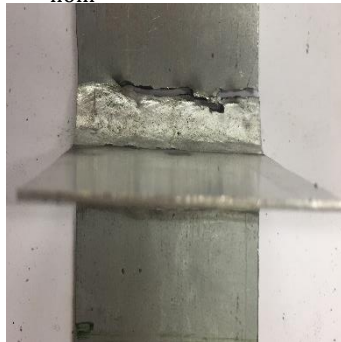
- Tee_-1_08
- $N_f=257386$ cycles to failure
- $\Delta\sigma_{nom} = 240$ MPa



- Tee_-1_09
- $N_f=847412$ cycles to failure
- $\Delta\sigma_{nom} = 230$ MPa



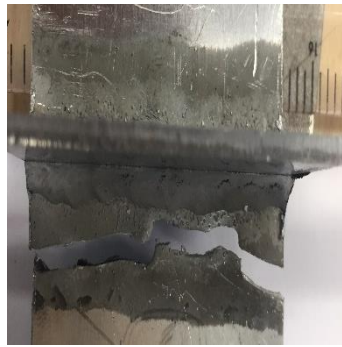
- Tee_-1_10
- $N_f=400377$ cycles to failure
- $\Delta\sigma_{nom} = 230$ MPa



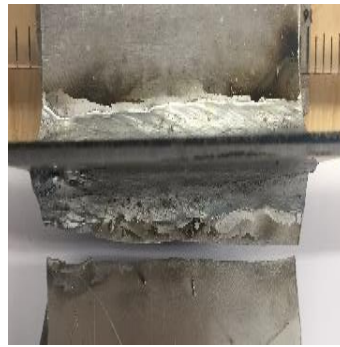
- Tee_-1_0
- $N_f=694024$ cycles to failure
- $\Delta\sigma_{nom} = 210$ MPa

Figure D.6 Fatigue failure of tee-welded joints with load ratio, $R=-1$.

Appendix D Fatigue data of aluminium-to-steel welded joints (chapter 7)



- Cr_0.1_01
- $N_f=1656$ cycles to failure
- $\Delta\sigma_{nom} = 60$ MPa



- Cr_0.1_02
- $N_f=52093$ cycles to failure
- $\Delta\sigma_{nom} = 55$ MPa



- Cr_-0.1_03
- $N_f=51492$ cycles to failure
- $\Delta\sigma_{nom} = 50$ MPa



- Cr_0.1_04
- $N_f=327683$ cycles to failure
- $\Delta\sigma_{nom} = 50$ MPa



- Cr_0.1_05
- $N_f=21171$ cycles to failure
- $\Delta\sigma_{nom} = 60$ MPa



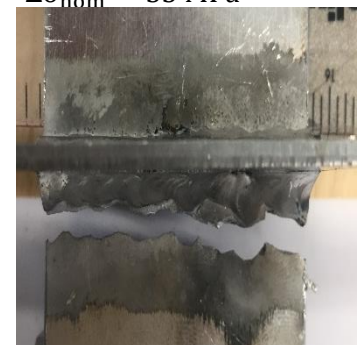
- Cr_0.1_06
- $N_f=564736$ cycles to failure
- $\Delta\sigma_{nom} = 55$ MPa



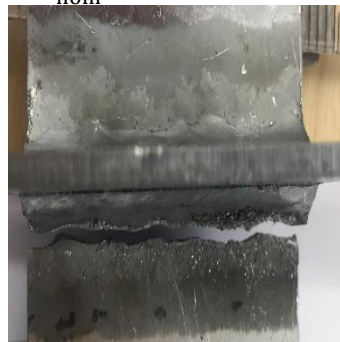
- Cr_0.1_07
- $N_f=564974$ cycles to failure
- $\Delta\sigma_{nom} = 40$ MPa



- Cr_01_08
- $N_f=279615$ cycles to failure
- $\Delta\sigma_{nom} = 40$ MPa



- Cr_0.1_09
- $N_f=86145$ cycles to failure
- $\Delta\sigma_{nom} = 45$ MPa



- Cr_0.1_10
- $N_f=2456047$ cycles to failure
- $\Delta\sigma_{nom} = 45$ MPa

Figure D.7 Fatigue failure of cruciform-welded joints with load ratio, $R=0.1$



- Cr_-1_01
- $N_f=44535$ cycles to failure
- $\Delta\sigma_{nom} = 60$ MPa



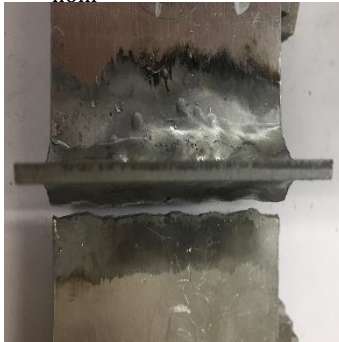
- Cr_-1_02
- $N_f=122917$ cycles to failure
- $\Delta\sigma_{nom} = 60$ MPa



- Cr_-1_03
- $N_f=289083$ cycles to failure
- $\Delta\sigma_{nom} = 55$ MPa



- Cr_-1_04
- $N_f=220433$ cycles to failure
- $\Delta\sigma_{nom} = 55$ MPa



- Cr_-1_05
- $N_f=417151$ cycles to failure
- $\Delta\sigma_{nom} = 50$ MPa



- Cr_-1_06
- $N_f=242154$ cycles to failure
- $\Delta\sigma_{nom} = 50$ MPa



- Cr_-1_08
- $N_f=297435$ cycles to failure
- $\Delta\sigma_{nom} = 55$ MPa



- Cr_-1_09
- $N_f=188002$ cycles to failure
- $\Delta\sigma_{nom} = 48$ MPa



- Cr_-1_10
- $N_f=699617$ cycles to failure
- $\Delta\sigma_{nom} = 48$ MPa



- Cr_-1_12
- $N_f=89987$ cycles to failure
- $\Delta\sigma_{nom} = 58$ MPa

Figure D.8 Fatigue failure of cruciform-welded joints with load ratio, $R=-1$.

Appendix D Fatigue data of aluminium-to-steel welded joints (chapter 7)

Table D.1 Experimental data and stress components relative to the critical plane calculated in terms of Pint Method for the butt-welded joints (2D and 3D FE models).

Code	R	$\Delta\sigma_{nom}$ [MPa]	2D FE analysis			3D FE analysis			Run-out
			$\Delta\tau$ [MPa]	$\Delta\sigma_n$ [MPa]	ρ_w	$\Delta\tau$ [MPa]	$\Delta\sigma_n$ [MPa]	ρ_w	
Butt_0.1_1	0.1	60	73.1	23.1		69.1	43.9		
Butt_0.1_2	0.1	50	60.9	19.2		57.6	36.6	✓	
Butt_0.1_3	0.1	54	65.8	20.8		62.2	39.5		
Butt_0.1_4	0.1	57	69.5	21.9		65.7	41.7		
Butt_0.1_5	0.1	57	69.5	21.9		65.7	41.7		
Butt_0.1_6	0.1	54	65.8	20.8		62.2	39.5		
Butt_0.1_7	0.1	52	63.4	20.0		59.9	38.1		
Butt_0.1_8	0.1	50	60.9	19.2	3.17*	57.6	36.6	1.57*	
Butt_0.1_9	0.1	50	60.9	19.2		57.6	36.6		
Butt_0.1_10	0.1	60	73.1	23.1		69.1	43.9		
Butt_0.1_11	0.1	50	60.9	19.2		57.6	36.6		
Butt_0.1_12	0.1	50	60.9	19.2		57.6	36.6		
Butt_0.1_13	0.1	35	42.7	13.5		40.3	25.6		
Butt_0.1_14	0.1	40	48.8	15.4		46.1	29.3	✓	
Butt_0.1_15	0.1	45	54.9	17.3		51.9	32.9		
Butt_-1_1	-1	35	99.3	29.5		64.3	58.1		
Butt_-1_2	-1	42	119.2	35.4		77.1	69.7		
Butt_-1_3	-1	32	90.8	26.9		58.7	53.1		
Butt_-1_4	-1	35	99.3	29.5		64.3	58.1		
Butt_-1_5	-1	30	85.1	25.3		55.1	49.8		
Butt_-1_6	-1	28	79.5	23.6	3.37*	51.4	46.4	1.11	
Butt_-1_7	-1	40	113.5	33.7		73.4	66.4		
Butt_-1_8	-1	32	90.8	26.9		58.7	53.1		
Butt_-1_9	-1	35	99.3	29.5		64.3	58.1	✓	
Butt_-1_10	-1	28	79.5	23.6		51.4	46.4	✓	
Butt_-1_11	-1	38	107.8	32.0		69.8	63.0		
Butt_-1_12	-1	28	79.5	23.6		51.4	46.4		

* $\rho_{w,lim} = 1.5$ is used for these series

Appendix D Fatigue data of aluminium-to-steel welded joints (chapter 7)

Table D.2 Experimental data and stress components relative to the critical plane calculated in terms of Pint Method for the lap welded joints (2D and 3D FE models).

Code	R	$\Delta\sigma_{nom}$ [MPa]	2D FE analysis			3D FE analysis			Run-out	
			$\Delta\tau$ [MPa]	$\Delta\sigma_n$ [MPa]	ρ_w	$\Delta\tau$ [MPa]	$\Delta\sigma_n$ [MPa]	ρ_w		
Lap_0.1_1	0.1	60	54.5	30.3		44.4	35.7			
Lap_0.1_2	0.1	60	54.5	30.3		44.4	35.7			
Lap_0.1_3	0.1	65	59.0	32.8		48.1	38.7			
Lap_0.1_4	0.1	65	59.0	32.8		48.1	38.7			
Lap_0.1_5	0.1	55	49.9	27.8	1.80*	40.7	32.7	1.24		
Lap_0.1_6	0.1	55	49.9	27.8		40.7	32.7			
Lap_0.1_7	0.1	50	45.4	25.3		37.0	29.7			
Lap_0.1_8	0.1	45	40.8	22.7		33.3	26.8			
Lap_0.1_9	0.1	45	40.8	22.7		33.3	26.8			
Lap_0.1_10	0.1	50	45.4	25.3		37.0	29.7			
Lap_0.5_1	0.5	30	32.3	18.7			24.2		20.8	
Lap_0.5_2	0.5	35	37.6	21.8			28.3		24.2	
Lap_0.5_3	0.5	35	37.6	21.8			28.3		24.2	
Lap_0.5_4	0.5	30	32.3	18.7			24.2		20.8	
Lap_0.5_5	0.5	32	34.4	20.0	1.73*	25.8	22.2	1.17		
Lap_0.5_6	0.5	32	34.4	20.0		25.8	22.2			
Lap_0.5_7	0.5	28	30.1	17.5		22.6	19.4			
Lap_0.5_8	0.5	38	40.9	23.7		30.7	26.3			
Lap_0.5_9	0.5	38	40.9	23.7		30.7	26.3			
Lap_0.5_10	0.5	28	30.1	17.5		22.6	19.4			
										✓

* $\rho_{w,lim} = 1.5$ is used for these series

Appendix D Fatigue data of aluminium-to-steel welded joints (chapter 7)

Table D.3 Experimental data and stress components relative to the critical plane calculated in terms of Pint Method for the cruciform welded joints (2D and 3D FE models).

Code	R	$\Delta\sigma_{nom}$ [MPa]	2D FE analysis			3D FE analysis			Run-out
			$\Delta\tau$ [MPa]	$\Delta\sigma_n$ [MPa]	ρ_w	$\Delta\tau$ [MPa]	$\Delta\sigma_n$ [MPa]	ρ_w	
Cr_0.1_1	0.1	60	48.9	22.0		44.4	35.7		
Cr_0.1_2	0.1	55	44.8	20.2		40.7	32.7		
Cr_0.1_3	0.1	50	40.8	18.3		37.0	29.7		
Cr_0.1_4	0.1	50	40.8	18.3		37.0	29.7		
Cr_0.1_5	0.1	60	48.9	22.0	2.22*	44.4	35.7	1.24	
Cr_0.1_6	0.1	55	44.8	20.2		40.7	32.7		
Cr_0.1_7	0.1	40	32.6	14.7		29.6	23.8		
Cr_0.1_8	0.1	40	32.6	14.7		29.6	23.8		
Cr_0.1_9	0.1	45	36.7	16.5		33.3	26.8		
Cr_0.1_10	0.1	45	36.7	16.5		33.3	26.8		
Cr_-1_1	-1	60	59.5	27.4		47.1	44.7		
Cr_-1_2	-1	60	59.5	27.4		47.1	44.7		
Cr_-1_3	-1	55	54.6	25.1		43.2	41.0		
Cr_-1_4	-1	55	54.6	25.1		43.2	41.0		
Cr_-1_5	-1	50	49.6	22.8		39.3	37.3		
Cr_-1_6	-1	50	49.6	22.8	2.66*	39.3	37.3	1.05	
Cr_-1_7	-1	45	44.7	20.6		35.3	33.6		
Cr_-1_8	-1	55	54.6	25.1		43.2	41.0		
Cr_-1_9	-1	48	47.6	21.9		37.7	35.8		
Cr_-1_10	-1	48	47.6	21.9		37.7	35.8		
Cr_-1_11	-1	48	47.6	21.9		37.7	35.8		
Cr_-1_12	-1	58	57.6	26.5		45.6	43.2		

* $\rho_{w,lim} = 1.5$ is used for these series

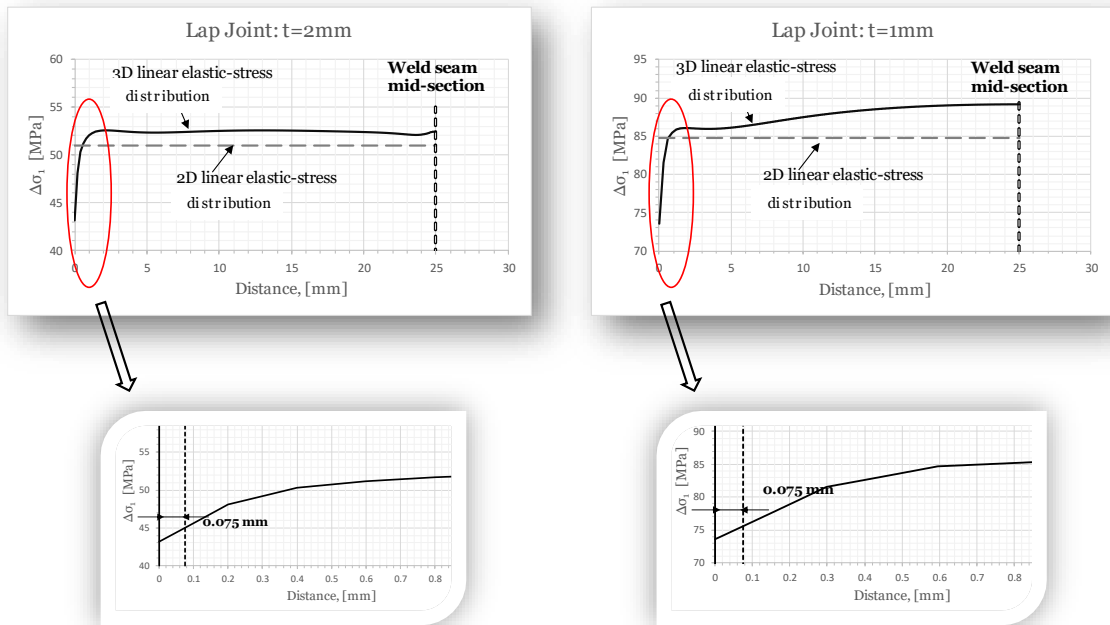


Figure D.9 2D and 3D linear elastic stress distribution along the weld seam for the lap-welded joints.

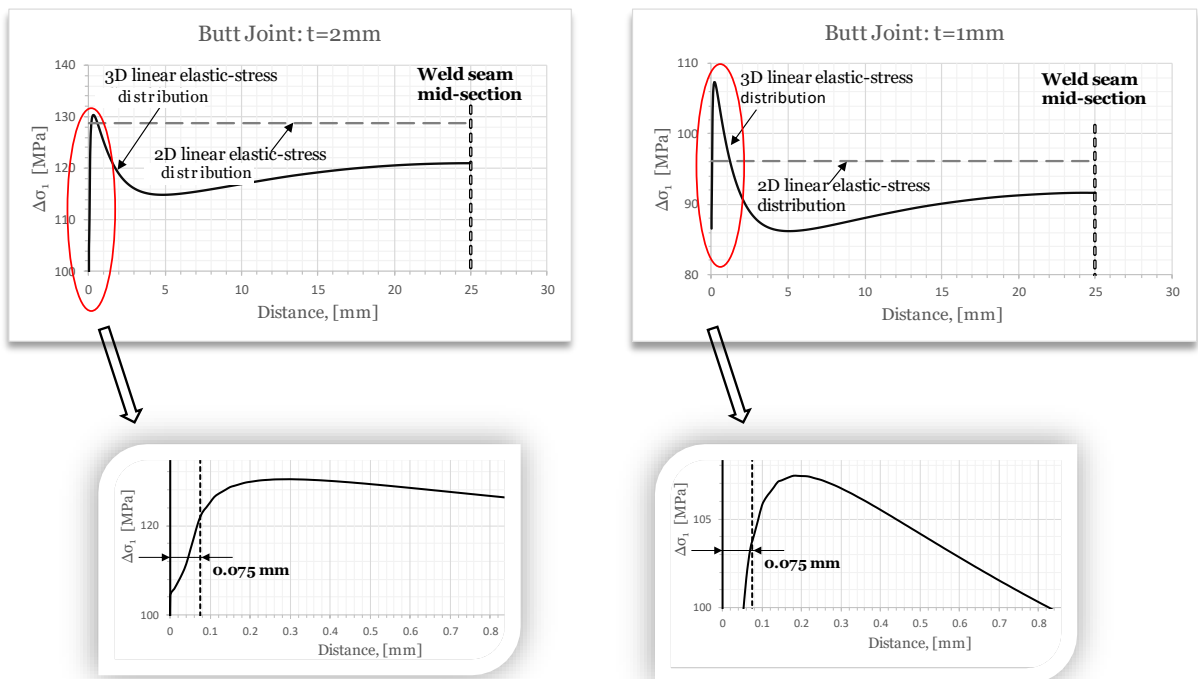


Figure D.10 2D and 3D linear elastic stress distribution along the weld seam for the butt-welded joints.